Miscible Flow Through Porous Media

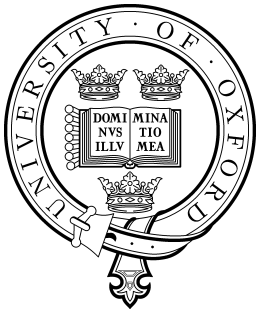

Richard Booth

Linacre College

University of Oxford

A thesis submitted for the degree of

Doctor of Philosophy

Trinity 2008

Acknowledgements

I would like to begin by thanking my supervisors John Ockendon and Chris Farmer for their continued advice and support. I would like to thank Schlumberger and EPSRC for their financial support. I would also like to thank the entire OCIAM community for making postgraduate life so enjoyable.

Finally I would like to thank my parents for their kindness and generosity.

Abstract

This thesis is concerned with the modelling of miscible fluid flow through porous media, with the intended application being the displacement of oil from a reservoir by a solvent with which the oil is miscible. The primary difficulty that we encounter with such modelling is the existence of a fingering instability that arises from the viscosity and the density differences between the oil and solvent.

We take as our basic model the Peaceman model, which we derive from first principles as the combination of Darcy's law with the mass transport of solvent by advection and hydrodynamic dispersion. In the oil industry, advection is usually dominant, so that the Péclet number, Pe, is large.

We begin by neglecting the effect of density differences between the two fluids and concentrate only on the viscous fingering instability. A stability analysis and numerical simulations are used to show that the wavelength of the instability is proportional to $\mathrm{Pe}^{-1/2}$, and hence that a large number of fingers will be formed. We next apply homogenisation theory to investigate the evolution of the average concentration of solvent when the mean flow is one-dimensional, and discuss the rationale behind the Koval model. We then attempt to explain why the mixing zone in which fingering is present grows at the observed rate, which is different from that predicted by a naïve version of the Koval model. We associate the shocks that appear in our homogenised model with the tips and roots of the fingers, the tip-regions being modelled by Saffman-Taylor finger solutions.

We then extend our model to consider flow through porous media that are heterogeneous at the macroscopic scale, and where the mean flow is not one-dimensional. We compare our model with that of Todd & Longstaff and also models for immiscible flow through porous media.

Finally, we extend our work to consider miscible displacements in which both density and viscosity differences between the two fluids are relevant.

Contents

List of Figures

Chapter 1

Introduction

This thesis is primarily concerned with the modelling of the flow of miscible fluids through a porous medium. The motivation behind studying these flows lies in the recovery of oil in a process known as miscible displacement, in which a solvent, such as a short-chain hydrocarbon or pressurised carbon-dioxide, is injected into the oil reservoir. We shall see that such flows are subject to a fingering instability, which leads to difficulty in accurate computation of the miscible displacement process. Although throughout this thesis our focus will be on miscible flow, we will spend some time, primarily in this introductory chapter, discussing immiscible flow, so that we are able to make comparisons between the two mechanisms.

We begin this introduction by giving an overview of the oil recovery process, and a more detailed explanation of the difference between miscible and immiscible flows. We introduce the standard model for flow of a single fluid through a porous medium, and investigate some simple free boundary problems for the displacement of one fluid by another. Strictly speaking these free boundary problems are only applicable to immiscible displacement, but they will be found to be limiting cases of miscible flood flows that shed light on the mechanism by which the fingering instability arises. We then give a brief review of some of the models applied in the oil industry which we shall revisit through the remainder of the thesis. We conclude the introduction with an overview of diffusion in porous media, which will be an important physical mechanism in many flows involving miscible displacement.

1.1 Oil recovery

Crude oil is found trapped inside the pore-space of rock formations several kilometres below ground. Various techniques have been developed to enable the recovery of oil to the surface, which we now outline.

1.1.1 Primary and secondary oil recovery

The simplest form of oil recovery is primary oil recovery, in which a well is drilled into the oil reservoir and the oil is pushed up the well due to the naturally high pressure in the oil reservoir. The high pressure is the result of denser rock and water resting above the level of the lighter oil. Pockets of trapped compressed gas may also contribute to the higher pressure. As oil is produced from the well, the natural reservoir pressure drops and the flow of oil to the surface may become greatly reduced. Some techniques that are used to maximise the amount of oil recovered during this primary phase include the use of pumps to lift oil up the well, and the use of explosives and high pressure pumps to fracture the rock formation. In a typical oil reservoir only around 10% of the total amount of oil available can be recovered by primary oil recovery.

In many oil reservoirs, once primary oil recovery has ceased, more of the oil may still be recovered by secondary oil recovery. In secondary oil recovery, water is injected into the oil reservoir through one well, displacing the oil so that it can be extracted from a neighbouring well. Since the water is less viscous than the oil and the permeability of the rock is often highly heterogeneous, the time before 'breakthrough' - i.e. when the water finds a path between the injection well and the production well - is often very short. When a large fraction of water is being extracted from the production well, the secondary recovery process becomes uneconomical. The amount of oil that may thus be extracted depends heavily on the structure of the rock in which the oil is contained and the properties of the oil to be extracted; however, even under optimal conditions more than half of the total amount of oil available will usually be left behind after primary and secondary recovery is complete.

1.1.2 Enhanced oil recovery

With large amounts of oil remaining unrecovered in mature oil reservoirs, the oil recovery industry has developed numerous techniques to extract this oil, referred to under the catchall phrase 'enhanced oil recovery'. The one feature that most enhanced oil recovery schemes share is that they attempt to alter the physical properties of the oil.

For some applications, thermal recovery is appropriate. Here the oil is heated either by the injection of steam or by 'in-situ combustion', where a controlled combustion is started underground using the oil itself as a fuel source. Heating the oil reduces its viscosity thus aiding recovery. Thermal recovery is particularly suited to the extraction of extremely viscous heavy oils [53], for which the amount recovered by primary and secondary oil recovery is particularly small. When the temperature of heavy oil is increased, its viscosity dramatically decreases, vastly improving the effectiveness of primary and secondary oil

recovery techniques.

During secondary recovery, it is possible to add various chemicals to the injected water. The chemicals added are chosen to either increase the viscosity of the water or to be surface active and reduce the surface-tension at the interface between the oil and water.

An increasingly important method of enhanced oil recovery, and one which forms the basis for this thesis, is miscible displacement. Miscible displacement involves the injection of a fluid which, unlike water, is miscible with the oil.

1.1.3 Miscible displacements

There are two advantages of using a fluid which is miscible with oil. Firstly, there are no surface-tension effects, and so the two fluids may more freely displace each other within the porous medium. Secondly, the introduction of a miscible fluid, less viscous than the oil, leads to a mixture with a viscosity less than that of the oil, thus reducing the applied pressure gradient required to displace the oil, and aiding recovery. Before we continue with more details of the industrial process, we make precise the difference between miscible and immiscible fluids.

1.1.3.1 What is meant by 'miscible' and 'immiscible'?

Two fluids are defined as *miscible* if the molecules of the one fluid are free to mix with the molecules of the other fluid. There is no interface between two miscible fluids. A common example of two miscible fluids is water and ethanol. In any proportions it is possible to mix the water and ethanol together to form a single homogeneous phase. When two gases meet, they are always miscible; for example oxygen and nitrogen readily mix in air.

Two fluids are defined as *immiscible* if the two fluids scarcely mix at all at the molecular level, and not at all at the macroscale. The two phases remain distinct and there is a well-defined interface between the two fluids. Common examples of two immiscible fluids are water and most vegetable oils.

It is possible for two fluids to be neither completely miscible nor completely immiscible. The molecules of the first fluid may mix with the molecules of the second fluid until the concentration of the first fluid reaches a certain saturation concentration. The saturation concentration may be affected by the temperature and pressure of the system. A common example of two partially miscible fluids is water and carbon dioxide. Some of the carbon dioxide may dissolve in the water but there is still a well-defined interface between the carbon dioxide gas and the water containing dissolved CO_2. At room temperature and pressure, the amount of dissolved carbon dioxide will be reasonably small, but at the

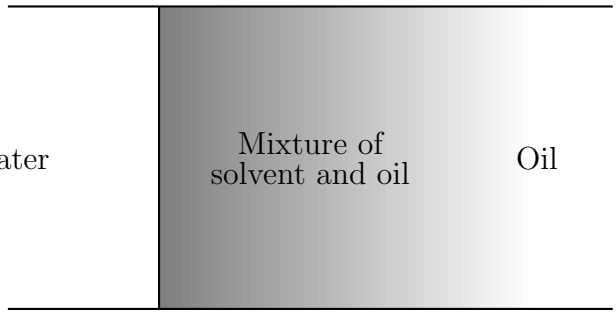

Figure 1.1: A pad of solvent between the water and oil.

temperatures and pressures experienced deep in an oil reservoir, there may be a significant quantity of carbon dioxide dissolved in the water. At sufficiently high pressures carbon dioxide and water eventually become completely miscible.

It should be emphasised that when we speak of the two fluids 'mixing' we are referring to mixing at the molecular level and not at the pore scale. When two immiscible fluids flow through a porous medium, it is possible that the two fluids will be simultaneously present in an individual pore; however, the two fluids will not freely displace each other within the pore and any modelling needs to account for this.

1.1.3.2 Introduction of solvents

The earliest miscible displacement processes used short-chain hydrocarbons, such as methane or propane, as a solvent. These solvents are fully miscible with oil and are considerably less viscous than oil; however, they may also be expensive to use. Due to the high cost of these solvents they are also sometimes used in small quantities to form a 'pad' between water and oil in a secondary oil recovery process. The solvents used are immiscible with the water and the viscosity of the solvent is less than that of water. It is found that the mixing region, where both the solvent and oil are present, grows quite quickly. In this thesis we will be concerned with modelling this mixing region, and shall assume that no water is present.

1.1.3.3 Introduction of carbon dioxide

A more economically viable alternative to injection of hydrocarbon solvents is the injection of carbon dioxide. Carbon dioxide can be captured from industrial processes above ground and injected at high pressure into the oil reservoir. At typical reservoir conditions, carbon dioxide is a supercritical fluid, with the carbon dioxide fully miscible with the oil, and is less viscous than the oil, so the mixing region may spread faster than one might naïvely expect. Carbon dioxide is also less dense than oil and so it tends to move upwards through the reservoir.

An additional advantage to the use of carbon dioxide in miscible displacements is that once the oil recovery process is complete the carbon dioxide is left behind in the oil reservoir. This removal of carbon dioxide from the atmosphere has attracted attention as a possible means of combating global warming. There is now also considerable interest in sequestering carbon dioxide in aquifers, where the carbon dioxide displaces water rather than oil.

1.2 Single-phase flow

For flow of one phase through a saturated porous medium the basic equation is Darcy's law,

$$\mathbf{u} = -\frac{\mathbf{K}}{\mu}\left(\nabla p - \rho \mathbf{g}\right), \tag{1.1}$$

where $\mathbf{u}$ is the flux of fluid per unit area. The flux or 'Darcy velocity' $\mathbf{u}$ is related to $\overline{\mathbf{v}}$, the averaged velocity through the pores, by

$$\mathbf{u} = \phi \overline{\mathbf{v}}, \tag{1.2}$$

where the porosity ϕ is the volume fraction of pore space. The permeability tensor $\mathbf{K}$ may be empirically determined from a sample of the porous medium, and has the dimensions of length squared, being proportional to the square of the microscopic pore scale. Darcy's law was originally suggested as an empirical law [13], but can also be formally derived by homogenisation of steady Stokes flow, as we present in the next section.

1.2.1 Derivation of Darcy's law from steady Stokes flow

Conservation of mass of the fluid inside the pores gives

$$\frac{\partial \rho}{\partial t} + \nabla \cdot (\rho \mathbf{v}) = 0, \tag{1.3}$$

where ρ is the density of the fluid and $\mathbf{v}$ is the actual velocity of the fluid inside the pores. The pore-scale Reynolds number in all oil recovery processes will be small (e.g. water flowing through pores of radius 0.1mm at a rate of 5mday^{-1} gives $\mathrm{Re} = 5 \times 10^{-4}$) and we therefore apply Stokes flow,

$$-\nabla p + \mu \nabla^2 \mathbf{v} + (4\mu/3 + \mu_b)\, \nabla \left(\nabla \cdot \mathbf{v}\right) = \rho \mathbf{g}, \tag{1.4}$$

where p is the pressure, μ is the viscosity of the fluid, μ_b is the bulk viscosity of the fluid and $\mathbf{g}$ is the acceleration due to gravity. We must also assume an equation of state

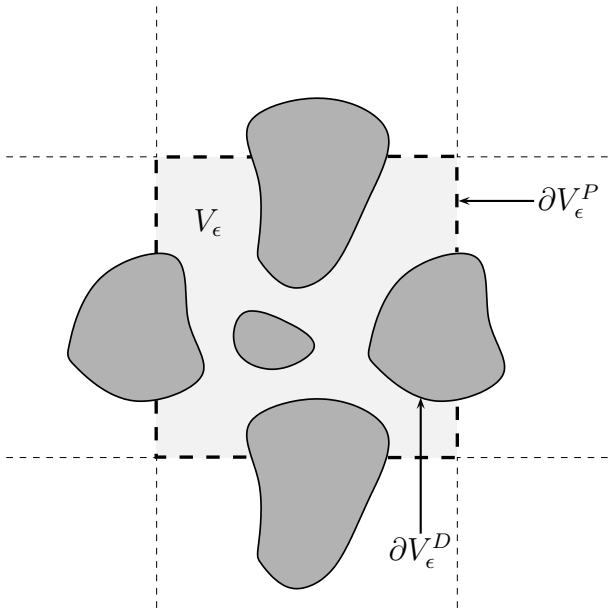

Figure 1.2: Definition of V_ϵ in a periodic medium.

$p = p(\rho)$. At the interface between the fluid space and the rock matrix we apply a no-slip boundary condition for the fluid.

The equations (1.3), (1.4) are only valid inside the pores, and are not valid at the macroscopic scale. We define a microscopic length scale (i.e. the length of a pore) to be L, and a macroscopic length scale, over which the pressure gradient is applied, to be l.[1] The macroscopic length scale of interest (e.g. between two wells, or between large heterogeneities in the rock) is much larger than the pore length scale, so that $\epsilon = L/l \ll 1$. We nondimensionalise the pressure with Δp, a typical pressure drop, $\mathbf{x}$ with l, the density with a reference value $\tilde{\rho}$, the velocity $\mathbf{v}$ with $U = L^2\Delta p/l\mu$, and t with l/U. The nondimensionalisation for the velocity is motivated by the scaling of the pressure in Poiseuille flow [20].

To apply homogenisation theory, one must make some assumptions about the structure of the porous medium that the fluid is flowing through. In principle one can apply homogenisation either by assuming that the medium is periodic at the microscale or by assuming that the medium is constructed by some random process with reasonable statistical properties such as stationarity and ergodicity [8]. In practice there are many technical details that arise when one derives Darcy's law for a random porous medium, particularly related to the connectedness of the fluid space, although these can be overcome [3]. Since the derivation of Darcy's law for periodic porous media is much simpler to follow and applies the same basic physical principles, we shall present the theory only for

[1] Throughout this thesis we shall use lower-case letters to represent macroscopic variables and upper-case letters to represent microscopic variables.

flow through periodic media. At least for this problem, the assumption that the medium is periodic is simply for analytical convenience, and we recognise that natural porous media will not be periodic.

We define V_ϵ as the volume of pore space over which the medium is ϵ-periodic in $\mathbf{x}$. The boundary of V_ϵ, ∂V_ϵ, is composed of two surfaces as depicted in Figure 1.2. The interface between the solid rock matrix and the pore space is denoted by ∂V_ϵ^D and the periodic surface between adjacent volumes of pore space is denoted by ∂V_ϵ^P. Inside V_ϵ our non-dimensionalised model is

$$\frac{\partial \rho}{\partial t} + \nabla \cdot (\rho \mathbf{u}) = 0, \tag{1.5}$$

$$-\nabla p + \epsilon^2 \left(\nabla^2 \mathbf{v} + \lambda \nabla (\nabla \cdot \mathbf{v}) \right) = -G\rho \mathbf{e}_3, \tag{1.6}$$

where $\lambda = 4/3 + \mu_b/\mu$ and $G = \tilde{\rho} g l / \Delta p$ are dimensionless constants that will be of order one (compared with ϵ) for most oil recovery applications, and $\mathbf{e}_3$ is the unit vector in the vertical (x_3) direction. We still have the equation of state $p = p(\rho)$, and on ∂V_ϵ^D we apply the no-slip condition that $\mathbf{v} = \mathbf{0}$. We now apply the first crucial step to any homogenisation argument: we allow the velocity, pressure and density to vary both slowly over the macroscopic length scale and rapidly over the microscopic length scale of the pores. This is achieved by proposing multiple-scales expansions of the form

$$\begin{aligned} \mathbf{v} &\sim \mathbf{v}_0(\mathbf{x}, \mathbf{X}, t) + \epsilon \mathbf{v}_1(\mathbf{x}, \mathbf{X}, t) + \dots , \\ p &\sim p_0(\mathbf{x}, \mathbf{X}, t) + \epsilon p_1(\mathbf{x}, \mathbf{X}, t) + \dots , \\ \rho &\sim \rho_0(\mathbf{x}, \mathbf{X}, t) + \epsilon \rho_1(\mathbf{x}, \mathbf{X}, t) + \dots , \end{aligned}$$

where the microscale variable $\mathbf{X} = \mathbf{x}/\epsilon$. We are on the manifold $\mathbf{x} = \epsilon \mathbf{X}$ and so

$$\nabla = \frac{1}{\epsilon} \nabla_X + \nabla_x,$$

as a result of the chain rule. This is equivalent to treating $\mathbf{x}$ and $\mathbf{X}$ as independent variables.

The next key step to the homogenisation argument is to ensure that the expansion remains valid as $\epsilon \to 0$. Since our problem is 1-periodic in $\mathbf{X}$, we shall require that $\mathbf{v}_0, \mathbf{v}_1, p_0, p_1, \rho_0, \rho_1, \dots$ are all 1-periodic in $\mathbf{X}$ since otherwise we would find that terms in our expansion would grow unboundedly as $\epsilon \to 0$ and $|\mathbf{X}| \to \infty$. We cannot allow terms in our expansion to grow unboundedly as this will lead to the expansion breaking down when, for instance we no longer satisfy $\epsilon p_1 \ll p_0$. The analogue to periodicity in random porous media is stationarity (i.e. invariance under translation), and to avoid unbounded

growth of terms in the expansion, we require stationarity of the terms in the expansion. To leading order in (1.6) we find $\nabla_X p_0 = \mathbf{0}$ and so $p_0 = p_0(\mathbf{x}, t)$. Also, from the equation of state $p = p(\rho)$, we conclude that $\rho_0 = \rho_0(\mathbf{x}, t)$. The leading order term in (1.5) and the $O(1)$ terms in (1.6) give

$$\nabla_X \cdot \mathbf{v}_0 = 0, \tag{1.7}$$

$$\nabla_X p_1 = \nabla_X^2 \mathbf{v}_0 - \nabla_x p_0 + \rho_0 G \mathbf{e_3}, \tag{1.8}$$

$$\mathbf{v}_0 = \mathbf{0} \quad \text{on} \quad \partial V_\epsilon^D. \tag{1.9}$$

We must consider local cell-problems in V_ϵ. We need to find functions $\mathbf{w}^j(\mathbf{X})$, $P^j(\mathbf{X})$ which are 1-periodic in $\mathbf{X}$ and solve the cell problem,

$$\nabla_X \cdot \mathbf{w}^j = 0, \tag{1.10}$$

$$\nabla_X P^j = \nabla_X^2 \mathbf{w}^j + \mathbf{e}_j, \tag{1.11}$$

$$\mathbf{w}^j = \mathbf{0} \quad \text{on} \quad \partial V_\epsilon^D, \tag{1.12}$$

where $\mathbf{e}_j$ is the unit basis vector in the X_j direction. Crucially equations (1.10)-(1.12) are linear and so we find that

$$\mathbf{v}_0 = -\frac{\partial p_0}{\partial x_j}\mathbf{w}^j + \rho_0 G \mathbf{w}^3. \tag{1.13}$$

The $O(1)$ term of (1.5) is

$$\frac{\partial \rho_0}{\partial t} + \nabla_x \cdot (\rho_0 \mathbf{v}_0) + \nabla_X \cdot (\rho_0 \mathbf{v}_1 + \rho_1 \mathbf{v}_0) = 0. \tag{1.14}$$

We now come to the final important step of the homogenisation process, we integrate the above equation over V_ϵ to obtain an integrability condition that gives an averaged equation. Integrating (1.14) over V_ϵ and applying the divergence theorem gives

$$\int_{V_\epsilon} \frac{\partial \rho_0}{\partial t} + \nabla_x \cdot (\rho_0 \mathbf{v}_0)\, \mathrm{d}\mathbf{X} = \int_{\partial V_\epsilon} (\rho_0 \mathbf{v}_1 + \rho_1 \mathbf{v}_0) \cdot \mathbf{n}\, \mathrm{d}s.$$

We can apply the no-slip condition on ∂V_ϵ^D and the periodicity condition on ∂V_ϵ^P to see that the right-hand side of the above equation vanishes. Applying summation convention, we are left with the homogenised problem:

$$\phi \frac{\partial \rho_0}{\partial t} + \frac{\partial}{\partial x_i}\left(-\rho_0 K_{ij}^* \frac{\partial p_0}{\partial x_j} + \rho_0 G K_{i3}^*\right) = 0, \tag{1.15}$$

where ϕ, the porosity, is equal to the volume of V_ϵ, and

$$K^*_{ij} = \int_{V_\epsilon} w^j_i \, \mathrm{d}\mathbf{X}, \tag{1.16}$$

is the permeability tensor; for some porous media it is reasonable to assume that the pore structure is isotropic so that $K_{ij} = k\delta_{ij}$. After redimensionalisation we obtain

$$\phi \frac{\partial \rho_0}{\partial t} - \nabla \cdot \left(\frac{\rho_0 \mathbf{K}}{\mu} \left(\nabla p_0 - \rho_0 \mathbf{g} \right) \right) = 0,$$

where the dimensional permeability tensor is given by $\mathbf{K} = L^2 \mathbf{K}^*$, i.e. the permeability tensor is proportional to the square of the pore length scale. It is also convenient to work with the flux of the fluid,

$$\mathbf{u} = \int_{V_\epsilon} \mathbf{v}_0 \, \mathrm{d}\mathbf{X} = -\frac{\mathbf{K}}{\mu} \left(\nabla p_0 - \rho_0 \mathbf{g} \right), \tag{1.17}$$

which satisfies

$$\phi \frac{\partial \rho_0}{\partial t} + \nabla \cdot (\mathbf{u} \rho_0) = 0.$$

Note that throughout this thesis we will use $\mathbf{u}$ to represent the flux of fluid per unit area, rather than the average velocity within the pores. The flux of fluid per unit area, also known as the superficial velocity or the Darcy velocity, is simply related to the average velocity within the pores, $\bar{\mathbf{v}}_0$ by the expression

$$\mathbf{u} = \phi \bar{\mathbf{v}}_0,$$

where ϕ is the porosity.

Although compressibility of the fluid may be important near to injection wells where the pressure gradient may be large, it is usually possible to justify neglecting the compressibility throughout most of the reservoir. For incompressible flow we simply have that

$$\nabla \cdot \mathbf{u} = 0,$$

where $\mathbf{u}$ is the flux as defined in (1.17). For the remainder of this thesis we shall assume that the fluids are incompressible. It is possible to justify this assumption, a posteriori, by the absence of large pressure gradients in all of our future models. In saturated, one-phase flow with no free surfaces, we may also incorporate the gravity term into the pressure gradient. When two or more fluids are present gravity may only be incorporated into the pressure gradient when the fluids are neutrally buoyant (i.e. they have equal densities).

In a homogeneous, isotropic porous medium, the effective pressure (actual pressure minus the hydrostatic pressure) in an incompressible fluid satisfies Laplace's equation $\nabla^2 p = 0$. This allows many simple analytical solutions to be found for one-phase incompressible flow through homogeneous, isotropic media.

1.2.2 The Hele-Shaw cell analogue

A useful analogue of flow through a porous medium is the Hele-Shaw cell. A Hele-Shaw cell consists of a viscous fluid flowing between two parallel plates separated by a small distance, h. It is easy to show (see for example [41]) that when the reduced Reynolds number and the aspect ratio of the Hele-Shaw cell are both much less than 1, the velocity, averaged between the two plates, is given by

$$\bar{\mathbf{u}} = -\frac{h^2}{12\mu}\nabla p.$$

The averaged velocity also satisfies

$$\nabla \cdot \bar{\mathbf{u}} = 0,$$

and so flow through a Hele-Shaw cell is analogous to incompressible flow through a two-dimensional porous medium with a permeability of $h^2/12$. It is often difficult to construct experiments for flow through porous media, and so a Hele-Shaw cell is used instead.

1.2.3 Homogenisation of the permeability

Homogenisation is not only useful for the derivation of Darcy's law from pore-scale models. The technique also allows us to determine the effective permeability of a porous medium that is heterogeneous below the length scale of interest. Rock formations typically exhibit heterogeneities over many different length scales. Suppose a porous medium exhibits heterogeneities with a characteristic length scale L, and the length scale of interest, i.e. the length scale over which a pressure difference is applied or the size of the reservoir, is l. For it to be possible to obtain an effective homogeneous permeability, without variations over the length scale L, we require that the two length scales are well-separated, i.e. we now have a small parameter $\epsilon = l/L \ll 1$.

The permeability can be described by $\mathbf{K} = K_{ij}(\mathbf{x}, \mathbf{X})$, where $\mathbf{X} = \mathbf{x}/\epsilon$. To be able to obtain an effective homogenised permeability, we require that the permeability has a sensibly defined local average on the microscopic scale. A well-defined local average of

the permeability is ensured if, for instance, the permeability is a strictly-stationary[2] and ergodic[3] random variable, and it is then possible to obtain a homogenised permeability, as shown in [43]. A simpler, but more restrictive, assumption that leads to a well-defined local average, is to assume that the permeability is 1-periodic in $\mathbf{X}$, which we now apply. The pressure must solve

$$\nabla \cdot (\mathbf{K}(\mathbf{x}, \mathbf{X}) \nabla p) = 0,$$

and so we introduce the multiple-scales expansion for the pressure,

$$p \sim p_0(\mathbf{x}, \mathbf{X}) + \epsilon p_1(\mathbf{x}, \mathbf{X}) + \dots \ ,$$

where $\mathbf{x}$ and $\mathbf{X}$ are treated as independent variables. The pressure must be 1-periodic in $\mathbf{X}$, as otherwise the pressure will grow unboundedly as $\epsilon \to 0$ and $|\mathbf{X}| \to \infty$.

The leading order pressure satisfies

$$\nabla_X \cdot (\mathbf{K}(\mathbf{x}, \mathbf{X}) \nabla_X p_0) = 0,$$

which only holds for periodic p_0 when $p_0 = p_0(\mathbf{x})$. At next order we find that

$$\nabla_X \cdot (\mathbf{K}(\mathbf{x}, \mathbf{X}) \nabla_X p_1) + \nabla_X \cdot (\mathbf{K}(\mathbf{x}, \mathbf{X}) \nabla_x p_0) = 0,$$

which has a solution of the form

$$p_1 = F_k(\mathbf{x}, \mathbf{X}) \frac{\partial p_0}{\partial x_k} + \hat{p}_1(\mathbf{x}),$$

where summation convention has been applied and F_k satisfies

$$\frac{\partial}{\partial X_i} \left(K_{ik} \frac{\partial F_j}{\partial X_k} \right) + \frac{\partial K_{ij}}{\partial X_i} = 0, \tag{1.18}$$

and is 1-periodic in $\mathbf{X}$. Once the cell problems (1.18) are solved, we may proceed to next order to find that

$$\nabla_X \cdot (\mathbf{K}(\mathbf{x}, \mathbf{X}) \nabla_X p_2) + \nabla_X \cdot (\mathbf{K}(\mathbf{x}, \mathbf{X}) \nabla_x p_1) + \nabla_x \cdot (\mathbf{K}(\mathbf{x}, \mathbf{X}) \nabla_X p_1) + \nabla_x \cdot (\mathbf{K}(\mathbf{x}, \mathbf{X}) \nabla_x p_0) = 0,$$

and, on integrating with respect to $\mathbf{X}$ over the unit cell, and applying the condition of periodicity to p_0 and p_1 we find that

$$\nabla_x \cdot \left(\tilde{\mathbf{K}} \nabla_x p_0 \right) = 0,$$

[2] I.e. the random variable representing the permeability is unchanged under translations in $\mathbf{X}$.
[3] I.e. the average of the permeability over many realisations is the same as the average over $\mathbf{X}$.

where

$$\tilde{K_{ij}} = \int_0^1 \int_0^1 \int_0^1 K_{ik} \frac{\partial F_j}{\partial X_k} + K_{ij} \, \mathrm{d}X_1 \mathrm{d}X_2 \mathrm{d}X_3.$$

The solutions to the cell problems, (1.18) are only unique up to the addition of a function of $\mathbf{x}$; however, since it is only the gradient of F_k with respect to $\mathbf{X}$ that appears in the homogenised permeability this function may be chosen arbitrarily. In general, there is no analytical solution to the cell problems, (1.18). A simple and physically-relevant example for which an analytical solution exists is a layered porous medium, in which $K_{ij} = k(\mathbf{x}, X_2)\delta_{ij}$. We then find that without loss of generality $F_1 = 0$ and that

$$F_2 = A(\mathbf{x}) \int_0^{X_2} \frac{1}{k} \, \mathrm{d}X_2 - X_2,$$

and so F_2 will only be periodic if

$$A = k^* = \left(\int_0^1 \frac{1}{k} \, \mathrm{d}X_2 \right)^{-1},$$

the harmonic average of the permeability. The homogenised permeability is therefore given by

$$\tilde{K}_{11} = \bar{k}, \quad \tilde{K}_{22} = k^*,$$

where $\bar{k}$ is the arithmetic mean of the permeability and k^* is the harmonic mean of the permeability. Since the harmonic mean is always smaller than the arithmetic mean, it is always more difficult for fluid to flow across layers than along them.

The appearance of the arithmetic mean for flow along layers and the harmonic mean for flow across layers may be familiar to the reader from studies of resistors in electrical circuits. The mean resistance of resistors connected in series is given by the arithmetic mean of their resistance, while the mean resistance of resistors connected in parallel is given by their harmonic mean. Equivalently the mean conductance (reciprocal of resistance) of resistors connected in series is given by the harmonic mean of their conductance, while the mean conductance of resistors connected in parallel is given by their arithmetic mean.

1.3 Two-phase flow

1.3.1 The Muskat problem

One of the simplest models for two-phase flow in a porous medium or a Hele-Shaw cell is the Muskat problem. Two fluids are separated by an interface that is modelled by a

moving boundary. We use subscript 1 to represent the properties of the displacing fluid and subscript 2 to represent the properties of the displaced fluid. In each fluid we must satisfy

$$\mathbf{u}_i = -\frac{k}{\mu_i}\nabla p_i, \quad \nabla \cdot \mathbf{u}_i = 0 \quad \text{for} \quad i = 1, 2. \tag{1.19}$$

At the moving boundary we have a dynamic boundary condition,

$$p_1 = p_2, \tag{1.20}$$

and a kinematic boundary condition

$$\mathbf{u}_1 \cdot \mathbf{n} = \mathbf{u}_2 \cdot \mathbf{n} = v_n, \tag{1.21}$$

where $\mathbf{n}$ is the normal to the boundary and v_n is the normal velocity of the boundary.

The single-phase Muskat problem, often referred to as the Hele-Shaw problem, considers a single fluid with a moving boundary separating a saturated region where the fluid is present from an unsaturated region where it is not. In the saturated region the fluid velocity satisfies

$$\mathbf{u} = -\frac{k}{\mu}\nabla p,$$

the dynamic boundary condition is

$$p = \text{constant},$$

and the kinematic boundary condition is

$$\mathbf{u} \cdot \mathbf{n} = v_n.$$

The Hele-Shaw problem may be recovered from the Muskat problem by taking the limit as the viscosity of either the displacing fluid or the displaced fluid tends to zero.

The Muskat model appears to follow immediately from Darcy's law, but in fact several assumptions have been implicitly made. The microscopic flow near the interface is difficult to analyse and so the true interface between the two fluids may be complicated. In particular, if we do not include any additional physics, as we apply no-slip boundary conditions at solid surfaces we should conclude that the interface should not move from any point where it meets the solid surface. This assumption will quickly lead to the formation of a tortuous moving boundary and the averaged equations for the flow that we have wrote down in section 1.2 will not be relevant. In reality there are often extra physical phenomena that allow one to apply the Muskat model. In immiscible flow the

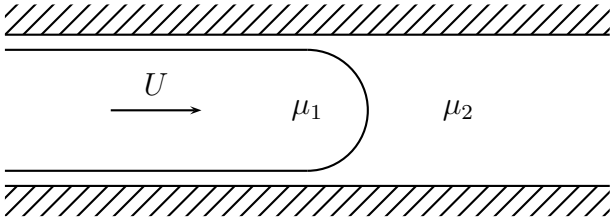

Figure 1.3: Cross-sectional view of two-phase flow in a Hele-Shaw cell.

physical phenomena are surface tension and the wettability of the fluids at the interface. For two-phase flow in a Hele-Shaw cell it is possible to derive a moving boundary problem as demonstrated in a paper by Park and Homsy [45]. For two-phase flow in a porous medium the situation is more complicated and it is not clear when the Muskat problem is applicable.

For miscible flows there is no longer a strict interface between the two fluids. Nevertheless we shall see in Chapter 2 that the Muskat problem can be recovered as a limiting case of the so-called Peaceman model for miscible flow in porous media.

1.3.2 Stability analysis of a planar interface

The Muskat problems permits a planar solution with an interface given by $x = Ut$ with fluid of viscosity μ_1 in $x < Ut$ and fluid of viscosity μ_2 in $x > Ut$. The pressure in the two fluids is given by

$$p_i = -U\frac{\mu_i}{k}\xi,$$

where $\xi = x - Ut$. We now seek a solution where the interface is given by

$$\xi = \epsilon f(y,t),$$

where ϵ is again a small parameter, and we have an initial condition,

$$f(y,0) = f_0(y).$$

We seek p_i of the form

$$p_i \sim -U\frac{\mu_i}{k}\xi + \epsilon\Re\left(\tilde{p}_i(\xi)\mathrm{e}^{\sigma t + \mathrm{i}\alpha y}\right),$$

where α is real. In each fluid the pressure must satisfy

$$\frac{\partial^2\tilde{p}_i}{\partial\xi^2} - \alpha^2\tilde{p}_i = 0,$$

and so the disturbance to the pressure is given by

$$\begin{aligned} \tilde{p}_1 &= P_1 \mathrm{e}^{|\alpha|\xi} \quad \text{for} \quad \xi < 0, \\ \tilde{p}_2 &= P_2 \mathrm{e}^{-|\alpha|\xi} \quad \text{for} \quad \xi > 0, \end{aligned}$$

where we have ensured that the disturbance decays as $|\xi| \to \infty$. The dynamic boundary condition yields

$$-U\frac{\mu_1}{k} + P_1 = -U\frac{\mu_2}{k} + P_2,$$

and the kinematic boundary condition gives

$$-\frac{k}{\mu_1}|\alpha| P_1 = \frac{k}{\mu_2}|\alpha| P_2 = \sigma.$$

We find the dispersion relation

$$\sigma = U|\alpha|\frac{\mu_2 - \mu_1}{\mu_1 + \mu_2}. \tag{1.22}$$

When a less viscous fluid displaces a more viscous fluid the interface is unstable, and the smallest wavelength disturbances grow at the fastest rate.

More generally the interface will be given by

$$\xi = \epsilon f(y,t),$$

where $f(y,t)$ is a linear combination of the exponential solutions already obtained, and is given by

$$f(y,t) = \frac{1}{2\pi}\int_{-\infty}^{\infty} \hat{f}_0(\alpha)\mathrm{e}^{\sigma(\alpha)t - \mathrm{i}\alpha y}\,\mathrm{d}\alpha, \tag{1.23}$$

where $\hat{f}_0(\alpha)$ is the Fourier transform of f_0, defined by

$$\hat{f}_0(\alpha) = \int_{-\infty}^{\infty} f_0(y)\mathrm{e}^{\mathrm{i}\alpha y}\,\mathrm{d}y,$$

and $\sigma(\alpha)$ is the growth rate given by (1.22). If, for example,

$$f_0(y) = \frac{1}{\pi}\frac{1}{1+y^2}, \quad \Rightarrow \quad \hat{f}_0(\alpha) = \mathrm{e}^{-|\alpha|};$$

then when $\sigma(\alpha) > 0$, (1.23) will only be integrable for

$$t < \frac{|\alpha|}{\sigma(\alpha)} = \frac{\mu_1 + \mu_2}{U(\mu_2 - \mu_1)},$$

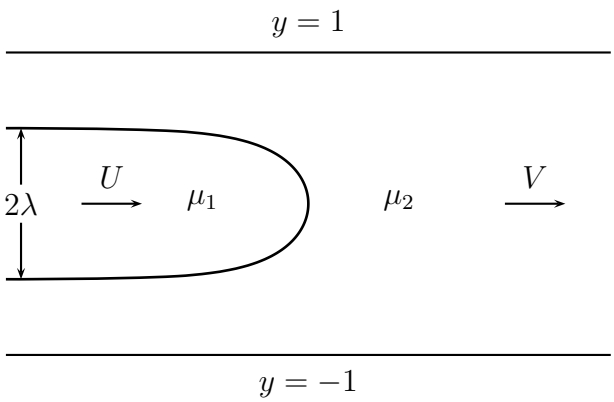

Figure 1.4: The Saffman-Taylor finger.

and so an initially smooth solution may 'blow up' in finite time. If

$$f_0(y) = \frac{1}{2}\mathrm{e}^{-|y|}, \quad \Rightarrow \quad \hat{f}_0(\alpha) = \frac{1}{1+\alpha^2},$$

then when $\sigma(\alpha) > 0$, (1.23) is not integrable for any $t > 0$, and the solution blows up immediately. We see that the linearised Muskat problem is ill-posed, as the solution need not always exist. Indeed, the full Muskat problem with an analytic initial condition has been shown to develop, in finite time, a singularity in the curvature of the free surface [52], suggesting that it too is ill-posed. In practice there is always a previously-neglected physical phenomenon that regularises the Muskat problem and ensures that the true problem to be solved is well-posed. We shall review some of these regularisation mechanisms in section 1.3.4.

1.3.3 The Saffman-Taylor finger solution

There is a well-known solution to the Muskat problem, known as the Saffman-Taylor finger. We consider a single 'finger' of fluid, with viscosity μ_1, penetrating a second fluid, with viscosity μ_2, lying in the infinite channel, $-\infty < x < \infty$, $-1 < y < 1$ (see Figure 1.4). Saffman and Taylor [49] found a family of travelling wave solutions, where as $x \to -\infty$ the displacing fluid occupies a fraction of the channel λ and as $x \to \infty$ the velocity of the displaced fluid is V. The displacing fluid moves as a rigid body with constant velocity U. The interface between the two fluids is given by

$$x - Ut = \frac{1-\lambda}{\pi}\log\left(\frac{1+\cos\left(\frac{\pi y}{\lambda}\right)}{2}\right), \tag{1.24}$$

and the velocity of the finger is given by

$$U = \frac{MV}{1+\lambda(M-1)}, \tag{1.25}$$

where the mobility ratio is

$$M = \frac{\mu_2}{\mu_1}.$$

We have a different solution for each value of λ between 0 and 1. The speed of the finger may take any value between V and MV.

Saffman-Taylor fingers can be obtained as the large time limit of flows which initially possess an almost planar interface [31, 48, 28]. While Saffman-Taylor fingers are perhaps not stable [38], their existence as the only travelling-wave, symmetric, finger solutions [28] and their appearance as the steady state of many particular solutions suggests they are at least important transient states.

It is worth noting that for the Hele-Shaw problem, one can find a Saffman-Taylor finger solution with arbitrarily large velocity by choosing λ to be arbitrarily small, and so one can find solutions close to a planar interface that blow up almost instantaneously. It is perhaps, therefore, not surprising that the Hele-Shaw problem should be ill-posed. For the full Muskat problem, the velocity of the Saffman-Taylor finger solutions may not exceed MV, suggesting that instantaneous blow-up of solutions is less likely.

1.3.4 Regularisation of the Muskat problem

We have seen that the linearised Muskat problem is ill-posed, when $M > 1$, with probable finite-time blow-up of solutions. The Hele-Shaw problem, in which the viscosity of the displacing fluid is set to zero, is known to be ill-posed for a retreating interface [29], and curvature singularities can appear in the full Muskat problem.

The physical problem cannot be ill-posed, and the ill-posedness of the mathematical model is an indication that we have neglected an important physical effect. For the flow of two immiscible fluids in a Hele-Shaw cell, the missing physical effect is often surface tension. A crude model for the effect of surface tension can be constructed [26] via a change in the dynamic boundary condition (1.20), so that

$$p_2 - p_1 = \frac{\pi}{4}\gamma\kappa,$$

where γ is the surface tension between the two fluids and κ is the curvature of the interface. The dispersion relation obtained is then

$$\sigma = \frac{1}{\mu_1 + \mu_2}\left(U(\mu_1 - \mu_2)\,|\alpha| - \gamma\frac{h^2}{12}\,|\alpha|^3\right),$$

where we recall that h is the separation between the plates.

The inclusion of surface tension stabilises large wavenumber disturbances, leading to

the existence of a least-stable wavenumber, for which the growth rate is largest, and a cutoff wavenumber, with all higher wavenumber disturbances being stable. The existence of the least-stable and cutoff wavenumbers suggests a natural wavelength for the disturbances, which was not present in the zero surface-tension problem. When the modified capillary number,

$$\mathrm{Ca}' = \frac{12\mu_2}{\gamma}(h/L)^2,$$

is large (L is the macroscopic length scale), the least-stable wavenumber will be of order $\mathrm{Ca}'^{1/2}$, suggesting that disturbances with a wavelength of order $\mathrm{Ca}'^{-1/2}$ will be observed, and this has been confirmed in experiments [59, 44]. The dispersion relation yields a growth rate that is bounded, and so the linearised problem does not admit solutions which blow-up in finite time such as those found in section 1.3.2. This result shows that surface tension can act to regularise the Muskat problem.

In miscible displacements, there is no interface between the displacing and displaced fluids, and hence surface tension cannot act. Instead of surface tension we shall see in Chapter 2 that transverse diffusion can regularise the Muskat problem, with the wavelength of disturbances observed depending on the magnitude of diffusion. The method by which diffusion regularises the Muskat problem, is quite different theoretically to the regularisation by surface tension, since we cannot perturb about a known solution to a moving boundary problem.

1.3.4.1 Kinetic undercooling

While surface tension is the physically-relevant regularisation mechanism for immiscible flow of two fluids, it is possible to associate the Muskat model with other physical mechanisms. One such physical problem is the Stefan problem, used to model a phase-change in a material, such as the freezing of water. The one-phase Stefan problem, with negligible specific heat (i.e. large Stefan number), is simply

$$\nabla \cdot (k\nabla T) = 0,$$

on one side of a curve $\Gamma(t)$, and with boundary conditions on the curve $\Gamma(t)$

$$T = T_0, \quad v_n = -\frac{k}{\rho L}\frac{\partial T}{\partial n},$$

where T represents the temperature, and may be associated with the pressure in the Hele-Shaw problem. The problem is exactly equivalent to the Hele-Shaw problem, and so the problem may be ill-posed. An appropriate regularisation mechanism for this problem may be kinetic undercooling, the rate at which the interface moves is too fast for the phase-

change process to be in thermodynamic equilibrium at the free surface and so instead of applying $T = T_0$ at the free surface we apply, as in [16],

$$T = T_0 + \beta v_n,$$

where v_n is the normal velocity of the free surface and β is the kinetic undercooling parameter.

As in section 1.3.2 one can seek a travelling wave solution in which the interface travels at speed U with the temperature given by

$$T = T_0 + \beta U - \frac{\rho L U}{k}(x - Ut).$$

If a small sinusoidal disturbance of wavenumber α is made to this base-state solution then we find that the growth rate of the disturbance is given by

$$\sigma = -\frac{U\,|\alpha|}{1 + \frac{\beta k}{\rho L}\,|\alpha|}.$$

A receding interface, corresponding to e.g. the freezing of a fluid cooled below T_0, is unstable. Even with kinetic undercooling included the process is unstable for all wavenumbers; however, the dispersion relation shows that for large wavenumbers the growth rate is constant, and so the solution will again not exhibit the finite-time blow-up that we observed in section 1.3.2, and so the linearised problem is well-posed. This observation suggests that while kinetic undercooling allows instability at all wavenumbers, it is still a possible regularisation mechanism of the Hele-Shaw problem.

We shall see in Chapter 2 that the action of longitudinal diffusion, in which a sharp interface is replaced by a region of non-zero width in which the fraction of solvent and oil gradually changes can be related to the kinetic undercooling regularisation.

1.3.4.2 Other possible regularisations

One can conceive of many different regularisation mechanisms for the Muskat problem, depending on the exact physical circumstances. One such regularisation, applicable for very porous media and therefore unlikely to be appropriate for oil recovery applications, is presented in Appendix B.

In Chapter 2 we shall see that diffusion acts as a regularisation mechanism, although we are unable to continue to use a free boundary model.

1.3.4.3 Shape selection of Saffman-Taylor fingers

The Saffman-Taylor finger solution, described in section 1.3.3, is valid for each value of λ between 0 and 1. In experiments [49] it is often observed that only the solution corresponding to $\lambda = 1/2$ is obtained. There do not appear to be any simple physical arguments as to why this particular solution should be preferred. It has, however, been shown that when a small regularisation mechanism is included, such as surface tension [12, 9] or kinetic undercooling [10], the only possible solution is close to that of the Saffman-Taylor finger with $\lambda = 1/2$. In both cases the selection is a consequence of terms that are exponentially small in the regularising parameter. The shape-selection of the Saffman-Taylor finger demonstrates the important role that small regularisation mechanisms play in determining the solution of the Muskat problem.

1.4 Other models used in the oil industry

1.4.1 The Peaceman model

The first mathematical model developed specifically for the simulation of miscible displacements was that of Peaceman [46]. The Peaceman model assumes that the flow is incompressible, and described by Darcy's law, with a viscosity that is dependent on the 'concentration' of solvent (defined to be the volume fraction of solvent in the oil-solvent mixture). The Peaceman model is

$$\nabla \cdot \mathbf{u} = 0, \qquad \mathbf{u} = -\frac{\mathbf{K}}{\mu(c)} \left(\nabla p - \rho(c)\mathbf{g} \right), \tag{1.26}$$

$$\phi \frac{\partial c}{\partial t} + \nabla \cdot (\mathbf{u}c) = \nabla \cdot (\mathbf{D} \nabla c), \tag{1.27}$$

where c is the concentration of solvent, $\mathbf{u}$ is the total volume flux of fluid per unit area, $\mathbf{K}$ and $\mathbf{D}$ are tensors representing respectively the permeability of the rock and the effective diffusion of the solvent, $\mu(c)$ is the viscosity of the mixture, $\rho(c)$ is the density of the mixture, and ϕ is the porosity of the medium. The viscosity of the solvent and oil mixture may be experimentally determined, and is found to be a function of c. There is no general relationship for the viscosity of a mixture of two fluids as a function of the fraction of each fluid present; however, for the mixtures under consideration in miscible displacement a commonly used relationship is due to Koval [33]:

$$\mu(c) = \left(\frac{c}{\mu_s^{1/4}} + \frac{1-c}{\mu_o^{1/4}} \right)^{-4}, \tag{1.28}$$

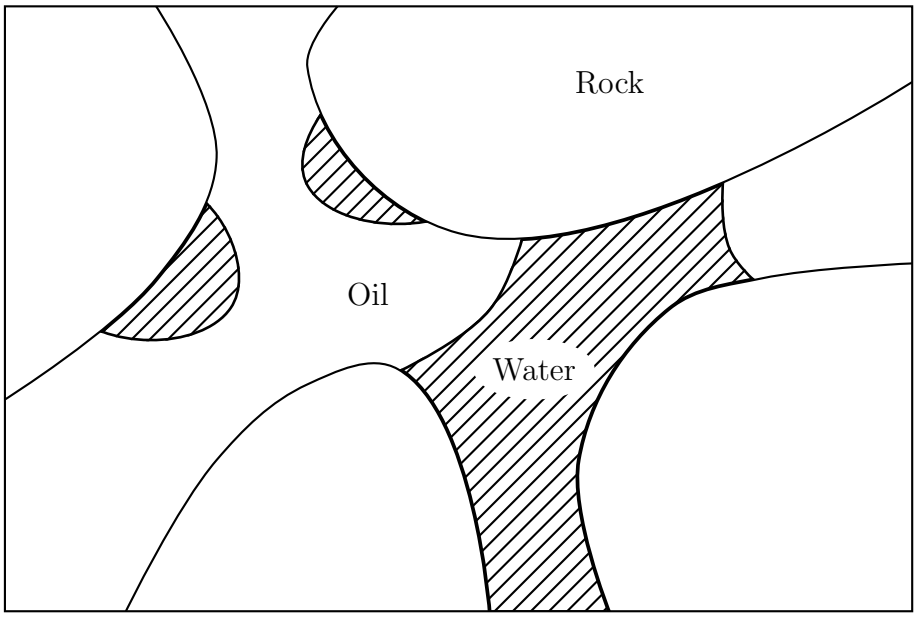

Figure 1.5: Oil and water are both present within the pores. One phase may close off some of the pores, affecting the flow of the other phase.

where μ_s and μ_o are the viscosities of the pure solvent and oil respectively. Similarly there is no general relationship for the density of a mixture of two fluids as a function of the fraction of each fluid present, but since the volume change on mixing of the two fluids is small, one typically assumes that the density is a linear function of c. We will take the Peaceman model to be the fundamental model for miscible flow through porous media, and we shall review it in much more detail in Chapter 2.

1.4.2 The Buckley-Leverett equation

The Buckley-Leverett equation models *immiscible* flow through porous media such as the displacement of oil by water. Although the fluids are considered to be completely immiscible at the molecular level, we nevertheless assume that the flow causes them to be mixed together at the scale of the pores as in Figure 1.5. We introduce saturations of oil and water, i.e. the fractions of pore space which are occupied by oil and water respectively, as S_o and S_w. The fluxes of oil and water are denoted by $\mathbf{u}_o$ and $\mathbf{u}_w$ respectively and the pressure in the oil and water is given by p_o and p_w. In two-phase flow, the flow of each phase through the porous medium will be affected by the presence of the other phase. Neglecting the effect of gravity for simplicity, this effect can be modelled by the introduction of relative permeabilities so that in each fluid,

$$\mathbf{u}_o = -\frac{k_{ro}}{\mu_o}\mathbf{K}\nabla p_o, \qquad \mathbf{u}_w = -\frac{k_{rw}}{\mu_w}\mathbf{K}\nabla p_w, \tag{1.29}$$

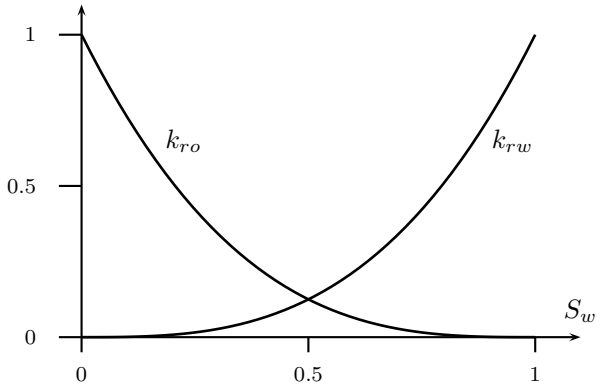

Figure 1.6: Relative permeability curves as used in the Buckley-Leverett equations.

where the relative permeabilities, k_{ro} and k_{rw} are empirically determined and depend on the fraction of the water-phase present, S_w. An example of relative permeability curves is given in Figure 1.6. Conservation of mass applied to the oil and water gives

$$\phi \frac{\partial S_w}{\partial t} + \nabla \cdot \mathbf{u}_w = 0, \tag{1.30}$$

$$\phi \frac{\partial S_o}{\partial t} + \nabla \cdot \mathbf{u}_o = 0, \tag{1.31}$$

where ϕ is the porosity of the rock. The difference between the pressure in the water phase and the pressure in the oil phase is given by the capillary pressure,

$$p_c(S_w) = p_o - p_w.$$

The capillary pressure is a consequence of surface tension, and for an individual pore, filled with water, the capillary pressure could be determined by

$$p_c = \frac{2\gamma \cos\theta}{r(S_w)},$$

where γ is the coefficient of surface tension, θ is the wetting angle at the point where the oil, water and rock meet, and $r(S_w)$ is a typical radius for a pore in which both water and oil are present. One can rearrange equations (1.29)-(1.31) in terms of the total flux, $\mathbf{u} = \mathbf{u_w} + \mathbf{u_o}$, to obtain:

$$\nabla \cdot \mathbf{u} = 0, \qquad \mathbf{u} = -\mathbf{K}\left(\frac{k_{rw}}{\mu_w} + \frac{k_{ro}}{\mu_o}\right)\nabla p_w - \mathbf{K}\frac{k_{ro}}{\mu_o}\nabla p_c, \tag{1.32}$$

$$\phi \frac{\partial S_w}{\partial t} + \nabla \cdot (F(S_w)\mathbf{u}) = -\nabla \cdot (G(S_w)\nabla p_c)\,, \tag{1.33}$$

where

$$F(S_w) = \left(1 + \frac{k_{ro}(S_w)\mu_w}{k_{rw}(S_w)\mu_o}\right)^{-1},$$

and

$$G(S_w) = \frac{k_{ro}(S_w)k_{rw}(S_w)}{k_{ro}(S_w)\mu_w + k_{rw}(S_w)\mu_o}.$$

The Buckley-Leverett equation is obtained by considering a one-dimensional problem and neglecting the capillary pressure term giving

$$\frac{\partial S_w}{\partial t} + U\frac{\partial F(S_w)}{\partial x} = 0, \tag{1.34}$$

where U is the (constant) total flux.

Even though the Buckley-Leverett equation models immiscible diffusionless flow of fluids that coexist on the pore scale, it has been used to model certain miscible flows through porous media [33, 58, 18]. If one interprets the saturation as the local concentration of solvent within the pores then, since the mixture of oil and solvent is homogeneous within the pores, the physically sensible relative permeabilities are

$$k_{ro} = \frac{\mu_o}{\mu(c)}(1-c), \quad \text{and} \quad k_{rs} = \frac{\mu_s}{\mu(c)}c,$$

leading us to recover the Peaceman model, although without diffusion.

It is possible to apply the Buckley-Leverett equation to modelling miscible flows by averaging the concentration over a larger scale than the pore scale, with the fluid not being homogeneous at this larger scale. The models that have been developed rely heavily on matching with empirical data and several, carefully considered, but occasionally ad hoc assumptions. It is desirable to place these models within a more systematic framework, with a better understanding of why the fluid is not homogeneous, and what the 'relative permeabilities' should be. One important model for miscible flow through porous media, which was originally derived via the Buckley-Leverett equations, is the Koval model, which we shall now examine.

1.4.3 The Koval model

It has been observed in experiments [6] that, in a miscible displacement through a channel, the evolution of the concentration of solvent is very different to that predicted by the one-dimensional Peaceman model. The cause of this difference is 'fingering' of the solvent, as we shall see in Chapter 2. Koval developed a simple one-dimensional model [33] to

describe the observations of Blackwell [6]. The Koval model is given by

$$\frac{\partial c}{\partial t} + U\frac{\partial F(c)}{\partial x} = 0, \quad \text{where} \quad F(c) = \frac{M_e c}{1 + (M_e - 1)c}, \tag{1.35}$$

and the effective mobility ratio, M_e is defined to be the ratio between the viscosity of the oil and a specific mixture of solvent and oil with a volume-fraction of solvent c_e. By matching with experiments, Koval determined that $c_e = 0.22$. The Koval model was derived from the Buckley-Leverett equations, but, as explained above, it is not immediately clear why any model other than the Peaceman model should be appropriate. Indeed, it is not readily apparent under what conditions the Koval model applies, and one of the main objectives of this thesis is to obtain the Koval model as an averaged version of the Peaceman model.

1.5 Diffusion

Diffusion of a solvent through a porous medium is a complicated process, particularly when the transport is convection dominated. The magnitude of the diffusion may depend on the structure of the porous medium and the mean velocity of the fluid. When modelling miscible displacements, on the scale of an oil reservoir, the transport will be convection dominated and the small diffusion will be velocity-dependent and anisotropic. In this section we shall review some of the popular models of diffusion in porous media.

1.5.1 Molecular diffusion of solvent and oil

The mixing of solvent and oil is governed by molecular diffusion at the microscopic scale. Molecular diffusion is described by Fick's law,

$$\mathbf{F} = -D\nabla c, \tag{1.36}$$

where $\mathbf{F}$ is the diffusive flux, D is the coefficient of diffusion, and c is the concentration of solvent i.e. the (volume) fraction of the fluid that is composed of solvent. If the fluid is moving with a flux $\mathbf{u}$ then conservation of volume[4] gives

$$\frac{\partial c}{\partial t} + \nabla \cdot (\mathbf{u}c) = \nabla \cdot (D\nabla c)\,, \tag{1.37}$$

in free space. For low concentrations of solvent the coefficient of diffusion is constant; however, in the displacement of oil by a solvent the concentration of solvent is not ev-

[4]Strictly speaking we should conserve mass, rather than volume, however, for all the solvents and oils used in miscible displacements, the volume change on mixing is very small and so conservation of volume is equivalent to conservation of mass. This subject is dealt with in more detail in section 5.2.

erywhere small. In general D will be a function of the concentration of solvent, and in particular D should depend on the viscosity of the mixture [4]. If the oil and solvent have reasonably similar properties the diffusion will be nearly constant. In Chapter 2 we shall model the effective diffusion of solvent through a porous medium, but first we give an overview of the effective diffusion of a passive tracer, i.e. a substance that does not affect the properties of the flow.

When a passive tracer is transported through a porous medium, the effective diffusion coefficient may be very different from molecular diffusion in free space. The dispersion of a substance through a porous medium is enhanced by the rapidly varying velocity at the pore scale. Molecular diffusion does not adequately describe the effective diffusion at the macroscopic scale of a substance, and so we must investigate the interaction between diffusion and a rapidly varying velocity field.

1.5.2 Taylor diffusion in a capillary

The simplest example of velocity dependent diffusion is the famous Taylor dispersion [57]. Taylor dispersion describes the dispersal of a solute dissolved in a fluid flowing down a long thin pipe. The fluid flow is Poiseuille flow and we assume that the solute diffuses with a constant coefficient of diffusion. The shear in the velocity profile interacts with transverse diffusion across the pipe to yield an enhanced longitudinal diffusion. The concentration, to first approximation, is independent of the radial coordinate, is advected with the mean velocity of the fluid, and diffuses in the longitudinal direction with the coefficient of diffusion given by the famous Taylor-Aris dispersion coefficient [57, 1],

$$D_T = \frac{a^2 U^2}{48 D} + D,$$

where a is the radius of the pipe, U is the mean velocity of the fluid and D is the coefficient of molecular diffusion. Small molecular diffusion may lead to a much larger dispersion of the concentration than one would immediately expect.

1.5.3 Saffman dispersion

Taylor dispersion provides a simple model for local diffusion in porous media; however as Taylor dispersion describes an essentially one-dimensional problem it can not be used to describe the effective transverse diffusion in a porous medium. Saffman developed a model [50] in which the solute undergoes a random walk through a network of capillary pores. The flow of fluid in each capillary is described by Poiseuille flow. The solute particles travel deterministically through the capillary until they reach a junction, at which point

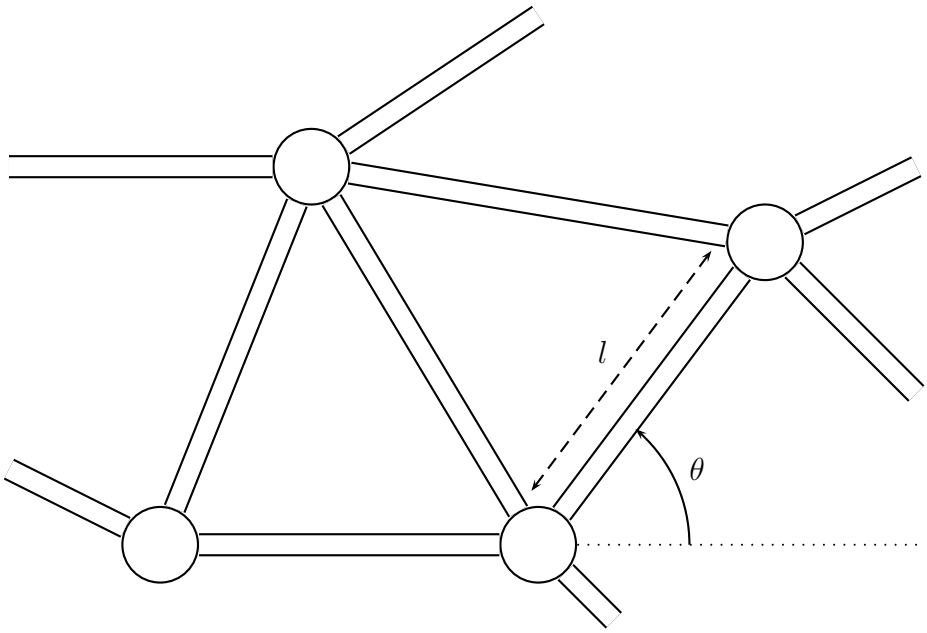

Figure 1.7: A schematic of Saffman's capillary network. Particles move deterministically through capillaries before randomly following a new streamline at each junction.

they follow a capillary which makes a random angle θ with the mean direction of flow (see Figure 1.7). The solute particle enters the capillary at a random distance from the central axis of the capillary. The probability of the solute following a given streamline is proportional to the speed of the fluid along that streamline.

When molecular diffusion is neglected the time that a particle takes to travel through a capillary is given by

$$t = \frac{L}{2u}\left(1 - \frac{r^2}{a^2}\right)^{-1},$$

where L is the length of the capillary, u is the mean speed of the fluid in the capillary, r is the distance of the particle from the central axis of the capillary and a is the radius of the capillary. The flux of fluid at a distance between r and $r + \mathrm{d}r$ from the central axis of the capillary is equal to

$$4\pi u r\left(1 - \frac{r^2}{a^2}\right)\mathrm{d}r,$$

for small $\mathrm{d}r$. With the time taken for a particle, entering the capillary at random, to traverse the capillary is given by T, we find that the expected value of T is

$$E(T) = \int_0^a \frac{4r}{a^2}\frac{L}{2u}\,\mathrm{d}r = \frac{L}{u},$$

and

$$E(T^2) = \int_0^a \frac{4r}{a^2}\frac{L^2}{4u^2}\left(1 - \frac{r^2}{a^2}\right)^{-1}\mathrm{d}r = \frac{L^2}{2u^2}\int_0^1 \frac{1}{1-\rho}\,\mathrm{d}\rho,$$

which is divergent. While the expected transit time of a particle passing through a capillary is finite, the variance is infinite, and so the central limit theorem does not apply after many transits through capillaries, and we therefore do not obtain a traditional diffusive model. The infinite variance is a consequence of a long transit time when the particle is close to the wall of the capillary, and leads to large longitudinal dispersion of the solute. Molecular diffusion will reduce the transit time for particles close to the capillary walls by allowing diffusion towards the faster central flow; however, when the effect of molecular diffusion is small, the long hold-up time for such particles will still lead to a large longitudinal dispersion of the solute.

Hold-up of the solute near the capillary walls is not the only mechanism by which dispersion develops, because there is also hold-up of the solute in capillaries that are aligned transversely to the direction of mean flow. The flux of fluid down a capillary making an angle θ with the mean direction of flow (and hence the applied pressure gradient), is proportional to $\cos\theta$, i.e. $u = \beta\cos\theta$, for some constant β. The component of the flux in each capillary, parallel to the mean direction of flow is $u\cos\theta$, and the fraction of pores for which the angle subtended between the pore and the mean direction of flow is between θ and $\theta + \mathrm{d}\theta$ is proportional to $\sin\theta\,\mathrm{d}\theta$. The total flux through the porous medium is therefore given by

$$U = \int_0^{\frac{\pi}{2}} \beta\cos^2\theta\sin\theta\,\mathrm{d}\theta,$$

and so we find that $\beta = 3U$. If we simply model the transit time of a particle through a capillary as equal to L/u then we find that for a capillary making a random angle with the mean direction of flow the expected transit time is given by

$$E(T) = \int_0^{\frac{\pi}{2}} \frac{2L}{3U}\sin\theta\,\mathrm{d}\theta = \frac{2L}{3U},$$

and

$$E(T^2) = \int_0^{\frac{\pi}{2}} \frac{2L^2}{9U^2}\tan\theta\,\mathrm{d}\theta,$$

which is also divergent. Here the long transit times are a consequence of particles travelling along a capillary that is nearly perpendicular to the mean direction of flow so that the flux of fluid through the capillary is small. Molecular diffusion will reduce these long transit times by allowing the particle to diffuse straight through the capillary.

Saffman suggested a simple formula [50] to represent the transit time of a solvent

through the capillary without neglecting molecular diffusion:

$$t = \begin{cases} \frac{L}{2u}\left(1 - \frac{r^2}{a^2}\right)^{-1}, & t < t_1, \\ t_1 + \frac{L}{u}, & t_1 \leq t < t_0, \\ t_0, & \text{otherwise.} \end{cases}, \tag{1.38}$$

where $t_1 = a^2/8D$ is the timescale for molecular diffusion towards the centre of the capillary and $t_0 = L^2/2D$ is the timescale for diffusion through the capillary. With this representation of the transit time one finds that the variance of the transit time is finite and it becomes possible to produce a theory of diffusion via the central limit theorem. The dispersion described in Saffman's paper [50] assumes that at the microscopic scale convection dominates, so that the timescales t_0 and t_1 are large. Saffman finds that the effective diffusion in the longitudinal direction is given by

$$D_\parallel = UL\left(\frac{1}{3}\log\frac{3UL}{2D} + \frac{1}{12}\left(\log\frac{3Ua^2}{4DL}\right)^2 - \frac{1}{4}\log\frac{3Ua^2}{4DL} + \frac{19}{24}\right),$$

and the transverse diffusion is given by

$$D_\perp = \frac{3}{16}UL.$$

Writing $\mathrm{Pe}_l = UL/D$ for the Péclet number at the scale of the capillary, and $\epsilon = L/l$, where l is the macroscopic length scale, we see that

$$\frac{1}{\mathrm{Pe}_\parallel} = O(\epsilon(\log \mathrm{Pe}_l)^2) + O(\epsilon \log \mathrm{Pe}_l) + O(\epsilon), \tag{1.39}$$

$$\frac{1}{\mathrm{Pe}_\perp} = O(\epsilon), \tag{1.40}$$

where $\mathrm{Pe}_\parallel = Ul/D_\parallel$ and $\mathrm{Pe}_\perp = Ul/D_\perp$. We see that, at the macroscopic length scale, convection will always be dominant since ϵ is small. We also see that the effective longitudinal diffusion has a weak dependence on the capillary Péclet number, but the effective transverse diffusion does not.

The available experimental evidence [5, 50, 21] appears to give reasonable qualitative agreement with Saffman's model, with the effective transverse diffusion simply proportional to UL and the ratio of the effective diffusion and UL appearing to show a weak dependence on Pe_l. While the Saffman model seems to agree fairly well with experiments, the model has attracted some criticism [7, 47] for the *ad hoc* assumptions involved in its derivation. In particular, the assumed geometry of the medium is not particularly realistic and, as noted by Saffman [50], the result for the transverse diffusion is somewhat dubious,

at least for two-dimensional flow. For periodic porous media it is possible to apply the technique of homogenisation to develop a model for the effective diffusion [7, 47], and unlike Saffman's model, it is not necessary to assume that the pore-scale Péclet number is large. We will revisit this in Chapter 2; however, periodic media are not representative of real-life porous media [32].

1.6 Structure of the thesis

In the next chapter we shall derive the Peaceman model by first considering the problem at the pore-scale. We thereby gain an understanding of the transport of the solvent through the porous medium, both by convection and dispersion, and show that, for many problems relevant to the oil industry, the flow will be dominated by convection, and that dispersion is small.

We have already seen that instabilities may arise when a less viscous fluid displaces a more viscous fluid through a porous medium, and so in Chapter 2 we will also investigate the nature of these instabilities when the two fluids are miscible. We show that instabilities persist in the miscible problem, but that there is now a maximum possible growth rate, shown to be a consequence of the smooth transition between the solvent and oil. Also large-wavenumber disturbances are shown to be stable as a consequence of transverse diffusion. Although the ill-posedness of the linear problem observed in section 1.3.1 is removed, instabilities persist in the Peaceman model, and we show that the Péclet number is critical in determining the appropriate length scale of these instabilities.

To conclude Chapter 2, we conduct numerical simulations of the Peaceman model. These are used to confirm the results of our stability analysis, and in particular to show the importance of the Péclet number in determining the length-scale of the fingers that are formed. For the applications under consideration, the length scale of the instabilities that form is small, and so accurate simulation of the Peaceman model requires a fine grid-size. Although we show that it is possible to numerically simulate the Peaceman model, it is a numerically intensive task, and it may become unfeasible in three-dimensions at the oil reservoir-scale.

Our numerical simulations predict small scale variations well below the reservoir scale, yet it is only the locally-averaged solvent concentration that is of practical interest. Hence, in Chapter 3, we develop an averaged model which does not capture the detailed fingering behaviour but does accurately capture the spread of the solvent through the porous medium on the reservoir scale. It is an important feature of the averaged model that it should not exhibit the same instability that existed prior to averaging. We begin by considering flow in which the applied pressure gradient is unidirectional and the medium

is entirely homogeneous. For large values of the Péclet number, the amplitude of the fingering instabilities is shown to be an order one fraction of the distance displaced by the solvent, but the wavelength of the fingering instabilities is proportional to $\mathrm{Pe}^{-1/2}$. On the basis of these observations, we make the important assumption that the fingers that are formed are long, thin and parallel. This assumption allows us to apply homogenisation theory to the problem, allowing us to explicitly solve for the velocity field, given the concentration field.

We show that development of a model for the evolution of the averaged concentration of solvent is possible if one can solve a closure problem, which is equivalent to determining how the concentration of solvent varies across the finger. A simple solution to the closure problem is obtained by assuming that the solvent and oil do not mix locally; however, it is found that this model significantly overpredicts the rate at which the solvent spreads. Nevertheless, with additional empirical assumptions, this solution leads to a derivation of the Koval model, which we confirm to be in very close agreement with our numerical simulations, at least for large Pe where the aspect ratio of the fingers is large.

In an effort to be able to predict the rate at which the solvent spreads out, we then study the behaviour of the homogenised Peaceman model. As a special case we suppose that the solvent is only slightly less viscous than the oil. This simplifies the homogenised model and enables us to find a particular solution which contains "shocks" corresponding to the finger tips and finger roots. In the vicinity of these shocks we can no longer make our original assumptions concerning the large aspect ratio of the fingers. By rescaling in the vicinity of these shocks, we are led to a local problem with some similarities to the Saffman-Taylor finger problem. The resolution of the closure problem relies on finding a solution to these local problems, and this gives us some new understanding of the rate at which the solvent disperses.

In practical application the applied pressure gradient may not be unidirectional or there may be macroscopic heterogeneities present. In Chapter 4, we therefore extend the model developed in Chapter 3 to more general flows. We continue to apply the assumption that the fingers are long and thin, and the closure problem obtained is the same as that encountered in Chapter 3. The crucial difference between the one-dimensional model of Chapter 3 and the two-dimensional model of Chapter 4, is the appearance of an effective viscosity that must also be determined to close the problem. We are able to find a simple formula for the effective viscosity, motivated by our tip-scale modelling, and checked against our numerical simulations.

Our two-dimensional model also allows us to accurately predict the pressure drop through the porous medium, in addition to the rate at which the solvent spreads. We compare our two-dimensional Koval model with the Todd and Longstaff model used in oil

recovery, and also with the Buckley-Leverett equations for immiscible flow through porous media. Our analysis sheds light on the significant advantage that miscible displacement has over immiscible displacement. We also investigate the stability of our two-dimensional model, and comment on the possibility of further instabilities.

Up to this point we have focused our attention only on the effect of viscosity differences between the solvent and oil. In fact the difference in the density between the two fluids is also important, particularly when carbon-dioxide is used as the solvent, and in Chapter 5 we will show how these density differences lead to "density fingering". We shall show that density fingering shares many similarities with viscous fingering and that much of the work of the previous sections can be extended to allow for density variations. However, we will find that there are a few subtleties to the stability of miscible displacements in which the densities and viscosities of the solvent and oil both differ. In particular we will show that it is possible for dispersion of the solvent to have a destabilising effect, with a miscible displacement allowing instabilities to form while the corresponding immiscible displacement does not. We also develop an averaged model, extending the work of Chapter 3 to average over fingers resulting from both density and viscosity differences.

1.7 Statement of originality

In Chapter 2 the derivation of the Peaceman model from first principles in section 2.1 is original, extending the work of Rubinstein & Mauri [47]. The stability analysis of the multi-layer Muskat problem in section 2.2.1 is also novel. Although the stability analysis of section 2.2.4 is taken from the paper [24], the WKB analysis in this paper is not applicable for the largest growth-rate disturbance, and we have corrected this.

In Chapter 3 the derivation of the naïve Koval model found in section 3.2 is not original, but the justification for the large aspect ratio - based on the large aspect ratio of the fingers, rather than the large aspect ratio of the medium - is new. Although the hyperbolic system in section 3.4.1 has been studied before, our explicit solution is novel. The order-one aspect-ratio tip-rescaling of section 3.5.1 is entirely original.

Chapter 4 is entirely original work.

In Chapter 5 the stability analysis of section 5.2.1 is novel to the precise application considered. Sections 5.3 and 5.4 extend the work of Chapters 3 and 4 respectively, and are both novel.

1.8 A short note on notation

Throughout this thesis we shall make use of several small parameters, typically being the ratio between two well-separated length-scales. To emphasise the smallness of these parameters we shall denote many of them by ϵ. In Chapters 3 and 4 the small aspect-ratio of the fingers is exclusively represented by ϵ.

Chapter 2

The Peaceman model

In this chapter we shall investigate the applicability of the Peaceman model for miscible flow through porous media. The Peaceman model, sometimes referred to as the miscible displacement equations, was first suggested in the paper of Peaceman and Rachford [46]. The model couples an equation for the transport of solvent with Darcy's law for the flow of fluid through the porous medium. It is possible formally to derive the Peaceman model from microscopic models of fluid flow, and for this reason we consider the Peaceman model to be the fundamental model for miscible flow through porous media. We shall start with a detailed derivation of the Peaceman model, to make clear the exact physical circumstances under which the model applies.

The most difficult concept within the Peaceman model is the introduction of an effective diffusion or "dispersion" term. Our formal derivation allows us to gain an understanding of diffusion in porous media and hence to explain the physical origin of this term, and gain a better understanding of diffusion in porous media. Miscible porous media flow leads to *hydrodynamic dispersion*, which is represented by an effective diffusion of the solvent resulting from interaction between molecular diffusion and a rapidly varying velocity field; these occur both at the pore-scale and at the larger scale of macroscopic inhomogeneities. We shall show that oil recovery flows are usually convection dominated and that there will be some anisotropy in the effective diffusion.

In the singular limit in which one entirely neglects diffusion in the Peaceman model, it is possible to recover the Muskat problem. We shall compare and contrast the stability properties of the moving boundary Muskat problem with the stability analysis of the Peaceman model. We shall see that the Peaceman model exhibits instabilities, just as the Muskat problem does, but the growth rate of these instabilities is bounded and so the linearised problem is not ill-posed.

There have been many numerical simulations of the Peaceman model, from the original simulations of Peaceman and Rachford [46], to more recent simulations by Tan and Homsy

[56] and Yang and Yortsos [62]. We shall comment on these existing numerical simulations and present our own numerical simulations. We will have to be particularly careful in carrying out our numerical simulations to ensure that we accurately simulate the small physical diffusion.

We now begin our formal derivation of the Peaceman model, by studying the microscopic flow of fluids at the pore-scale.

2.1 Derivation of the Peaceman model

2.1.1 Physical properties of mixtures of fluids

When two fluids mix at the molecular level, the resulting mixture will have physical properties that are different from either of its constituent substances. The physical properties of the mixture that will be of most interest to us are the viscosity and density. In general, when two substances mix there will be a volume change associated with the mixing; however, for the substances involved in miscible displacements, the associated volume change is negligible. The density of a mixture is then given by the volume-average of the densities of the two substances that constitute the mixture,

$$\rho(c) = \rho_s c + \rho_o(1-c), \tag{2.1}$$

where c is the volume fraction of the solvent, and ρ_s, ρ_o are the densities of the solvent and oil respectively. When the volume change on mixing is negligible the fraction of volume by mass C is related to the fraction of solvent by volume by

$$C = \frac{\rho_s c}{\rho_s c + \rho_o(1-c)}.$$

There is no general formula for the viscosity of a mixture of two substances. Indeed it is possible for the viscosity to have a complicated dependence on the fractions of the two constituents; for example the viscosity of an equal mixture of ethanol and water is larger than the viscosity of either ethanol or water, [19]. For the viscosity of mixtures of oil fractions, a formula used in oil refineries, and reported by Koval [33], is the quarter-power mixing rule:

$$\mu(c) = \left(\frac{c}{\mu_s^{1/4}} + \frac{1-c}{\mu_o^{1/4}} \right)^{-4}, \tag{2.2}$$

where c is the volume fraction of the solvent, and μ_s, μ_o are the viscosities of the solvent and oil respectively. This formula is applicable to the oil-solvent mixtures that we will consider. The solvents used in miscible displacements are less viscous than the oil that is

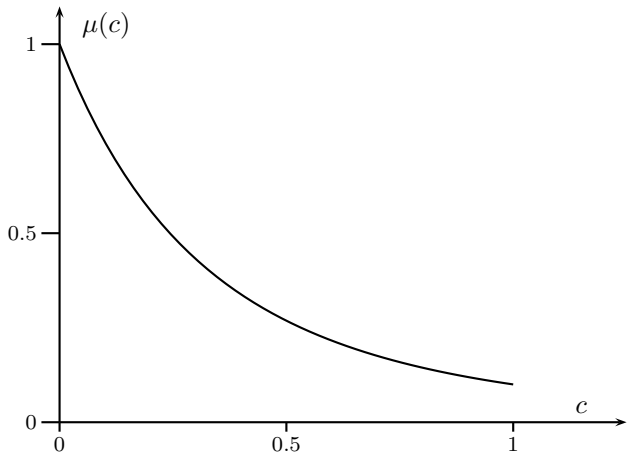

Figure 2.1: Viscosity of a mixture of solvent, with a mobility ratio of 10 (the viscosity is nondimensionalised with the viscosity of the oil). Note that the dependence of the viscosity on the fraction of solvent is nonlinear, and a small concentration of solvent mixed with the oil leads to a large reduction in viscosity.

displaced, with the mobility ratio defined as

$$M = \frac{\mu_o}{\mu_s},$$

taking values anywhere from 1 to 100. The viscosity exhibits a nonlinear dependence on the concentration of solvent, so that, when the mobility ratio between the two fluids is large, only a small amount of solvent must be added to lead to a large reduction in the viscosity of the mixture.

We shall begin by considering only the effect of viscosity variations, and neglecting any density variations. In general the effects of density variations between the solvent and the oil may be important, and we consider them in Chapter 5. Density variations might be neglected when the densities of the oil and solvent are similar or, as we shall show in Chapter 5, when the flow is quite fast. For an incompressible fluid with constant density conservation of mass is equivalent to conservation of volume.

We now seek to derive, as rigorously as possible, the Peaceman model of section 1.4.1, from the appropriate microscale equations. Our exposition will make clear the necessary assumptions that must be made, and will provide a derivation of the diffusive term.

2.1.2 Homogenisation of miscible Stokes' flow

Our derivation of the Peaceman model will be based on the method of homogenisation applied to the miscible version of Stokes' flow. It is an adaptation of the standard derivation of Darcy's law by homogenisation, presented in section 1.2.1, and some of the arguments found in the paper by Rubinstein and Mauri [47] for the homogenisation of diffusion in

porous media.

Inside the pores we require that the fluid is incompressible so that conservation of mass gives

$$\nabla \cdot \mathbf{v} = 0, \tag{2.3}$$

where $\mathbf{v}$ is the physical (non-superficial) velocity of the fluid as it travels through the pores. A typical value of the pore-scale Reynolds number for the flow in miscible displacements is 10^{-4} and so we may apply the Stokes' flow approximation, neglecting inertial terms, when considering the conservation of momentum. The equation for conservation of momentum is then

$$\sum_j \frac{\partial \sigma_{ij}}{\partial x_j} = 0,$$

where σ_{ij} is the stress tensor defined as

$$\sigma_{ij} = -p\delta_{ij} + \mu(c)\frac{\partial v_i}{\partial x_j},$$

for a mixture with a concentration of solvent c. The fluid therefore satisfies

$$\frac{\partial p}{\partial x_i} = \frac{\partial}{\partial x_j}\left(\mu(c)\frac{\partial v_i}{\partial x_j}\right), \tag{2.4}$$

where we have used the summation convention with implied summation over the repeated index. We now require a separate equation for the transport of the solvent. The solvent will be advected with the fluid and will also diffuse under molecular diffusion. As we are not necessarily considering dilute concentrations of solvent we allow for non-Fickian diffusion, with the diffusive flux being given by

$$\mathbf{F} = -D(c)\nabla c.$$

Although we are not aware of any experiments that determine the concentration-dependence of the diffusion coefficient for the solvents and oils under consideration, for both diffusion of a dilute substance and for self-diffusion it is known that the coefficient of diffusion is inversely proportional to the viscosity of the fluid in which the diffusion occurs [4]. We therefore might assume that the concentration-dependence of diffusion may be related to the concentration-dependence of viscosity. By considering the conservation of mass of the solvent we find that

$$\frac{\partial c}{\partial t} + \nabla \cdot (\mathbf{v}c) = \nabla \cdot (D(c)\nabla c)\,. \tag{2.5}$$

The solvent and oil flow through a porous medium in which the microscopic pore scale is much smaller than the macroscopic scale of interest. We write L for the characteristic

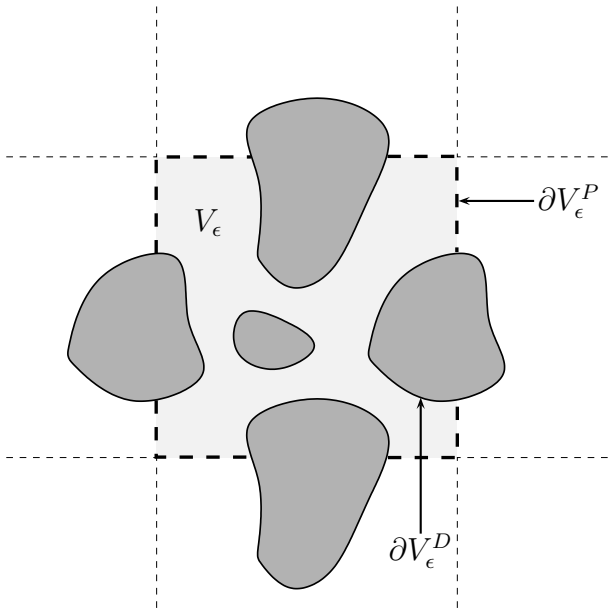

Figure 2.2: The unit cell, V_ϵ, of a periodic medium.

microscopic length scale (i.e. the length of a pore) and l for the characteristic macroscopic length scale (i.e. the distance over which a pressure gradient is applied) with $\epsilon = L/l \ll 1$. As we intend to apply a homogenisation argument we assume, for simplicity, that the porous medium is periodic at the microscopic scale, with a periodic cell ∂V_ϵ (see Figure 2.2). The assumption of periodicity is applied for mathematical convenience, with the hope that a periodic medium may serve as a good representation of more general media. In fact we shall see that the assumption of periodicity may not always be a reasonable assumption, and we shall comment on exactly when it might be applicable. At the interface between the solid rock and the pore space ∂V_ϵ^D we must satisfy the boundary conditions

$$\mathbf{v} = \mathbf{0} \qquad \text{and} \qquad \mathbf{n} \cdot \nabla c = 0.$$

We nondimensionalise $\mathbf{x}$ with l, the velocity with U, $\mu(c)$ with the viscosity of the oil, μ_o and the coefficient of molecular diffusion with a reference value D_0. The appropriate nondimensionalisation for the pressure[1] is to scale p with $l\mu_o U/L^2$. There are four time scales associated with the problem, namely

$$t_1 = \frac{l^2}{D_0}, \quad t_2 = \frac{l}{U}, \quad t_3 = \frac{L^2}{D_0}, \quad t_4 = \frac{L}{U}. \tag{2.6}$$

The time scales in (2.6) respectively represent the time scales for diffusion and convection at the macroscopic length scale, and diffusion and convection at the microscopic length

[1]One can obtain this scaling by considering Poiseuille flow through a pipe of length l and radius L.

scale. Some typical values for the parameters in (2.6) are

$$U \approx 10^{-5}\,\mathrm{m\,s^{-1}}, \qquad D_0 \approx 10^{-9}\,\mathrm{m^2\,s^{-1}}, \qquad L \approx 10^{-4}\,\mathrm{m}, \qquad l \approx 1\,\mathrm{m}.$$

We observe that the microscale Péclet number,

$$\mathrm{Pe}_l = \frac{t_3}{t_4} = \frac{UL}{D_0} = O(1),$$

and so convection balances diffusion at the microscopic length scale. We shall use the macroscopic convective time scale t_2 to nondimensionalise t giving (2.3)-(2.5) in dimensionless form as

$$\nabla \cdot \mathbf{v} = 0, \qquad \frac{\partial p}{\partial x_i} = \epsilon^2 \frac{\partial}{\partial x_j}\left(\mu(c)\frac{\partial v_i}{\partial x_j}\right), \tag{2.7}$$

$$\frac{\partial c}{\partial t} + \nabla \cdot (\mathbf{v}c) = \frac{\epsilon}{\mathrm{Pe}_l}\nabla \cdot (D(c)\nabla c), \tag{2.8}$$

with boundary conditions

$$\mathbf{v} = \mathbf{0} \quad \text{and} \quad \mathbf{n} \cdot \nabla c = 0 \quad \text{on} \quad \partial V_\epsilon^D, \tag{2.9}$$

and an initial condition

$$c = C_0(\mathbf{x}, \mathbf{X}) \quad \text{when} \quad t = 0.$$

In addition to the two well-separated length scales the problem contains three well-separated time scales: t, the time scale for convection on the macroscopic length scale; $T = t/\epsilon$, the fast time scale for both convection and diffusion on the microscopic length scale and $\tau = \epsilon t$, the slow time scale for diffusion on the macroscopic length scale. We shall initially consider the problem for reasonably short times where $t = O(1)$ and we may therefore neglect variations over the slow time scale τ.

2.1.2.1 Behaviour at short times

We propose the following multiple-scales expansions

$$\begin{aligned} p &\sim p_0(\mathbf{x}, \mathbf{X}, t, T) + \epsilon p_1(\mathbf{x}, \mathbf{X}, t, T) + \dots, \\ \mathbf{v} &\sim \mathbf{v}_0(\mathbf{x}, \mathbf{X}, t, T) + \epsilon \mathbf{v}_1(\mathbf{x}, \mathbf{X}, t, T) + \dots, \\ c &\sim c_0(\mathbf{x}, \mathbf{X}, t, T) + \epsilon c_1(\mathbf{x}, \mathbf{X}, t, T) + \dots, \end{aligned}$$

where we shall treat $\mathbf{x}, \mathbf{X}$ and t, T as independent variables so that

$$\nabla = \frac{1}{\epsilon}\nabla_X + \nabla_x,$$

and

$$\frac{\partial}{\partial t} = \frac{1}{\epsilon}\frac{\partial}{\partial T} + \frac{\partial}{\partial t}.$$

We shall also require that $p_0, p_1, c_0, c_1, \mathbf{v}_0, \mathbf{v}_1, \ldots$ are all 1-periodic in $\mathbf{X}$. If this were not the case then we would find that terms in the expansion would grow unboundedly as $\epsilon \to 0$ and $|\mathbf{X}| \to \infty$. It is this secularity condition that is key to all homogenisation arguments. At $O(\epsilon^{-1})$ in (2.7) and (2.8) we find that

$$\nabla_X \cdot \mathbf{v}_0 = 0, \qquad \nabla_X p_0 = \mathbf{0}, \qquad \frac{\partial c_0}{\partial T} + \nabla_X \cdot (\mathbf{v}_0 c_0) = \frac{1}{\mathrm{Pe}_l}\nabla_X \cdot (D(c_0)\nabla_X c_0)\,. \tag{2.10}$$

We expect that there will be an initial boundary layer, in which $T = O(1)$, where c_0 depends on $\mathbf{X}$ and T; however, as T becomes large c_0 will reach a steady-state solution, with c_0 independent of $\mathbf{X}$ and T. Integrating over V_ϵ we find that

$$\phi\frac{\partial \bar{c}_0}{\partial T} + \int_{\partial V_\epsilon} c_0 \mathbf{v}_0 \cdot \mathbf{n}\,\mathrm{d}S = \frac{1}{\mathrm{Pe}_l}\int_{\partial V_\epsilon} D(c_0)\nabla_X c_0 \cdot \mathbf{n}\,\mathrm{d}S,$$

where for a function $f(X)$, periodic over V_ϵ, we have defined

$$\bar{f} = \frac{1}{|V_\epsilon|}\int_{V_\epsilon} f(\mathbf{X})\,\mathrm{d}\mathbf{X},$$

and $\phi = 1/|V_\epsilon|$ is the porosity. Using the boundary conditions (2.9) together with the condition that both $\mathbf{v}_0$ and c_0 must be periodic in $\mathbf{X}$ we find that

$$\frac{\partial \bar{c}_0}{\partial T} = 0.$$

By multiplying the final equation of (2.10) by $(c_0 - \bar{c}_0)$ and then integrating over V_ϵ we find that

$$\phi\frac{\partial}{\partial T}\left(\frac{1}{2}\overline{(c_0 - \bar{c}_0)^2}\right) = -\int_{V_\epsilon} D(c_0)\,|\nabla_X c_0|^2\,\mathrm{d}\mathbf{X},$$

and so, since $D(c_0)$ is positive, it is indeed true that, for large T, c_0 reaches a steady-state solution, independent of $\mathbf{X}$. Matching with this initial boundary layer shows us that c_0 satisfies the initial condition

$$c_0 = \overline{C_0(\mathbf{x}, \mathbf{X})}, \tag{2.11}$$

when $t = 0$. Hence c_0 is just a function of $\mathbf{x}$ and t for large T and is independent of the microscale variable: the concentration converges strongly to its homogenised limit as $\epsilon \to 0$.

With the leading order concentration independent of $\mathbf{X}$ we may now proceed to con-

sider the flow problem. The $O(1)$ terms in (2.7) are

$$\nabla_X \cdot \mathbf{v}_1 + \nabla_x \cdot \mathbf{v}_0 = 0, \tag{2.12}$$

and

$$\frac{\partial p_1}{\partial X_i} + \frac{\partial p_0}{\partial x_i} = \frac{\partial}{\partial X_j}\left(\mu(c_0)\frac{\partial v_{0i}}{\partial X_j}\right). \tag{2.13}$$

As in section 1.2.1, we introduce the cell problems

$$\begin{aligned} \nabla_X \cdot \mathbf{w}^j &= 0, \\ \nabla_X P^j &= \nabla_X^2 \mathbf{w}^j + \mathbf{e}_j, \\ \mathbf{w}^j &= \mathbf{0} \quad \text{on} \quad \partial V_\epsilon^D, \end{aligned}$$

where $\mathbf{e}_j$ is the unit vector in the X_j direction and P, $\mathbf{w}^j$ are periodic over V_ϵ. By linearity (with respect to $\mathbf{X}$) of (2.13), $\nabla_X \cdot \mathbf{v}_0 = 0$ and the boundary conditions, we then find that

$$\mathbf{v}_0 = -\frac{\mathbf{w}^j}{\mu(c_0)}\frac{\partial p_0}{\partial x_j}, \quad \text{and} \quad p_1 = -P^j \frac{\partial p_0}{\partial x_j}. \tag{2.14}$$

Integrating (2.12) gives

$$\begin{aligned} \nabla_x \cdot \left(\int_{V_\epsilon} \mathbf{v}_0 \,\mathrm{d}\mathbf{X}\right) &= -\int_{\partial V_\epsilon} \mathbf{v}_1 \cdot \mathbf{n} \,\mathrm{d}S \\ &= 0, \end{aligned}$$

after applying the boundary condition $\mathbf{v}_1 = \mathbf{0}$ on the solid interface. We therefore find that

$$\nabla_x \cdot \left(\frac{1}{\mu(c_0)}\frac{\partial p_0}{\partial x_j}\int_{V_\epsilon} \mathbf{w}^j \,\mathrm{d}\mathbf{X}\right) = 0,$$

and so p_0 satisfies

$$\nabla_x \cdot \left(\frac{\mathbf{K}}{\mu(c_0)}\nabla_x p_0\right) = 0, \tag{2.15}$$

where the permeability tensor $\mathbf{K}$ is given by

$$K_{ij} = \int_{V_\epsilon} w_i^j \,\mathrm{d}\mathbf{X}.$$

Recall that (2.10) shows the leading order pressure to be independent of $\mathbf{X}$, or alternatively that the pressure converges strongly to the homogenised leading order pressure as $\epsilon \to 0$. In contrast, the leading order velocity is still dependent on $\mathbf{X}$, and so, as $\epsilon \to 0$, the velocity becomes rapidly oscillating, and only converges to the homogenised velocity in

a weak sense. It is the rapidly oscillating velocity that will ultimately be responsible for dispersion of the solvent.

We now return to equation (2.8) and look at the $O(1)$ term for large T, remembering that, for large T, c_0 is independent of both $\mathbf{X}$ and T,

$$\frac{\partial c_0}{\partial t} + \frac{\partial c_1}{\partial T} + \nabla_X \cdot (\mathbf{v}_0 c_1 + \mathbf{v}_1 c_0) + \nabla_x \cdot (\mathbf{v}_0 c_0) = \frac{1}{\mathrm{Pe}_m} \nabla_X \cdot (D(c_0) \nabla_X c_1).$$

Integrating over V_ϵ and applying boundary conditions gives

$$\phi \frac{\partial c_0}{\partial t} + \phi \frac{\partial \bar{c}_1}{\partial T} + \nabla_x \cdot (\phi \bar{\mathbf{v}}_0 c_0) = -D(c_0) \nabla_x c_0 \cdot \int_{\partial V_\epsilon^D} \mathbf{n} \, \mathrm{d}S,$$

where the right-hand side evaluates to zero. We find that

$$\phi \frac{\partial \bar{c}_1}{\partial T} = -\phi \frac{\partial c_0}{\partial t} - \nabla_x \cdot (\phi \bar{\mathbf{v}}_0 c_0),$$

and since, for large T, the right-hand side is independent of T, we conclude that $\bar{c}_1$ is independent of T, otherwise c_1 would grow unboundedly as $T \to \infty$. We conclude that for $O(1)$ values of t the concentration is simply advected with the mean velocity satisfying

$$\phi \frac{\partial c_0}{\partial t} + \nabla_x \cdot (\phi \bar{\mathbf{v}}_0 c_0) = 0, \tag{2.16}$$

or

$$\phi \frac{\partial c_0}{\partial t} + \nabla_x \cdot (\mathbf{u_0} c_0) = 0,$$

where $\mathbf{u}_0 = \phi \bar{\mathbf{v}}_0$ is the (leading-order) flux of fluid per unit area (or superficial velocity). To introduce any diffusion term into the leading-order problem one must proceed to the longer time scale.

2.1.2.2 Behaviour at longer times

Since the global Péclet number is $O(\epsilon^{-1})$, diffusion does not appear in the global problem until $t = O(\epsilon^{-1})$. We therefore introduce the long time scale $\tau = \epsilon t$. At this large time the initial concentration profile will have moved on by a distance of $O(\epsilon^{-1})$, as described by (2.16). We therefore introduce Lagrangian coordinates,

$$\boldsymbol{\xi} = \mathbf{x} - \int_0^t \bar{\mathbf{v}}_0(\mathbf{x}(s)) \, \mathrm{d}s.$$

Equation (2.8) becomes

$$\frac{\partial c}{\partial t} + \nabla_\xi \cdot (\mathbf{v} c_0) - \bar{\mathbf{v}}_0 \cdot \nabla_\xi c_0 = \frac{\epsilon}{\mathrm{Pe}_l} \nabla_\xi \cdot (D(c) \nabla_\xi c) \,.$$

We now arrive at some difficulty in deciding whether it is appropriate to use Eulerian or Lagrangian coordinates for the micro-length scale. Since small rapid variations in the concentration are a consequence of rapid variations in the fixed, periodic medium, the rapid variations in c will therefore not follow the fluid, and so we should continue to use the Eulerian variable $\mathbf{X}$ for the microscale variable. We therefore propose asymptotic expansions of the form

$$\begin{aligned} p &\sim p_0(\boldsymbol{\xi}, \mathbf{X}, t, T, \tau) + \epsilon p_1(\boldsymbol{\xi}, \mathbf{X}, t, T, \tau) + \dots \,, \\ \mathbf{v} &\sim \mathbf{v}_0(\boldsymbol{\xi}, \mathbf{X}, t, T, \tau) + \epsilon \mathbf{v}_1(\boldsymbol{\xi}, \mathbf{X}, t, T, \tau) + \dots \,, \\ c &\sim c_0(\boldsymbol{\xi}, \mathbf{X}, t, T, \tau) + \epsilon c_1(\boldsymbol{\xi}, \mathbf{X}, t, T, \tau) + \dots \,, \end{aligned}$$

where we treat $\boldsymbol{\xi}$ rather than $\mathbf{x}$ as being independent of $\mathbf{X}$, and also take T, t, τ as independent. Our derivatives become

$$\nabla = \frac{1}{\epsilon} \nabla_X + \nabla_\xi,$$

$$\frac{\partial}{\partial t} = \frac{1}{\epsilon} \frac{\partial}{\partial T} + \frac{\partial}{\partial t} - \bar{\mathbf{v}}_0 \cdot \nabla_\xi + \epsilon \frac{\partial}{\partial \tau}.$$

Our leading order equations are

$$\nabla_X \cdot \mathbf{v}_0 = 0, \quad \nabla_X p_0 = 0, \quad \frac{\partial c_0}{\partial T} + \nabla_X \cdot (\mathbf{v}_0 c_0) = \frac{1}{\mathrm{Pe}_l} \nabla_X \cdot (D(c_0) \nabla_X c_0).$$

Once again, as $T \to \infty$ the leading order concentration will reach a steady state solution, in which c_0 is independent of $\mathbf{X}$, and when we match the $t = O(1)$ region to this initial boundary layer we find that

$$c_0 = \bar{C}_0(\boldsymbol{\xi}) \quad \text{when} \quad t = 0.$$

The next order term in the equation for the transport of solvent is

$$\frac{\partial c_1}{\partial T} + \nabla_X \cdot (\mathbf{v}_0 c_1) - \frac{1}{\mathrm{Pe}_l} \nabla_X \cdot (D(c_0) \nabla_X c_1) = -\frac{\partial c_0}{\partial t} - \nabla_\xi \cdot (\mathbf{v}_0 c_0) + \bar{\mathbf{v}}_0 \cdot \nabla_\xi c_0 - \nabla_X \cdot (\mathbf{v}_1 c_0). \quad (2.17)$$

Integrating over V_ϵ and applying boundary conditions and the condition of periodicity gives

$$\frac{\partial \bar{c}_1}{\partial T} = -\frac{\partial c_0}{\partial t},$$

and, since c_1 must be bounded as $T \to \infty$, and since the right-hand side is independent of T, we conclude that for large T

$$\frac{\partial c_0}{\partial t} = 0 \quad \text{and} \quad \frac{\partial \bar{c}_1}{\partial T} = 0.$$

We can eliminate $\mathbf{v}_1$ from (2.17) using the identity

$$\nabla_\xi \cdot \mathbf{v}_0 + \nabla_X \cdot \mathbf{v}_1 = 0,$$

so that we then obtain

$$\frac{\partial c_1}{\partial T} + \nabla_X \cdot (\mathbf{v}_0 c_1) - \frac{D(c_0)}{\mathrm{Pe}_l} \nabla_X^2 c_1 = -(\mathbf{v}_0 - \bar{\mathbf{v}}_0) \cdot \nabla_\xi c_0. \tag{2.18}$$

We also find that the leading order velocity is exactly the same as that found for $t = O(1)$. Equation (2.18), together with the boundary condition

$$\mathbf{n} \cdot \nabla_X c_1 + \mathbf{n} \cdot \nabla_\xi c_0 = 0,$$

shows that c_1 has a linear dependence on $\nabla_\xi c_0$, leading us to seek a solution of the form

$$c_1 = \hat{\boldsymbol{\chi}} \cdot \nabla_\xi c_0 + \hat{c}_1(\boldsymbol{\xi}, t, \tau), \tag{2.19}$$

where $\hat{\boldsymbol{\chi}} = \hat{\boldsymbol{\chi}}(\boldsymbol{\xi}, \boldsymbol{X}, t, T, \tau)$. We are then led towards a cell problem which requires us to solve

$$\frac{\partial \hat{\chi}_i}{\partial T} + \nabla_X \cdot (\mathbf{v}_0 \hat{\chi}_i) - \frac{D(c_0)}{\mathrm{Pe}_l} \nabla_X^2 \hat{\chi}_i = -(v_{0i} - \bar{v}_{0i}), \tag{2.20}$$

while satisfying the boundary condition

$$\mathbf{n} \cdot \nabla_X \hat{\chi}_i = -n_i \quad \text{on} \quad \partial V_\epsilon^D.$$

On integrating over V_ϵ we find that

$$\frac{\partial \overline{\hat{\boldsymbol{\chi}}}}{\partial T} = \mathbf{0},$$

and so we may assume that $\overline{\hat{\boldsymbol{\chi}}} = \mathbf{0}$ so that $\hat{c}_1 = \bar{c}_1$. For large T, $\hat{\boldsymbol{\chi}}$ will reach a steady state solution $\boldsymbol{\chi}$ satisfying the condition that $\overline{\boldsymbol{\chi}} = \mathbf{0}$. The velocity is still given by (2.14)

and so the cell problem is to solve

$$\alpha_j \left(\mathbf{w}^j \cdot \nabla_X \chi_i + w_i^j - \overline{w_i^j} \right) = \nabla_X^2 \chi_i, \tag{2.21}$$

with the boundary condition

$$\mathbf{n} \cdot \nabla_X \chi_i = -n_i \quad \text{on} \quad \partial V_\epsilon^D, \tag{2.22}$$

where

$$\alpha_j = -\frac{\mathrm{Pe}_l}{\mu(c_0) D(c_0)} \frac{\partial p_0}{\partial \xi_j},$$

and χ_i is periodic with $\overline{\chi_i} = 0$. Note that, since c_0 only depends on $\boldsymbol{\xi}$ and τ, we have that $\boldsymbol{\chi} = \boldsymbol{\chi}(\boldsymbol{\xi}, \mathbf{X}, \tau)$. The dependence of the cell problem (2.21),(2.22) on α_j is not simple, and so, to fully close the problem, one has to first solve the cell problem for all possible values of α_j. The cell problem does not obey any simple relationship with the mean velocity and this is one of the main reasons why a simple description of diffusion in porous media is lacking.

Once the cell problems (2.21),(2.22) are solved, we may proceed to the $O(\epsilon)$ terms of equation (2.8), yielding

$$\begin{aligned}
\frac{\partial c_2}{\partial T} &+ \nabla_X \cdot (\mathbf{v}_0 c_2) - \frac{1}{\mathrm{Pe}_l} \nabla_X \cdot (D(c_0) \nabla_X c_2) = \\
&- \frac{\partial c_0}{\partial \tau} - \frac{\partial \bar{c}_1}{\partial t} - \nabla_\xi \cdot (\mathbf{v}_0 c_1) + \bar{\mathbf{v}}_0 \cdot \nabla_\xi c_1 \\
&- \nabla_\xi \cdot (\mathbf{v}_1 c_0) - \nabla_X \cdot (\mathbf{v}_1 c_1) - \nabla_X \cdot (\mathbf{v}_2 c_0) \\
&+ \frac{1}{\mathrm{Pe}_l} \nabla_X \cdot \left(D(c_0) \nabla_\xi c_1 + c_1 D'(c_0) (\nabla_X c_1 + \nabla_\xi c_0) \right) \\
&+ \frac{1}{\mathrm{Pe}_l} \nabla_\xi \cdot \left(D(c_0) \left(\nabla_X c_1 + \nabla_\xi c_0 \right) \right),
\end{aligned} \tag{2.23}$$

and the boundary condition

$$\mathbf{n} \cdot \nabla_X c_2 + \mathbf{n} \cdot \nabla_\xi c_1 = 0 \quad \text{on} \quad \partial V_\epsilon^D.$$

As usual we require that c_2 is periodic in $\mathbf{X}$, as otherwise c_2 would grow unboundedly as

$|\mathbf{X}| \to \infty$. Integrating (2.23) over V_ϵ and applying the ansatz, (2.19), gives

$$\begin{aligned}\phi\frac{\partial \bar{c}_2}{\partial T} &+ \frac{D(c_0)}{\mathrm{Pe}_l}\int_{\partial V_\epsilon}\mathbf{n}\cdot\nabla_\xi c_1\,\mathrm{d}S = -\phi\frac{\partial c_0}{\partial \tau} - \phi\frac{\partial \bar{c}_1}{\partial t}\\ &- \frac{\partial}{\partial \xi_i}\left(\int_{V_\epsilon} v_{0i}\chi_j\,\mathrm{d}\mathbf{X}\frac{\partial c_0}{\partial \xi_j}\right) - \nabla_\xi\cdot(\phi\bar{\mathbf{v}}_1 c_0) + \frac{D(c_0)}{\mathrm{Pe}_l}\int_{\partial V_\epsilon}\mathbf{n}\cdot\nabla_\xi c_1\,\mathrm{d}S\\ &+ \frac{\phi}{\mathrm{Pe}_l}\frac{\partial}{\partial \xi_i}\left(D(c_0)\overline{\frac{\partial \chi_j}{\partial X_i}}\frac{\partial c_0}{\partial \xi_j}\right) + \frac{\phi}{\mathrm{Pe}_l}\nabla_\xi\cdot(D(c_0)\nabla_\xi c_0)\,, \end{aligned} \tag{2.24}$$

which we may write as

$$\phi\left(\frac{\partial c_0}{\partial \tau} + \frac{\partial \bar{c}_1}{\partial t} + \frac{\partial \bar{c}_2}{\partial T}\right) + \nabla_\xi\cdot(\phi\bar{\mathbf{v}}_1 c_0) = \frac{1}{\mathrm{Pe}_l}\frac{\partial}{\partial \xi_i}\big(D_{ij}\frac{\partial c_0}{\partial \xi_j}\big), \tag{2.25}$$

where

$$D_{ij} = \phi\left(\delta_{ij} + \overline{\frac{\partial \chi_j}{\partial X_i}}\right)D(c_0) - \phi\mathrm{Pe}_l\overline{v_{0i}\chi_j}. \tag{2.26}$$

Now since $\partial\bar{c}_2/\partial T$ is the only term depending on T, (2.25) must hold with the term $\partial\bar{c}_2/\partial T$ set equal to zero, as otherwise c_2 would grow unboundedly as $T \to \infty$. Similarly as $\partial\bar{c}_1/\partial t$ is the only term depending on t we must set the term $\partial\bar{c}_1/\partial t$ equal to zero, as otherwise c_1 would grow unboundedly as $t \to \infty$. We conclude that

$$\phi\frac{\partial c_0}{\partial \tau} + \nabla_\xi\cdot(\bar{\mathbf{u}}_1 c_0) = \frac{1}{\mathrm{Pe}_l}\frac{\partial}{\partial \xi_i}\big(D_{ij}\frac{\partial c_0}{\partial \xi_j}\big), \tag{2.27}$$

where $\bar{\mathbf{u}}_1 = \phi\bar{\mathbf{v}}_1$. It is theoretically possible to calculate the $O(\epsilon)$ velocity term, $\mathbf{v}_1$; however, for most practical purposes it is only the diffusion term that we are interested in. Locally there may be large concentration gradients, in which the small diffusion term becomes important, but the small correction to the velocity does not become important.

One particular example of a periodic, porous medium, for which we can explicitly solve the cell problems, is a medium consisting of straight cylindrical pipes. This example corresponds to Taylor dispersion in a capillary pipe. If the capillaries all point in the $x-$direction then the only non-zero component of $\boldsymbol{\chi}$ will be $\chi_1 = \alpha_1\chi_1^*(Y,Z)$, where χ_1^* satisfies

$$\frac{\partial^2\chi_1^*}{\partial Y^2} + \frac{\partial^2\chi_1^*}{\partial Z^2} = w_1^1 - \overline{w_1^1},$$

with $\partial\chi_1^*/\partial n = 0$ on the boundaries of the pipes and the cross-sectional average of χ_1^* equal to zero. For a pipe with a circular cross-section with radius a, $w_1^1 = (a^2 - r^2)/4$, where r measures the distance from the centre of the pipe. We then find that

$$\chi_1^*(r) = \frac{a^2r^2}{32} - \frac{r^4}{64} - \frac{a^4}{96},$$

and so $D_{ij} = \phi\delta_{ij}D(c_0)$ except for $i = j = 1$ where

$$D_{11} = \phi D(c_0) + \phi\frac{\mathrm{Pe}_l^2\bar{v}_0^2a^2}{48D(c_0)},$$

and $\bar{v}_0$ is the mean velocity through the pores. This is equivalent to the expression for the effective diffusion found by Taylor [57], and modified by Aris [1], presented in section 1.5.2.

2.1.2.3 Effective diffusion for $\mathrm{Pe}_l \ll 1$

When at the microscopic scale diffusion dominates over convection, we obtain a much simpler form for the diffusion. The limit $\mathrm{Pe}_l \ll 1$ is not a singular limit of the problem for $\boldsymbol{\chi}$ (2.21),(2.22) and we find, in this limit, that the effective diffusion is given by

$$D_{ij} = \phi\left(\delta_{ij} + \overline{\frac{\partial\tilde{\chi}_i}{\partial X_j}}\right)D(c_0), \tag{2.28}$$

where $\tilde{\chi}_i$ satisfies

$$\nabla_X^2\tilde{\chi}_i = 0, \quad \text{with} \quad \mathbf{n}\cdot\nabla_X\tilde{\chi}_i = -n_i \quad \text{on} \quad \partial V_\epsilon^D.$$

For a stationary fluid, the difference between the effective diffusion of a substance in a porous medium, and the diffusion of a substance in free space, may be attributed to the tortuosity of the porous medium. It has been shown by Bear [2] that the ratio of the effective diffusion to the molecular diffusion is equal to the tortuosity and so one could apply (2.28) as the definition of the tortuosity of a periodic, porous medium.

2.1.2.4 Effective diffusion for $\mathrm{Pe}_l \gg 1$

The limit $\mathrm{Pe}_l \gg 1$ is a singular limit of the cell problem (2.21), (2.22). On neglecting the advection terms from (2.20) we obtain a reaction-diffusion equation in which the source term is positive wherever v_{0i} is below $\bar{v}_{0i}$, and negative wherever v_{0i} is above $\bar{v}_{0i}$. Eventually a steady state is reached where the gradient of χ_i is large enough for diffusion to act, requiring $\chi_i = O(\mathrm{Pe}_l)$. Since χ_i will tend to be negative for v_{0i} larger than $\bar{v}_{0i}$ and positive for v_{0i} smaller than $\bar{v}_{0i}$, we see that $\overline{\chi_i v_{0i}}$ will be of order Pe_l and, reassuringly, negative so that the effective diffusion is of order Pe_l^2 and positive.

When the advection terms are reintroduced the picture becomes somewhat more complicated. One might try to apply a similar argument along each particle-path/streamline,

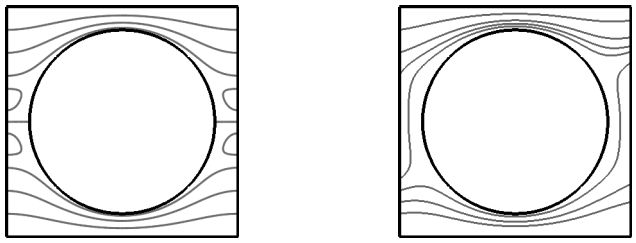

(a) **(b)**

Figure 2.3: Streamlines for flow past a periodic array of cylinders. In Figure 2.3a the mean flow is aligned with the array of cylinders so that the streamlines are periodic. In Figure 2.3b the mean flow is slightly misaligned to the array of cylinders and the streamlines are not periodic. For large Pe_l the effective longitudinal diffusion for 2.3a is much larger than the effective diffusion for 2.3b.

as follows. The average[2] of $v_{0i} - \bar{v}_{0i}$ will be positive on certain streamlines and negative on others. This leads to growth of χ_i on certain streamlines while χ_i will decrease along other streamlines. Eventually diffusion will act once $\chi_i = O(\mathrm{Pe}_l)$. The problem with this argument is that we have implicitly assumed that an average of $v_{0i} - \bar{v}_{0i}$ exists along a given streamline. Although the velocity is periodic the streamlines need not be, as shown in Figure 2.3, and a particle that enters the periodic cell at one point does not necessarily leave at the opposite point. When the streamlines are not periodic it is not possible to define an average of $v_{0i} - \bar{v}_{0i}$. When the streamlines are periodic, such as flow through a cylinder, we will always find that $\chi = O(\mathrm{Pe}_l)$ and so the effective diffusion will be of the order Pe_l^2. In contrast, when the streamlines are not periodic, there may not be such a large growth in χ_i, and the effective diffusion may be smaller.

Whether the streamlines are periodic or not will depend on the direction of the flow. However, we do not physically expect that the magnitude of the effective diffusion will depend strongly on the direction of the flow, at least for anisotropic porous media. The dependence that we find here seems to be a consequence of the fact that we are looking at periodic media. For large Pe_l, effective diffusion through periodic media is quite different from effective diffusion through random porous media. The idea that diffusion through periodic, porous media would behave in a qualitatively different way from diffusion through random, porous media has been previously suggested by Koch & Brady [32]. We often expect periodic media to behave similarly to random media, but here this is not the case. When $\mathrm{Pe}_l \gg 1$ the effect of molecular diffusion is not significant until

[2]Here, by average we mean the time-averaged value that a particle travelling along a streamline observes.

the fluid has travelled a distance of $O(\epsilon \mathrm{Pe}_l)$. Since the effective diffusion depends on a length scale much larger than that of the microscopic length scale, we expect that the structure of the porous medium over a distance $O(\epsilon \mathrm{Pe}_l)$ is important, and so a periodic porous medium cannot be viewed as generic. When Pe_l is not large the structure beyond that of the periodic cell is not so important and the behaviour of a periodic medium will be closer to the behaviour of a random porous medium. Hence we have gained some intuitive understanding as to when it is appropriate to assume that the medium is periodic for general problems: one may assume that the medium is periodic, without significantly altering the results, provided that there is no long range interaction between the periodic cells.

We may also predict that the diffusion will be anisotropic, even for isotropic media. The cause of this anisotropy is that, for a typical flow, the variation in the velocity about its mean value will be somewhat larger in the direction of the mean flow than in the transverse direction.

2.1.2.5 'Upscaling' of diffusion in porous media

The enhanced diffusion that is observed in flow through porous media [22] is not only the consequence of effects at the pore scale. The rocks through which oil flows are heterogeneous on many different length scales, and these heterogeneities also lead to an enhanced diffusion. Where the length scale of the heterogeneities is much smaller than the macroscopic length scale of interest, we can determine an effective permeability by applying the method of homogenisation, as shown in section 1.2.3. The only properties of the superficial velocity field, $\mathbf{u}(\mathbf{x}, \mathbf{X})$ that we require in order to be able to follow our above derivation of the Peaceman model is that $\nabla \cdot \mathbf{u} = 0$, and that $\mathbf{u}$ is periodic in $\mathbf{X}$. Provided that the Péclet number at the length scale of the microscopic heterogeneities is of order one, it is possible to apply a similar argument to our above derivation of the Peaceman model. The only significant difference between modelling dispersion produced by permeability variations, and dispersion produced by velocity variations at the pore scale, is that we no longer have to concern ourselves with the interface between the solid rock matrix and the fluid-filled pore-space. The effective diffusion, as defined in (2.27), is given by

$$D_{ij} = \delta_{ij} D(c_0) - \mathrm{Pe}_l \overline{u_{0i} \chi_j},$$

where χ_i solves

$$\mathbf{u}_0 \cdot \nabla_X \chi_i + u_{0i} - \bar{u}_{0i} = \frac{D(c_0)}{\mathrm{Pe}_l} \nabla_X^2 \chi_i,$$

and χ_i is periodic over the unit cell with $\overline{\chi_i} = 0$.

We see that dispersion resulting from flow past small-scale heterogeneities in the rock

is qualitatively similar to dispersion resulting from shear in the flow of fluid through microscopic pores. It is observed that the magnitude of dispersion depends strongly on the length scale over which it is measured [22]. Our investigation suggests that, just as the rapidly varying velocity at the pore scale may lead to an enhanced dispersion, so too may small-scale heterogeneities in the porous medium lead to an enhanced dispersion. However, provided that the length scale of the heterogeneities is well-separated from the length scale over which dispersion is measured, the ratio of the macroscopic dispersion to the microscopic dispersion must surely be much smaller than the ratio of the two length scales. This ensures that the Péclet number increases as the length scale under consideration increases. The field-scale data reviewed in [22] seem to support this assumption, with larger values of dispersion, along with larger values of the Péclet number, found in larger aquifers.

2.1.3 The Peaceman model

The Peaceman model is in general given by

$$\nabla \cdot \mathbf{u} = 0, \tag{2.29}$$

$$\mathbf{u} = -\frac{\mathbf{K}}{\mu(c)}\nabla p, \tag{2.30}$$

$$\phi\frac{\partial c}{\partial t} + \nabla \cdot (\mathbf{u}c) = \nabla \cdot (\mathbf{D}\nabla c)\,, \tag{2.31}$$

where $\mathbf{u}$ represents the flux of fluid per unit area through the porous medium: i.e. the superficial Darcy velocity which is equal to the product of the porosity and the average pore-velocity. We shall be primarily concerned with isotropic porous media, so that the permeability tensor can be replaced by a scalar permeability k. However, as we have seen in our derivation of the Peaceman model the diffusion/dispersion term is complicated. The dispersion tensor $\mathbf{D}$ depends on the concentration of solvent, the velocity of the fluid and is likely to be anisotropic. Perhaps the most surprising property of the dispersion tensor is its dependence on the scale of measurement, which has been observed in field-scale studies [22]. We have explained the origin of this scale-dependence and showed that, while the magnitude of the effective diffusion increases as the scale of measurement increases, the effective Péclet number will always be large. The dispersion will be largest in the direction longitudinal to the flow, and smallest in the direction transverse to the flow. The ratio between the longitudinal dispersion and the transverse dispersion has been measured to be in the range of $10 - 100$, [5, 22]. For general porous media the dependence of this ratio on the velocity of the fluid appears to be quite weak, with Saffman and Koch and

Brady [50, 32] suggesting that the ratio is proportional to the logarithm of the microscale Péclet number. There does not appear to be much evidence that the dispersion tensor is concentration dependent, and so we shall neglect this possibility.

We nondimensionalise the Peaceman model, nondimensionalising: $\mathbf{u}$ with a typical flux U; $\mathbf{x}$ with the size of the reservoir L; $\mu(c)$ with the viscosity of the oil μ_o; k with a reference value k_0; $\mathbf{D}$ with a reference value of diffusion D_0; p with $UL\mu_o/k_0$ and t with $\phi L/U$. The nondimensionalised Peaceman model is then

$$\nabla \cdot \mathbf{u} = 0, \qquad \mathbf{u} = -\frac{k}{\mu(c)}\nabla p, \tag{2.32}$$

$$\frac{\partial c}{\partial t} + \nabla \cdot (\mathbf{u}c) = \frac{1}{\mathrm{Pe}}\nabla \cdot (\mathbf{D}\nabla c)\,, \tag{2.33}$$

$$\mu(c) = \left(M^{1/4}c + 1 - c\right)^{-4}. \tag{2.34}$$

The problem contains two important nondimensional parameters, the mobility ratio, M and the Péclet number. Since the Péclet number is large we are led to consider the singular limit in which the right-hand side of (2.33) is neglected.

2.1.4 The Muskat limit

We now consider the singular limit of the Peaceman model in which diffusion is entirely neglected, and as an initial condition we take the oil and solvent to be entirely separate, at least at the macroscopic scale. The concentration is advected according to

$$\phi\frac{\partial c}{\partial t} + \mathbf{u} \cdot \nabla c = 0, \tag{2.35}$$

and so, if initially the oil and solvent are separated, then they will remain so. Away from the discontinuity in the concentration where the oil meets the solvent it is clear from (2.32) that we must solve $\nabla^2 p = 0$. In general the pressure must satisfy

$$\nabla \cdot \left(\frac{k}{\mu(c)}\nabla p\right) = 0,$$

and so, if c is discontinuous across a curve Γ then, for a weak solution, we require that

1. p is continuous across Γ,
2. $\dfrac{k}{\mu(c)}\nabla p \cdot \mathbf{n}$ is continuous across Γ,

where $\mathbf{n}$ is the normal to the curve Γ. These are exactly the conditions satisfied by the Muskat problem.

Even when diffusion produces a slightly diffuse interface, it is still possible to derive the Muskat problem as we now show. If we suppose that μ is initially a smooth function, and then neglect the effect of diffusion, then we must solve

$$\nabla \cdot \left(\frac{1}{\mu} \nabla p \right) = 0, \tag{2.36}$$

and

$$\frac{\partial \mu}{\partial t} = \nabla^2 p, \tag{2.37}$$

where the last equation is obtained by combining the equation for conservation of the viscosity of a fluid particle with Darcy's law. We suppose that the initial condition for μ is such that μ takes the constant values μ_- and μ_+ away from either side of a curve Γ, and that near Γ

$$\mu = \tilde{\mu} \left(\frac{r}{\delta}, s \right),$$

where s measures arc-length along Γ, r is a coordinate perpendicular to s and $\delta \ll 1$. The function $\tilde{\mu}$ is such that as $r/\delta \to \pm\infty$, $\tilde{\mu} \to \mu_\pm$ exponentially fast. At later times the viscosity will take the constant values μ_- and μ_+ either side of a curve $\Gamma(t)$, and near $\Gamma(t)$ the viscosity will be of the form

$$\mu = \mu \left(\frac{r}{\delta}, s, t \right).$$

Away from $\Gamma(t)$ we have

$$\nabla^2 p_0 = 0, \qquad \nabla^2 p_1 = 0 \quad \ldots \ .$$

We parametrise $\Gamma(t)$ by $(X(s,t), Y(s,t))$ where s is the arc-length so that r, s are defined (sufficiently close to $\Gamma(t)$) such that

$$\mathbf{x}(r,s,t) = \mathbf{X}(s,t) + r\mathbf{n}(s,t), \tag{2.38}$$

where $\mathbf{n}$ is the unit normal to the curve, defined by

$$\mathbf{n} = \frac{\mathrm{d}^2\mathbf{X}}{\mathrm{d}s^2} \Bigg/ \left| \frac{\mathrm{d}^2\mathbf{X}}{\mathrm{d}s^2} \right|.$$

Near $\Gamma(t)$ equations (2.36), (2.37) then become

$$\frac{1}{1+\delta\kappa R} \frac{\partial}{\partial R} \left(\frac{1+\delta\kappa R}{\mu} \frac{\partial p}{\partial R} \right) + \frac{\delta^2}{1+\delta\kappa R} \frac{\partial}{\partial s} \left(\frac{1}{\mu(1+\delta\kappa R)} \frac{\partial p}{\partial s} \right) = 0, \tag{2.39}$$

and

$$-\delta v_n \frac{\partial \mu}{\partial R} + \delta^2 \frac{\partial \mu}{\partial t} = \frac{1}{1+\delta\kappa R}\frac{\partial}{\partial R}\left((1+\delta\kappa R)\frac{\partial p}{\partial R}\right) + \frac{\delta^2}{1+\delta\kappa R}\frac{\partial}{\partial s}\left(\frac{1}{1+\delta\kappa R}\frac{\partial p}{\partial s}\right) \quad (2.40)$$

where $R = r/\delta$, κ is the curvature of $\Gamma(t)$, defined by

$$\kappa = \left|\frac{\mathrm{d}^2\mathbf{X}}{\mathrm{d}s^2}\right|,$$

and v_n is the normal velocity of $\Gamma(t)$, defined by

$$v_n = \mathbf{n} \cdot \frac{\mathrm{d}^2\mathbf{X}}{\mathrm{d}s^2}.$$

We introduce the asymptotic expansions

$$\begin{aligned} p &\sim p_0 + \delta p_1 + \dots , \\ \mu &\sim \mu_0 + \delta \mu_1 + \dots , \end{aligned}$$

and similarly for κ and v_n. We find that p_0 is independent of R and that p_1 solves

$$\frac{\partial}{\partial R}\left(\frac{1}{\mu_0}\frac{\partial p_1}{\partial R}\right) = 0, \qquad -v_{n0}\frac{\partial \mu_0}{\partial R} = \frac{\partial^2 p_1}{\partial R^2},$$

so that

$$p_1 = \hat{p}_1(s,t) - v_{n0}\int_0^R \mu_0(R',s,t)\,\mathrm{d}R'.$$

We now need to match our expansions in the inner region to our expansion away from $\Gamma(t)$. Matching with the solution as $R \to -\infty$, using Van Dyke's rule, we find that

$$(2 \text{ t.i.})(2 \text{ t.o.}) = p_0|_{\Gamma^-} + \delta R \left.\frac{\partial p_0}{\partial n}\right|_{\Gamma^-} + \delta\, p_1|_{\Gamma^-} ,$$

$$(2 \text{ t.i.}) = \hat{p}_0 + \delta\hat{p}_1 - \delta v_{n0}\int_0^{r/\delta} \mu_0\,\mathrm{d}R'.$$

Since r/δ is large and negative we find that

$$\int_0^{r/\delta} \mu_0\,\mathrm{d}R' \sim \frac{r}{\delta}\mu_- - \int_{-\infty}^0 (\mu_0 - \mu_-)\,\mathrm{d}R' + \text{exponentially small terms.}$$

We then find from matching that

$$p_0|_{\Gamma^-} = \hat{p}_0, \qquad \left.\frac{\partial p_0}{\partial n}\right|_{\Gamma^-} = -v_{n0}\mu_-,$$

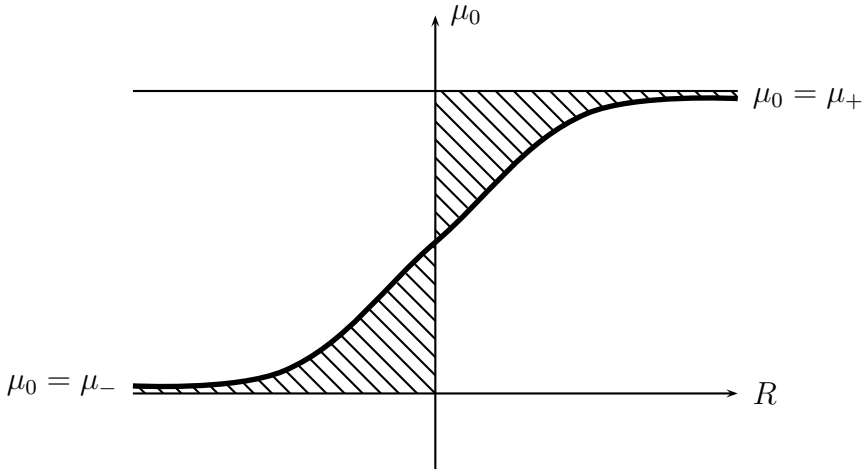

Figure 2.4: Viscosity profile in the inner region, where $R = O(1)$.

and

$$p_1|_{\Gamma^-} = \hat{p}_1(t) + v_{n0} \int_{-\infty}^{0} (\mu_0 - \mu_-)\, \mathrm{d}R'.$$

We can similarly match with the solution as $R \to +\infty$ and find that

$$p_0|_{\Gamma^+} = \hat{p}_0, \qquad \left.\frac{\partial p_0}{\partial n}\right|_{\Gamma^+} = -v_{n0}\mu_+,$$

and

$$p_1|_{\Gamma^+} = \hat{p}_1(t) - v_{n0} \int_{0}^{\infty} (\mu_0 - \mu_+)\, \mathrm{d}R'.$$

To leading order we find the usual Muskat conditions at the free surface, namely

$$p_0|_{\Gamma^-} = p_0|_{\Gamma_+} \quad \text{and} \quad \frac{1}{\mu_-}\frac{\partial p_0}{\partial n} = \frac{1}{\mu_+}\frac{\partial p_0}{\partial n} = -v_{n0}.$$

At next order we find that

$$p_1|_{\Gamma^+} - p_1|_{\Gamma^-} = -v_n \left(\int_{0}^{\infty} (\mu_0 - \mu_+)\, \mathrm{d}R' + \int_{-\infty}^{0} (\mu_0 - \mu_-)\, \mathrm{d}R' \right).$$

The value of the coefficient of v_{n0} in the above equation depends on the exact location of $\Gamma(t)$ up to $O(\delta)$. The exact location of $\Gamma(t)$ up to $O(\delta)$ is unimportant in the free boundary problem and so we are free to shift R by a function of s and t. It is sensible for us to make this shift so that the jump in p_1 across $\Gamma(t)$ is zero. We will then have that

$$\beta = \int_{-\infty}^{0} \mu_0 - \mu_-\, \mathrm{d}R' = \int_{0}^{\infty} \mu_+ - \mu_0\, \mathrm{d}R' \geq 0,$$

with $\beta = 0$ only when μ is a step function. The next order condition at the free surface is then given by

$$p_1|_{\Gamma^-} = p_1|_{\Gamma^+} = \hat{p}_1 + \beta v_{n0}.$$

We have found the next order correction term to the dynamic condition, i.e.

$$p|_{\Gamma^-} = p|_{\Gamma^+} = \hat{p} + \delta\beta v_{n0} + O(\delta^2),$$

and it is equivalent to the kinetic undercooling free surface condition that is applied to the Stefan problem. In the Stefan problem the temperature is analogous to the pressure and the analogue of $\hat{p}$, the melting temperature, is known; however, for the Muskat problem, $\hat{p}$ is not known beforehand and so we may incorporate the $\delta\beta v_{n0}$ term into $\hat{p}$. We have not obtained the next order correction to the kinematic condition. We note that this derivation of the Muskat problem is not applicable when the curvature of the interface $\kappa = O(\delta^{-1})$, since both our asymptotic expansion and our coordinate system (2.38) will break down in this regime.

Since we have seen in the introduction that the Muskat problem is unstable to small wavelength instabilities, we might expect similar behaviour of the Peaceman model, especially when diffusion is small and there are jumps in the concentration of solvent. In the next section we investigate the linear stability of solutions to the Peaceman model.

2.2 Stability analysis

In this section we shall investigate the stability of some solutions to the Peaceman model. We have seen that in the singular limit of zero diffusion and taking a step function for the initial condition, the Peaceman model reverts to the Muskat problem. We therefore expect that the Peaceman model will exhibit a similar instability to the Muskat problem. We expect, however, that the introduction of small diffusion will act as a regularisation mechanism, preventing the blow-up of solutions that we have witnessed when considering the Muskat problem. We can foresee two mechanisms by which the introduction of diffusion might help to stabilise large wavenumber disturbances:

1. Diffusion transverse to the direction of growth of fingers will become important at the small length scale of large wavenumber disturbances, and will act to promote decay of large wavenumber disturbances.

2. Longitudinal diffusion will act to produce a diffuse interface between the oil and solvent. There is no longer such a sharp jump in the viscosity, and this may help stabilise the problem.

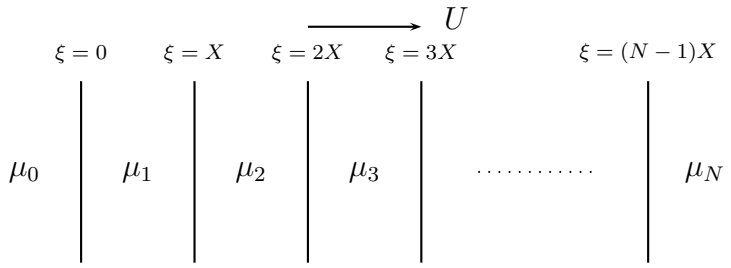

Figure 2.5: Muskat problem with many fluids

The first of these two mechanisms is simply a consequence of the ability of diffusion to cause large wavenumber disturbances to decay rapidly. Disturbances to the heat equation with wavenumber k decay at a rate that is proportional to k^2, and so large wavenumber disturbances decay at a very large rate. The second mechanism is somewhat more subtle and to illustrate the stabilising effect of a diffuse interface, we now consider the stability analysis of a many-fluid system in the Muskat problem.

2.2.1 The many-fluid Muskat problem

Suppose that, rather than simply having a single fluid displacing another we consider a whole series of fluids sequentially displacing each other as shown in Figure 2.5. The many-fluid Muskat problem, and in particular the three-fluid Muskat problem, has been the subject of several papers by Daripa [14, 15]. Our base state consists of $(N+1)$ fluid layers travelling with velocity U in the x-direction. To simplify the algebra somewhat, we assume that the separation between each layer is constant and equal to X. We introduce travelling coordinates, $\xi = x - Ut$, so that the position of the interfaces is given by $\xi = nX$, $n = 0, 1, \ldots (N-1)$. In each fluid the velocity and pressure satisfies

$$\nabla \cdot \mathbf{u} = 0, \quad \text{and} \quad \mathbf{u} = -\frac{k}{\mu_i}\nabla p.$$

At each interface we must satisfy the kinematic condition that the normal velocity of the fluid to the interface is continuous and equal to the normal velocity of the interface. We must also satisfy the dynamic boundary condition that the pressure is continuous. The pressure in the base-state solution is given by

$$p_0 = \begin{cases} -\mu_0 U\xi/k & \xi < 0, \\ UX\left(\mu_n - \sum_{i=1}^{n-1}(n-i)\mu_i\right)/k - \mu_n U\xi/k & (n-1)X < \xi < nX, \\ UX\left(\mu_N - \sum_{i=1}^{N-1}(N-i)\mu_i\right)/k - \mu_N U\xi/k & (N-1)X < \xi. \end{cases}$$

We now seek a solution where the interfaces are slightly perturbed so that the positions of the interfaces are given by

$$\xi = nX + \epsilon f_n \Re\left(\mathrm{e}^{\mathrm{i}\alpha y + \sigma t}\right),$$

and the pressure is given by

$$p \sim p_0 + \epsilon P_1(\xi) \Re\left(\mathrm{e}^{\mathrm{i}\alpha y + \sigma t}\right),$$

where $\epsilon \ll 1$ and α is real. The disturbance to the pressure satisfies

$$\frac{\mathrm{d}^2 P_1}{\mathrm{d}\xi^2} = \alpha^2 P_1,$$

and so we have the solution

$$P_1 = A_n \mathrm{e}^{|\alpha|\xi} + B_n \mathrm{e}^{-|\alpha|\xi}$$

in the region occupied by the fluid with viscosity μ_n. Since the disturbance to pressure must decay as $|\xi| \to \infty$, we require that $B_0 = A_N = 0$. We now need to apply the kinematic and dynamic boundary conditions at each interface. The kinematic boundary condition applied at each interface gives

$$\begin{aligned} k\,|\alpha|\,\frac{A_n \mathrm{e}^{n|\alpha|X} - B_n \mathrm{e}^{-n|\alpha|X}}{\mu_n} &= k\,|\alpha|\,\frac{A_{n+1}\mathrm{e}^{n|\alpha|X} - B_{n+1}\mathrm{e}^{-n|\alpha|X}}{\mu_{n+1}}, \\ &= -\sigma f_n, \end{aligned} \tag{2.41}$$

for $n = 0, 1, \ldots, N-1$. We may also apply the dynamic boundary condition at each interface to find that

$$\begin{aligned} &(A_n \mathrm{e}^{n|\alpha|X} + B_n \mathrm{e}^{-n|\alpha|X}) - (A_{n+1}\mathrm{e}^{n|\alpha|X} + B_{n+1}\mathrm{e}^{-n|\alpha|X}) \\ &\qquad = U\,|\alpha|\,(\mu_{n+1} - \mu_n)\frac{A_n \mathrm{e}^{n|\alpha|X} - B_n \mathrm{e}^{-n|\alpha|X}}{\sigma \mu_n}, \end{aligned} \tag{2.42}$$

for $n = 0, 1, \ldots, N-1$. We now have $2N+2$ equations, namely (2.41), (2.42) and the conditions $B_0 = A_N = 0$, for $2N+2$ unknowns. In general this yields a polynomial for σ with order N and so we may have difficulty finding an explicit expression for σ when N is large. It is of particular interest to solve the problem for large wavenumbers so that $|\alpha|\,X \gg 1$. The problem can be expressed in the form

$$\mathbf{A}\mathbf{x} = \mathbf{0},$$

where $\mathbf{x}$ is the vector $(B_0, A_0, B_1, A_1, \ldots, B_N, A_N)$. If we write $\delta = \mathrm{e}^{-|\alpha|X}$, then, for small δ, the *order of magnitude* of the entries of the matrix $\mathbf{A}$ is given by

$$\begin{pmatrix} 1 & 0 & 0 & 0 & 0 & 0 & 0 & & 0 \\ 1 & 1 & 1 & 1 & 0 & 0 & 0 & & 0 \\ 1 & 1 & 1 & 1 & 0 & 0 & 0 & & 0 \\ 0 & 0 & \delta & \delta^{-1} & \delta & \delta^{-1} & 0 & & 0 \\ 0 & 0 & \delta & \delta^{-1} & \delta & \delta^{-1} & 0 & & 0 \\ 0 & 0 & 0 & 0 & \delta^2 & \delta^{-2} & \delta^2 & & 0 \\ 0 & 0 & 0 & 0 & \delta^2 & \delta^{-2} & \delta^2 & & 0 \\ & & & & & & & \ddots & \\ 0 & 0 & 0 & 0 & 0 & 0 & 0 & 0 & 1 \end{pmatrix}. \tag{2.43}$$

To find σ we must solve $\det \mathbf{A} = 0$, since otherwise only the trivial solution is possible. We note that for small δ, the leading order term in the determinant of this matrix is equivalent to the determinant of a block-diagonal matrix where the entries have the order of magnitude

$$\begin{pmatrix} 1 & 0 & 0 & 0 & 0 & 0 & 0 & & 0 \\ 0 & 1 & 1 & 0 & 0 & 0 & 0 & & 0 \\ 0 & 1 & 1 & 0 & 0 & 0 & 0 & & 0 \\ 0 & 0 & 0 & \delta^{-1} & \delta & 0 & 0 & & 0 \\ 0 & 0 & 0 & \delta^{-1} & \delta & 0 & 0 & & 0 \\ 0 & 0 & 0 & 0 & 0 & \delta^{-2} & \delta^2 & & 0 \\ 0 & 0 & 0 & 0 & 0 & \delta^{-2} & \delta^2 & & 0 \\ & & & & & & & \ddots & \\ 0 & 0 & 0 & 0 & 0 & 0 & 0 & 0 & 1 \end{pmatrix}. \tag{2.44}$$

To leading order, the condition that $\det \mathbf{A} = 0$ can thus be expressed as

$$\prod_{n=0}^{N-1} \frac{1}{\mu_n \mu_{n+1}} \left(U\,|\alpha|\, \frac{\mu_{n+1} - \mu_n}{\sigma} - (\mu_{n+1} + \mu_n) \right) = 0, \tag{2.45}$$

and so we have that for some n,

$$\sigma = U\,|\alpha|\, \frac{\mu_{n+1} - \mu_n}{\mu_{n+1} + \mu_n}.$$

The growth rate depends on the viscosities of only one pair of adjacent fluids. In contrast to the two-fluid Muskat problem there are now multiple eigensolutions, each with its own growth rate. For general initial conditions the growth rate observed will be that of the fastest growing eigensolution, and so, for an unstable miscible displacement, the growth rate is given by

$$\sigma = U\,|\alpha| \max_{n=0\ldots N-1} \frac{\mu_{n+1} - \mu_n}{\mu_{n+1} + \mu_n}. \tag{2.46}$$

Since for large $|\alpha|\, X$, the growth rate depends on only the jump in viscosities at each interface, it is therefore possible to reduce the growth rate of large wavenumber insta-

bilities, when a less viscous fluid displaces a more viscous one, by introducing a fluid of intermediate viscosity between them.

On the basis of the above calculation, one could try to model a diffuse interface as a large number of small jumps in the viscosity. If the separation between each interface is δx, and the jump in viscosity is $\delta x \mathrm{d}\mu/\mathrm{d}x$, then the maximum growth rate for wavenumbers satisfying $\alpha \gg 1/\delta x$ will be

$$\sigma = \frac{U|\alpha|}{2} \max_x \frac{1}{\mu}\frac{\mathrm{d}\mu}{\mathrm{d}x}\delta x.$$

In the limit $\delta x \to 0$, we find that $\mathrm{d}\sigma/\mathrm{d}\alpha \to 0$ as $\alpha \to \infty$. One might therefore imagine that, in the continuum limit, the growth rate would be constant for large α. We shall see that in the continuum limit this is indeed the case, and the existence of a diffuse interface does indeed lead to a growth rate that remains bounded for all wavenumbers.

Another special case that yields to analysis is when $|\alpha| X \ll 1$. One finds that

$$\begin{pmatrix} A_{n+1} \\ B_{n+1} \end{pmatrix} = \frac{1}{2\sigma\mu_n} \mathbf{P}^1_n \begin{pmatrix} A_n \\ B_n \end{pmatrix},$$

where

$$\mathbf{P}^k_n = \begin{pmatrix} \sigma a^k_n - U|\alpha| b^k_n & \sigma b^k_n + U|\alpha| b^k_n \\ \sigma b^k_n - U|\alpha| b^k_n & \sigma a^k_n + U|\alpha| b^k_n \end{pmatrix} \quad \text{and} \quad \begin{aligned} a^k_n &= \mu_{n+k} + \mu_n, \\ b^k_n &= \mu_{n+k} - \mu_n. \end{aligned}$$

We find a similar relationship between A_{n+2}, B_{n+2} and A_n, B_n, with $\mathbf{P}^1_n$ replaced with $\mathbf{P}^2_n$, and so by induction we have

$$\begin{pmatrix} 0 \\ B_N \end{pmatrix} = \frac{1}{2\sigma\mu_0} \mathbf{P}^N_0 \begin{pmatrix} A_0 \\ 0 \end{pmatrix},$$

and so we find that when $|\alpha| X \ll 1$,

$$\sigma = U|\alpha| \frac{\mu_N - \mu_0}{\mu_0 + \mu_N}.$$

It is only the far field viscosities that are of any importance in determining the growth rate of small wavenumber disturbances, and we recover the same growth rate for these small wavenumber disturbances as when there are only two fluids involved. We shall see that in the continuum limit too, we recover the same growth rate as the traditional two-fluid Muskat problem.

The analysis of the multi-layer Muskat problem has real practical importance in industrial applications. One technique for enhanced oil recovery involves introducing a polymer into the water used during secondary oil recovery [23]. The introduction of the polymer

allows one to control the viscosity of the water so that there is a gradual change in viscosity, rather than a single large jump in viscosity at the oil-water interface. This may lead to a reduction of the growth rate of any instabilities. With this in mind, we now return to the stability analysis of the Peaceman model.

2.2.2 The linearised problem

When considering linear stability analysis of the Peaceman model, we are concerned with the initial growth rate of small disturbances. Since the enhanced diffusive terms are only relevant after a long time, we make the basic assumption that the coefficients of diffusion are entirely determined by the base-state, and are independent of any small disturbances to the base state. We shall also assume that the permeability is constant to avoid complicating the stability analysis. We wish to consider a one-dimensional flow, and so we take as our base-state velocity $u = 1$ and $v = 0$. As the base state has a constant velocity, we may assume that diffusion is constant and anisotropic, so that the equation for the advection of concentration is

$$\frac{\partial c}{\partial t} + \nabla \cdot (\mathbf{u}c) = \frac{1}{\mathrm{Pe}_{\parallel}} \frac{\partial^2 c}{\partial x^2} + \frac{1}{\mathrm{Pe}_{\perp}} \frac{\partial^2 c}{\partial y^2}. \tag{2.47}$$

The base-state concentration profile $c_0(x, t)$ satisfies

$$\frac{\partial c_0}{\partial t} + \frac{\partial c_0}{\partial x} = \frac{1}{\mathrm{Pe}_{\parallel}} \frac{\partial^2 c_0}{\partial x^2}. \tag{2.48}$$

We face a significant difficulty when investigating the stability of solutions in that this equation does not accept any non-trivial, time-independent solutions, unless we neglect longitudinal diffusion. With no time-independent base-state, our linearised problem will contain an explicit time-dependence and so we will not obtain solutions with an exponential time dependence. As a consequence there is no longer a constant, globally-defined growth rate, and the linear stability analysis yields a system of partial differential equations rather than ordinary differential equations.

As we want to compare our stability results with the stability results of the Muskat problem, we therefore seek a base state which, initially, shows a sharp jump in concentration of solvent at the boundary between solvent and oil. We therefore find that our base state is given by

$$c_0 = \frac{1}{2}\mathrm{erfc}\left(\sqrt{\mathrm{Pe}_{\parallel}}\frac{x-t}{2\sqrt{t}}\right).$$

The base-state pressure is then given by

$$p_0(\xi,t) = -\int^{\xi} \mu(c_0(\xi,t))\,\mathrm{d}\xi,$$

where $\xi = x - t$. We seek a solution that is slightly perturbed from the base state with

$$\begin{aligned} c &= c_0(\xi,t) + \epsilon c_1(\xi,y,z,t), \\ p &= p_0(\xi,t) + \epsilon p_1(\xi,y,z,t), \\ u &= 1 + \epsilon u_1(\xi,y,z,t), \end{aligned}$$

where $\epsilon \ll 1$. The disturbances to the velocity and concentration then satisfy the pair of partial differential equations

$$\frac{\partial^2 u_1}{\partial \xi^2} + \frac{1}{\mu(c_0)}\frac{\mathrm{d}\mu}{\mathrm{d}c}(c_0)\frac{\partial c_0}{\partial \xi}\frac{\partial u_1}{\partial \xi} + \frac{\partial^2 u_1}{\partial y^2} + \frac{\partial^2 u_1}{\partial z^2} + \frac{1}{\mu(c_0)}\frac{\mathrm{d}\mu}{\mathrm{d}c}(c_0)\frac{\partial^2 c_1}{\partial y^2} = 0, \tag{2.49}$$

$$\frac{\partial c_1}{\partial t} + \frac{\partial c_0}{\partial \xi}u_1 = \frac{1}{\mathrm{Pe}_{\|}}\frac{\partial^2 c_1}{\partial \xi^2} + \frac{1}{\mathrm{Pe}_{\perp}}\frac{\partial^2 c_1}{\partial y^2} + \frac{1}{\mathrm{Pe}_{\perp}}\frac{\partial^2 c_1}{\partial z^2}. \tag{2.50}$$

Since these equations have no explicit dependence on y or z, we may seek solutions with an exponential dependence on y and z,

$$c_1 = \Re\left(C(\xi,t)\mathrm{e}^{\mathrm{i}\alpha_y y + \mathrm{i}\alpha_z z}\right),$$

$$u_1 = \Re\left(U(\xi,t)\mathrm{e}^{\mathrm{i}\alpha_y y + \mathrm{i}\alpha_z z}\right),$$

where α_y and α_z are real. We then find that

$$\left(\frac{\partial^2}{\partial \xi^2} + \frac{\partial \lambda_0}{\partial \xi} - \alpha^2\right)U = \alpha^2\frac{\mathrm{d}\lambda_0}{\mathrm{d}c}C, \tag{2.51}$$

$$\left(\frac{\partial}{\partial t} - \frac{1}{\mathrm{Pe}_{\|}}\frac{\partial^2}{\partial \xi^2} + \frac{\alpha^2}{\mathrm{Pe}_{\perp}}\right)C = -\frac{\partial c_0}{\partial \xi}U, \tag{2.52}$$

where $\lambda_0 = \log(\mu(c_0))$ is the log-viscosity of the base-state solution and $\alpha^2 = \alpha_y^2 + \alpha_z^2$, with α taken to be positive.

2.2.3 Boussinesq approximation

In the paper of Wooding [60], the pair of partial differential equations, (2.51) and (2.52), are tackled head-on. Wooding makes a Boussinesq-like approximation that the differences in viscosities between the two fluids is small, allowing him to treat the viscosity as constant

except when it appears as a derivative, in which case the derivative of the viscosity is treated as constant. More precisely, when the mobility ratio is close to 1, we may write $\lambda_0 = -Rc_0$, where $R = \log(M) \ll 1$. Equation (2.51) becomes

$$\frac{\partial^2 U}{\partial \xi^2} - R\frac{\partial c_0}{\partial \xi}\frac{\partial U}{\partial \xi} - \alpha^2 U = -R\alpha^2 C,$$

and so when $C = O(1)$ we find that $U = O(R)$. We write

$$U = RF(\xi, T)\mathrm{e}^{-\alpha^2 \frac{\mathrm{Pe}_\parallel}{\mathrm{Pe}_\perp} T}, \qquad C = G(\xi, T)\mathrm{e}^{-\alpha^2 \frac{\mathrm{Pe}_\parallel}{\mathrm{Pe}_\perp} T},$$

where $T = t/\mathrm{Pe}_\parallel$, and obtain the equations

$$\left(\frac{\partial^2}{\partial \xi^2} - \alpha^2\right) F = -\alpha^2 G + O(R), \tag{2.53}$$

and

$$\left(\frac{\partial}{\partial T} - \frac{\partial^2}{\partial \xi^2}\right) G = R\mathrm{Pe}_\parallel \frac{\mathrm{e}^{-\frac{\xi^2}{4T}}}{2\sqrt{\pi T}} F + O(R^2). \tag{2.54}$$

If we neglect R entirely in (2.54) we will simply find that the initial concentration disturbance spreads out. When (2.53) and (2.54) are combined we see that the term involving R in (2.54) provides the leading order correction for small R and so we may neglect all other terms involving R. Wooding found a series solution to (2.53), (2.54) by taking G of the form

$$G = G(X, T) = T^{-1/2}\mathrm{e}^{-X^2} \sum_{n=0}^{\infty} T^{-n/2} A_n(T) H_n(X), \quad \text{where} \quad X = \frac{\xi}{2\sqrt{T}},$$

and H_n are Hermite polynomials. We may solve (2.53) by the use of Green's functions so that

$$F(X, T) = \alpha \sum_{n=0}^{\infty} A_n(T) F_n(X, T),$$

where

$$F_n(X, T) = \mathrm{e}^{-2\sqrt{T}\alpha X} \int_{-\infty}^{X} \mathrm{e}^{2\sqrt{T}\alpha u - u^2} H_n(u)\,\mathrm{d}u + \mathrm{e}^{2\sqrt{T}\alpha X} \int_{X}^{\infty} \mathrm{e}^{-2\sqrt{T}\alpha u - u^2} H_n(u)\,\mathrm{d}u,$$

and we have assumed, without loss of generality, that $\alpha > 0$. On substituting our series solutions into (2.54) we find that

$$T^{-1/2}\mathrm{e}^{-X^2} \sum_{n=0}^{\infty} \frac{\mathrm{d}A_n}{\mathrm{d}T} T^{-n/2} H_n(X) = \frac{\alpha R \mathrm{Pe}_\parallel}{2\sqrt{\pi}} T^{-1/2}\mathrm{e}^{-X^2} \sum_{n=0}^{\infty} A_n(T) F_n(X, T).$$

Since Hermite polynomials obey an orthogonality condition, we can multiply by $H_m(X)$ and integrate with respect to X to find that

$$\frac{\mathrm{d}A_m}{\mathrm{d}T} = \frac{\alpha R\mathrm{Pe}_\parallel}{2\pi}\sum_{n=0}^{\infty} A_n(T)\frac{I_{mn}(T)}{2^m m!},$$

where

$$I_{mn}(T) = \int_{-\infty}^{\infty} \mathrm{e}^{-X^2} H_m(X) F_n(X,T)\,\mathrm{d}X.$$

It is possible to calculate all the I_{mn} by repeated integration by parts. Wooding suggests that a good representation of the behaviour of the disturbance is provided when one only considers the leading order term $A_0(T)$. This approximation will be particularly good for small values of $\alpha\sqrt{T}$ where I_{00} is much larger than all other values of I_{mn}. When we only consider the first term of the series we find that

$$\frac{1}{A_0}\frac{\mathrm{d}A_0}{\mathrm{d}T} = \frac{\alpha R\mathrm{Pe}_\parallel}{2\pi} I_{00} = \frac{R\mathrm{Pe}_\parallel \alpha}{2}\mathrm{e}^{2\alpha^2 t/\mathrm{Pe}_\parallel}\mathrm{erfc}\Big(\alpha\sqrt{2t/\mathrm{Pe}_\parallel}\Big) \tag{2.55}$$

The rate of change of A_0 is a measure of the global growth rate, in that it measures the rate of growth of the total magnitude of the disturbance. The local growth-rate will differ from the global growth-rate due to spreading of the disturbance. The total magnitude of the disturbance to concentration is given by

$$C^*(t) = \int_{-\infty}^{\infty} C(\xi,t)\,\mathrm{d}\xi = 2\sqrt{\pi}A_0(T)\mathrm{e}^{-\alpha^2\frac{\mathrm{Pe}_\parallel}{\mathrm{Pe}_\perp}T}.$$

After redimensionalisation we find that the rate of growth of the total magnitude of the disturbance is given by

$$\sigma = \frac{1}{C^*}\frac{\partial C^*}{\partial t} = -\alpha^2 D_\perp + \frac{RU}{2}\alpha \mathrm{e}^{2D_\parallel \alpha^2 t}\mathrm{erfc}\big(\alpha\sqrt{2D_\parallel t}\big). \tag{2.56}$$

There is a key non-dimensional variable, $\alpha\sqrt{D_\parallel t}$. When $\alpha\sqrt{D_\parallel t} \ll 1$, i.e. the wavelength of the disturbance is much larger than the diffusive length scale associated with the spreading of the base-state, we see that the growth rate is given by

$$\sigma = -\alpha^2 D_\perp + \frac{RU}{2}\alpha,$$

with the second term being similar to the instability present in the Muskat problem (1.22). For large values of $\alpha\sqrt{D_\parallel t}$ the growth rate is given by

$$\sigma = -\alpha^2 D_\perp + \frac{RU}{2\sqrt{2\pi D_\parallel t}},$$

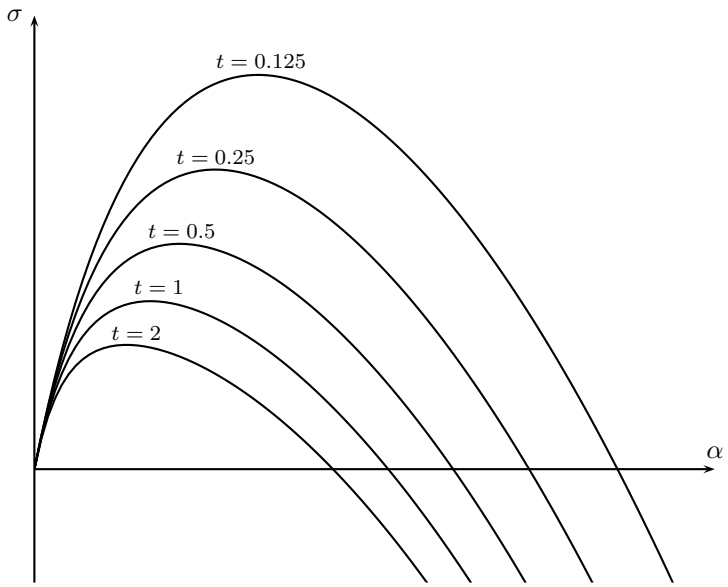

Figure 2.6: Changing dispersion relation over time, as given by Wooding's stability analysis (2.56).

and so the second term does not grow large with α, but instead only depends on the length scale associated with the spreading of the base state. This behaviour is similar to the behaviour that we predicted of the multilayer Muskat problem when the number of layers became large in section 2.2.1.

Crucially the linear problem is no longer ill-posed, due to the combined effects of longitudinal and transverse diffusion. There is a cutoff wavenumber, with all larger wavenumbers being stable, and there is a least-stable wavenumber, for which the growth rate is largest. For a general initial disturbance we expect to observe disturbances with a wavenumber close to the least-stable wavenumber. We have already seen that, for oil recovery applications, both $\mathrm{Pe}_{\|}$ and $\mathrm{Pe}_{\perp}$ will be large. We find that at these large wavenumbers the cutoff wavenumber, $\alpha_c = O(\mathrm{Pe}^{3/4})$, with

$$\alpha_c \sim \frac{R^{1/2}\mathrm{Pe}_{\|}^{3/4}}{2^{3/4}\delta^{1/2}\pi^{1/2}t^{1/2}},$$

where $\delta = \mathrm{Pe}_{\|}/\mathrm{Pe}_{\perp}$. The least-stable wavenumber α_m is of $O(\mathrm{Pe}^{5/8})$ and is given by

$$\alpha_m \sim \frac{R^{1/4}\mathrm{Pe}_{\|}^{5/8}}{4^{1/4}\delta^{1/4}\pi^{1/8}(2t)^{3/8}}.$$

2.2.4 The work of Hickernell and Yortsos

In the paper due to Homsy [55], it is suggested that the "quasi-steady-state assumption" (QSSA) might be useful in studying the pair of equations (2.51) and (2.52); the QSSA assumes that the rate of growth of the disturbances is much larger than the rate at which the base state changes. The QSSA applies to this problem when $\mathrm{Pe}_{\|} \gg 1$ and the initial concentration profile is smooth. However, since we are considering an initially sharp concentration profile, the rate of growth of the base state is large for $t = o(\mathrm{Pe}_{\|})$ and the QSSA does not hold.

The QSSA is useful in investigating the stability when the initial concentration profile is not sharp. This allows us to gain an understanding of the effect of longitudinal diffusion without having to assume that the difference in viscosities is small. The non-sharp initial profile is also of more direct practical interest in some enhanced oil recovery applications, because one technique applied to improve the yield from secondary recovery processes is to introduce a polymer which allows the viscosity of the injected solution to be controlled. We shall now show why a slowly changing viscosity profile may be preferable to a sharp jump in the viscosity.

When there is an initially smooth concentration profile and $\mathrm{Pe}_{\|} \gg 1$ the solution to (2.48) is of the form

$$c \sim c_0(\xi) + \frac{1}{\mathrm{Pe}_{\|}} c_1(\xi, t) + \dots ,$$

where $\xi = x - t$. This solution is valid provided $t = o(\mathrm{Pe}_{\|})$. The leading-order base-state pressure is also time-independent and is given by

$$p_0 = -\int^{\xi} \mu(c_0)\, \mathrm{d}\xi.$$

Our base state is now time-independent, and as the effect of diffusion is negligible the stability analysis of Hickernell & Yortsos [24] applies. Since the base-state is time-independent we may seek a perturbed solution satisfying the ansatz,

$$c \sim c_0(\xi) + \epsilon \Re\left(C(\xi) \mathrm{e}^{\mathrm{i}\alpha y + \sigma t}\right) + O\left(\epsilon^2, \frac{1}{\mathrm{Pe}_{\|}}\right),$$
$$p \sim p_0(\xi) + \epsilon \Re\left(P(\xi) \mathrm{e}^{\mathrm{i}\alpha y + \sigma t}\right) + O\left(\epsilon^2, \frac{1}{\mathrm{Pe}_{\|}}\right),$$

where $\frac{1}{\mathrm{Pe}_{\|}} \ll \epsilon \ll 1$, and α is real and, without loss of generality, positive. On substituting this ansatz into (2.32),(2.47) we find that,

$$\frac{\mathrm{d}}{\mathrm{d}\xi}\left(\frac{1}{\mu(c_0)}\frac{\mathrm{d}\mu}{\mathrm{d}c}(c_0)C + \frac{1}{\mu(c_0)}\frac{\mathrm{d}P}{\mathrm{d}\xi}\right) - \frac{\alpha^2}{\mu(c_0)}P = 0, \tag{2.57}$$

$$\sigma C - \frac{1}{\mu(c_0)}\frac{\mathrm{d}\mu}{\mathrm{d}c}(c_0)\frac{\mathrm{d}c_0}{\mathrm{d}\xi}C - \frac{1}{\mu(c_0)}\frac{\mathrm{d}c_0}{\mathrm{d}\xi}\frac{\mathrm{d}P}{\mathrm{d}\xi} = 0. \tag{2.58}$$

We can eliminate C to obtain the equation

$$\frac{\mathrm{d}}{\mathrm{d}\xi}\left(\frac{\sigma\frac{\mathrm{d}P}{\mathrm{d}\xi}}{\sigma\mu(c_0) - \frac{\mathrm{d}\mu}{\mathrm{d}c}(c_0)\frac{\mathrm{d}c_0}{\mathrm{d}\xi}}\right) = \frac{\alpha^2}{\mu(c_0)}P. \tag{2.59}$$

Following Hickernell & Yortsos [24] we introduce a stream function defined by

$$\frac{\mathrm{d}\psi}{\mathrm{d}\xi} = \frac{P}{\mu(c_0)}.$$

After integrating (2.59) we obtain

$$\frac{\mathrm{d}}{\mathrm{d}\xi}\left(\mu_0\frac{\mathrm{d}\psi}{\mathrm{d}\xi}\right) = \alpha^2\left(\mu_0 - \frac{1}{\sigma}\frac{\mathrm{d}\mu_0}{\mathrm{d}\xi}\right)\psi,$$

where $\mu_0(\xi) = \mu(c_0(\xi))$. Since $\mu_0 > 0$ we may simplify the problem further by introducing a new variable, X such that $\mathrm{d}X = \mathrm{d}\xi/\mu_0$, obtaining

$$\frac{\mathrm{d}^2\psi}{\mathrm{d}X^2} = \alpha^2\left(\mu_0^2 - \frac{1}{\sigma}\frac{\mathrm{d}\mu_0}{\mathrm{d}X}\right)\psi. \tag{2.60}$$

We also need the disturbance to decay as $\xi \to \pm\infty$ and so require that ψ tends to zero as $X \to \pm\infty$.

As noted in the paper by Hickernell & Yortsos [24], for there to exist a nontrivial solution to (2.60) with decaying boundary conditions at infinity, we require that, for some X, the coefficient of ψ on the right-hand side of (2.60) must be negative[3]. We therefore require that for some X

$$\sigma < \frac{1}{\mu_0^2}\frac{\mathrm{d}\mu_0}{\mathrm{d}X},$$

or equivalently, for some ξ,

$$\sigma < V(\xi) = \frac{1}{\mu_0}\frac{\mathrm{d}\mu_0}{\mathrm{d}\xi}.$$

The growth rate is therefore bounded by

$$\sigma < \sigma_m = \sup_{\xi} V(\xi). \tag{2.61}$$

This result is in contrast to the stability analysis of section 1.3.1 in which μ_0 is a step

[3]It is easy to see that the coefficient of ψ on the right-hand side of (2.60) must be nonpositive. For there to be a nontrivial solution, $\psi(X)$ must have either a maximum with $\psi > 0$ or a minimum with $\psi < 0$. In either case we require that the coefficient of ψ on the right-hand side of (2.60) must be nonpositive.

function and we see from (1.22) that the growth rate may grow unboundedly for large-wavenumber disturbances.

2.2.4.1 Small wavenumber disturbances

We consider the case of $\alpha \ll 1$. As a direct result of the bounds on the rate of growth considered in [24] we can conclude that $\sigma = O(\alpha)$. We therefore have an expansion for σ,

$$\sigma \sim \sigma_1\alpha + \sigma_2\alpha^2 + \dots .$$

We first look at outer solutions away from $X = 0$. We make the scaling $X = x/\alpha$ and assume that the derivative of c_0 decays exponentially fast at infinity. Our outer problems are

$$\frac{\mathrm{d}^2\psi^{\pm}}{\mathrm{d}x^2} = \mu_{\pm}^2\psi^{\pm},$$

where $\psi^{\pm}$ are the solutions for X large and positive/negative respectively and $\mu_{\pm}$ represents the limiting value of μ as $X \to \pm\infty$. We introduce the expansions

$$\psi^{\pm} \sim \psi_0^{\pm} + \alpha\psi_1^{\pm} + \dots ,$$

and obtain the solutions

$$\psi_0^{\pm} = \Psi_0^{\pm}\exp(\mp\mu_{\pm}x), \quad \psi_1^{\pm} = \Psi_1^{\pm}\exp(\mp\mu_{\pm}x),$$

where $\Psi_0^{\pm}$, $\Psi_1^{\pm}$ are constants. In the inner region where $X = O(1)$, we have the expansion

$$\psi \sim \psi_0 + \alpha\psi_1 + \dots ,$$

and find to leading order

$$\frac{\mathrm{d}^2\psi_0}{\mathrm{d}X^2} = 0.$$

The only solution that can match with our outer solutions is a constant. This constant is arbitrary and so, without loss of generality, we have

$$\psi_0 = \Psi_0^{\pm} = 1.$$

The next order equation is

$$\sigma_1\frac{\mathrm{d}^2\psi_1}{\mathrm{d}X^2} = -\frac{\mathrm{d}\mu_0}{\mathrm{d}X},$$

so that

$$\sigma_1\frac{\mathrm{d}\psi_1}{\mathrm{d}X} = -\mu_0 + \text{constant}.$$

Matching with the outer solutions gives

$$\sigma_1 = \frac{\mu_+ - \mu_-}{\mu_+ + \mu_-},$$

and so for our problem where $\mu_+ = 1$ and $\mu_- = 1/M$, the growth rate for small wavenumbers is given by

$$\sigma = \frac{M-1}{M+1}\alpha. \tag{2.62}$$

This is the same dispersion relation as for the moving boundary problem as given by (1.22).

2.2.4.2 Large wavenumber disturbances

For large wavenumbers, the growth rate will approach the bound (2.61), i.e.

$$\sigma \sim \sigma_m = \sup_\xi \frac{1}{\mu_0}\frac{\mathrm{d}\mu_0}{\mathrm{d}\xi}, \quad \text{for} \quad \alpha \gg 1,$$

as we shall now demonstrate. We write

$$Q(X) = \mu_0^2 - \frac{1}{\sigma}\frac{\mathrm{d}\mu_0}{\mathrm{d}X},$$

so that (2.60) becomes

$$\frac{\mathrm{d}^2\psi}{\mathrm{d}X^2} = \alpha^2 Q(X)\psi. \tag{2.63}$$

For $\alpha \gg 1$, we may apply the WKB method, seeking a solution that satisfies the WKB ansatz,

$$\psi(X) = \Re\left(A(X)\mathrm{e}^{\alpha u(X)}\right).$$

We find that

$$\frac{\mathrm{d}u}{\mathrm{d}X} = \pm\sqrt{Q(X)}$$

and

$$A(X) \propto Q(X)^{-1/4}.$$

If $Q(X)$ is always strictly positive then our WKB ansatz is always valid and there are no nontrivial solutions which decay as $X \to \pm\infty$, as shown earlier. There are therefore no nontrivial solutions to (2.63) with $\alpha \gg 1$ unless $Q(X) \leq 0$ for some X.

We define the function

$$Q_m(X) = \mu_0(X)^2 - \frac{1}{\sigma_m}\frac{\mathrm{d}\mu_0}{\mathrm{d}X}(X),$$

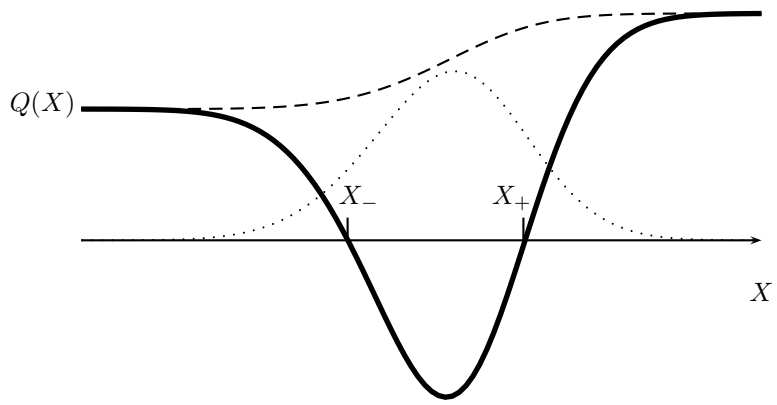

Figure 2.7: A typical form of the function $Q(X)$. The dashed line shows μ_0^2 and the dotted line shows $\frac{\mathrm{d}\mu_o}{\mathrm{d}X}$.

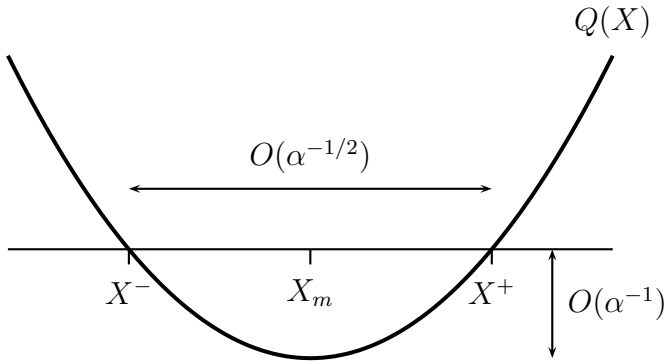

Figure 2.8: Turning points of $Q(X)$.

where σ_m is the bounding value of the growth rate. By construction $Q_m(X) = 0$ for precisely one value of X, X_m (assuming that the viscosity profile is monotonic) and $Q_m > 0$ for all other values of X. When $\sigma = \sigma_m$ we must rescale near $X = X_m$, to find an inner problem where $X - X_m = O(\alpha^{-1/2})$. We find that the inner problem has no solution that can match with our WKB expansions. The maximum value of σ that gives us a solution must therefore be slightly smaller than σ_m so that $Q(X) < 0$ near $X = X_m$.

Since the size of the region in which the WKB approximation is not valid is of order $\alpha^{-1/2}$ we consider a situation in which two turning points are separated by a distance of $O(\alpha^{-1/2})$. Since Q_m takes its minimum value at $X = X_m$, this will occur when $\sigma_m - \sigma = O(\alpha^{-1})$ as shown in Figure 2.8. Writing

$$\sigma = \sigma_m - \frac{S}{\alpha},$$

(2.60) becomes

$$\frac{\mathrm{d}^2\psi}{\mathrm{d}X^2} = \alpha^2 \left(Q_m(X) - \frac{S}{\sigma_m^2 \alpha} \frac{\mathrm{d}\mu_0}{\mathrm{d}X}(X) \right) \psi.$$

Applying the WKB ansatz

$$\psi \sim A(X) \exp\left(\alpha u(X)\right),$$

gives

$$\frac{\mathrm{d}u}{\mathrm{d}X} = \pm\sqrt{Q_m(X)},$$

and so applying boundary conditions at infinity we find that

$$u(X) = -\int_{X_m}^{X} \sqrt{Q_m(X)}\,\mathrm{d}X, \quad \text{for} \quad X > X_m, \tag{2.64}$$

$$u(X) = \int_{X_m}^{X} \sqrt{Q_m(X)}\,\mathrm{d}X, \quad \text{for} \quad X < X_m. \tag{2.65}$$

Note that $Q_m \geq 0$ for all X and so we find no highly oscillatory solutions; however, since $Q_m(X_m) = 0$ the WKB expansion will not be valid for X close to X_m. At next order we find that A satisfies

$$\frac{\mathrm{d}A}{\mathrm{d}X} = \left(\pm\frac{S}{2\sigma_m^2} \frac{1}{\sqrt{Q_m(X)}} \frac{\mathrm{d}\mu_0}{\mathrm{d}X} - \frac{1}{4Q_m(X)} \frac{\mathrm{d}Q_m}{\mathrm{d}X} \right) A, \tag{2.66}$$

in $X \lessgtr X_m$. We find that

$$A(X) = \frac{A_\pm}{Q_m(X)^{1/4}} \exp\left(\pm\frac{S}{2\sigma_m^2} \int_{X_m}^{X} \frac{1}{2\sqrt{Q_m(X)}} \frac{\mathrm{d}\mu_0}{\mathrm{d}X}(X)\,\mathrm{d}X \right) \quad \text{in} \quad X \lessgtr X_m. \tag{2.67}$$

We now rescale X near X_m, writing $X - X_m = \alpha^{-1/2} x$, and Taylor expand Q_m near X_m. We find that ψ satisfies

$$\frac{\mathrm{d}^2\psi}{\mathrm{d}x^2} = \left(x^2 \frac{\mathrm{d}^2 Q_m}{\mathrm{d}X^2}(X_m) - \frac{S}{\sigma_m^2} \frac{\mathrm{d}\mu_0}{\mathrm{d}X}(X_m) \right) \psi,$$

and so rewriting $x = Q_m''(X_m)^{1/4} r$ we find that

$$\frac{\mathrm{d}^2\psi}{\mathrm{d}r^2} = (r^2 - c^2)\psi, \tag{2.68}$$

where

$$c^2 = \frac{S}{\sigma_m^2 Q_m''(X_m)^{1/2}} \frac{\mathrm{d}\mu_0}{\mathrm{d}X}(X_m). \tag{2.69}$$

Equation (2.68) is the famous equation for the quantum harmonic oscillator and for

parabolic cylinder functions, and it is well known that this equation only possesses non-trivial solutions, decaying as $r \to \pm\infty$, when c^2 is an odd integer. When $c^2 = 2n+1$ the solution is

$$\psi(r) = H_n(r)\exp(-r^2/2),$$

where H_n is the nth Hermite polynomial. We must now check that the inner solution matches with our outer WKB expansion. We introduce an intermediate variable

$$X - X_m = \alpha^{-1/4} Q_m''(X_m)^{1/4} s,$$

so that $r = \alpha^{1/4}s$. In the inner region, expanding in the intermediate variable with $s = O(1)$ gives

$$\psi \sim 2^n \alpha^{n/4} s^n \mathrm{e}^{-\alpha^{1/2}s^2/2}.$$

In the outer WKB regions, expanding in the intermediate variables gives

$$\psi \sim \frac{A_\pm \alpha^{1/8}}{Q_m''(X_m)^{3/8} s^{1/2}} \exp\left(\frac{S}{2\sigma_m^2 Q_m''(X_m)^{1/2}} \frac{\mathrm{d}\mu_0}{\mathrm{d}X}(X_m)\log s\right) \mathrm{e}^{-\alpha^{1/2}s^2/2},$$

but applying (2.69) this is simply

$$\psi \sim \frac{A_\pm \alpha^{1/8} s^n}{Q_m''(X_m)^{3/8}} \mathrm{e}^{-\alpha^{1/2}s^2/2},$$

and so the inner solution can be matched with the outer solution.

The maximum growth rate occurs when $c^2 = 1$ so that

$$\sigma = \sigma_m - \frac{\sigma_m^2}{\alpha}\left(\frac{\mathrm{d}^2 Q_m}{\mathrm{d}X^2}(X_m)\right)^{1/2} \frac{\mathrm{d}\mu_0}{\mathrm{d}X}(X_m). \tag{2.70}$$

For large wavenumbers the maximum growth rate of instabilities is almost constant. Hence, although for small wavenumber disturbances the growth rate is identical to that of the moving boundary analysis, it is very different for large wavenumbers. The most important consequence of the boundedness of the growth rate is that, following the arguments of section 1.3.2, we see that the linearised problem is well-posed.

2.2.4.3 Transverse diffusion

For sufficiently large α, we will have $\alpha^2 = O(\mathrm{Pe})$ and we then expect transverse diffusion to become important. Unfortunately we cannot simply extend this analysis to this case. To be able to perform linear stability analysis and obtain a global growth rate we require:

1. A base state that is time independent. This yields the requirement that $1/\mathrm{Pe} \ll \epsilon$.

2. Our resulting problem must be linear and to ensure that this is the case we require that $\alpha^2 \ll 1/\epsilon$.

These two requirements lead us to the conclusion that we must have $\alpha^2 \ll \mathrm{Pe}$ to be able to carry out a linear stability analysis.

However, it is possible to see the effect of transverse diffusion if we neglect the terms involving longitudinal diffusion in (2.47), yielding

$$\frac{\partial c}{\partial t} + \nabla \cdot (\mathbf{u}c) = \frac{1}{\mathrm{Pe}} \frac{\partial^2 c}{\partial y^2}.$$

We can use the same base state as before, (2.57) still holds and (2.58) becomes

$$\sigma C - \frac{1}{\mu(c_0)} \frac{\mathrm{d}\mu}{\mathrm{d}c}(c_0) \frac{\mathrm{d}c_0}{\mathrm{d}\xi} C - \frac{1}{\mu(c_0)} \frac{\mathrm{d}c_0}{\mathrm{d}\xi} \frac{\mathrm{d}P}{\mathrm{d}\xi} = -\frac{\alpha^2}{\mathrm{Pe}} C.$$

We observe that if we write

$$\tilde{\sigma} = \sigma + \frac{\alpha^2}{\mathrm{Pe}},$$

we recover the equations (2.57),(2.58) with σ replaced by $\tilde{\sigma}$. We conclude that for $\alpha \ll 1$

$$\sigma \sim \tilde{\sigma} \sim \frac{M-1}{M+1}\alpha + O(\alpha^2),$$

and for $\alpha \gg 1$

$$\sigma \sim \tilde{\sigma} - \frac{\alpha^2}{\mathrm{Pe}} \sim -\frac{\alpha^2}{\mathrm{Pe}} + \sigma_m - \frac{\sigma_m^2}{\alpha} \left(\frac{\mathrm{d}^2 Q_m}{\mathrm{d}X^2}(X_m) \right)^{1/2} \frac{\mathrm{d}\mu_0}{\mathrm{d}X}(X_m)., \tag{2.71}$$

where σ_m is as defined in (2.61). With $\mathrm{Pe} \gg 1$ the cutoff wavenumber, beyond which all disturbances are stable, is given by $\alpha_c \sim \sqrt{\sigma_m}\mathrm{Pe}^{1/2}$. The least-stable wavenumber for which the disturbance grows at the fastest rate is given by

$$\alpha_m = \left(\frac{\sigma_m^2 Q_m''(X_m)}{2} \right)^{1/3} \left(\frac{\mathrm{d}\mu_0}{\mathrm{d}X}(X_m) \right)^{-1/2} \mathrm{Pe}^{1/3}.$$

2.3 Numerical solutions

There have been several numerical simulations of the Peaceman model. The Peaceman model is numerically simulated by first solving for the pressure field for a given concentration and then updating the concentration field. Various numerical techniques have been applied to model the evolution of the concentration of solvent, such as finite difference methods and finite volume methods [46, 62] and spectral methods [56]. We have elected

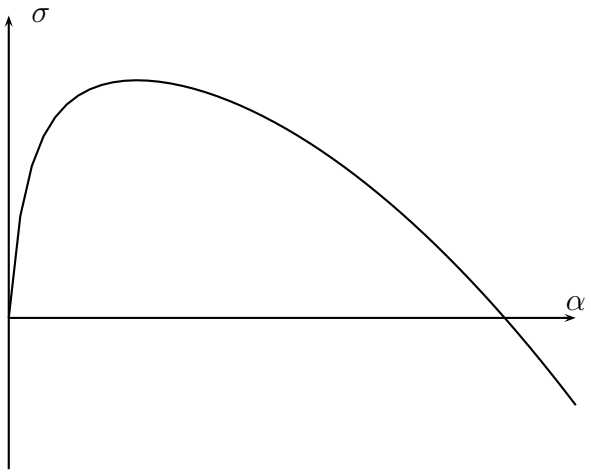

Figure 2.9: Sketch of the dispersion relation as given by (2.71).

to apply finite-volume techniques in our simulations of the Peaceman model. The finite-volume method is a natural method to use for solving hyperbolic problems and, in the large Péclet number limit, the equation for the advection of the solvent is approximately hyperbolic. Full details of the method that we have used are available in appendix A, but we present here a brief summary of the method used to give an idea of some of the challenges that are presented by numerical simulation of the Peaceman model.

At each time step we first solve for the pressure field, using the concentration field from the previous time step to determine the viscosity. Once we have solved for the pressure field, we can find the velocity of the fluid and proceed to advect the concentration of solvent. The greatest difficulty that we find with our finite-volume scheme is that in modelling the evolution of the concentration of solvent, our scheme produces an artificial numerical diffusion. The magnitude of the numerical diffusion is small, but the physical diffusion is also small. Our stability analysis has led us to expect that disturbances will form in which their length scale is determined by the magnitude of diffusion in the problem. It is for this reason that we need to be particularly careful about the magnitude of numerical diffusion. To ensure that we are accurately modelling diffusion, we must ensure that the numerical diffusion is much smaller than the physical diffusion. To minimise the numerical diffusion we have used a corner-transport upwinding scheme with a high-resolution flux-limiter, as may be found in [35], to simulate the transport of solvent by advection. It has also proved necessary to restrict ourselves to consider two-dimensional problems. Accurate simulation of fingering in three-dimensional miscible displacements remains a significant numerical challenge. When considering unidirectional flow through a homogeneous porous medium, we also move into travelling coordinates and have implemented the largest time-step satisfying the Courant condition. Both of these steps help to reduce the magnitude of numerical diffusion. Once the advective part of the evolution

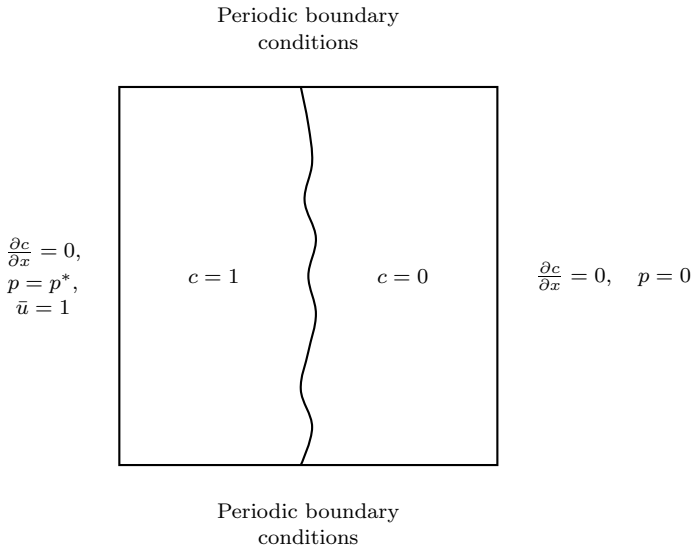

Figure 2.10: Schematic of the computational domain.

of concentration has been simulated, we can add the physical diffusion to the problem, concluding the time-step.

For most of our numerical simulations we have simply assumed that the diffusion tensor is constant. We have already suggested that this is appropriate when considering linearised stability problems. In practice we expect that the diffusion tensor will not be constant. It has been shown in previous numerical simulations [64, 65] that physically-reasonable changes to the magnitude and velocity-dependence of longitudinal diffusion does not, at least for large Péclet number, significantly change the solution.

We solve a linear flood problem so that the flow is essentially one-dimensional, as shown in Figure 2.10. Since the flow is essentially one-dimensional, the direction of longitudinal diffusion is always in the x-direction. Since the magnitude of the longitudinal diffusion was not found to be important in [64] we have usually taken the diffusion to be isotropic.

In our numerical simulations the fingering instability is initiated by a small random disturbance to the initial sharp interface, as applied in [56]. An example of the initial interface used is presented in Figure 2.11. The fingering instability could also have been initiated by including a slightly heterogeneous permeability as in [46, 62] with similar results, but note that heterogeneity is not required to drive the instability, only to initiate it. If no effort is made to initiate the disturbance then the upwinding part of our numerical scheme will be exact for this particular problem, and so we cannot rely on numerical errors to initiate the instability.

Our numerical simulations show the formation of many long, thin fingers whenever there is an adverse mobility ratio (see Figure 2.12). We also find that the rate of growth of the fingers increases as the mobility ratio between the solvent and the oil increases.

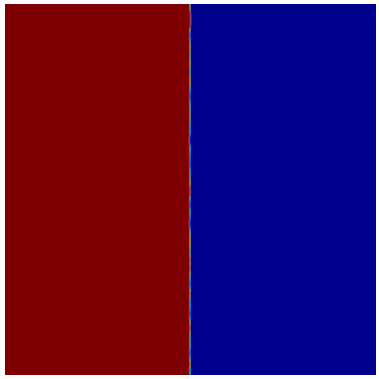

Figure 2.11: Initial condition for the concentration of solvent, with red representing the solvent ($c = 1$) and blue representing the oil ($c = 0$). The (barely visible) changes to the concentration at the interface initiate the fingering instability.

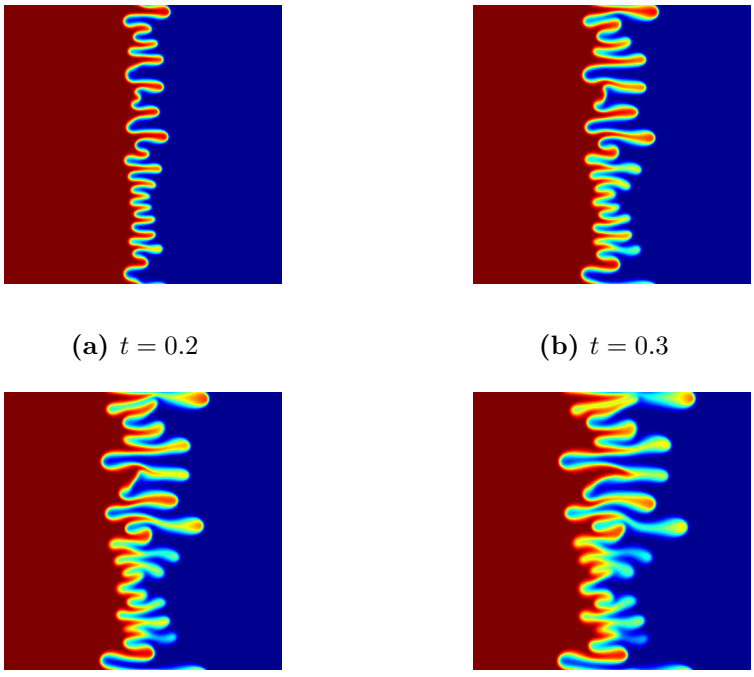

(a) $t = 0.2$ **(b)** $t = 0.3$

(c) $t = 0.4$ **(d)** $t = 0.5$

Figure 2.12: Numerical simulation of the Peaceman model for an unstable miscible displacement. Here $M = 5$ and $\mathrm{Pe} = 2000$, with red representing the less viscous solvent ($c = 1$) and blue representing the more viscous, oil ($c = 0$).

Our linear stability analysis has provided suggestions for the typical wavenumber of the disturbances, and it is interesting to see if the numerical results for the nonlinear growth of finger-like disturbances agree. To provide a measurement of the number of fingers we

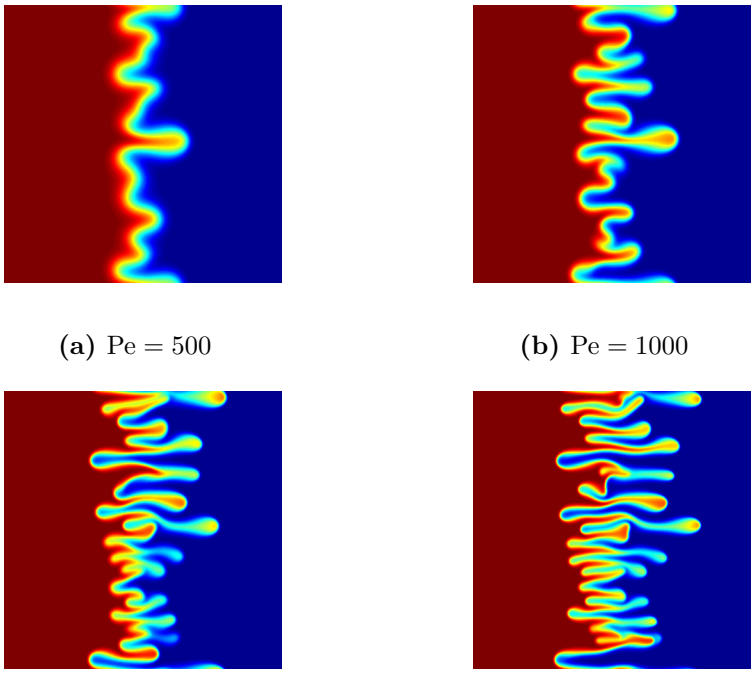

(a) Pe = 500 **(b)** Pe = 1000

(c) Pe = 2000 **(d)** Pe = 3000

Figure 2.13: Numerical simulation of an unstable miscible displacement for various values of the Péclet number. Here $M = 5$ and $t = 0.5$, with red representing the less viscous solvent ($c = 1$) and blue representing the more viscous, oil ($c = 0$).

use a 'perimeter' function,

$$P = \frac{1}{2}\int_0^1 \left|\frac{\partial c}{\partial y}\right| \mathrm{d}y, \tag{2.72}$$

as suggested in [39]. This function gives a measure of the number of times that the concentration varies from 0 to 1 as y increases. In Figure 2.14 we show how P varies as we vary Pe. The gradient of the log-log plot suggests that, for large Péclet number, $P \propto \mathrm{Pe}^{1/2}$. The linear stability analysis will not be valid at this stage; however, we find the dependence of the wavenumber on Pe is in agreement with the cutoff wavenumber obtained from (2.71).

While we have shown that it is possible to simulate the detailed fingering patterns produced by the Peaceman model, it may not be numerically feasible to simulate the detailed fingering patterns for a three-dimensional simulation over an entire oil reservoir. The detailed fingering pattern is not of practical interest in oil recovery, and it is only the averaged flow of solvent and oil through the reservoir that is of interest. The existence of fingers is, however, important since they will lead to both earlier breakthrough of solvent than one would find for a stable interface, and since they will lead to enhanced mixing of the solvent and oil. It appears that the detailed structure of the fingers is random; however, it has been observed [62, 56, 64, 65] that, at least for large Péclet numbers, the

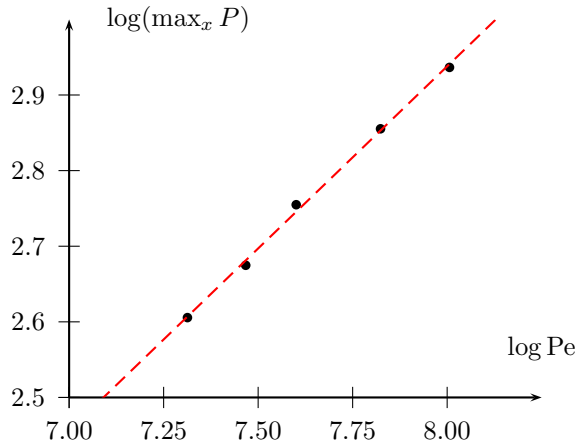

Figure 2.14: Log-log plot of the number of fingers as a function of the Péclet number, $M = 5$, $t = 0.5$. In these simulations we have assumed that the diffusion is isotropic and constant. The dashed, red line represents the line of best fit to the numerical results, and has a gradient of 0.48.

average of the concentration of solvent, transverse to the direction of flow, is independent of the precise fingering pattern. In Figure 2.15 we present several simulations, with the only change between them being the random disturbance that initialised the instability. It is clear that the different simulations each give a different fingering pattern, but qualitative, averaged features are consistent between the various simulations. In Figure 2.16 we present the transverse average of the concentration profile of the simulations shown in Figure 2.15. The transverse average appears fairly consistent between the simulations, and it appears [56] that with increasing Pe, the total number of fingers becomes large, and the transverse average of the concentration becomes deterministic and hence predictable. In Chapter 3 we shall attempt to develop models that predict the averaged concentration, allowing us to avoid the detailed numerical simulations of this section.

2.4 Conclusions

In this chapter we have derived the Peaceman model from consideration of the microscale behaviour at the pore-scale. Since the Peaceman model may be derived in this systematic fashion, we view it as the fundamental model for miscible displacements in porous media. Fluid flowing through a porous medium leads to an enhanced diffusion that is the result of an interaction between the rapidly varying velocity of the fluid at the pore-scale and molecular diffusion. This enhanced diffusion is referred to as hydrodynamic dispersion. The hydrodynamic dispersion is anisotropic, with the largest component longitudinal to the direction of flow. Microscale variations in the permeability will also contribute to an enhanced hydrodynamic dispersion, by a similar mechanism to that which yields hy-

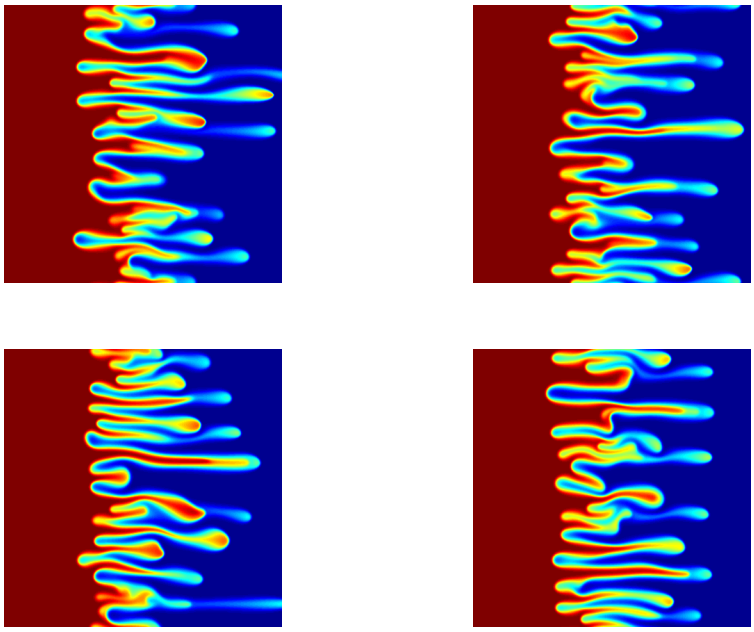

Figure 2.15: Numerical simulations of an unstable miscible displacement with slightly different initial conditions. Here $M = 10$, $\mathrm{Pe} = 2500$ and $t = 0.5$, with red representing the less viscous solvent ($c = 1$) and blue representing the more viscous, oil ($c = 0$).

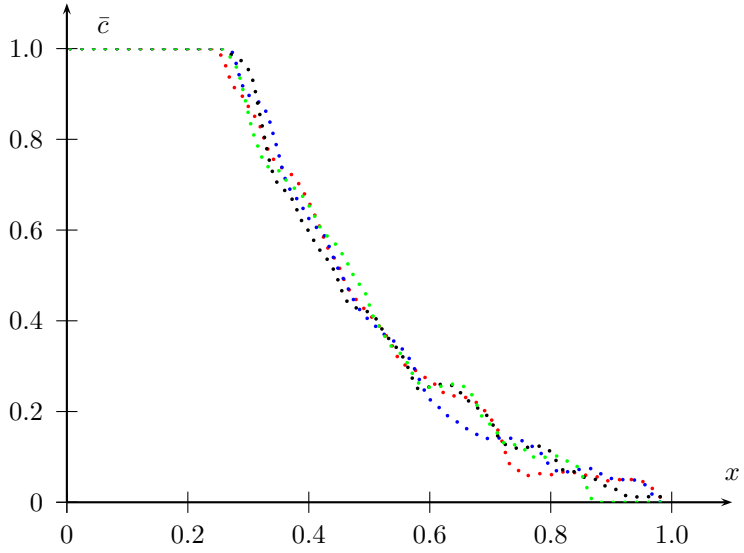

Figure 2.16: Transverse average of the numerical simulations presented in Figure 2.15, with each different colour representing a different simulation

drodynamic dispersion at the pore-scale. Permeability variations may also lead to the magnitude of diffusion depending on the length scale of the problem, and this property has been observed in field-scale data [22]. Although the magnitude of the effective dif-

fusion may increase over increasing length scales, we have shown that, nevertheless, the magnitude of the macroscale Péclet number will increase as the length scale of the problem increases. For miscible displacements used in the oil recovery industry, the Péclet number will be large, and the flow will be convection dominated.

We have confirmed that the Muskat problem may be obtained as a singular limit of the Peaceman model. We therefore expect that the Peaceman model will exhibit small-wavelength instabilities, although we anticipate that the introduction of diffusion may regularise the problem, and prevent the ill-posedness that was observed of the linearised Muskat problem. We have investigated the linear stability properties of one-dimensional solutions of the Peaceman model. We found that there are two mechanisms by which diffusion acts to prevent the large growth rates of small wavelength disturbances. The first mechanism is that transverse diffusion causes large wavenumber disturbances to decay. The second mechanism is a consequence of the ability of longitudinal diffusion to smear out the sharp jump in the concentration of solvent. When the wavelength of the disturbance is comparable to the size of the diffuse region between the solvent and oil, the growth rate is constant and does not continue to increase with increasing wavenumber. Either of the two mechanisms is sufficient to prevent the ill-posedness of the linearised Muskat problem, and together they lead to a characteristic length scale for the wavelength of the disturbances.

Our numerical simulations support the predictions of our stability analysis. At large Péclet number we have found that a large number of finger-like disturbances are formed. It is not numerically feasible to accurately simulate these fingers at the scale of an entire oil-reservoir; however any numerical simulation of the Peaceman model that does not simulate these fingers will underpredict the spread of the solvent into the oil. The detailed behaviour of the fingers appears to be very complicated but our numerical simulations support previous works [56, 64, 65, 62] that have observed that, at least for large Pe, the transverse average of the concentration is independent of the detailed fingering pattern. The detailed fingering pattern is not particularly important for practical purposes, but the prediction of the evolution of the averaged concentration of solvent through the reservoir certainly is. Our next chapter will therefore be devoted to trying to understand why, for large Pe, the average concentration of solvent is independent of the detailed fingering behaviour, and attempting to develop an averaged model for the spreading of the solvent through the reservoir.

Chapter 3

Unidirectional fingering

We have seen in the last chapter that numerical simulation of the Peaceman model leads to the formation of many thin fingers. Although detailed features of the fingers are sensitive to small disturbances in the initial condition, it nevertheless seems to be the case that the averaged behaviour is independent of this detailed information.

Accurate simulation of the Peaceman model at the scale of an entire oil reservoir is numerically intractable. As we have seen in Chapter 2, when the numerical simulation of the Peaceman model is performed on too coarse a scale, we do not correctly reproduce the fingering behaviour observed in finer scale simulations, and consequently we underpredict the rate of growth of the mixing zone. Since we cannot accurately model all the details of the fingering, we instead aim to produce a model for the average concentration of solvent which faithfully reproduces the correct rate of growth of the mixing zone as predicted by the fine scale simulations.

In this chapter we shall develop models that describe the evolution of the mean concentration of an essentially one-dimensional flow, in which the fingers are unidirectional. We show that, for there to be a sensible averaged model, there must be a large number of fingers and that this corresponds to the large Péclet number limit. In the large Péclet number limit we are able to formally derive a homogenised model for the mixing zone, with the pressure given explicitly in terms of the concentration of solvent. By averaging this homogenised model we develop a naïve version of the Koval model, and demonstrate the regrettable fact that this model significantly overpredicts the rate of growth of fingers due to the important rôle of diffusion. In the oil industry this problem has been largely overcome by the introduction of an empirical assumption, but there is as yet in the literature no clear explanation as to why this assumption works. The key difficulty that arises in developing a model for the evolution of the mean concentration lies in finding canonical solutions of the homogenised model.

We will show that when the mobility ratio between the two fluids is close to 1 we

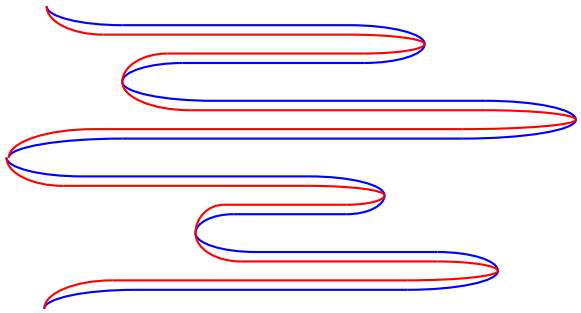

Figure 3.1: Idealised morphology of numerical simulations of the Peaceman model. The red line represents a contour for a high concentration of solvent and the blue line represents a contour for a low concentration of solvent.

recover a somewhat simpler model, that has previously been investigated by Wooding [61] in relation to fingering driven by density differences inside an inclined Hele-Shaw cell. We find a particular solution to this simplified problem which exhibits shock solutions. Our numerical simulations suggest that the formation of these shocks is a generic feature of our homogenised model for the mixing zone. However, a difficulty arises in determining the correct shock conditions, and this is the fundamental problem that must be solved to determine the correct growth rate of the mixing zone. We shall attempt to derive appropriate shock conditions by rescaling near the finger tips and finger roots. In contrast to previous works, [39, 63], this rescaling involves the reversion to the full flow problem in the vicinity of the finger tip/root, rather than the reintroduction of longitudinal diffusion.

3.1 Background Ideas

In the large Péclet number limit, our numerical simulations of the Peaceman model in section 2.3 produced many thin fingers with clearly defined roots and tips. An idealised morphology of the fingers is shown in Figures 3.1 and 3.2. The existence of many thin fingers suggests that a "mushy region" or "homogenised" model may be applied, at least away from the roots and tips of individual fingers. The small finger width leads to a concentration of solvent that varies rapidly across the fingers, and consequently a viscosity that varies rapidly across the fingers. We expect that this rapidly-varying viscosity will lead to a homogeneous pressure, in exactly the same way that a rapidly-varying permeability did in section 1.2.3. The large aspect ratio of the finger also leads us to expect that, at least away from roots and tips, transverse diffusion will be much more important than longitudinal diffusion.

We shall now use homogenisation to derive a model that is applicable in the large aspect-ratio region.

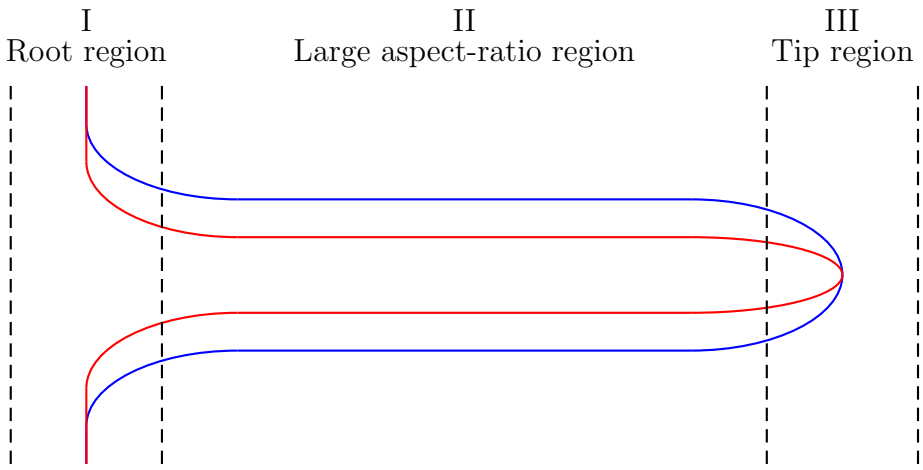

Figure 3.2: A cartoon depicting an idealised finger, with the red line representing a contour for a high concentration of solvent and the blue line representing a contour for a low concentration of solvent. The large aspect-ratio model is only valid in region II. In the root region (I) and the tip region (III) the model breaks down and further analysis is required.

3.2 Homogenisation of pressure

In Chapter 2 we saw that, at large Péclet numbers, small wavelength transverse disturbances in physically relevant solutions to the Peaceman model were unstable. The introduction of transverse diffusion led to a cutoff wavelength, with all disturbances of wavelength smaller than the cutoff wavelength being stable, and a least-stable wavelength, for which the disturbances grow at the fastest rate. The existence of the cut-off wavelength and least-stable wavelength led to a small natural length scale, at least for the linear problem, that is determined by the small amount of diffusion present. Our numerical simulations led us to predict that the fully nonlinear problem would show the formation of long parallel finger-like solutions, with a width comparable to the wavelength of the least-stable disturbance.

In this chapter we shall assume that the flow is essentially one-dimensional with all the fingers pointing in the direction of the x-axis. The one-dimensional mean-flow suggests that the diffusive term in the Peaceman model is anisotropic, with the larger coefficient of diffusion acting in the $x-$direction. As noted in Chapter 2, both $\mathrm{Pe}_{\|}$ and $\mathrm{Pe}_{\perp}$ are large, with the smaller $\mathrm{Pe}_{\|}$ being at least 1000. The ratio between them may be as large as 50, but this is still somewhat smaller than the value of the Péclet numbers themselves. We will therefore treat the longitudinal and transverse Péclet numbers as being large and of the same order of magnitude. We shall also model the diffusion as constant, since numerical simulations [64, 65] have shown that physically reasonable velocity-dependence of longitudinal diffusion is not important for large Péclet number displacements.

Since the fingers are much longer than they are wide, we make the rescaling $y = \epsilon Y$,

where $\epsilon \ll 1$ is the typical aspect ratio of a finger. The numerical simulations of section 2.3 suggest that the length scale of the fingers is proportional to $\mathrm{Pe}^{-1/2}$. We therefore propose that $\epsilon = O(\mathrm{Pe}_\perp^{-1/2})$, and write

$$\mathrm{Pe}^* = \epsilon^2 \mathrm{Pe}_\perp,$$

where $\mathrm{Pe}^* = O(1)$. From (2.32) the velocity must satisfy

$$\frac{\partial u}{\partial x} + \frac{1}{\epsilon}\frac{\partial v}{\partial Y} = 0, \tag{3.1}$$

and so to ensure that we obtain a sensible balance we require that the transverse velocity is small with $v = \epsilon V$. The equation for conservation of solvent, (2.33), becomes

$$\frac{\partial c}{\partial t} + \frac{\partial}{\partial x}(uc) + \frac{\partial}{\partial Y}(Vc) = \frac{\epsilon^2}{\delta \mathrm{Pe}^*}\frac{\partial^2 c}{\partial x^2} + \frac{1}{\mathrm{Pe}^*}\frac{\partial^2 c}{\partial Y^2}, \tag{3.2}$$

where $\delta = \mathrm{Pe}_\parallel/\mathrm{Pe}_\perp \sim O(1)$. If our earlier analysis had suggested that $\mathrm{Pe}^* \ll 1$, then we would have found that transverse diffusion would quickly eliminate any instability. Conversely, if our analysis had suggested that $\mathrm{Pe}^* \gg 1$ then diffusion would have been so small, even at the finger length scale, that this regime may be vulnerable to the development of further instabilities. Moreover, were our analysis in this regime to result in the development of further instabilities, it would suggest that our choice for the length scale of the fingers was inconsistent. These arguments suggest that our choice for the finger length scale, such that $\mathrm{Pe}^* = O(1)$, is indeed correct.

With this scaling of diffusion, the pressure and concentration satisfy

$$\nabla \cdot \left(\frac{1}{\mu(c)}\nabla p\right) = 0, \tag{3.3}$$

$$\frac{\partial c}{\partial t} - \nabla \cdot \left(\frac{c}{\mu(c)}\nabla p\right) = \frac{\epsilon^2}{\delta \mathrm{Pe}^*}\frac{\partial^2 c}{\partial x^2} + \frac{\epsilon^2}{\mathrm{Pe}^*}\frac{\partial^2 c}{\partial y^2}. \tag{3.4}$$

To model the unidirectional thin fingers, we assume a multiple scales solution for the concentration of the form

$$c \sim c_0(x, y, Y, t) + \epsilon c_1(x, y, Y, t) + \dots ,$$

where $Y = y/\epsilon$, and y, Y are treated as independent variables. Similarly, we seek a multiple scales solution for the pressure,

$$p \sim p_0(x, y, Y, t) + \epsilon p_1(x, y, Y, t) + \epsilon^2 p_2(x, y, Y, t) + \dots$$

At leading order we find that

$$\frac{\partial}{\partial Y}\left(\frac{1}{\mu(c_0)}\frac{\partial p_0}{\partial Y}\right) = 0,$$

so that

$$p_0(x,y,Y,t) = a(x,y,t)\int_0^Y \mu(c_0(x,y,Y,t))\,\mathrm{d}Y + \hat{p}_0(x,y,t), \tag{3.5}$$

where a is an arbitrary function, and we may choose the location of the line $Y = 0$ arbitrarily by altering $\hat{p}_0$. We now suppose that there is a well-defined local average of $\mu(c_0)$, $\bar{\mu}$, so that for large Y

$$\int_0^Y \mu(c_0(x,y,Y,t))\,\mathrm{d}Y \sim \bar{\mu}(x,y,t)Y. \tag{3.6}$$

This requirement is ensured if, for instance, c_0 has the statistical property of being stationary with respect to Y and ergodic, in which case $\bar{\mu}$ should be interpreted as the ensemble average of $\mu(c_0)$. The assumption is also ensured if c_0 is periodic in Y, with

$$\bar{\mu} = \int_0^1 \mu(c_0(x,y,Y,t))\,\mathrm{d}Y,$$

where, without loss of generality, we have taken c_0 to be 1-periodic in Y. For any function $F(x,y,Y,t)$, which is 1-periodic in Y, we shall henceforth define the average as

$$\bar{F}(x,y,t) = \int_0^1 F(x,y,Y,t)\,\mathrm{d}Y.$$

We see from (3.5) that as $Y \to \infty$,

$$p_0 \sim a(x,y,t)\bar{\mu}(x,y,t)Y + \dots\ , \tag{3.7}$$

for large Y, which grows unboundedly unless $a = 0$, and so we require that $a = 0$, so that p_0 is independent of Y. At next order we find that

$$\frac{\partial}{\partial Y}\left(\frac{1}{\mu(c_0)}\frac{\partial p_1}{\partial Y}\right) + \frac{\partial}{\partial Y}\left(\frac{1}{\mu(c_0)}\frac{\partial \hat{p}_0}{\partial y}\right) = 0 \quad \Rightarrow$$

$$p_1 = -Y\frac{\partial \hat{p}_0}{\partial y} + b(x,y,t)\int_0^Y \mu(c_0(x,y,Y,t))\,\mathrm{d}Y + \hat{p}_1(x,y,t), \tag{3.8}$$

where b is an arbitrary function. We see from (3.8) that

$$p_1 \sim -Y\frac{\partial \hat{p}_0}{\partial y}(x,y,t) + b(x,y)\bar{\mu}(x,y,t)Y,$$

for large Y, whence, to ensure that p_1 does not grow unboundedly,

$$b(x,y,t) = \frac{1}{\bar{\mu}(x,y,t)}\frac{\partial \hat{p}_0}{\partial y}(x,y,t). \tag{3.9}$$

The $O(1)$ terms in (3.3) are

$$\frac{\partial}{\partial Y}\left(\frac{1}{\mu(c_0)}\frac{\partial p_2}{\partial Y} + \frac{1}{\mu(c_0)}\frac{\partial p_1}{\partial y} - c_1\frac{\mu'(c_0)}{\mu(c_0)^2}\left(\frac{\partial \hat{p}_0}{\partial y} + \frac{\partial p_1}{\partial Y}\right)\right) + \frac{\partial}{\partial x}\left(\frac{1}{\mu(c_0)}\frac{\partial \hat{p}_0}{\partial x}\right) + \frac{\partial}{\partial y}\left(\frac{1}{\mu(c_0)}\left(\frac{\partial \hat{p}_0}{\partial y} + \frac{\partial p_1}{\partial Y}\right)\right) = 0.$$

Integrating with respect to Y we see that

$$\begin{aligned}\frac{\partial p_2}{\partial Y} &= -\frac{\partial p_1}{\partial y} + c_1\frac{\mu'(c_0)}{\bar{\mu}}\frac{\partial \hat{p}_0}{\partial y} + d(x,y,t)\mu(c_0) \\ &- \mu(c_0)\int_0^Y \frac{\partial}{\partial x}\left(\frac{1}{\mu(c_0)}\frac{\partial \hat{p}_0}{\partial x}\right) + \frac{\partial}{\partial y}\left(\frac{1}{\bar{\mu}}\frac{\partial \hat{p}_0}{\partial y}\right)\mathrm{d}Y,\end{aligned}$$

where d is an arbitrary function, and so, recalling that $\hat{p}_0 = \hat{p}_0(x,y,t)$,

$$\begin{aligned}&p_2(x,y,Y,t) = \hat{p}_2(x,y,t) + \\ &\int_0^Y d(x,y,t)\mu(c_0(x,y,Y',t)) - \frac{\partial p_1}{\partial y}(x,y,Y',t) + c_1(x,y,Y',t)\frac{\mu'(c_0(x,y,Y',t))}{\bar{\mu}(x,y,t)}\frac{\partial \hat{p}_0}{\partial y}\,\mathrm{d}Y' - \\ &\int_0^Y \mu(c_0(x,y,Y',t))\int_0^{Y'}\frac{\partial}{\partial x}\left(\frac{1}{\mu(c_0(x,y,Y'',t))}\frac{\partial \hat{p}_0}{\partial x}\right) + \frac{\partial}{\partial y}\left(\frac{1}{\bar{\mu}(x,y,t)}\frac{\partial \hat{p}_0}{\partial y}\right)\mathrm{d}Y''\,\mathrm{d}Y'.\end{aligned}$$

For large Y we find that

$$p_2 \sim \frac{1}{2}\bar{\mu}(x,y,t)\left(\frac{\partial}{\partial x}\left(\frac{1}{\mu^*(x,y,t)}\frac{\partial \hat{p}_0}{\partial x}(x,y,t)\right) + \frac{\partial}{\partial y}\left(\frac{1}{\bar{\mu}(x,y,t)}\frac{\partial \hat{p}_0}{\partial y}(x,y,t)\right)\right)Y^2 + O(Y),$$

where we have defined the harmonic average of the viscosity as

$$\frac{1}{\mu^*(x,y,t)} = \overline{\left(\frac{1}{\mu(c_0(x,y,Y,t))}\right)}. \tag{3.10}$$

To ensure that p_2 remains bounded as $Y \to \infty$ we require that

$$\frac{\partial}{\partial x}\left(\frac{1}{\mu^*(x,y,t)}\frac{\partial \hat{p}_0}{\partial x}(x,y,t)\right) + \frac{\partial}{\partial y}\left(\frac{1}{\bar{\mu}(x,y,t)}\frac{\partial \hat{p}_0}{\partial y}(x,y,t)\right) = 0, \tag{3.11}$$

and this is our homogenised equation for the lowest order pressure.

For the mean flow to be one-dimensional we require that $\hat{p}_0 = \hat{p}_0(x,t)$ and $c_0 = c_0(x,Y,t)$, and, once we have applied the condition that the mean velocity, $\bar{u}_0 = 1$, we find that

$\partial \hat{p}_0/\partial x = -\mu^*(x,t)$. Clearly

$$u_0(x,Y,t) = \frac{\mu^*(x,t)}{\mu(c_0(x,Y,t))} \tag{3.12}$$

and the transverse velocity is given by the expansion $v \sim \epsilon v_1(x,Y,t)$, with v_1 satisfying

$$\frac{\partial u_0}{\partial x} + \frac{\partial v_1}{\partial Y} = 0. \tag{3.13}$$

Equation (3.4) gives

$$\frac{\partial c_0}{\partial t} + \frac{\partial}{\partial x}\left(u_0 c_0\right) + \frac{\partial}{\partial Y}\left(v_1 c_0\right) = \frac{1}{\mathrm{Pe}^*}\frac{\partial^2 c_0}{\partial Y^2}, \tag{3.14}$$

at leading order. Together, equations (3.12)-(3.14) describe the flow in the homogenised region. One can integrate (3.13) with respect to Y to obtain

$$v_1 = -\int_0^Y \frac{\partial}{\partial x}\left(\frac{\mu^*(x,t)}{\mu(c_0(x,Y',t))}\right)\mathrm{d}Y' + \tilde{v}(x,t), \tag{3.15}$$

where $\tilde{v}$ is an arbitrary function which, when there is a line of symmetry of c_0, parallel to the x-axis, can be set equal to zero by appropriate choice of the line $Y = 0$. We can therefore combine (3.12)-(3.14) to obtain the following single integrodifferential equation for $c_0(x,Y,t)$:

$$\frac{\partial c_0}{\partial t} + \frac{\partial}{\partial x}\left(\frac{\mu^*(x,t)}{\mu(c_0)}c_0\right) + \frac{\partial}{\partial Y}\left(\left(-\int_0^Y \frac{\partial}{\partial x}\left(\frac{\mu^*(x,t)}{\mu(c_0(x,Y',t))}\right)\mathrm{d}Y' + \tilde{v}(x,t)\right)c_0\right) = \frac{1}{\mathrm{Pe}^*}\frac{\partial^2 c_0}{\partial Y^2}. \tag{3.16}$$

This equation describes the flow of solvent in the mixing region where fingering takes place, and it still involves the rapidly-varying concentration of solvent. It is our fundamental model for the growth of fingers, at least away from their roots and tips, and we shall return to analyse this equation in more detail in section 3.4, but first we shall try to develop a model for the average concentration of solvent by averaging the concentration across the fingers.

3.3 The Koval model

To develop an averaged model we simply integrate (3.14) with respect to Y, giving (for some arbitrary function $e(x,y,t)$)

$$\begin{aligned}\frac{1}{\mathrm{Pe}^*}\frac{\partial c_0}{\partial Y} - v_1 c_0 &= \int_0^Y \frac{\partial c_0}{\partial t} + \frac{\partial}{\partial x}\left(\frac{\mu^*}{\mu(c_0)}c_0(\right)\mathrm{d}Y' + e(x,y,t) \\ &\sim \left(\frac{\partial \bar{c}_0}{\partial t}(x,t) + \frac{\partial}{\partial x}\left(\mu^*(x,t)\overline{\left(\frac{c_0}{\mu(c_0)}\right)}\right)\right)Y,\end{aligned}$$

for large Y, and so to ensure that the left-hand side of the equation does not grow unboundedly as $Y \to \infty$ we require that

$$\frac{\partial \bar{c}}{\partial t} + \frac{\partial}{\partial x}\left(\mu^*\overline{\left(\frac{c}{\mu(c)}\right)}\right) = 0, \tag{3.17}$$

where we have now dropped the 0 subscript from c. However, (3.17) is not closed since μ^* and $\overline{(c/\mu)}$ are not known as functions of $\bar{c}$. One way of closing this problem, previously suggested by Yortsos in [63], is to assume that, even on the microscopic scale, diffusion is unimportant. Initially the concentration is either 0 (in the oil) or 1 (in the solvent); hence with no diffusion the concentration may only ever take these two values, and so

$$\mu^* = \left(\int_0^1 \frac{1}{\mu(c)}\,\mathrm{d}Y\right)^{-1} = \frac{1}{M\bar{c} + 1 - \bar{c}},$$

and

$$\overline{\left(\frac{c}{\mu(c)}\right)} = \int_0^1 \frac{c}{\mu(c)}\,\mathrm{d}Y = M\bar{c},$$

where we recall that $M = \mu_o/\mu_s > 1$ is the mobility ratio between the solvent and the oil. This leads us to the "naïve" Koval model:

$$\frac{\partial \bar{c}}{\partial t} + \frac{\partial}{\partial x}\left(\frac{M\bar{c}}{M\bar{c} + 1 - \bar{c}}\right) = 0, \tag{3.18}$$

which can be easily solved by the method of characteristics. With the initial condition

$$\bar{c} = \begin{cases} 1 & x < 0 \\ 0 & x > 0 \end{cases},$$

we obtain the solution

$$\bar{c} = \begin{cases} 1 & x < \frac{t}{M} \\ \frac{\sqrt{\frac{Mt}{x}}-1}{M-1} & \frac{t}{M} < x < Mt \\ 0 & Mt < x \end{cases}, \tag{3.19}$$

provided $M > 1$. When $M < 1$ a shock forms so that, assuming the usual Rankine-Hugoniot condition since (3.18) is a conservation law,

$$\bar{c} = \begin{cases} 1 & x < t \\ 0 & x > t \end{cases}. \tag{3.20}$$

When $M < 1$ the displacement is stable, we do not expect any fingering to occur, and the only mixing between solvent and oil will be as a direct result of diffusion. When diffusion is negligible, the "piston-like" shock solution (3.20) is the expected result.

3.3.1 Limitations of the naïve Koval model

Equation (3.18) is a possible model for the growth of the mixing zone and so we now compare the predictions of this model with the numerical simulations of the Peaceman model presented in section (2.3). In view of the comment made at the end of the previous section, we will restrict attention to the unstable case $M > 1$.

As shown in Figure 3.3, we find that the naïve Koval model that we have presented here vastly overpredicts the rate at which the fingers grow. The cause of this failure is the unjustified assumption that, for large Pe, the effect of diffusion is negligible. As we discussed at the start of section 3.2, the correct scaling for the width of the fingers is of order $\mathrm{Pe}^{-1/2}$ and so it is *never* possible to neglect the effect of diffusion. This statement is supported by the observation that our numerical simulations show that the concentration takes values other than 0 and 1, this feature being observed in the accurate numerical solution of the Peaceman model, however large the Péclet number is.

Koval [33] suggested that rather than entirely abandoning (3.18), we instead postulate the existence of an "effective" concentration of solvent. To derive Koval's improved model, one supposes that the effect of the varying concentration of solvent is equivalent to the displacement of the oil by an effective fluid, immiscible with the oil. The effective fluid consists of a particular mixture of solvent and oil with a fixed concentration of solvent, c_e. We may then model the effect of the varying concentration of solvent by replacing the mobility ratio M in the naïve Koval model by an effective mobility ratio M_e representing the mobility ratio between the effective fluid and the oil. This leads us to the modified Koval model,

$$\frac{\partial \bar{c}}{\partial t} + \frac{\partial}{\partial x}\left(\frac{M_e \bar{c}}{M_e \bar{c} + 1 - \bar{c}}\right) = 0, \tag{3.21}$$

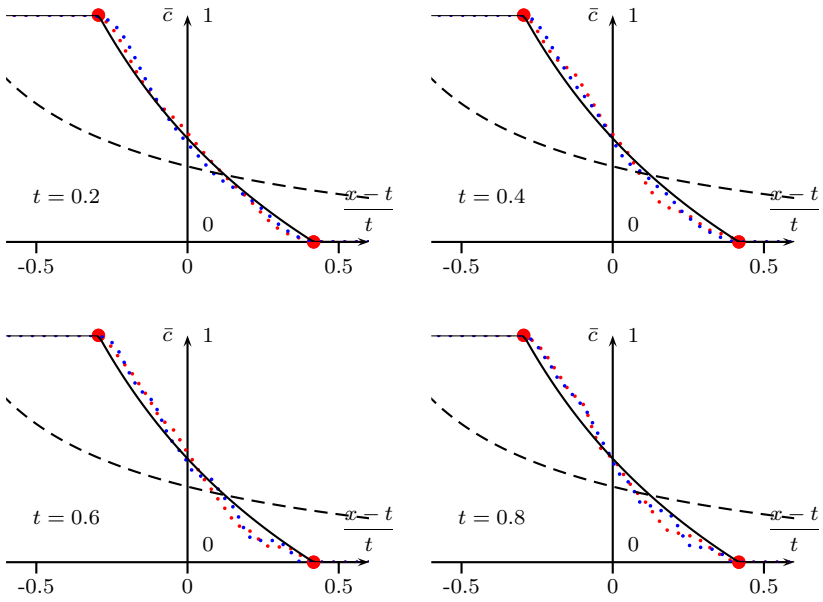

Figure 3.3: Transversely-averaged concentration profiles of two-dimensional simulations of the Peaceman model. The red and blue dotted lines represent the transverse averages of two simulations, with small random differences in the initial data. In the simulations we have taken $M = 4$, so that $M_e = 1.417$, and $\mathrm{Pe} = 2000$. The black dashed line represents the (incorrect) predicted concentration profile when the naïve Koval model is applied. The black unbroken line represents the predicted concentration profile of the modified Koval model in which Koval's effective mobility ratio is applied. The large red dots represent the ends of the mushy region, as predicted by the modified Koval model. The ends of the mushy region as predicted by the naïve Koval model are outside the plotted range. The transverse average of the two numerical simulations appear to approximately coincide with each other, but the naïve Koval model vastly overpredicts the spread of the mixing zone.

where M_e is given by

$$M_e = \left(M^{1/4} c_e + 1 - c_e\right)^4, \tag{3.22}$$

and we have used the formula for the viscosity of a mixture (1.28).

The concentration of solvent in the effective displacing mixture, c_e, is an unknown parameter. Koval found, by fitting with the experiments of Blackwell [5], that he could predict the average concentration profile by choosing $c_e = 0.22$. Our own numerical simulations also suggest that taking an effective concentration close to 0.22 gives good agreement with the transverse average of two-dimensional numerical simulations, as can be seen in Figure 3.3 and Figure 3.4. By applying least-squares to fit c_e to our numerical simulations, we find values for c_e in the range of $0.18 - 0.24$. The model (3.21) also appears to be effective in predicting the growth rate of the mixing zone over a wide range of mobility ratios: the same model seems to give good agreement with our numerical simulations for both $M = 4$ and $M = 20$.

In summary, the model (3.21) appears to be effective in predicting the average concen-

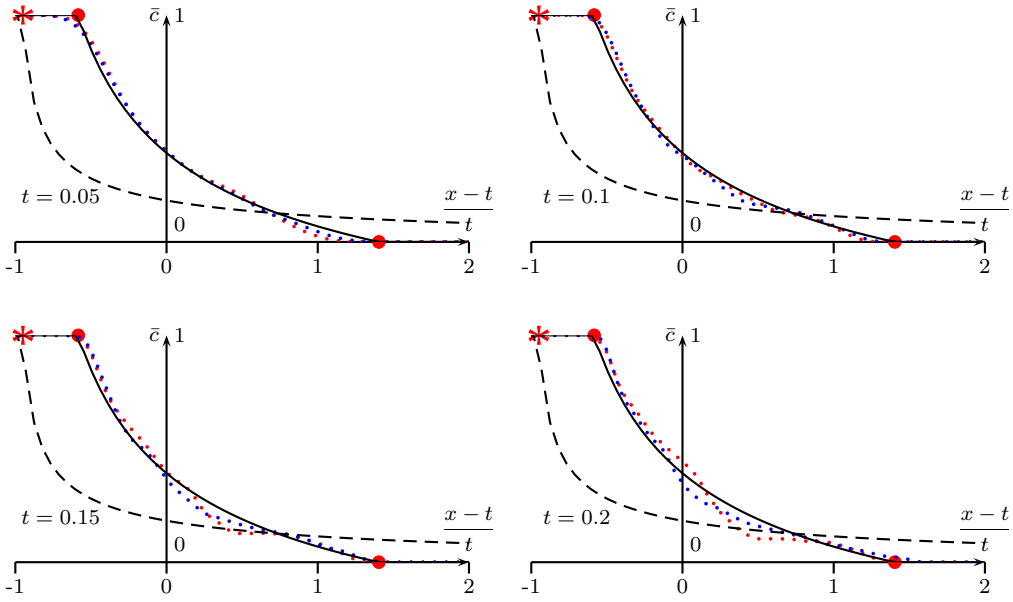

Figure 3.4: Transversely-averaged concentration profiles of two-dimensional simulations of the Peaceman model. In the simulations we have taken $M = 20$, so that $M_e = 2.404$, and $\mathrm{Pe} = 2000$. The representation of each curve follows those of Figure 3.3. The large red dots represent the ends of the mixing region, as predicted by the modified Koval model. The large red asterisks represent the boundary between the solvent region and mushy region, as predicted by the naïve Koval model, with the boundary between the oil region and mushy region far outside the plotted area (at $(x-t)/t = 19$). As in Figure 3.3 the naïve Koval model vastly overpredicts the spread of the mixing region, but the modified Koval model is reasonably effective at capturing both the size of the mixing region and the average concentration profile within.

tration, but it is not apparent that the assumption underlying it can be readily justified. Thus, it is still of interest to explain why the mixing zone grows at the rate that it does. To proceed in a more rigorous fashion, we return to the equation for the evolution of the concentration prior to averaging, namely (3.16).

3.4 The homogenised problem

In the remainder of this chapter we shall attempt to predict the growth rate of the mushy region, and support the assumptions made in the Koval model, by returning to the homogenised problem, prior to averaging, (3.16). Recall that the homogenised problem (3.16) requires us to solve, on dropping 0 subscripts from the leading order concentration,

$$\frac{\partial c}{\partial t} + \frac{\partial}{\partial x}\left(\frac{\mu^*}{\mu(c)}c\right) + \frac{\partial}{\partial Y}\left(\left(-\int_0^Y \frac{\partial}{\partial x}\left(\frac{\mu^*}{\mu(c)}\right)\mathrm{d}Y + \tilde{v}\right)c\right) = \frac{1}{\mathrm{Pe}^*}\frac{\partial^2 c}{\partial Y^2}, \tag{3.23}$$

where μ^* is the harmonic average of the viscosity across the fingers defined in (3.10) and we will set $\tilde{v}$ to zero by assuming $Y = 0$ is a line along which c is symmetric. We begin by making some preliminary observations about special solutions of (3.23). There is a large class of solutions that can be obtained by seeking solutions independent of x. If $c = \hat{c}(Y, t)$, and there is no applied transverse velocity as $Y \to \pm\infty$, then we need only solve

$$\frac{\partial \hat{c}}{\partial t} = \frac{1}{\mathrm{Pe}^*} \frac{\partial^2 \hat{c}}{\partial Y^2}.$$

Such solutions may represent the finger through much of its length; however since we have solvent displacing oil, our boundary conditions will require that $c = 1$ for sufficiently small values of x and $c = 0$ for sufficiently large values of x, and so we cannot have a solution independent of x.

We can also seek solutions that are independent of Y, and with $c = \hat{c}(x, t)$ satisfying

$$\frac{\partial \hat{c}}{\partial t} + \frac{\partial \hat{c}}{\partial x} = 0.$$

The stability of such one-dimensional solutions to (3.23) has already been studied by Yortsos [62]; for sufficiently large values of Pe^*, such solutions are unstable as we now show. Our base state solution is $c = \hat{c}(\xi)$, where $\xi = x - t$, and so we seek a solution of the form

$$c = \hat{c}(\xi) + \delta C(\xi, Y, t),$$

where δ is a small parameter. We find at leading order that C satisfies

$$\frac{\partial C}{\partial t} - \frac{1}{\mu(\hat{c})} \left(C - \bar{C}\right) \frac{\mathrm{d}\mu(\hat{c})}{\mathrm{d}\xi} = \frac{1}{\mathrm{Pe}^*} \frac{\partial^2 C}{\partial Y^2}.$$

By integrating with respect to Y, we see that $\bar{C}$ is independent of t, and so writing

$$V(\xi) = \frac{1}{\mu(\hat{c})} \frac{\mathrm{d}\mu(\hat{c})}{\mathrm{d}\xi},$$

we can write

$$C(\xi, Y, t) = \bar{C}(\xi) + W(\xi, Y, t) \exp\left(V(\xi)t\right),$$

where W satisfies the heat equation

$$\frac{\partial W}{\partial t} = \frac{1}{\mathrm{Pe}^*} \frac{\partial^2 W}{\partial Y^2}.$$

For periodic fingers, with period 1, the maximum growth rate is given by

$$\sigma = \max_{\xi} V(\xi) - \frac{\pi^2}{\mathrm{Pe}^*},$$

and so, when the viscosity gradient is large or when Pe^* is large, the solution $c = \hat{c}(\xi)$ will be unstable. This stability result is very similar to the the large-wavenumber stability analysis of the Peaceman model (2.71), which is not surprising since, by assuming thin fingers we are limiting ourselves to the large-wavenumber regime. If the one-dimensional solution were to be stable, then this would suggest that we have incorrectly estimated the finger width, and we should look at wider fingers, chosen so that this one-dimensional solution is unstable.

Since neither solutions independent of x or Y fully represent the desired behaviour we have performed some numerical simulations of (3.23).[1] Our preliminary simulations of (3.23), with only numerical diffusion acting in the longitudinal direction, led to the formation of discontinuities in the concentration along a line parallel to the Y-axis, suggesting that (3.23) may have weak solutions with shocks. These numerical simulations suffered from spurious oscillations in the concentration along the line of discontinuity, and large transverse velocities along the line across which c was discontinuous were observed. We have attempted to regularise the numerical problem by adding a small artificial longitudinal diffusion term into our numerical simulations. Although there is longitudinal diffusion in the original model, we should be careful about introducing it into the large aspect-ratio model, as other terms have been neglected which are at least as large as longitudinal diffusion. Some simulations are depicted in Figure 3.5, and we note here that the shocks in the solution are formed at the finger-tips and finger-roots. Our numerical simulations also show that equation (3.23) alone does not predict sensible interaction between fingers, near the shocks, with extremely large transverse velocities for all points with the same $x-$coordinate as the shock.

In all of our simulations we have observed large transverse velocities along the line across which c appears discontinuous, and we are able to explain the large transverse velocities observed, since the transverse velocity is given by

$$v_1 = -\int_0^Y \frac{\partial}{\partial x}\left(\frac{\mu^*(x,t)}{\mu(c(x,Y',t))}\right) \mathrm{d}Y',$$

it will, in general, become infinite wherever c is discontinuous in x. Note that the variable of integration is different to the variable in which c is discontinuous. The appearance

[1] The numerical scheme used is the same as that used to model advection and diffusion in the Peaceman model in Chapter 2.

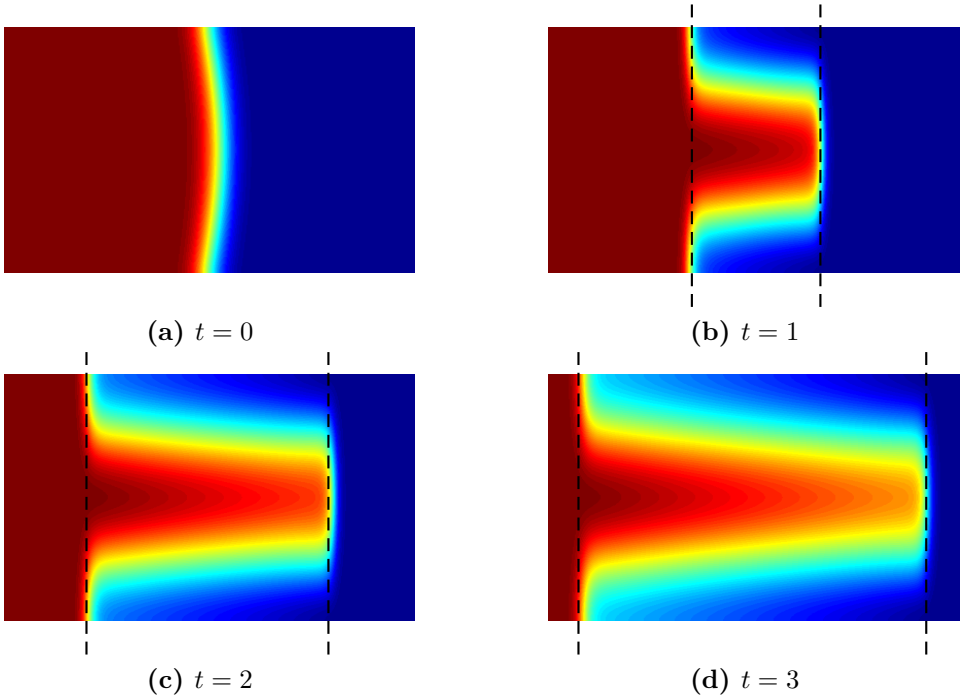

(a) $t = 0$ **(b)** $t = 1$ **(c)** $t = 2$ **(d)** $t = 3$

Figure 3.5: Numerical simulations of solutions of (3.23) in the moving frame $\xi = x - t$. Red represents the less viscous solvent ($c = 1$) and blue represents the more viscous oil ($c = 0$). The dashed, black lines represent the locations of the shocks representing the root and tip regions. We have taken $M = 2$ and $\mathrm{Pe}^* = 1/100$ for this simulation.

of an infinite transverse velocity is symptomatic of the fact that the large aspect-ratio assumption has broken down, and it prevents us from numerically solving (3.23), even when using a conservative scheme. When shocks appear, one often attempts to seek physically relevant weak solutions; however, it is not clear that a weak solution of (3.12)-(3.14) may be found, as we now show. Since (3.13) holds, we may introduce a stream function defined by

$$\frac{\partial \psi}{\partial Y} = \frac{\mu^*(x,t)}{\mu(c(x,Y,t))},$$

so that (3.14) becomes

$$\frac{\partial c}{\partial t} + \frac{\partial}{\partial c}\left(\frac{\partial \psi}{\partial Y}c\right) - \frac{\partial}{\partial Y}\left(\frac{\partial \psi}{\partial x}c\right) = \frac{1}{\mathrm{Pe}^*}\frac{\partial^2 c}{\partial Y^2}.$$

In attempting to derive a weak formulation we will obtain a term of the form

$$\int\int \frac{\partial \phi}{\partial Y}\frac{\partial \psi}{\partial x}c \,\mathrm{d}x\,\mathrm{d}Y,$$

where ϕ is our test function. It is not possible to pass the x derivative of ψ on to the test function ϕ without causing an x derivative of c to also be present. We expect c to be discontinuous in x, and so we also expect ψ to be discontinuous in x; however, because ψ

depends on the global behaviour of c, it is not possible to write ψ as a function of c, and it is not possible to produce a weak formulation.

We have already anticipated that the large aspect-ratio model will break down near the tips and roots of individual fingers, and we therefore expect that, to determine the correct behaviour near the shock, we will need to rescale the original Peaceman model, (3.3)-(3.4), to produce a model for the finger-tip region and the finger-root region (regions I and III in Figure 3.2). However, before working towards a model for the finger-tip and root regions in section 3.5 we shall investigate further the formation of shocks in (3.23), and the solution of (3.23) away from any shocks.

3.4.1 The Wooding problem

We have not been able to obtain physically useful analytical solutions to (3.23). However, further progress can be made by considering the slight simplification in which the mobility ratio is close to 1, allowing us to linearise the concentration dependence of the viscosity, so that $\mu(c) = 1 - \Lambda\delta c$, where $0 < \delta = O(1/M - 1) \ll 1$. The homogenised problem becomes

$$\frac{\partial c}{\partial t} + \frac{\partial c}{\partial x} + \Lambda\delta\left(\frac{\partial}{\partial x}\left((c-\bar{c})c\right) - \frac{\partial}{\partial Y}\left(c\int_0^Y \frac{\partial}{\partial x}(c-\bar{c})\,\mathrm{d}Y\right)\right) = \frac{1}{\mathrm{Pe}^*}\frac{\partial^2 c}{\partial Y^2}.$$

If we move into travelling coordinates $x' = x - t$ and rescale t and Pe^* with δ we obtain, after dropping primes from x,

$$\frac{\partial c}{\partial t} + \Lambda\frac{\partial}{\partial x}\left((c-\bar{c})c\right) - \Lambda\frac{\partial}{\partial Y}\left(c\int^Y \frac{\partial}{\partial x}\left(c-\bar{c}\right)\mathrm{d}Y\right) = \frac{1}{\mathrm{Pe}^*}\frac{\partial^2 c}{\partial Y^2}. \tag{3.24}$$

This problem, first studied by Wooding [61], retains many of the features of (3.23), but it is algebraically simpler, and even admits a useful analytical solution which we will show shortly. We shall also show in Chapter 5 that (3.24) can also be derived as the model for fingering driven by gravity through the density differences between two miscible fluids, and so it is of physical importance in its own right.

We are fortunate in that special exact, periodic solutions to this problem may be found of the form

$$c = c_0(x,t) + c_1(x,t)\cos 2\pi Y, \tag{3.25}$$

even though the problem is nonlinear. Substituting the ansatz (3.25) into (3.24) we find,

$$\frac{\partial c_0}{\partial t} + \frac{\partial c_1}{\partial t}\cos 2\pi Y + \Lambda\left(c_1\frac{\partial c_0}{\partial x}\cos 2\pi Y + c_1\frac{\partial c_1}{\partial x}\cos^2 2\pi Y + c_1\frac{\partial c_1}{\partial x}\sin^2 2\pi Y\right) = -\frac{4\pi^2}{\mathrm{Pe}^*}\cos 2\pi Y, \tag{3.26}$$

and fortunately, this simplifies to eliminate all of the nonlinear terms in $\cos 2\pi Y$. (Un-

fortunately this technique does not work if we include any more terms from the Fourier series.) We may now find solutions satisfying (3.25) by solving the system

$$\frac{\partial c_0}{\partial t} + \Lambda c_1 \frac{\partial c_1}{\partial x} = 0, \tag{3.27}$$

$$\frac{\partial c_1}{\partial t} + \Lambda c_1 \frac{\partial c_0}{\partial x} = -\alpha c_1, \tag{3.28}$$

where $\alpha = 4\pi^2/\mathrm{Pe}^*$, whose solution can be found by the method of characteristics, with the solution determined along characteristic curves, $(x(s), t(s))$. We find that the characteristic curves are described by

$$\dot{x} = \pm \Lambda c_1 \dot{t}, \tag{3.29}$$

where $\dot{}$ represents $\mathrm{d}/\mathrm{d}s$. The system of equations (3.27),(3.28) is hyperbolic whenever c_1 is nonzero, but becomes degenerate when $c_1 = 0$. We also find that c_0 and c_1 satisfy

$$\dot{c_0} \pm \dot{c_1} = \mp \alpha c_1 \dot{t}, \tag{3.30}$$

on $\dot{x} = \pm \Lambda c_1 \dot{t}$, and so we find, amazingly, that the system of equations possesses the Riemann invariants

$$c_0 \pm c_1 + \frac{\alpha}{\Lambda} x = \text{constant} \quad \text{on} \quad \dot{x} = \pm \Lambda c_1 \dot{t}. \tag{3.31}$$

In line with section 3.3, we consider the initial condition

$$\begin{aligned} c_0 = 1 \quad \text{and} \quad c_1 = 0 \qquad \text{in} \quad x < 0, \\ c_0 = 0 \quad \text{and} \quad c_1 = 0 \qquad \text{in} \quad x > 0. \end{aligned}$$

If initially $c_1 = 0$ at $x = 0$, i.e. the initial condition for c is entirely independent of Y, then we obtain a discontinuity at $x = 0$, but no characteristics cross as shown in Figure 3.6, and so this discontinuity does not represent a shock. This solution corresponds to the special case in which the boundary between the solvent and oil is precisely one-dimensional, and the initial condition is the solution for all t, with characteristics x=constant. If $c_1 \neq 0$ at $x = 0$ then, as shown in Figure 3.7 characteristics emanating from $x = 0$ will immediately cross one of the vertical characteristics in $x < 0$ and in $x > 0$, and so a shock must immediately form.

We have already suggested that shock formation is the genesis of the regions containing roots and tips of fingers, and so it is of no surprise that shocks will immediately form. The formation of shocks leads to considerable difficulties in our analysis within the large aspect-ratio region, since it is not obvious how to determine the shock conditions. Although we

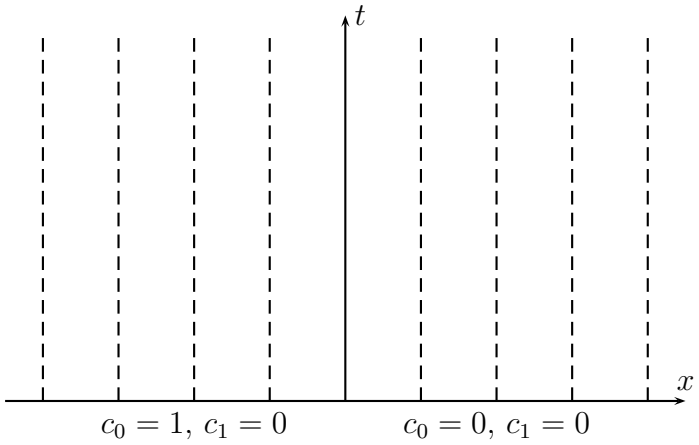

Figure 3.6: Characteristic diagram for the Wooding solution with the initial condition $c_1(x, 0) = 0$, even at $x = 0$. The dashed lines represent characteristics, and along each line there are two coincident characteristics. A discontinuity at $x = 0$ persists for all t, but characteristics do not cross and no shock is formed.

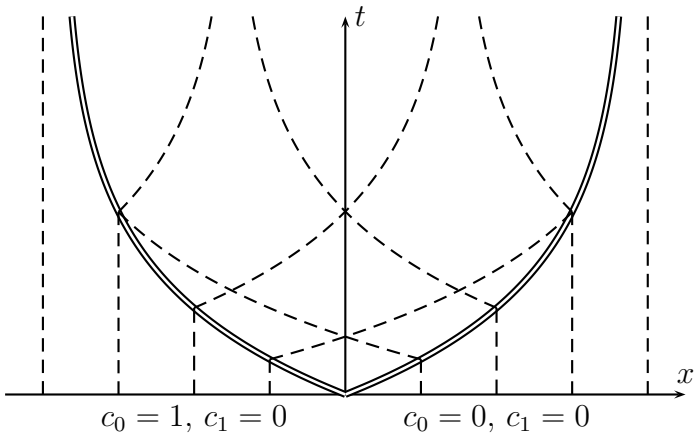

Figure 3.7: Characteristic diagram for the Wooding solution with initial condition $c_1 = 0$ for $x \lesseqgtr 0$ and $c_1(0, 0) \neq 0$. The dashed lines represent characteristics and the double, unbroken lines represent shocks. Along the vertical dashed lines there are two coincident characteristics.

cannot obtain all the shock conditions without matching to a tip/root region, we can obtain a single shock condition by integrating the equation for conservation of solvent from $Y = 0$ to $Y = 1$. The integrated equation automatically conserves mass across the shock, and conservation of solvent across the shock requires that the speed of the shock satisfies

$$U = \frac{\Lambda}{2} \frac{[c_1^2]_-^+}{[c_0]_-^+}. \tag{3.32}$$

Moreover, from (3.27) and (3.28) we may be able to obtain the missing, second shock condition, up to an undetermined constant, by simple scaling arguments as follows. We first note that the problem is unchanged under the mapping $c_0 \to 1 - c_0$ and $x \to -x$.

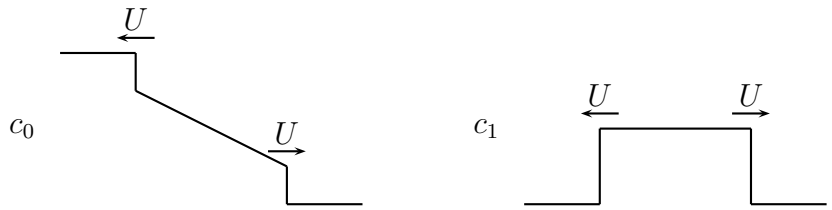

Figure 3.8: Profile of c_0 and c_1.

Note that this symmetry property is a feature of (3.24) but not of the full homogenised problem, (3.23); this lack of symmetry is one of the principal differences between (3.23) and (3.24). For our solution to (3.27)-(3.28) to possess this symmetry, we require that there is either a single stationary shock at $x = 0$ or that there are two shocks of equal magnitude, travelling at the same speed, but in opposite directions. With $\Lambda > 0$ we will obtain the second case, as shown in Figure (3.8). With this symmetry we need only consider the problem in $x > 0$, setting $c_0 = 1/2$ on $x = 0$. At the shock the $-\alpha c_1$ term on the right-hand side of (3.28) is negligible and we note that the remaining system of equations is invariant under the rescalings:

$$c_0 \to \lambda c_0, \quad c_1 \to \lambda c_1, \quad U \to \lambda U,$$

where U is the speed of the shock. This invariance of (3.27)-(3.28) close to the shock, implies that c_1^- depends linearly on c_0^- or

$$c_1^- = \beta c_0^-, \tag{3.33}$$

for some constant β. Since $c_0^+ = c_1^+ = 0$, the shock condition (3.32) becomes

$$U = \beta^2 \frac{\Lambda}{2} \, c_0|_{x=F^-} \, ,$$

where $x = F(t)$ is the position of the shock. We are not, however, able to determine β without further investigation of the tip and root regions.

We have found that the solution in the mixing region can be obtained by seeking a solution with c_1 independent of x, and c_0 a linear function of x, independent of t in $x < F(t)$. Equation (3.27) is automatically solved and writing $C(t) = c_0|_{x=F^-}$ we have

$$\frac{\partial c_0}{\partial x} = \frac{C(t) - 1/2}{F(t)}, \quad c_1 = \beta C(t), \quad \text{and} \quad F(t) = \beta^2 \frac{\Lambda}{2} \int_0^t C(t) \, \mathrm{d}t.$$

Equation (3.28) becomes

$$\beta\frac{\mathrm{d}C}{\mathrm{d}t}+\frac{\beta C(2C-1)}{\beta^2\int_0^t C\,\mathrm{d}t}=-\alpha\beta C.$$

Since $C>0$,

$$\chi=\int_0^t C\,\mathrm{d}t,$$

can be used as our independent variable so that C solves

$$\frac{\mathrm{d}C}{\mathrm{d}\chi}=\frac{1-2C}{\beta^2\chi}-\alpha C.$$

As the solution must be valid as $\chi\to 0$ we find that

$$C=\frac{1}{2}-\frac{\alpha\chi}{1+2/\beta^2}.$$

Since $C(t)=\mathrm{d}\chi/\mathrm{d}t$ we find that

$$\chi=\frac{2+\beta^2}{\alpha\beta^2}\left(1-\exp\left(-\frac{\alpha\beta^2 t}{2+\beta^2}\right)\right),$$

$$C=\frac{1}{2}\exp\left(-\frac{\alpha\beta^2 t}{2+\beta^2}\right),$$

and

$$F(t)=\frac{\Lambda(2+\beta^2)}{4\alpha}\left(1-\exp\left(-\frac{\alpha\beta^2}{2+\beta^2}t\right)\right), \tag{3.34}$$

and so we find that in $|x|<F(t)$

$$c_0 = c_0(x)=\frac{1}{2}-\frac{2\alpha}{\Lambda(2+\beta^2)}x, \tag{3.35}$$

$$c_1 = c_1(t)=\frac{\beta}{2}\exp\left(-\frac{\alpha\beta^2}{2+\beta^2}t\right). \tag{3.36}$$

In Figure 3.9 we show a surface plot of this solution, and it is in qualitative agreement with the numerical simulations depicted in Figure 3.5.

More generally, we can write

$$c=c_0(x,t)+\sum_{n=1}^{\infty}c_n(x,t)\cos 2n\pi Y,$$

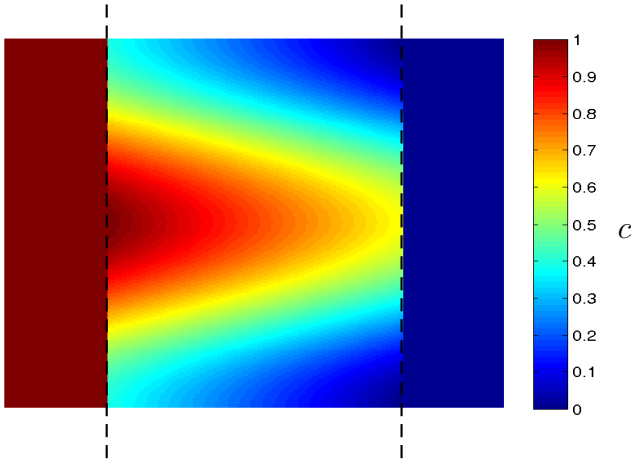

Figure 3.9: The concentration of solvent in solution to (3.24). The solution is obtained from (3.35) and (3.36) with $\alpha = 0.5$, $\beta = 1$, $\Lambda = 1$ and $t = 3$. Red represents the less viscous solvent ($c = 1$) and blue represents the more viscous oil ($c = 0$). The dashed, black lines represent the locations of the shocks representing the root and tip regions. Compare with Figure 3.5.

for a symmetric disturbance. The c_n's satisfy

$$\frac{\partial c_0}{\partial t} + \Lambda \sum_{n=1}^{\infty} c_n \frac{\partial c_n}{\partial x} = 0,$$

$$\frac{\partial c_n}{\partial t} + \Lambda c_n \frac{\partial c_0}{\partial x} + \frac{\Lambda}{2} \sum_{r=1}^{n-1} \left(\frac{n-2r}{n-r} c_r \frac{\partial c_{n-r}}{\partial x} + \frac{2r-n}{r} c_{n-r} \frac{\partial c_r}{\partial x} \right)$$
$$+ \frac{\Lambda}{2} \sum_{r=1}^{\infty} \left(\frac{n+2r}{n+r} c_r \frac{\partial c_{n+r}}{\partial x} + \frac{n+2r}{r} c_{n+r} \frac{\partial c_r}{\partial x} \right) = -\frac{4\pi^2}{\mathrm{Pe}^*} n^2 c_n.$$

The diffusive term leads to exponential decay in time for $c_1, c_2, \ldots$, with the rate of decay proportional to n^2. The c_2 term will therefore decay 4 times faster than the c_1 term, and so the dominant behaviour is likely to come from just c_0 and c_1, at least for large αt. Hence, although our solution is only valid for a specific shape of the initial disturbance, we might expect (3.35)-(3.36) to be reasonably accurate for more general disturbances.

The Wooding solution helps us to understand the behaviour of (3.23) in region II, between the finger-tip and finger-root, and in particular helps to explain the genesis of shocks, which must correspond to the tips and roots of the fingers. While we have been able to find an explicit analytical solution, (3.35)-(3.36), which even incorporates the effect of transverse diffusion, it is only valid if we can match it to a valid solution in the tip- and root- regions. One might expect that the reintroduction of longitudinal diffusion into the problem would allow us to determine the correct shock speed, analogously to the rôle of viscosity in the famous 'viscous shock' solutions of Burgers' equation. This possibility is considered in the next section.

3.4.2 The Yortsos problem

In a paper by Yortsos & Salin [63] the model

$$\frac{\partial c}{\partial t}+\frac{\partial}{\partial x}\left(\frac{\mu^*(c)}{\mu(c)}c\right)-\frac{\partial}{\partial y}\left(c\int_0^y\frac{\partial}{\partial x}\left(\frac{\mu^*(c)}{\mu(c)}\right)\mathrm{d}y\right)=\frac{1}{\mathrm{Pe}}\left(\frac{\partial^2 c}{\partial x^2}+\frac{\partial^2 c}{\partial y^2}\right), \tag{3.37}$$

is studied, where

$$\mu^*=\left(\int_0^1\frac{1}{\mu(c(x,y))}\,\mathrm{d}y\right)^{-1}.$$

The model is somewhat similar to (3.23), but the physical motivation that leads to its derivation is slightly different, and there is the notable addition of a diffusive term in the $x-$direction. The model was derived by applying the large aspect-ratio assumption, but as a consequence of the porous medium having a large aspect ratio rather than the fingers. Boundary conditions of $\partial c/\partial y=0$ are applied on the boundaries of the porous medium at $y=0,1$. A typical oil reservoir may have a length of 2km and a depth of 100m, so the aspect ratio of a typical oil reservoir is indeed quite large. It is not clear why the longitudinal diffusion term should be retained in (3.37), although perhaps some attempt to model the anisotropy of diffusion could justify its appearance.

In (3.37) the large aspect ratio assumption is independent of the Péclet number. Since for the unstable case, $1/M<\mu^*<1$, [63] showed that it is possible to bound solutions to (3.37), above and below, by solutions to the one-dimensional problems

$$\frac{\partial c^*}{\partial t}+\frac{1}{\mu(c^*)}\frac{\partial c^*}{\partial x}=\frac{1}{\mathrm{Pe}}\frac{\partial^2 c^*}{\partial x^2},\quad \frac{\partial c_*}{\partial t}+\frac{1}{M\mu(c_*)}\frac{\partial c_*}{\partial x}=\frac{1}{\mathrm{Pe}}\frac{\partial^2 c_*}{\partial x^2}, \tag{3.38}$$

respectively. When $\mathrm{Pe}\gg 1$, (3.38) will have viscous shock solutions in which the solutions will change rapidly over a distance of $O(\mathrm{Pe}^{-1})$ at the shock, where they are of the form

$$c^*=c^*(\mathrm{Pe}(x-v^*t)),\quad c_*=c_*(\mathrm{Pe}(x-v_*t)).$$

If the upstream concentration is $c=1$, and the downstream concentration is $c=0$, then the velocities of the two bounding solutions will be given by

$$v^*=\int_0^1\frac{1}{\mu(c)}\,\mathrm{d}c,\quad v_*=\frac{1}{M}\int_0^1\frac{1}{\mu(c)}\,\mathrm{d}c. \tag{3.39}$$

Since $1/M\le\mu(c)\le 1$ we see that

$$\frac{1}{M}<v_*<1<v^*<M,$$

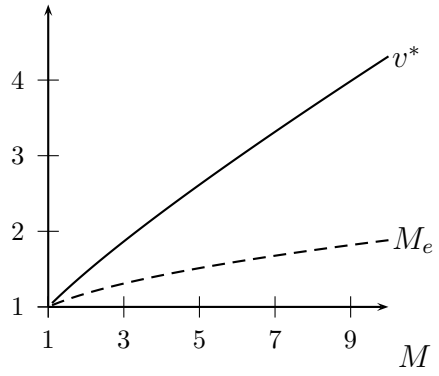

Figure 3.10: Plot of v^* and M_e, the predictions for the speed of the leading finger-tip of [63] and [33] respectively.

i.e. the concentration must spread at a rate that is slower than that predicted by the naïve Koval model, (3.18).

Since (3.37) is derived using the assumption of a large aspect-ratio porous medium, and not on the large-aspect ratio of fingers, it is legitimate to consider the behaviour near a finger-tip without making any rescalings. Suppose there exists an arbitrarily thin and solitary leading finger-tip, i.e. $c = 0$ for all values of y away from a thin region so that $\mu^* \approx 1$ near the tip. Assuming that the finger is parallel to the x-axis near the tip, we have that, along the line where the concentration of solvent takes its maximum value, $\partial c/\partial y = 0$. The maximum concentration near the leading finger-tip then satisfies

$$\frac{\partial c}{\partial t} + \frac{1}{\mu(c)}\frac{\partial c}{\partial x} = \frac{1}{\mathrm{Pe}}\frac{\partial^2 c}{\partial x^2}.$$

This suggests that c^* represents the maximum concentration near an arbitrarily thin and solitary leading finger-tip. Similarly c_* describes the minimum concentration near an arbitrarily thin and solitary trailing finger-root.

The bounds on the leading and trailing velocities, (3.39), do not give a tight bound when compared with the solution of the Koval model, (3.21), as we now show. With $\mu(c)$ defined as usual by (1.28), we find that

$$v^* = \frac{M^{5/4} - 1}{5(M^{1/4} - 1)},$$

whereas (3.21) predicts that the leading edge of the mushy region travels with speed $M_e = (0.22M^{1/4} + 0.78)^4$. In Figure 3.10 we see that $v^* > M_e$, for all M, and so the bound is not tight. Similarly we find that v_* is not a tight bound for the speed of the trailing finger-root.

We do not believe that it is justified in [63] to make the large aspect-ratio assumption

independently of the assumption of $\mathrm{Pe} \gg 1$. The large aspect-ratio assumption, as applied in this chapter, has been a consequence of the large aspect-ratio of the fingers. Near the tips and roots of the fingers, where shocks have formed, the large aspect-ratio assumption is no longer valid. We believe that the appropriate rescaling near the shock is one that reintroduces a fully two-dimensional flow problem rather than simply reintroducing longitudinal diffusion. It is this rescaling that we shall consider in the next section.

3.5 Tip rescaling

We have seen that the equation (3.23) generally leads to the formation of shocks. We have also seen that the equation cannot be derived in conservative form and so the shock conditions cannot be found. To determine the shock conditions we need to rescale the problem in the tip and root regions, identified in Figure 3.2, and then match with our solutions in the outer region where (3.23) is still valid.

3.5.1 Order-one aspect-ratio tip-rescaling

We recall that the length scale for the width of the fingers is given by ϵ where $\epsilon = O(\mathrm{Pe}^{-1/2})$. To reintroduce longitudinal diffusion into (3.23) we must rescale x with ϵ^2 near the shock. We note, however, that on this latter length scale, we no longer conclude that p is independent of Y. In fact we recover a two-dimensional elliptic problem for the pressure when x is rescaled with ϵ near the shock.

Near the shock we therefore seek a solution with $c = c(X, Y, t) + O(\epsilon)$ and

$$p \sim p_0(t) + \epsilon P(X, Y, t) + \ldots,$$

where

$$X = \frac{x - F(t)}{\epsilon},$$

and p_0 is the pressure obtained from matching to the regions away from the shock. The elliptic problem for P is

$$\frac{\partial}{\partial X}\left(\frac{1}{\mu(c)}\frac{\partial P}{\partial X}\right) + \frac{\partial}{\partial Y}\left(\frac{1}{\mu(c)}\frac{\partial P}{\partial Y}\right) = 0, \tag{3.40}$$

and the concentration satisfies

$$\frac{\partial c}{\partial t} - \frac{U}{\epsilon}\frac{\partial c}{\partial X} - \frac{1}{\epsilon}\frac{\partial}{\partial X}\left(\frac{c}{\mu(c)}\frac{\partial P}{\partial X}\right) - \frac{1}{\epsilon}\frac{\partial}{\partial Y}\left(\frac{c}{\mu(c)}\frac{\partial P}{\partial Y}\right) + \frac{\partial}{\partial X}(u_1 c) + \frac{\partial}{\partial Y}(v_1 c) = \frac{1}{\mathrm{Pe}^*}\left(\frac{\partial^2 c}{\partial X^2} + \frac{\partial^2 c}{\partial Y^2}\right),$$

where $U = \dot{F}(t)$. The coefficient of $\partial c/\partial t$ is small compared to ϵ^{-1}, and so the quasi-steady-state assumption applies: c and P only depend on t through the boundary conditions and through U. We find that, after an initial transient where $t = O(\epsilon)$,

$$U\frac{\partial c}{\partial X} + \frac{\partial}{\partial X}\left(\frac{c}{\mu(c)}\frac{\partial P}{\partial X}\right) + \frac{\partial}{\partial Y}\left(\frac{c}{\mu(c)}\frac{\partial P}{\partial Y}\right) = 0. \tag{3.41}$$

Equations (3.40) and (3.41) form our model for the tip region. We also need to determine the boundary conditions by matching with the homogenised region II and with regions ahead of the tips in which only oil is present.[2] At a shock representing a finger tip, we have

$$c \to c_{\pm}(Y), \qquad \frac{\partial P}{\partial X} \to -\mu^*_{\pm}, \quad \text{as} \quad X \to \pm\infty, \tag{3.42}$$

where $\mu^*_{\pm}$ are independent of X and Y and are defined by

$$\frac{1}{\mu^*_{\pm}} = \overline{\left(\frac{1}{\mu(c_{\pm})}\right)}.$$

To make further progress we shall restrict ourselves to considering the behaviour of leading finger tips (see Figure 3.11), which may be isolated or may form an array, and which match upstream to the region in which only oil is present. For leading finger tips we therefore have the boundary conditions $c \to 0$ and $\partial P/\partial X \to -1$ as $X \to \infty$. The rate of growth of the leading finger-tips governs the rate of growth of the edge of the mixing zone, and so understanding the growth of these leading finger tips will hopefully lead to an explanation of the origin of the effective mobility ratio M_e that appears in the modified Koval model (3.21). We can conceive of three possible scenarios for the structure of the fingering near to the leading finger-tips:

a) All the fingers are periodic in Y, so that all the finger-tips are aligned, occurring at the same value of x. In the tip region the problem is periodic in Y with period 1. This scenario of *periodic fingers* is depicted in Figure 3.11a.

b) The leading finger-tips are periodic, but further "interior" finger-tips may exist. In the tip region the problem is periodic in Y with period W, a measure of the number of interior finger-tips that exist between the leading finger-tips. Any interior finger-tips are assumed to be separated from the leading finger-tips by distance in x much larger than ϵ, and so there is no direct interaction between the interior finger-tip region and the leading finger-tip region. This scenario of *periodic leading finger-tips* is depicted in Figure 3.11b.

[2]Equations (3.40)-(3.41) also hold near the finger-roots, where we must match with the homogenised region II and a region behind the roots in which only solvent is present.

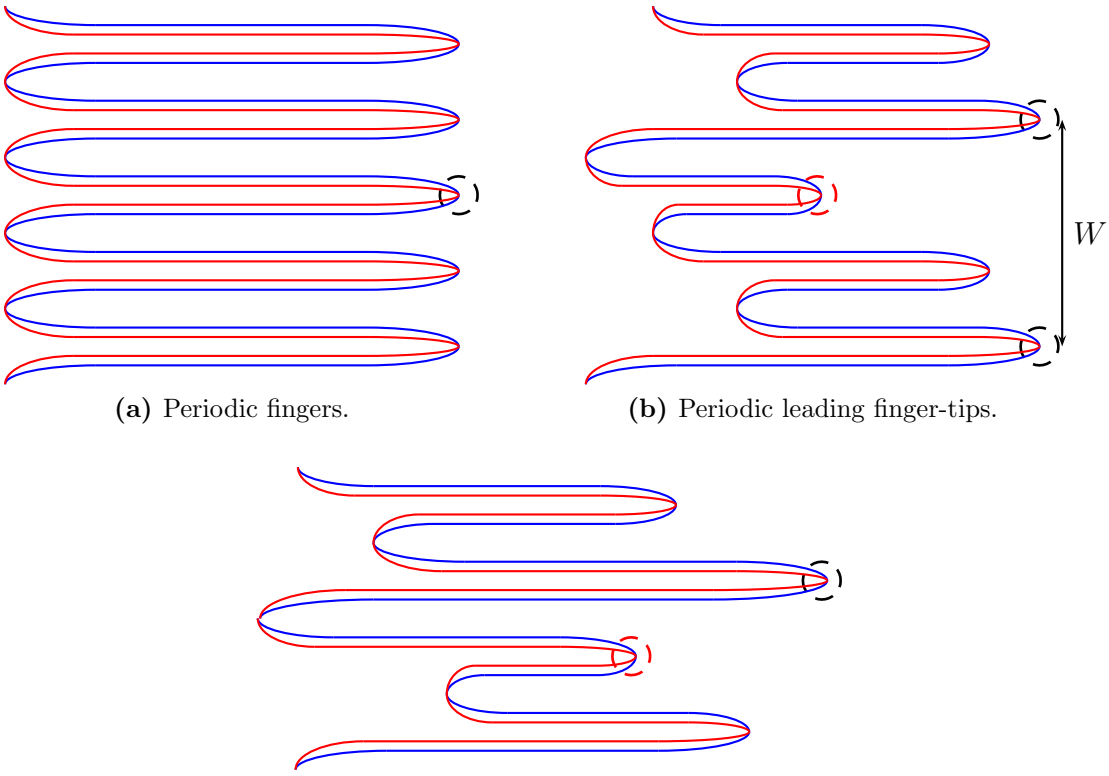

(a) Periodic fingers.

(b) Periodic leading finger-tips.

(c) Solitary leading finger-tip.

Figure 3.11: Illustrations of the three possible scenarios for the structure of the fingering near to the leading finger-tip/s. Some leading finger-tips are shown inside black circles and some interior finger-tips are shown inside red circles. In the second figure, depicting periodic leading finger-tips, the period between the finger tips is shown as W.

c) A solitary leading finger-tip, which does not interact with any other finger-tips. This scenario of a *solitary leading finger-tip* is depicted in Figure 3.11c.

We begin by considering scenarios a and b, periodic fingers and periodic leading finger-tips.

3.5.1.1 Periodic finger tips

The solution should be periodic in Y and away from the shock, as $X \to -\infty$, should match with the solution given by (3.23). If the fingers are themselves periodic (as in Figure 3.11a) then the finger-tips will have period 1; however, if it is only the finger-tips themselves that are periodic (as in Figure 3.11b) then the period will be larger, say equal to W. We shall therefore treat scenario a as a special case of scenario b, periodic leading finger-tips, with $W = 1$. The solution is W periodic in Y, as $X \to -\infty$ should match with the solution in the homogenised region II, and as $X \to \infty$ should match with a region containing only oil. We can arbitrarily translate the solution in Y so that the maximum

value of c, as $X \to -\infty$ lies on $Y = 0$, and we will then have the boundary conditions

$$\frac{\partial P}{\partial Y} = 0, \quad \frac{\partial c}{\partial Y} = 0, \quad \text{on} \quad Y = 0, W$$

and

$$c \to c_-(Y), \quad \frac{\partial P}{\partial X} = -\mu_-^* \quad \text{as} \quad X \to -\infty,$$

where $c_-(Y)$ is the concentration behind the shock and, μ_-^* is the usual harmonic average of $\mu(c_-(Y))$. As $X \to +\infty$, the concentration matches with the concentration ahead of the shock, i.e. $c \to 0$, and $\partial P/\partial X \to -1$.

We can determine a relationship between the concentration behind the shock and the velocity of the shock, U, as we now show. Integrating (3.41) over $-\infty < X < \infty$, $0 < Y < W$ and applying the boundary conditions (3.42) with $c_+ = 0$ and $\mu_+^* = 1$ we find that

$$U = \frac{\mu_-^*}{W\bar{c}_-} \int_0^W \frac{c_-(Y)}{\mu_-(Y)} \, \mathrm{d}Y, \tag{3.43}$$

where

$$\bar{c}_- = \frac{1}{W} \int_0^W c_-(Y) \, \mathrm{d}Y.$$

In addition to being periodic in Y, we also expect that the concentration will be symmetric in Y about $Y = 0$. We then only need to consider the solution in $0 < Y < W/2$, to obtain the solution for all Y. We note that (3.40)-(3.41) are invariant under the rescalings

$$X \to \lambda X', \quad Y \to \lambda Y', \quad \text{and} \quad P \to \lambda P',$$

as are the boundary conditions

$$\frac{\partial P}{\partial X} \to -\mu_\pm^* \quad \text{as} \quad X \to \pm\infty,$$

and so we can therefore rescale X, Y and P by $W/2$ without altering the problem. The period between fingers W only appears in the downstream concentration of solvent where it is a measure of the finger width as a fraction of the spacing between fingers. One particular family of symmetric, weak solutions with discontinuous boundary conditions as $X \to -\infty$ corresponds to the Saffman-Taylor fingers of section 1.3.3 When the downstream viscosity is given by

$$\mu_-(Y) = \begin{cases} 1/M & 0 < Y < \lambda, \\ 1 & \lambda < Y < 1, \end{cases} \tag{3.44}$$

we find from (3.43) that the velocity of the tip is given by

$$U = \frac{M}{1 + \lambda(M-1)},$$

as found in [49], and we note that $\lambda \propto 1/W$. The Saffman-Taylor finger solution is clearly a possible weak solution of (3.40)-(3.41) when periodic fingers are sought, although diffusion will act in an inner-inner region at the boundary between the solvent and oil. In fact the Saffman-Taylor finger is the only possible solution, when periodic fingers are sought, as we shall now show.

We note that in our tip-scale model (3.40)-(3.41), diffusion does not appear. It is only possible for the oil and solvent to mix in "inner regions" of our tip-scale problem where there is a sharp jump in the concentration. The rate at which oil mixes with solvent over these inner regions is small, and so we must not only conserve the total mass of fluid and the total mass of solvent, but also the total mass of 'pure oil', i.e. oil that is not mixed with any solvent. The total flux of pure oil upstream must therefore be equal to the total flux of pure oil downstream, and there must be a finite-width region of pure oil downstream of the finger tip. If this region is given by $\lambda < Y < 1$ then we find from equating the flux of pure oil upstream and downstream of the finger tip that

$$(1-\lambda)(\mu_-^* - U) = 1 - U, \tag{3.45}$$

where as usual

$$\frac{1}{\mu_-^*} = \int_0^1 \frac{1}{\mu(c_-(Y))}\,\mathrm{d}Y.$$

Using (3.43) to find U, (3.45) becomes

$$1 - \lambda + \frac{\lambda}{\bar{c}_-}\int_0^1 \frac{c_-(Y)}{\mu(c_-(Y))}\,\mathrm{d}Y = \frac{1}{\mu_-^*}.$$

We can write

$$\begin{aligned}\int_0^1 \frac{1}{\mu(c_-(Y))}\,\mathrm{d}Y &= \int_0^\lambda \frac{1}{\mu(c_-(Y))}\,\mathrm{d}Y + \int_\lambda^1 \mathrm{d}Y \\ &= 1 - \lambda + \int_0^\lambda \frac{1}{\mu(c_-(Y))}\,\mathrm{d}Y,\end{aligned}$$

and so we obtain the condition that

$$\frac{\lambda}{\bar{c}_-}\int_0^1 \frac{c_-(Y)}{\mu(c_-(Y))}\,\mathrm{d}Y = \int_0^\lambda \frac{1}{\mu(c_-(Y))}\,\mathrm{d}Y,$$

or, since $c_-(Y) = 0$ in $\lambda < Y < 1$,

$$\int_0^\lambda \frac{c_-(Y)}{\mu(c_-(Y))}\,\mathrm{d}Y = \frac{1}{\lambda}\int_0^\lambda c_-(Y)\,\mathrm{d}Y \int_0^\lambda \frac{1}{\mu(c_-(Y))}\,\mathrm{d}Y. \tag{3.46}$$

However, since μ is a monotonic decreasing function of c we require that

$$\frac{1}{\lambda}\int_0^\lambda \frac{c_-(Y)}{\mu(c_-(Y))}\,\mathrm{d}Y \geq \frac{1}{\lambda^2}\int_0^\lambda c_-(Y)\,\mathrm{d}Y \int_0^\lambda \frac{1}{\mu(c_-(Y))}\,\mathrm{d}Y,$$

with equality if and only if $c_-(Y)$ is constant in $0 < Y < \lambda$. Since (3.46) implies that equality holds we see that $c_-(Y)$ must be constant in $0 < Y < \lambda$, and the only permissible downstream concentration profile corresponds to that of the Saffman-Taylor finger with a region of oil separated from a region with a constant concentration of solvent. This result strongly suggests that the only possible tip-scale solution corresponds to a Saffman-Taylor finger.

The speed at which the Saffman-Taylor fingers travel will depend on the value of λ. The modified Koval model (3.21) predicts that the leading edge of the mixing zone, and hence the leading finger-tips, grow at a rate equal to M_e. If the Saffman-Taylor finger solution at the tip corresponds to pure solvent displacing pure oil then its velocity is given by (3.44), and if it is to travel at the speed predicted by (3.21) then we require

$$\lambda = \frac{M/M_e - 1}{M - 1}. \tag{3.47}$$

As noted in section 1.3.4.3, in Hele-Shaw cell experiments of the Saffman-Taylor finger, with immiscible fluids, a particular value of λ appears to be chosen, namely $\lambda = 1/2$ [49]. It has proved possible to explain the selection of the $\lambda = 1/2$ Saffman-Taylor finger by the introduction of both surface-tension [12, 9] and kinetic undercooling [10] as regularisations of the Muskat problem. It is possible that the reintroduction of diffusion near the jump in concentration will have a similar effect; however, unlike the surface-tension and kinetic undercooling regularisations we do not hope that the $\lambda = 1/2$ finger is selected, since (3.47) predicts that λ will be a function of M, with values ranging from 0 for very large values of the mobility ratio to $1 - c_e = 0.78$ for values of M close to 1. A complete understanding of the shape selection mechanism that occurs near the finger-tip requires much further work, including a reintroduction of diffusion into an inner region along the boundary between the solvent and oil.

Even without introducing the concept of "conservation of pure oil", we can show that there is no non-trivial, classical solution to (3.40) and (3.41). For a classical solution, one does not need to leave (3.41) in conservative form, and after multiplying by μ^α and using

(3.40) one can rewrite (3.41) as

$$U\frac{\partial \mu^{\alpha+1}}{\partial X} + \nabla \cdot \left(\mu^{\alpha}\frac{\partial P}{\partial X}\right) = 0,$$

for arbitrary α. On integrating over the entire domain we find that

$$U = \frac{\mu_-^* \overline{\mu_-^{\alpha}} - 1}{\overline{\mu_-^{\alpha+1}} - 1}.$$

For this to be true for all α we may multiply the above equation through by $\overline{\mu_-^{\alpha+1}} - 1$ and differentiate both sides with respect to α to obtain the condition

$$\int_0^1 \mu_-^{\alpha}(U\mu_- - \mu_-^*)\log\mu_- \,\mathrm{d}Y = 0.$$

Since $0 < \mu_- \leq 1$ and $\log\mu_- \leq 0$ the only part of the integrand of the above expression that changes sign is $(U\mu_- - \mu_-^*)$ which, for appropriately chosen U, will be negative for small values of the viscosity and positive for values of the viscosity closer to 1. If for a given α we have found a U such that the integral is equal to zero, then changing α must change the value of the integral *unless* $(U\mu_- - \mu_-^*)\log\mu_-$ is identically equal to zero for all Y. The condition that $(U\mu_- - \mu_-^*)\log\mu_-$ is identically equal to zero leads us to conclude that $\mu_-(Y)$ can only take two values, one of which must be equal to 1. Therefore, either (3.41) only holds in conservative form or the boundary conditions for c must be those of a Saffman-Taylor finger, both of which indicate that we do not have a classical solution.

With periodic leading finger-tips, the rate of growth of the leading edge of the homogenised region is related to the separation W between the leading finger-tips. It is not immediately clear why the leading finger-tips should be periodic in Y, and one might expect that instead a solitary leading finger-tip would exist as in Figure 3.11c. We shall therefore now look at the behaviour of a solitary leading finger-tip.

3.5.1.2 A solitary leading finger tip

Since each individual finger is thin, a solitary leading finger-tip makes a small contribution to the harmonic average of the viscosity. The harmonic average of the viscosity both downstream and upstream of the leading finger is therefore equal to 1 (the viscosity of the oil). The boundary conditions as $X \to \pm\infty$ are $\partial P/\partial X \to -1$, $c(Y) \to 0$ as $X \to \infty$, and $c(Y) \to c_-(Y)$ as $X \to -\infty$. The first observation that we can make is that

$$\int_{-\infty}^{\infty}\left(\frac{1}{\mu(c)}\frac{\partial P}{\partial X}\right)_{X\to\infty} - \left(\frac{1}{\mu(c)}\frac{\partial P}{\partial X}\right)_{X\to-\infty}\mathrm{d}Y = \int_{-\infty}^{\infty}\left(\frac{1}{\mu(c_-(Y)}-1\right)\mathrm{d}Y,$$

which in general will not be equal to zero, and so there appears to be a difference between the total fluxes of fluid upstream and downstream of the finger. This difference between the fluxes of fluid as $X \to \pm\infty$ can be explained by the existence of a finite flux of fluid as $Y \to \pm\infty$. A solitary finger-tip therefore affects the flow far away (in Y) from the tip. By analogy with the zero-width Saffman-Taylor finger, the pressure near the tip will be of the form $p \sim O(\sqrt{r})$, where $r = \sqrt{X^2 + Y^2}$.

If a solitary leading finger-tip were to exhibit a sharp interface between the solvent and oil then the rate of growth of the finger-tip would be equal to that of the zero-width Saffman-Taylor finger, i.e. $U = M$. This growth rate is the same as that predicted by the naïve Koval model (3.18), and we have already seen (see Figure 3.3) that this is much larger than the observed growth rate of the leading fingers. Therefore, if the leading finger-tips in a miscible displacement are indeed solitary then to agree with our experimental observations, they may not exhibit a sharp interface between the solvent and oil. We therefore seek similarity solutions of (3.40)-(3.41) in which c changes smoothly. We have noticed in the previous section that (3.40)-(3.41) are invariant under the rescalings

$$X \to \lambda X', \quad Y \to \lambda Y', \quad \text{and} \quad P \to \lambda P',$$

and this suggests that we may be able to seek a similarity solution of the form $c = \tilde{f}(Y/X)$ and $P = X\tilde{g}(Y/x)$, or equivalently $c = f(\theta)$ and $P = rg(\theta)$, where $r = \sqrt{X^2 + Y^2}$ and $\theta = \tan^{-1}(Y/X)$. Seeking a solution of this form we find from (3.40)-(3.41) that

$$\frac{g(\theta)}{\mu(f(\theta))} + \frac{\mathrm{d}}{\mathrm{d}\theta}\left(\frac{g'(\theta)}{\mu(f(\theta))}\right) = 0, \quad \text{and} \quad -f'(\theta)\sin\theta + \frac{f(\theta)g(\theta)}{\mu(f(\theta))} + \frac{\mathrm{d}}{\mathrm{d}\theta}\left(\frac{f(\theta)g'(\theta)}{\mu(f(\theta))}\right) = 0,$$

from which we can find that

$$g(\theta) = -\mu(f(\theta))\cos\theta, \quad \text{and} \quad g'(\theta) = \mu(f(\theta))\sin\theta.$$

We conclude that $f'(\theta) = 0$, except possibly when $\theta = \pi/2$, and so we will have c constant in $\theta \leqslant \pi/2$. This solution simply corresponds to a one-dimensional interface, and does not help us to produce a solution with a smoothly varying concentration of solvent.

The interface near the very tip of a Saffman-Taylor finger is of a parabolic shape corresponding to the Ivantsov parabola [30, 34]. This suggests that we might also try to seek a similarity solution of (3.40)-(3.41) by changing to parabolic coordinates defined implicitly by

$$\begin{aligned} X &= \tfrac{1}{2}\left(\xi^2 - \eta^2\right), \\ Y &= \xi\eta. \end{aligned}$$

In parabolic coordinates (3.40)-(3.41) become

$$\frac{\partial}{\partial\xi}\left(\frac{1}{\mu(c)}\frac{\partial P}{\partial\xi}\right)+\frac{\partial}{\partial\eta}\left(\frac{1}{\mu(c)}\frac{\partial P}{\partial\eta}\right)=0,$$

and

$$U\left(\xi\frac{\partial c}{\partial\xi}-\eta\frac{\partial c}{\partial\eta}\right)+\frac{\partial}{\partial\xi}\left(\frac{c}{\mu(c)}\frac{\partial P}{\partial\xi}\right)+\frac{\partial}{\partial\eta}\left(\frac{c}{\mu(c)}\frac{\partial P}{\partial\eta}\right)=0.$$

If we seek solutions with $c=c(\xi)$, independent of η, then we find that the only possible solution corresponds to the Ivantsov parabola, with $\mathrm{d}c/\mathrm{d}\xi=0$, for almost all ξ. When solvent is displacing oil our solution is

$$c=1 \quad \text{in} \quad \xi<\xi_0, \qquad c=0 \quad \text{in} \quad \xi>\xi_0,$$

and

$$P=-\frac{U}{2M}(\xi^2-\eta^2),$$

in $\xi<\xi_0$, and

$$P=-\frac{U}{2M}(\xi^2-\eta^2)+U\left(\frac{1}{M}-1\right)\xi_0(\xi-\xi_0),$$

in $\xi>\xi_0$, where ξ_0 may be chosen arbitrarily. Once again there are no solutions in which we have a smooth transition between solvent and oil. Hence, it appears to be the case that there are no non-trivial solutions to (3.40)-(3.41) in which c varies smoothly, and that an interface between solvent and oil must always be present.

In summary it appears to be the case that a solitary leading finger-tip will grow at the same speed as a zero-width Saffman-Taylor finger, which does not agree with the growth rate of leading finger-tips in simulations (Figure 3.3). We therefore propose that solitary leading finger-tips do not appear in practice, and instead the leading edge of the homogenised region consists of periodic finger-tips as depicted in Figure 3.11b. We now endeavour to give a physical explanation to support this proposition.

3.5.1.3 The formation of periodic finger-tips

In this section we attempt to suggest a phenomenological explanation as to why periodic finger-tips form at the leading edge, rather than a solitary leading finger. An interesting phenomena has been observed in numerical simulations of miscible flow through porous media [64], referred to as *fading*. Fading occurs when one leading finger has advanced ahead of surrounding fingers. It is observed [64] that when a solitary leading finger advances far into the oil, the solvent "chooses" to flow into a shorter nearby finger, rather than flow into the tip of the leading finger, and the concentration of solvent in the tip of

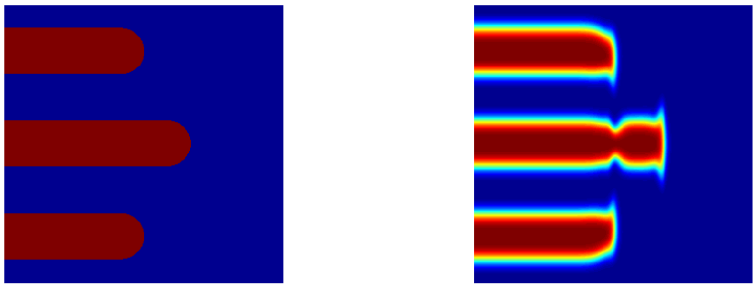

(a) $t = 0$ **(b)** $t = 0.05$

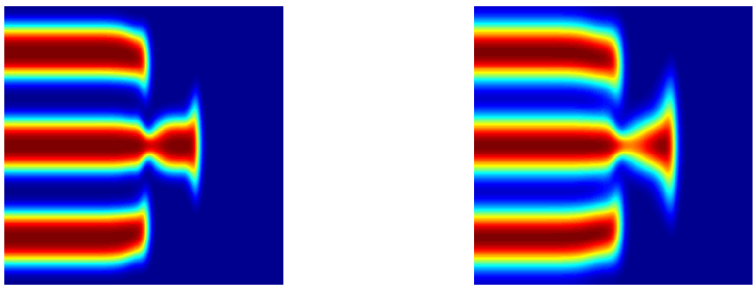

(c) $t = 0.1$ **(d)** $t = 0.2$

Figure 3.12: Numerical simulation of (3.23) in a moving frame $\xi = x - t$, with a small, artificial longitudinal diffusion term. Red represents the solvent ($c = 1$) and blue represents the oil ($c = 0$), and we have taken $M = 2$, and $\mathrm{Pe}^* = 1/200$ for this simulation. The initial condition in 3.12a consists of a leading finger surrounded by two trailing fingers, and we observe that, as time progresses, the tip of the leading finger is 'pinched-off', so that eventually these fingers are of approximately equal length.

the leading finger is observed to drop. Once the fading process is complete the leading finger is of the same length as the nearby finger that appears to have initiated the fading. The fading process is an interaction between the finger that follows the leading finger-tip and an interior finger-tip, in which the end of the finger that follows the leading finger-tip is pinched off. The pinching-off process can be observed (see Figure 3.12) in simulations of (3.23) regularised by longitudinal diffusion as in section 3.4, but we also expect that pinching-off will occur when the correct order-one aspect-ratio regularisation is introduced.

Further investigation of this fading process may be useful in understanding how periodic finger-tips form, and possibly determining a preferred separation. We suspect that the observed speed of the leading edge of the mixing-zone may be the result of a dynamic balance between the accelerated growth of leading fingers and this pinch-off mechanism.

3.5.2 Concluding remarks on tip-rescaling

In this section we have seen that, rather than reintroducing diffusion in a tip region, we should instead recover the tip-scale problem (3.40)-(3.41) in which the pressure variation is fully two-dimensional. This rescaling corresponds to a tip-region in which the large aspect-ratio assumption used to derive (3.23) is no longer valid. We have suggested that the leading finger-tips must be periodic (as in Figure 3.11b) rather than there existing a solitary leading finger-tip (as in Figure 3.11c), since the rate of growth of a solitary leading finger-tip does not correspond with experimental observations or numerical simulations. The only possible solution to (3.40)-(3.41) for the leading finger-tips corresponds to a Saffman-Taylor finger, with a sharp interface between the solvent and oil. The rate of growth of the edge of the homogenised region (region II), will depend on the separation between the leading finger-tips, and we suspect that a particular separation is selected. A possible explanation as to why the leading finger-tips formed are not solitary might be obtained by further investigation of the fading mechanism first reported in [64]; however, much more work is necessary.

3.6 Dynamic scaling of finger-width

In all of our previous work we have assumed that the finger-width is constant. If one were to consider a single finger in isolation then one would expect the width of the finger to increase over time as the finger spread out under transverse diffusion, with the rate of growth of the width of the finger under diffusion being proportional to $\sqrt{t}$. In experiments the mean finger width is indeed observed to increase at a rate proportional to $\sqrt{t}$; however, it is also observed that diffusion is not directly responsible for this increase in the mean width of the fingers. Rather, the mechanism by which the mean width of fingers is observed to increase is convective coalescence of nearby fingers, as can be observed in Figure 3.13. The two fingers at the centre of the circle when $t = 0.2$ are in the process of coalescing when $t = 0.3$ and have formed a single larger finger when $t = 0.4$. The width of an individual finger therefore increases discretely in time, rather than continually spreading out under transverse diffusion.

Since it is only the mean finger-width that is increasing in time and not the width of the individual fingers that is increasing, the analysis of the previous sections is still valid, provided the aspect-ratio of the fingers is still large. It is only when we come to decide upon an appropriate value for the diffusion parameter α that we must take into

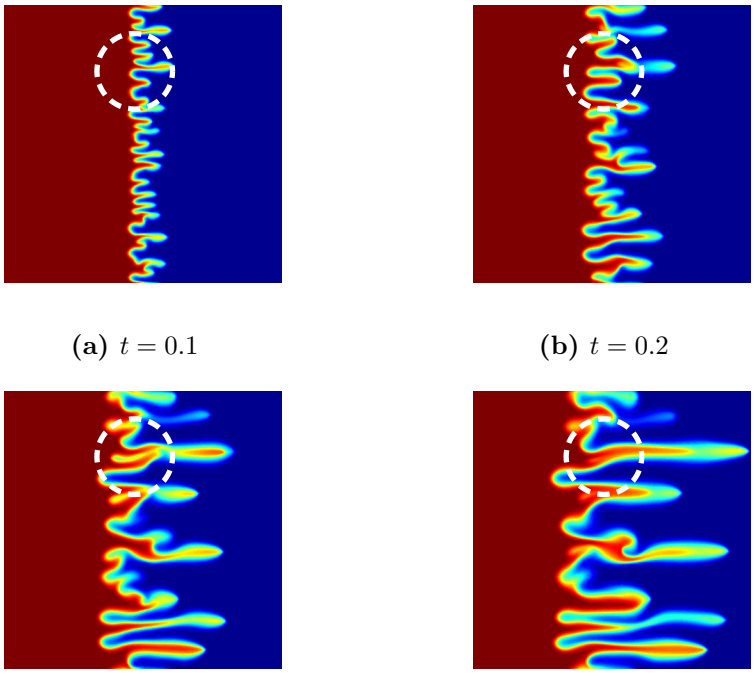

(a) $t = 0.1$ **(b)** $t = 0.2$

(c) $t = 0.3$ **(d)** $t = 0.4$

Figure 3.13: Numerical simulations of the Peaceman model with $M = 20$, $\mathrm{Pe} = 2000$. Red represents the solvent ($c = 1$) and blue represents the oil ($c = 0$). Note that in addition to the horizontal spreading of the mixing zone, the mean finger-width is also increasing with time. Inside the circled regions one can observe an example of the convective coalescence that is observed to be responsible for the increase in the mean finger-width.

consideration this coarsening effect. We recall that α is given by

$$\alpha = \frac{4\pi^2}{\epsilon^2 \mathrm{Pe}},$$

where ϵ is the aspect ratio of the fingers and Pe is the macroscopic Péclet number. Since the mean length of the fingers increases at a rate proportional to t and the mean width of the fingers increases at a rate proportional to $\sqrt{t}$ we find that the aspect ratio of the fingers must increase at a rate proportional to $\sqrt{t}$. This suggests that the mean value of α will decrease over time at a rate proportional to $1/t$.

When there are many fingers, all with slightly different widths, the general solution for the transversely averaged concentration will be of the form

$$\bar{c}(x,t) = \int_0^\infty f(t,\alpha) c_0(x,t,\alpha)\,\mathrm{d}\alpha, \tag{3.48}$$

where c_0 is the average of the solution to (3.23) with $\mathrm{Pe}^* = 4\pi^2/\alpha$ and f is a density function representing the distribution of fingers with a finger-width corresponding to α. Since the mean value of α decreases over time at a rate proportional to $1/t$, this suggests

that $f = f(\alpha t)$. We also note that (3.23) is invariant under the scaling

$$t \to \lambda t',\ x \to \lambda x',\ \mathrm{Pe}^* \to \lambda \mathrm{Pe}^{*\prime},$$

which suggests that $c_0 = c_0(x/t, \alpha t)$. The transverse average of the concentration only depends on x/t, and is of the form

$$\bar{c}(x/t) = \int_0^\infty f(s) c_0(x/t, s)\, \mathrm{d}s, \tag{3.49}$$

for some $f(s)$, where $s = \alpha t$. The function $f(s)$, representing the distribution of different finger-width solutions, is a consequence of the stability of, and interactions between, fingers of varying widths, and it is not at all easy to determine.

3.7 Conclusions

In this chapter we have shown that the derivation of the Koval model is only possible in the limiting case where the Péclet number is large, which results in the formation of many long, thin and straight fingers. The morphology in which there are many long, thin, straight fingers is necessary in order that both a sensible averaging direction and a sensible average exist. We have taken this average using a homogenisation theory which exploits the large aspect-ratio of the fingers. We emphasise that we have justified the large aspect ratio assumption as a consequence of the large Péclet number and the consequential large aspect-ratio of the fingers, rather than the aspect ratio of the medium itself. Previous works, for example [62], have developed a similar model to (3.23) under the large aspect ratio assumption that the porous medium in which the miscible displacement occurs has a large aspect-ratio. With this latter assumption, the connection between the Péclet number and the size of the aspect ratio is lost, and it is not clear where diffusion will be important.

One might naïvely have assumed that, in the large Péclet number limit, we would be able to entirely neglect diffusion and therefore there would be no appreciable mixing between the oil and the solvent. This assumption led us to the naïve Koval model (3.18), which fails to accurately predict the rate of growth of the fingers. The failure of the naïve Koval model is due to the fact that transverse diffusion is, in fact, important at the small length scale of the fingers. Indeed, the width of the fingers is determined by the length scale on which transverse diffusion becomes relevant. We have confirmed that the modified Koval model (3.21) gives a reasonably good approximation of the evolution of the averaged concentration, but there is no rigorous physical explanation for the assumptions

that it makes.

We have then proceeded to investigate the homogenised problem (3.23), in which transverse diffusion is retained. We have shown that, when the difference in viscosities between the solvent and oil is reasonably small, (3.23) becomes a somewhat simpler model, that has already been investigated by [61]. We have found explicit solutions of this simpler model in which shocks are formed, and our numerical simulations have suggested that shock formation is a generic feature of the original homogenised problem, (3.23). Although we expect shocks to form we cannot immediately determine their speed because we do not have a classical hyperbolic system. The only way to proceed is to consider a local problem near the finger-tips.

In this tip region the flow is fully two-dimensional but diffusion is not important to lowest order and the problem is similar to the Saffman-Taylor finger problem. Although, in principle, we may seek solutions to our tip-scale problem (3.40)-(3.41) in which the concentration of solvent varies smoothly downstream of the tip finger, we have shown that, at least for the leading finger-tips, no such solutions exist. At the leading finger-tips the transition from solvent to oil is sharp, and the flow is described by the Saffman-Taylor finger solution. The morphology of the leading finger-tips is such that they are periodic in Y, with a period greater than that of the interior-finger width in the homogenised region. The speed of the leading finger-tips is a function of their separation, and it seems that a particular separation (in Y) between the finger-tips is preferred. It is not at all easy to explain this shape selection mechanism and much more work is needed. A possible explanation for the formation of the periodic finger-tips, and perhaps their separation, lies in the fading, or pinching-off, mechanism described by Zimmerman and Homsy [64].

All of the work that we have done up to this point has assumed that the mean flow is unidirectional with the fingers pointing in the same direction. In practical applications this is not usually the case, either the direction of the applied pressure gradient varies throughout the medium or there are large-scale heterogeneities which the fluid may have to flow around. In the next chapter we shall extend the ideas that we have presented in this chapter to the situation in which the mean flow is not unidirectional.

Chapter 4

Multidirectional fingering

In the previous chapter we restricted ourselves to considering miscible displacements in entirely homogeneous media, and with the 'linear flood' geometry, so that the mean flux of fluid was one-dimensional. In practice solvent will be injected into oil reservoirs and oil will be recovered via several wells placed throughout the oil reservoir. The linear flood geometry is therefore not appropriate for modelling miscible displacements throughout the oil reservoir. Although the mean flux of fluid is no longer one-dimensional, we still expect the displacement of oil by a less viscous solvent to lead to the formation of fingering instabilities. Hence, provided that the width of the fingers is small compared to the length scale over which the mean flux of fluid varies, we may still apply the large aspect-ratio assumption that was crucial in the previous chapter.

True interaction between the heterogeneity of a porous medium and viscous fingering is an extremely difficult problem, with only a small number of entirely empirical results being available [33, 58], and some suggested crude bounds on the maximum rate of growth of the mixing zone [63]. Although we do not attempt to model viscous fingering when the length scale of the heterogeneities is comparable to that of the width of the fingers formed, in this chapter we shall allow for macroscopic heterogeneities that occur on a length scale much larger than the characteristic length scale of fingering. Most porous media contain large scale faults, where the permeability is very high, and also inclusions of nearly impermeable rock, where the permeability is very low, and so it is important that our model can deal with such features. In this chapter we shall therefore explicitly extend the Koval model of Chapter 3 to apply to geometries different to that of the linear flood, in porous media containing macroscopic heterogeneities.

When we have developed a two-dimensional Koval model, we will compare it with the standard models for immiscible flow through porous media, and comment on the Todd & Longstaff model [58], which is based on models of immiscible flow. Finally, we will investigate the stability of a disturbance to a one-dimensional solution. Our motivation

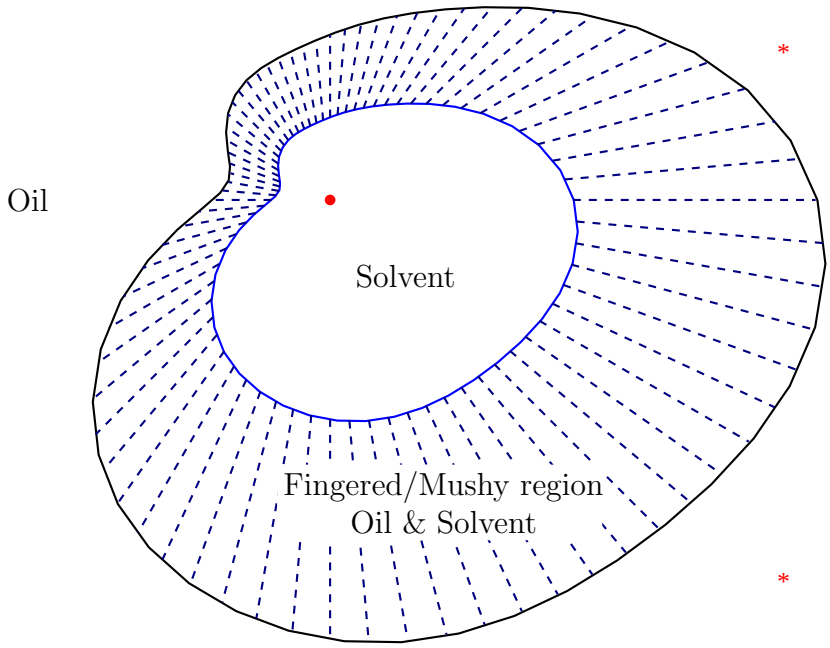

Figure 4.1: Schematic of a miscible displacement, with solvent introduced from an injector well (solid red dot) and recovered from producer wells (red asterisks). The oil and solvent are separated by a large fingered (or mushy) region in which there are many long fingers that point in the direction of flow.

for doing this lies in understanding whether the original viscous fingering instability is still present, and investigating to what extent the averaging process stabilises the problem.

4.1 The two-dimensional Koval model

The key practical limitation of the Koval model is that it is only capable of predicting the transverse average of the solution in a simple linear flood. In practice the geometry of the problem will not be as simple as a linear flood. The flow is driven by a series of oil wells, with solvent injected into some of the wells and oil or a mixture of oil and solvent, recovered from others as shown in Figure 4.1. There may also be some macroscopic heterogeneities in the reservoir, such as large regions of impermeable rock, around which the solvent and oil must flow. We shall develop a model for the averaged concentration of solvent across many fingers which does not assume that the macroscopic flow is one-dimensional as in the case of a linear flood. More precisely, we continue to make the assumption that the fingers are long and thin, but we do not a priori make an assumption about the direction in which they point.

As in Chapter 3, our fundamental model is the Peaceman model, in which we shall

now allow for a heterogeneous tensor permeability $\mathbf{K}(\mathbf{x})$, so that

$$\nabla \cdot \mathbf{u} = 0, \qquad \mathbf{u} = -\frac{\mathbf{K}(\mathbf{x})}{\mu(c)}\nabla p, \tag{4.1}$$

$$\frac{\partial c}{\partial t} + \nabla \cdot (\mathbf{u}c) = \frac{1}{\mathrm{Pe}}\nabla \cdot (\mathbf{D}\nabla c)\,. \tag{4.2}$$

We also expect, based on our previous findings in Chapter 2, that the concentration of solvent in the Peaceman model will show variation over two length scales, namely the macroscopic length scale of the reservoir and the length scale over which any fingering instabilities form. For large Péclet number miscible displacements, these two length scales will be well-separated, and indeed we have seen in section 2.3 that a large number of finger-like disturbances will form, with a characteristic width proportional to $\mathrm{Pe}^{-1/2}$. We therefore make the a priori assumption that the concentration of the solvent is of the form

$$c = c\left(\mathbf{x}, \frac{\mathbf{x}}{\epsilon}, t\right),$$

where $\epsilon = O(\mathrm{Pe}^{-1/2})$ is the aspect ratio of the fingers, and $\mathbf{x}$ and $\mathbf{X} = \mathbf{x}/\epsilon$ are treated as independent. To make analytical progress we have to separate behaviour at the macroscopic scale from behaviour at the fingering length scale. We therefore make the following two assumptions:

- We assume that the permeability does not vary over the short fingering length scale, so that the rock appears homogeneous at this length scale. The problem of interaction between heterogeneity and a fingering instability is too difficult for a full mathematical treatment; current theories either attempt to fit empirical data [33] or to bound the rate of growth of the mixing region [63].

- With a homogeneous permeability at the scale of the fingers, we assume that there will be a characteristic "fingering direction", with the flow being parallel to the fingering direction and the concentration varying rapidly across this fingering direction. Hence our model will only encompass flows in which any deviation from the straight, parallel fingers considered in Chapter 3 occurs at the macroscopic length scale $\mathbf{x}$ and not on the length scale of the finger width. This assumption may be violated close to the wells where the radius of the well-bore is comparable to the mean finger-width.

We introduce a coordinate system (r, s), chosen so that the vectors ∇r and ∇s are vectors parallel and perpendicular to the direction of fingering, the latter being in the $s-$direction. Since the direction of fingering only changes on the macroscopic length

scale, r and s only depend on $\mathbf{x}$ and not on $\mathbf{X}$, and since the concentration only varies across the fingering direction we have that

$$c = c(r, s, S, t),$$

where $S = s/\epsilon$. Applying this ansatz for the concentration of the solvent, the pressure satisfies

$$\nabla \cdot \left(\frac{\mathbf{K}(r,s)}{\mu(r,s,S,t)} \nabla p \right) = 0. \tag{4.3}$$

We need to express equation (4.3) in curvilinear coordinates, and to this end we shall need to introduce some simple tensor notation. Applying summation convention throughout, the contravariant metric tensor g^{ij} is defined by

$$g^{ij} = \frac{\partial \xi^i}{\partial x^k} \frac{\partial \xi^j}{\partial x^k},$$

where $\boldsymbol{\xi} = (r, s)$. The contravariant metric tensor is the inverse of the covariant metric tensor defined by

$$g_{ij} = \frac{\partial x^k}{\partial \xi^i} \frac{\partial x^k}{\partial \xi^j},$$

and we also use

$$g = \det(g_{ij}) = \frac{1}{\det(g^{ij})}.$$

Note that $g^{ij} = g^{ij}(r, s)$, i.e. the metric tensor is independent of S, and since r and s are orthogonal coordinates g^{ij} is diagonal, with $\det(g^{ij}) = g^{11} g^{22}$, $g^{11} = 1/g_{11}$ and $g^{22} = 1/g_{22}$. In r, s coordinates, the permeability tensor is $\tilde{K}^i{}_j(\boldsymbol{\xi})$ given by the tensor transformation relation,

$$\tilde{K}^i{}_j(\boldsymbol{\xi}) = \frac{\partial \xi^i}{\partial x^l} \frac{\partial x^m}{\partial \xi^j} K^l{}_m(\mathbf{x}) = \frac{\partial \xi^i}{\partial x^l} \frac{\partial x^m}{\partial \xi^j} K_{lm}(\mathbf{x}). \tag{4.4}$$

Applying the standard expressions from tensor analysis for the divergence and gradient (see e.g. [37]), (4.3) is equivalent to

$$\frac{1}{\sqrt{g}} \frac{\partial}{\partial \xi^i} \left(\frac{\sqrt{g}}{\mu} \tilde{K}^i{}_j g^{jk} \frac{\partial p}{\partial \xi^k} \right) = 0,$$

which can be expanded to give

$$\frac{\partial}{\partial r} \left(\sqrt{g} \left(\frac{g^{11} \tilde{K}^1{}_1}{\mu} \frac{\partial p}{\partial r} + \frac{g^{22} \tilde{K}^1{}_2}{\mu} \frac{\partial p}{\partial s} \right) \right) + \frac{\partial}{\partial s} \left(\sqrt{g} \left(\frac{g^{11} \tilde{K}^2{}_1}{\mu} \frac{\partial p}{\partial r} + \frac{g^{22} \tilde{K}^2{}_2}{\mu} \frac{\partial p}{\partial s} \right) \right) = 0. \tag{4.5}$$

For small ϵ we take the asymptotic expansions

$$\begin{aligned} p &\sim p_0(r,s,S,t) + \epsilon p_1(r,s,S,t) + \epsilon^2 p_2(r,s,S,t) + \dots \,, \\ c &\sim c_0(r,s,S,t) + \epsilon c_1(r,s,S,t) + \dots \,, \\ \mu &\sim \mu_0(r,s,S,t) + \epsilon \mu_1(r,s,S,t) + \dots \,, \end{aligned}$$

where

$$\mu_0 = \mu(c_0) \quad \text{and} \quad \mu_1 = c_1 \frac{\mathrm{d}\mu}{\mathrm{d}c}(c_0).$$

We apply the method of multiple scales and assume that s and S are independent, so that

$$\frac{\partial}{\partial s} = \frac{\partial}{\partial s} + \frac{1}{\epsilon}\frac{\partial}{\partial S}.$$

To leading order in (4.5) we find

$$\frac{\partial}{\partial S}\left(\sqrt{g}\frac{g^{22}(r,s)\tilde{K}^2{}_2(r,s)}{\mu_0(r,s,S,t)}\frac{\partial p_0}{\partial S}\right) = 0,$$

which has the solution

$$p_0 = \frac{a(r,s,t)}{\sqrt{g}g^{22}(r,s)\tilde{K}^2{}_2(r,s)}\int_0^S \mu_0(r,s,S',t)\,\mathrm{d}S' + \hat{p}_0(r,s,t),$$

where a and $\hat{p}_0$ are arbitrary functions, independent of S. Provided there exists a well-defined local average of μ_0 we can expand the integral in the above equation, for large S, as

$$\int_0^S \mu_0(r,s,S',t)\,\mathrm{d}S' \sim S\bar{\mu}(r,s,t),$$

where $\bar{\mu}$ is the average of μ_0. If the concentration is 1-periodic in S then

$$\bar{\mu}(r,s,t) = \int_0^1 \mu_0(r,s,S,t)\,\mathrm{d}S,$$

and if c_0 is described by a stationary and ergodic random variable then $\bar{\mu}$ is simply the expectation of μ_0. The leading order pressure is then given by

$$p_0 \sim \frac{a(r,s,t)\bar{\mu}(r,s)}{\sqrt{g}g^{22}(r,s)\tilde{K}^2{}_2(r,s)}S + \hat{p}_0(r,s,t) + \dots,$$

for large S, and so to ensure that the pressure remains bounded as $\epsilon \to 0$ and $S \to \infty$ we require that $a(r,s,t) = 0$; this is the analogue of (3.7). The next order terms in (4.5)

yield

$$\frac{\partial}{\partial S}\left(\frac{\sqrt{g}g^{11}(r,s)\tilde{K^2}_1(r,s)}{\mu_0(r,s,S,t)}\frac{\partial\hat{p}_0}{\partial r}(r,s,t)+\frac{\sqrt{g}g^{22}(r,s)\tilde{K^2}_2(r,s)}{\mu_0(r,s,S,t)}\left(\frac{\partial\hat{p}_0}{\partial s}(r,s,t)+\frac{\partial p_1}{\partial S}(r,s,S,t)\right)\right)=0,$$

from which we find that

$$\begin{aligned}p_1 &= \frac{b(r,s,t)}{\sqrt{g}g^{22}(r,s)\tilde{K^2}_2(r,s)}\int_0^S\mu_0(r,s,S',t)\,\mathrm{d}S'-\frac{g^{11}(r,s)\tilde{K^2}_1(r,s)}{g^{22}(r,s)\tilde{K^2}_2(r,s)}\frac{\partial\hat{p}_0}{\partial r}(r,s,t)S\\ &\quad -\frac{\partial\hat{p}_0}{\partial s}(r,s,t)S+\hat{p}_1(r,s,t),\end{aligned}$$

where b and $\hat{p}_1$ are arbitrary functions, independent of S, and so, for large S,

$$p_1 \sim \left(\frac{b(r,s,t)\bar{\mu}(r,s,t)}{\sqrt{g}g^{22}(r,s)\tilde{K^2}_2(r,s)}-\frac{g^{11}(r,s)\tilde{K^2}_1(r,s)}{g^{22}(r,s)\tilde{K^2}_2(r,s)}\frac{\partial\hat{p}_0}{\partial r}(r,s,t)-\frac{\partial\hat{p}_0}{\partial s}(r,s,t)\right)S+\ldots\,.$$

To ensure that p_1 remains bounded and our asymptotic expansion remains valid, we therefore require that

$$b(r,s,t)=\frac{1}{\bar{\mu}(r,s,t)}\left(\sqrt{g}g^{11}(r,s)\tilde{K^2}_1(r,s)\frac{\partial\hat{p}_0}{\partial r}(r,s,t)+\sqrt{g}g^{22}(r,s)\tilde{K^2}_2(r,s)\frac{\partial\hat{p}_0}{\partial s}(r,s,t)\right),$$

which is the analogue of (3.9). The order-one terms in (4.5) are

$$\begin{aligned}&\frac{\partial}{\partial r}\left(\sqrt{g}\left(\frac{g^{11}\tilde{K^1}_1}{\mu_0}\frac{\partial\hat{p}_0}{\partial r}+\frac{g^{22}\tilde{K^1}_2}{\mu_0}\frac{\partial\hat{p}_0}{\partial s}+\frac{g^{22}\tilde{K^1}_2}{\mu_0}\frac{\partial p_1}{\partial S}\right)\right)+\\ &\frac{\partial}{\partial s}\left(\sqrt{g}\left(\frac{g^{11}\tilde{K^2}_1}{\mu_0}\frac{\partial\hat{p}_0}{\partial r}+\frac{g^{22}\tilde{K^2}_2}{\mu_0}\frac{\partial\hat{p}_0}{\partial s}+\frac{g^{22}\tilde{K^2}_2}{\mu_0}\frac{\partial p_1}{\partial S}\right)\right)+\\ &\frac{\partial}{\partial S}\left(\sqrt{g}\left(\frac{g^{11}\tilde{K^2}_1}{\mu_0}\frac{\partial p_1}{\partial r}+\frac{g^{22}\tilde{K^2}_2}{\mu_0}\frac{\partial p_1}{\partial s}+\frac{g^{22}\tilde{K^2}_2}{\mu_0}\frac{\partial p_2}{\partial S}\right)\right)-\\ &\frac{\partial}{\partial S}\left(\sqrt{g}\frac{\mu_1}{\mu_0^2}\left(g^{11}\tilde{K^2}_1\frac{\partial\hat{p}_0}{\partial r}+g^{22}\tilde{K^2}_2\frac{\partial\hat{p}_0}{\partial s}+g^{22}\tilde{K^2}_2\frac{\partial p_1}{\partial s}\right)\right)=0.\end{aligned}\tag{4.6}$$

To ensure that p_2 does not have any terms that grow like S^2 for large S we require that the average over S of the first two terms is equal to zero, i.e.

$$\begin{aligned}&\frac{\partial}{\partial r}\left(\sqrt{g}\left(\frac{g^{11}\tilde{K^1}_1}{\mu^*}\frac{\partial\hat{p}_0}{\partial r}+\left(\frac{1}{\bar{\mu}}-\frac{1}{\mu^*}\right)\frac{g^{11}\tilde{K^1}_2\tilde{K^2}_1}{\tilde{K^2}_2}\frac{\partial\hat{p}_0}{\partial r}+\frac{g^{22}\tilde{K^1}_2}{\bar{\mu}}\frac{\partial\hat{p}_0}{\partial s}\right)\right)+\\ &\qquad\frac{\partial}{\partial s}\left(\sqrt{g}\left(\frac{g^{11}\tilde{K^2}_1}{\bar{\mu}}\frac{\partial\hat{p}_0}{\partial r}+\frac{g^{22}\tilde{K^2}_2}{\bar{\mu}}\frac{\partial\hat{p}_0}{\partial s}\right)\right)=0,\end{aligned}\tag{4.7}$$

where μ^* is the harmonic average of μ_0, which we recall is defined by

$$\frac{1}{\mu^*} = \overline{\left(\frac{1}{\mu_0}\right)}.$$

Equation (4.7), can be expressed in the form

$$\nabla \cdot (\mathbf{A}\nabla \hat{p}_0) = 0, \tag{4.8}$$

where the tensor

$$\mathbf{A} = \frac{1}{\bar{\mu}}\mathbf{K} + \left(\frac{1}{\mu^*} - \frac{1}{\bar{\mu}}\right)\boldsymbol{\kappa},$$

and, in r, s coordinates, $\tilde{\kappa}^i{}_j(\boldsymbol{\xi}) = 0$ except for $i = j = 1$ with

$$\tilde{\kappa}^1{}_1 = \tilde{K}^1{}_1 - \frac{\tilde{K}^1{}_2\tilde{K}^2{}_1}{\tilde{K}^2{}_2}.$$

The entries of $\boldsymbol{\kappa}$ in the original Cartesian coordinates are, by the tensor transformation rule,

$$\kappa^i{}_j(\mathbf{x}) = \frac{\partial x^i}{\partial r}\frac{\partial r}{\partial x^j}\tilde{\kappa}^1{}_1.$$

The partial derivatives in the two coordinate systems are related by

$$\begin{pmatrix} x_r & y_r \\ x_s & y_s \end{pmatrix} = \frac{1}{r_x s_y - r_y s_x}\begin{pmatrix} s_y & -s_x \\ -r_y & r_x \end{pmatrix}, \tag{4.9}$$

and since r, s are orthogonal coordinates we also have that

$$r_x s_x + r_y s_y = 0. \tag{4.10}$$

After applying (4.4) to write $\tilde{K}^i{}_j(\boldsymbol{\xi})$ in terms of $K^i{}_j(\mathbf{x})$ and using (4.9) and (4.10), we eventually find that, in the original Cartesian coordinates,

$$\boldsymbol{\kappa} = \frac{K^1{}_1K^2{}_2 - K^1{}_2K^2{}_1}{r_y^2K^1{}_1 - r_xr_y(K^1{}_2 + K^2{}_1) + r_x^2K^2{}_2}\begin{pmatrix} r_x^2 & r_xr_y \\ r_xr_y & r_y^2 \end{pmatrix}. \tag{4.11}$$

In (4.8), we have an equation that determines the pressure, provided that the arithmetic and harmonic averages of the viscosity across the fingers are known *and* the direction in which the fingers are aligned is also known. In the unidirectional case in Chapter 3 only the harmonic average of the viscosity is required.

We now make the further assumption that the fingers align themselves to be parallel to the mean flux of fluid on a time scale much shorter than the global penetration time scale.

Observations of the formation of fingers suggests that they should grow in the direction of the mean flux of fluid and so, provided that at any one location the direction of the mean flux does not rapidly change, this seems a reasonable assumption. The leading-order mean flux of fluid is given by

$$\bar{\mathbf{u}}_0 = -\mathbf{A}\nabla\hat{p}_0,$$

and, for the fingers to be parallel to the mean flux of fluid, we require that

$$\lambda = \frac{r_y}{r_x} = \frac{\bar{v}_0}{\bar{u}_0},$$

from which we find that

$$\lambda = \frac{K^2{}_1\frac{\partial\hat{p}_0}{\partial x} + K^2{}_2\frac{\partial\hat{p}_0}{\partial y}}{K^1{}_1\frac{\partial\hat{p}_0}{\partial x} + K^1{}_2\frac{\partial\hat{p}_0}{\partial y}}.$$

With the direction of fingering thus determined, we find that the mean velocity of fluid is given by

$$\begin{aligned}\bar{u}_0 &= -\frac{1}{\mu^*}\left(K^1{}_1\frac{\partial\hat{p}_0}{\partial x} + K^1{}_2\frac{\partial\hat{p}_0}{\partial y}\right),\\ \bar{v}_0 &= -\frac{1}{\mu^*}\left(K^2{}_1\frac{\partial\hat{p}_0}{\partial x} + K^2{}_2\frac{\partial\hat{p}_0}{\partial y}\right),\end{aligned}$$

and so the pressure satisfies

$$\nabla\cdot\left(\frac{\mathbf{K}}{\mu^*}\nabla p_0\right) = 0, \tag{4.12}$$

and therefore the harmonic average of the viscosity across the fingers acts as an effective viscosity in the homogenised model. Applying our "direction-of-fingering assumption" we also find that $b(r,s,t) = 0$, and hence that the leading order velocity parallel to the direction of fingering is

$$\begin{aligned}\tilde{u}_0 &= -\frac{1}{\mu_0}\left(\tilde{K}^1{}_1 g^{11}\frac{\partial\hat{p}_0}{\partial r} + \tilde{K}^1{}_2 g^{22}\left(\frac{\partial\hat{p}_0}{\partial s} + \frac{\partial p_1}{\partial S}\right)\right)\\ &= -\frac{g^{11}}{\mu_0}\left(\tilde{K}^1{}_1 - \frac{\tilde{K}^1{}_2\tilde{K}^2{}_1}{\tilde{K}^2{}_2}\right)\frac{\partial\hat{p}_0}{\partial r}\\ &= \frac{\mu^*}{\mu_0}\bar{\tilde{u}}_0,\end{aligned} \tag{4.13}$$

where $\bar{\tilde{u}}_0$ is the averaged leading-order velocity parallel to the direction of fingering in (r,s) coordinates, related to the mean speed of the fluid in Cartesian coordinates by

$$\bar{\tilde{u}}_0 = |\nabla r|\,|\bar{\mathbf{u}}_0|\,.$$

Equation (4.13) is the two-dimensional analogue of (3.12). Moreover, the leading order velocity transverse to the direction of fingering is

$$\tilde{v}_0 = -\frac{\tilde{K}^2{}_1 g^{11}}{\mu_0}\frac{\partial \hat{p}_0}{\partial r} - \frac{\tilde{K}^2{}_2 g^{22}}{\mu_0}\left(\frac{\partial \hat{p}_0}{\partial s} + \frac{\partial p_1}{\partial S}\right),$$

which is equal to zero, and so the velocity transverse to the direction of fingering is of order ϵ. More precisely, the $O(\epsilon)$ transverse velocity can be obtained from the continuity equation (4.1),

$$\frac{\partial}{\partial r}\left(\sqrt{g}\tilde{u}_0\right) + \frac{\partial}{\partial S}\left(\sqrt{g}\tilde{v}_1\right) = 0, \tag{4.14}$$

which, on integrating with respect to S, gives

$$\tilde{v}_1 = -\frac{1}{\sqrt{g}}\frac{\partial}{\partial r}\left(\sqrt{g}\bar{\tilde{u}}_0\mu^* \int_0^S \frac{1}{\mu_0}\,\mathrm{d}S\right) + \hat{v}_1(r,s,t),$$

where $\hat{v}_1$ is an arbitrary function, which, analogously to $\tilde{v}(x,t)$ that appeared in (3.15), may be set to zero provided c_0 is symmetric in S about the line $S = 0$. To ensure that $\tilde{v}_1$ does not grow unboundedly for large S, we must require that $\tilde{u_0}$ satisfies

$$\frac{\partial}{\partial r}\left(\sqrt{g}\bar{\tilde{u}}_0\right) = 0,$$

which is equivalent to requiring that the mean flux is constant in the one-dimensional flow of Chapter 3.

We now return to the equation for the transport of solvent, (4.2). Since the aspect-ratio of the fingers, $\epsilon = O(\mathrm{Pe}^{-1/2})$, we shall write $\mathrm{Pe}^* = \epsilon^2\mathrm{Pe}$, with $\mathrm{Pe}^* = O(1)$, so that (4.2) becomes

$$\frac{\partial c_0}{\partial t} + \nabla\cdot(\mathbf{u}c_0) = \frac{\epsilon^2}{\mathrm{Pe}^*}\nabla\cdot(\mathbf{D}\nabla c_0)\,. \tag{4.15}$$

The $O(1)$ terms in (4.15) are

$$\sqrt{g}\frac{\partial c_0}{\partial t} \quad + \quad \frac{\partial}{\partial r}\left(\sqrt{g}\tilde{u}_0 c_0\right) + \frac{\partial}{\partial S}\left(\sqrt{g}\tilde{v}_1 c_0\right) = \frac{1}{\mathrm{Pe}^*}\frac{\partial}{\partial S}\left(\sqrt{g}g^{22}\tilde{D}^2{}_2\frac{\partial c_0}{\partial S}\right) \tag{4.16}$$

and (4.16) together with (4.13) and (4.14) form our model for the flow within the fingered region. Integrating (4.16) with respect to S yields

$$g^{22}\tilde{D}^2{}_2\frac{\partial c_0}{\partial S} - \tilde{v}_1 c_0 = \int_0^S \frac{\partial c_0}{\partial t} + \frac{1}{\sqrt{g}}\frac{\partial}{\partial r}\left(\sqrt{g}\frac{\mu^* c_0}{\mu(c_0)}\bar{\tilde{u}}_0\right)\mathrm{d}S.$$

and so for large S we have that

$$g^{22}\tilde{D}^2{}_2\frac{\partial c_0}{\partial S} - \tilde{v}_1 c_0 \sim \left(\frac{\partial \bar{c}_0}{\partial t} + \frac{1}{\sqrt{g}}\frac{\partial}{\partial r}\left(\sqrt{g}\bar{\tilde{u}}_0 F\right)\right) S, \tag{4.17}$$

where

$$F = \mu^* \overline{\left(\frac{c_0}{\mu(c_0)}\right)}, \tag{4.18}$$

is the fractional flow function, previously encountered in (3.17). If c_0 is 1-periodic in S then F is defined by

$$F = \int_0^1 \frac{c_0}{\mu(c_0)}\,\mathrm{d}S \Big/ \int_0^1 \frac{1}{\mu(c_0)}\,\mathrm{d}S,$$

and similar expressions exist when c is described by a random variable. Since we require that the left-hand side of (4.17) remains bounded as $S \to \infty$, we require that $\bar{c}_0$ satisfies

$$\frac{\partial \bar{c}_0}{\partial t} + \frac{1}{\sqrt{g}}\frac{\partial}{\partial r}\left(\sqrt{g}\bar{\tilde{u}}_0 F\right) = 0,$$

which generalises (3.17).

In summary, in Cartesian coordinates the generalised Koval model is

$$\nabla \cdot \bar{\mathbf{u}}_0 = 0, \quad \bar{\mathbf{u}}_0 = -\frac{\mathbf{K}}{\mu^*}\nabla \hat{p}_0, \tag{4.19}$$

$$\frac{\partial \bar{c}_0}{\partial t} + \nabla \cdot (\bar{\mathbf{u}}_0 F) = 0, \tag{4.20}$$

which clearly reduces to (3.17) in the one-dimensional case. However this model is not closed, since the averaged quantities, F and μ^*, are unknown. As in section 3.3, we aim to close the problem by expressing F and μ^* as functions of $\bar{c}_0$. The model for the evolution of the concentration in the large aspect-ratio region is equations (4.13), (4.14) and (4.16), which combine to give

$$\begin{aligned}\sqrt{g}\frac{\partial c_0}{\partial t} &+ (\sqrt{g}\bar{\tilde{u}}_0)\frac{\partial}{\partial r}\left(\frac{\mu^*}{\mu(c_0)}c_0\right) - (\sqrt{g}\bar{\tilde{u}}_0)\frac{\partial}{\partial S}\left(c_0\int^S \frac{\partial}{\partial r}\left(\frac{\mu^*}{\mu(c_0)}\right)\mathrm{d}S\right)\\ &+ \frac{\partial}{\partial S}\left(\sqrt{g}\hat{v}_1 c_0\right) = \frac{1}{\mathrm{Pe}^*}\frac{\partial}{\partial S}\left(\sqrt{g}g^{22}\tilde{D}^2{}_2\frac{\partial c_0}{\partial S}\right).\end{aligned} \tag{4.21}$$

The equivalent equation in our unidirectional model is (3.16). We have shown that the expression $\sqrt{g}\bar{\tilde{u}}_0$ is independent of both r and S, and so, since there is no explicit appearance of s in (4.21), we may treat $\sqrt{g}\bar{\tilde{u}}_0$ as a constant. The resulting equation is still slightly different to that of (3.16), since $\sqrt{g}$ may be a function of r and the diffusion term is more complicated.

We expect (4.21) to form shocks in the $r-$direction just as (3.16) does, and so we may need to introduce a rescaled region, where $R = r/\epsilon = O(1)$, near the finger roots and tips just as in section 3.5. Since g^{ij} and $\mathbf{K}$ will be continuous near the tip/root, and they do not vary over an $O(\epsilon)$ length scale, we can treat them as constants in the tip region. If $\mathbf{K}$ is isotropic, the tip region problem is

$$\frac{\partial}{\partial R}\left(\frac{g^{11}}{\mu(c)}\frac{\partial P}{\partial R}\right) + \frac{\partial}{\partial S}\left(\frac{g^{22}}{\mu(c)}\frac{\partial P}{\partial S}\right) = 0,$$

and

$$U\frac{\partial c}{\partial R} + \frac{\partial}{\partial R}\left(\frac{kg^{11}c}{\mu(c)}\frac{\partial P}{\partial R}\right) + \frac{\partial}{\partial S}\left(\frac{kg^{22}c}{\mu(c)}\frac{\partial P}{\partial S}\right) = 0,$$

and since g is independent of R and S, we can rescale R, S and U to recover the tip-problem of section 3.5. Even when $\mathbf{K}$ is anisotropic, we can recover the tip-problem of section 3.5, provided the fingering direction is, as is likely, aligned with the principle direction of the anisotropy, so that $\mathbf{K}$ is diagonal in (r, s) coordinates. Our rescaling does not alter the cross-sectional shape of the finger, and so we suspect that the concentration profile near the tip will be the same as that for unidirectional fingering.

Since the problem in both the tip region and in the large aspect ratio region for multidirectional fingering appears to be similar to that of unidirectional fingering, it is reasonable to close the generalised Koval model, (4.19)-(4.20), by using F and μ^* determined from simulations of the Peaceman model in the linear flood geometry. We have already found an expression for the fractional flow function F in section 3.3.1, but we now need to find an expression for μ^*.

4.2 Determination of μ^*

In principle one could determine the harmonic average of the viscosity by averaging solutions to the full homogenised problem, (3.23). However, we have seen in sections 3.4 and 3.5 that the behaviour near the tips and roots of the fingers (regions I and III of Figure 3.2) is extremely important in determining the solution in the large finger-aspect-ratio region (region II of Figure 3.2), where the homogenised model is valid. As noted in Chapter 3, our incomplete understanding of the behaviour in the tip and root regions means we are unable to rigorously derive expressions for either the fractional flow function or the harmonic average of viscosity.

In section 3.3.1 we were able to suggest an appropriate form for the fractional flow function by making an empirical assumption before fitting with experiments and numerical simulations of the full Peaceman model. We shall now similarly attempt to suggest a

reasonable form for the harmonic average of the viscosity.

The suggested form of the fractional flow function in the Koval model was found by first considering the naïve approximation that the oil and solvent are entirely separate in the fingering region. We saw in section 3.3.1 that this naïve assumption yields a fractional flow function that does not agree with experiments or numerical simulations, and so Koval [33] suggested that we replace the smoothly varying viscosity with two immiscible fluids: the oil and an effective mixture of the solvent and oil. The concentration of solvent in Koval's effective mixture of solvent and oil was chosen to agree with experiments. Koval's assumption allowed us to produce the fractional flow function,

$$F(\bar{c}) = \frac{M_e \bar{c}}{1 + (M_e - 1)\bar{c}}, \tag{4.22}$$

which gives good agreement with experimental results; however, this "mixture model" does not have any systematic physical interpretation. With Koval's effective mixture model, the harmonic average of the viscosity becomes

$$\mu^*(\bar{c}) = \frac{1}{1 + (M_e - 1)\bar{c}},$$

which does not even satisfy the surely necessary condition that $\mu^*(1) = 1/M$!

The fractional flow function is a viscosity-weighted average of the concentration, and so we choose to write it as

$$F(\bar{c}) = \frac{\tilde{\mu}(\bar{c})}{\mu^*(\bar{c})}\bar{c},$$

where $\tilde{\mu}$ is the following concentration-weighted average of the viscosity,

$$\frac{1}{\tilde{\mu}(\bar{c})} = \frac{1}{\bar{c}}\overline{\left(\frac{c}{\mu(c)}\right)}. \tag{4.23}$$

To obtain the same fractional flow function applied in the Koval model, while also ensuring that $\mu^*(0) = 1$ and $\mu^*(1) = 1/M$, it is clear that we require that $\tilde{\mu}(0) = 1/M_e$ and $\tilde{\mu}(1) = 1/M$. Our motivation for introducing this average of the viscosity is our observation that in our numerical simulations $1/\tilde{\mu}$ is approximately a linear function of $\bar{c}$, leading us to the conjecture that

$$\frac{1}{\tilde{\mu}(\bar{c})} = M_e + (M - M_e)\bar{c}. \tag{4.24}$$

As shown in Figure 4.2, the above expression appears to be in reasonable agreement with numerical simulations, over a wide range of values for M, but a satisfactory explanation of this result would require further analysis of the tip-problem encountered in section 3.5, and in particular we would have to give further consideration to "interior" finger-tips

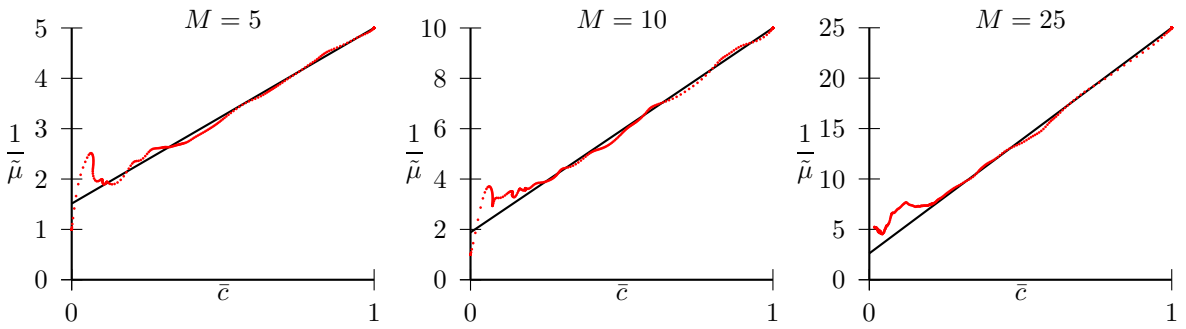

Figure 4.2: The red dots are a plot of $1/\tilde{\mu}$ against $\bar{c}$, as defined by (4.23), and determined by taking the transverse average of simulations of the Peaceman model, as found in section 2.3. The black line is given by $1/\tilde{\mu}(\bar{c}) = M_e + (M - M_e)\bar{c}$.

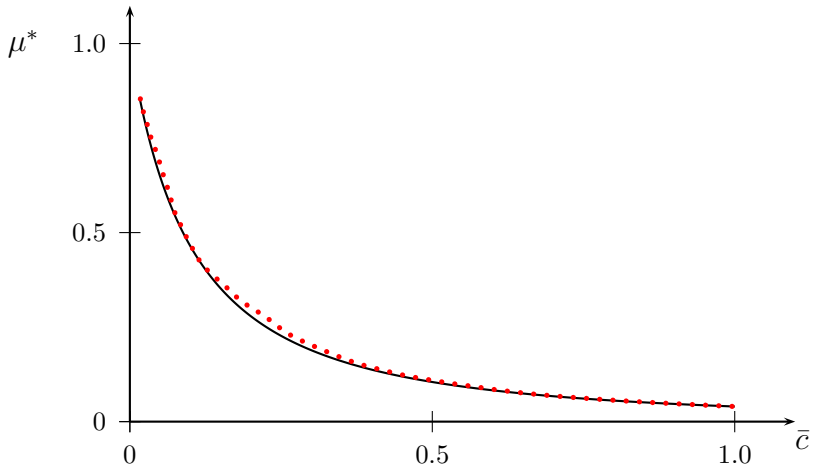

Figure 4.3: Plot of the harmonic average of viscosity as a function of the average concentration, for a linear flood with $M = 25$, $\mathrm{Pe} = 1500$ and $t = 0.3$. The red dotted curve represents the average of our 2-dimensional simulation of the Peaceman model, and the solid, black curve shows the expression given in (4.25).

in addition to the leading finger-tips that were our primary focus. Combining the two expressions (4.22) and (4.24) we are finally able to suggest the following expression for the harmonic average of the viscosity,

$$\frac{1}{\mu^*(\bar{c})} = (1 + (M_e - 1)\bar{c})\,(1 + (M/M_e - 1)\,\bar{c})\,. \tag{4.25}$$

This expression for the harmonic average of the viscosity gives good agreement with our numerical simulations (see Figure 4.3).

Since our model is now closed, and we are only now interested in the averaged concentration $\bar{c}$ and not the rapidly varying actual concentration c, we shall drop the bar from the averaged concentration for the remainder of this chapter.

4.3 Comparative studies for miscible and immiscible flow

We have seen in section 1.4.2 that the principal model for *immiscible* flow through porous media involves the concept of relative permeabilities, which represent the extent to which the water and oil hinder each other's progress through the porous medium. We recall that the relative permeability model is given by

$$\mathbf{u}_o = -\frac{k_{ro}(S_w)}{\mu_o}\mathbf{K}\nabla p_o, \qquad \mathbf{u}_w = -\frac{k_{rw}(S_w)}{\mu_w}\mathbf{K}\nabla p_w, \tag{4.26}$$

with

$$\phi\frac{\partial S_w}{\partial t} + \nabla\cdot\mathbf{u}_w = 0, \qquad \phi\frac{\partial S_o}{\partial t} + \nabla\cdot\mathbf{u}_o = 0, \tag{4.27}$$

and the pressure in the two fluids related by the capillary pressure $p_c(S_w) = p_o - p_w$. Note that since only oil and water are present we must have that $S_w + S_o = 1$. To make comparison with miscible flow, we replace subscript w, representing properties in the water phase, with subscript s, representing the solvent, associate the 'saturation' of water, S_w, with the averaged concentration of solvent c, and we neglect the capillary pressure. At first glance this model appears to be entirely different to the generalised Koval model, (4.19)-(4.20). However, by rearranging the equations in terms of the total flux $\mathbf{u} = \mathbf{u}_o + \mathbf{u}_s$, as in 1.4.2, and neglecting the capillary pressure we have that

$$\nabla\cdot\mathbf{u} = 0, \qquad \mathbf{u} = -\left(\frac{k_{rs}}{\mu_s} + \frac{k_{ro}}{\mu_o}\right)\mathbf{K}\nabla p, \tag{4.28}$$

$$\phi\frac{\partial c}{\partial t} + \nabla\cdot\left(\left(1 + \frac{k_{ro}\mu_s}{k_{rs}\mu_o}\right)^{-1}\mathbf{u}\right) = 0. \tag{4.29}$$

This is equivalent to the generalised Koval model provided we make the identification

$$\mu^*(c) = \left(\frac{k_{ro}(c)}{\mu_o} + \frac{k_{rs}(c)}{\mu_s}\right)^{-1}, \qquad F(c) = \left(1 + \frac{k_{ro}(c)\mu_s}{k_{rs}(c)\mu_o}\right)^{-1}, \tag{4.30}$$

or equivalently

$$k_{ro}(c) = \frac{\mu_o}{\mu^*(c)}(1 - F(c)), \qquad k_{rs}(c) = \frac{\mu_s}{\mu^*(c)}F(c). \tag{4.31}$$

We can therefore view the relative permeability model as an alternative way of expressing the generalised Koval model, which may provide us with extra intuitive understanding, and we can readily change between the two expressions. The effective relative permeabilities that are obtained when we use the fractional flow function and harmonic average of

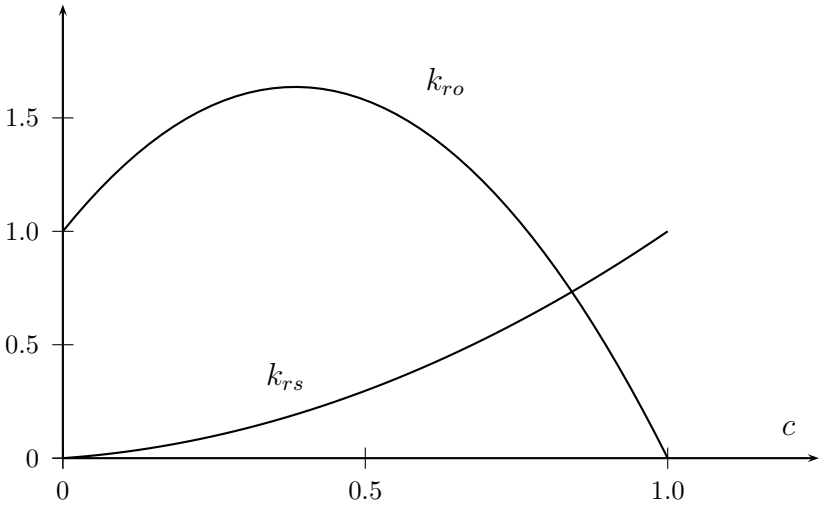

Figure 4.4: A plot of the effective relative permeabilities that may be identified with the Koval model (4.32)-(4.33), with $M = 10$ so that $M_e = 1.8817$. Note that k_{ro} is neither monotonic decreasing, nor less than one! Compare with Figure 1.6.

the viscosity of the generalised Koval model, are

$$k_{ro}(c) = \left(1 + \left(\frac{M}{M_e} - 1\right) c\right)(1 - c), \tag{4.32}$$

and

$$k_{rs}(c) = \frac{M_e}{M}\left(1 + \left(\frac{M}{M_e} - 1\right) c\right) c. \tag{4.33}$$

In immiscible flow the presence of water hinders the flow of oil and so the relative permeability of oil is a monotonic decreasing function of the fraction of water present, and is always less than or equal to $(1 - S_w)$. In contrast, in miscible flows, rather than hinder the flow of oil, the presence of solvent may actually increase the total flux of oil, as shown in Figure 4.4. The increase in flow of oil can be attributed to the significant diffusion of solvent into the oil in the fingering region, and the accompanied significantly reduced viscosity of this mixture. The increased flow of oil when a less viscous miscible solvent is introduced is in direct contrast to the decreased flow of oil when a less viscous immiscible fluid is introduced, and serves as the primary motivation for introducing miscible solvents rather than water. Since the mixing of solvent and oil only occurs in the fingered region, the occurrence of fingers is arguably a desirable feature of the miscible displacement. It is also worth noting that the naïve model, with

$$F(c) = \frac{Mc}{1 + (M-1)c} \quad \text{and} \quad \mu^*(c) = \frac{1}{1 + (M-1)c},$$

gives the relative permeabilities

$$k_{ro}(c) = (1-c) \quad \text{and} \quad k_{rs}(c) = c,$$

i.e. there is no interaction between the oil and solvent at the microscopic scale.

4.3.1 The Todd & Longstaff model

One of the principal models used in the oil recovery industry is the one suggested by Todd & Longstaff [58]. In dimensional form, the Todd & Longstaff model is

$$\mathbf{u}_o = -\frac{1-c}{\mu_o^{1-\omega}(\mu_m(c))^\omega}\mathbf{K}\nabla p, \qquad \mathbf{u}_s = -\frac{c}{\mu_s^{1-\omega}(\mu_m(c))^\omega}\mathbf{K}\nabla p,$$

$$-\phi\frac{\partial c}{\partial t} + \nabla\cdot\mathbf{u}_o = 0, \qquad \phi\frac{\partial c}{\partial t} + \nabla\cdot\mathbf{u}_s = 0,$$

where $\mu_m(c)$ is simply the viscosity of a mixture of solvent and oil with concentration of solvent c, and ω is an empirically determined 'mixing parameter'. The Todd & Longstaff model is derived from the relative permeability model (4.26)-(4.27), with no capillary pressure, relative permeabilities given by $k_{ro} = 1-c$ and $k_{rs} = c$, and the viscosities replaced by ad hoc effective viscosities,

$$\mu_{oe} = \mu_o^{1-\omega}(\mu_m(c))^\omega, \qquad \mu_{se} = \mu_s^{1-\omega}(\mu_m(c))^\omega.$$

Recall that c represents the averaged concentration across the fingers, in which the concentration is not uniform, whereas the function μ_m represents the viscosity of a uniform mixture of solvent and oil. We can therefore see no clear reason why $\mu_m(c)$ is a relevant quantity. From (4.30) we see that the Todd & Longstaff model predicts the fractional flow function to be

$$F(c) = \frac{M^{1-\omega}c}{1+(M^{1-\omega}-1)c}, \tag{4.34}$$

which is identical to the Koval fractional flow function only when $M_e = M^{1-\omega}$. It is not possible to choose ω to fit the Todd & Longstaff model to the Koval model for all M. In [58] it is suggested, by fitting with experiments with $M = 86$, that we should take $\omega = 2/3$. This value of ω gives agreement with the Koval model only when $M = 85$, and the Todd & Longstaff model does not appear to give particularly good agreement for linear flood simulations when M is much smaller than this value (see Figure 4.5).

While the concept of applying the relative permeability model to miscible displacements is not fundamentally flawed, the ad hoc assumptions that are made in the Todd & Longstaff model to determine the 'effective viscosity' are not reasonable. In addition to

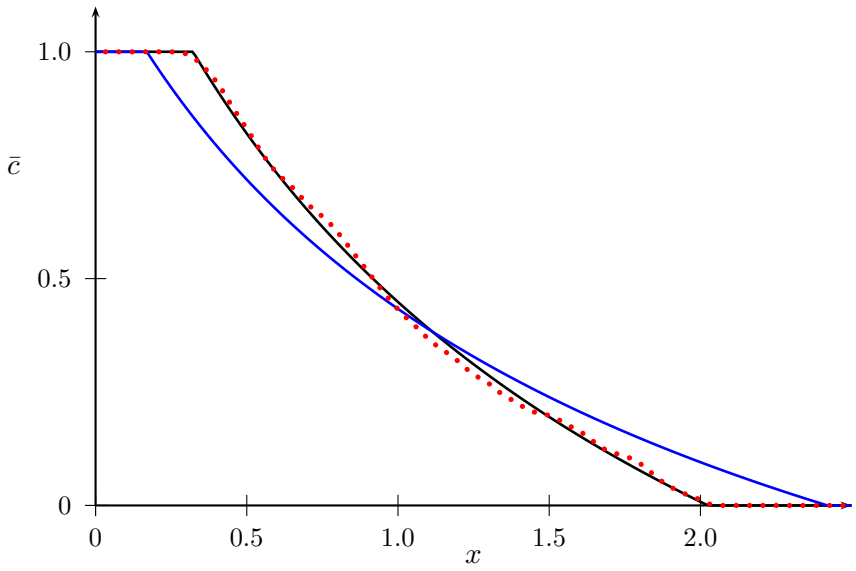

Figure 4.5: The red dotted line is the transverse average of a numerical simulation of the Peaceman model (see section 2.3) with Pe = 2500, $M = 5$ and $t = 0.5$. The solid black line is the prediction of the Koval model (3.21), and the solid blue line is the prediction of the Todd & Longstaff model with $\omega = 2/3$.

the failure of the Todd & Longstaff model to accurately capture the average concentration in a linear flood, there is no reason to suspect that the model leads to the correct choice of $\mu^*(c)$ either. The Todd & Longstaff model predicts that the harmonic average of the viscosity is

$$\mu^* = \frac{\mu_o^{1-\omega}(\mu_m(c))^\omega}{1 + (M^{1-\omega} - 1)c}, \tag{4.35}$$

and we see in Figure 4.3.1 that, even when ω is chosen to ensure that the correct concentration profile is produced, the Todd & Longstaff model does not reproduce the correct harmonic average of the viscosity.

4.4 Stability analysis

We shall now investigate the two-dimensional stability of one-dimensional solutions to the generalised Koval model in a homogeneous medium,

$$\nabla \cdot \mathbf{u} = 0, \qquad \mathbf{u} = -\frac{1}{\mu^*(c)}\nabla p,$$

$$\frac{\partial c}{\partial t} + \nabla \cdot (\mathbf{u}F(c)) = 0,$$

where $\mu^*(c)$ and $F(c)$ have been determined from the closure problem. It is just as easy to investigate the stability for general $\mu^*(c)$ and $F(c)$ as it is for specific functions, and

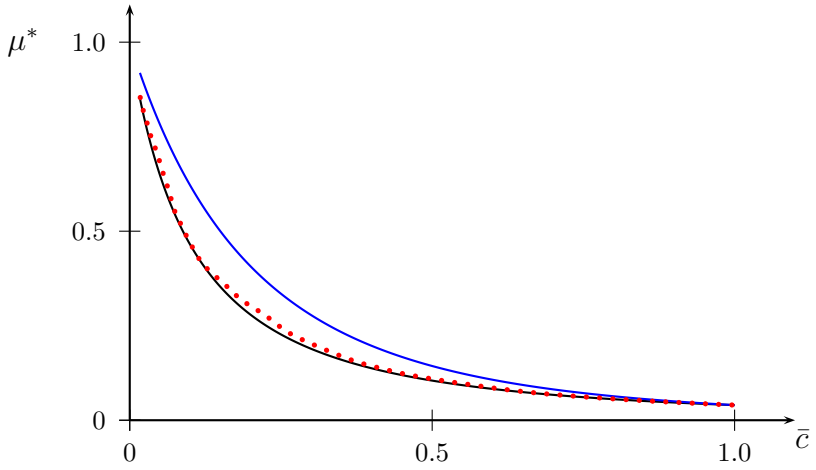

Figure 4.6: Plot of the harmonic average of viscosity as a function of the average concentration, for a linear flood with $M = 25$, $\mathrm{Pe} = 1500$ and $t = 0.3$. The red dotted curve represents the average of a 2-dimensional simulation of the Peaceman model, and the solid, black curve shows the expression given in (4.25). The blue solid curve shows the prediction of the Todd & Longstaff model when we take $\omega = 1 - \log(M_e)/\log(M)$ to ensure that the model predicts the correct value of $\bar{c}$.

so we shall postpone specifying these functions until the end of this section. This has the advantage of allowing us to also investigate the stability of the Todd & Longstaff model or any other model of the same form. Recall that c represents the concentration of solvent averaged over many fingers and so, if the averaging process has been successful, we do not expect our model to be susceptible to exactly the same instability observed in section 2.2.4. Our one-dimensional base-state solution will have the velocity $u = 1$ and $v = 0$ so that the concentration satisfies

$$\frac{\partial c}{\partial t} + \frac{\mathrm{d}F}{\mathrm{d}c}\frac{\partial c}{\partial x} = 0. \tag{4.36}$$

As we wish to consider the stability of an initially sharp interface, with solvent displacing oil, we take as the initial condition

$$c(x,0) = \begin{cases} 1, & x < 0, \\ 0, & x > 0. \end{cases}$$

Since $F(c)$ represents the fraction of the total flow which is comprised of flow of solvent it must satisfy $0 \leq F(c) \leq 1$ with $F(0) = 0$ and $F(1) = 1$. With solvent less viscous than the oil it is displacing we find that F is a monotonic increasing function of c; however, since an increased concentration of solvent will then also increase the mean velocity of the remaining oil, we also find that $F'(c)$ is monotonically decreasing in c, where $'$ denotes the derivative with respect to c. All of the above properties are satisfied by the usual Koval fractional flow function (4.22). When $F(c)$ satisfies the above conditions, the solution to

(4.36) is a rarefaction wave given by

$$c = c_0 = \begin{cases} 1 & x < F'(1)t \\ (F')^{-1}(x/t) & F'(1)t < x < F'(0)t \\ 0 & x > F'(0)t \end{cases},$$

and the base-state pressure is given by

$$p = p_0 = -\int^x \mu^*(c_0)\,\mathrm{d}x.$$

We also note the following identities which will soon prove useful:

$$F'(c_0) = \frac{x}{t} \quad \text{and} \quad \frac{\partial c_0}{\partial x} = \frac{1}{tF''(c_0)}.$$

We take this one-dimensional solution as our base state for a linear stability analysis, writing

$$u \sim 1 + \delta u_1(x,y,t), \quad v \sim \delta v_1(x,y,t), \quad c \sim c_0 + \delta c_1(x,y,t), \quad p \sim p_0 + \delta p_1(x,y,t),$$

where δ is a small parameter. Note that our base-state is time-dependent and so we will not be able to seek solutions that are exponential in time, and we will not necessarily be able to define a global growth rate. Equation (4.36) does not admit any non-trivial, time-independent solutions, and the problem contains only one time scale, so we cannot apply a quasi-steady-state assumption as in section 2.2.4. We will have to look at the growth or decay of solutions to a partial differential equation as in section 2.2.3 rather than an ordinary differential equation as in section 2.2.4.

The linearised equations are

$$\frac{\partial u_1}{\partial x} + \frac{\partial v_1}{\partial y} = 0, \tag{4.37}$$

$$u_1 = -\frac{1}{\mu^*(c_0)}\frac{\partial p_1}{\partial x} - \frac{\mu^{*'}(c_0)}{\mu^*(c_0)}c_1, \tag{4.38}$$

and

$$v_1 = -\frac{1}{\mu^*(c_0)}\frac{\partial p_1}{\partial y}. \tag{4.39}$$

In $F'(1)t < x < F'(0)t$ the disturbance to concentration satisfies

$$\frac{\partial c_1}{\partial t} + u_1 F'(c_0)\frac{\partial c_0}{\partial x} + F'(c_0)\frac{\partial c_1}{\partial x} + F''(c_0)\frac{\partial c_0}{\partial x}c_1 = 0. \tag{4.40}$$

We may eliminate p_1 and v_1 from (4.37)-(4.39) to obtain the single equation,

$$-\frac{\partial^2 u_1}{\partial y^2} - \frac{\mu^{*'}(c_0)}{\mu^*(c_0)}\frac{\partial^2 c_1}{\partial y^2} = \frac{\partial^2 u_1}{\partial x^2} + \frac{\mu^{*'}(c_0)}{\mu^*(c_0)}\frac{\partial c_0}{\partial x}\frac{\partial u_1}{\partial x}. \tag{4.41}$$

In $x < F'(1)t$ and $x > F'(0)t$ the disturbance to the concentration satisfies

$$\frac{\partial c_1}{\partial t} + F'(1)\frac{\partial c_1}{\partial x} = 0, \quad \frac{\partial c_1}{\partial t} + F'(0)\frac{\partial c_1}{\partial x} = 0 \tag{4.42}$$

respectively, and so any disturbance in these regions is simply advected along with the base state, giving neutral stability. In $F'(1)t < x < F'(0)t$ the disturbance to concentration satisfies

$$\frac{\partial c_1}{\partial t} + u_1 F'(c_0)\frac{\partial c_0}{\partial x} + F'(c_0)\frac{\partial c_1}{\partial x} + F''(c_0)\frac{\partial c_0}{\partial x}c_1 = 0. \tag{4.43}$$

Note that there is no explicit appearance of y in (4.41) or (4.43), and so we may seek solutions of the form

$$u_1(x,y,t) = \Re\left(U(x,t)\mathrm{e}^{\mathrm{i}\alpha y}\right), \quad \text{and} \quad c_1(x,y,t) = \Re\left(C(x,t)\mathrm{e}^{\mathrm{i}\alpha y}\right),$$

where α is real. Our equations for the evolution of a disturbance in $F'(1)t < x < F'(0)t$ become

$$\begin{aligned}\left(\frac{\partial^2}{\partial x^2} + \frac{\mu^{*'}(c_0)}{\mu^*(c_0)}\frac{\partial c_0}{\partial x}\frac{\partial}{\partial x} - \alpha^2\right)U &= \frac{\mu^{*'}(c_0)}{\mu^*(c_0)}\alpha^2 C,\\ \left(\frac{\partial}{\partial t} + \frac{x}{t}\frac{\partial}{\partial x} + \frac{1}{t}\right)C &= -\frac{F'(c_0)}{tF''(c_0)}U.\end{aligned}$$

If we introduce a new variable $\xi = x/t$, we find that

$$\left(\frac{\partial^2}{\partial \xi^2} + \frac{\mu^{*'}(c_0)}{\mu^*(c_0)}\frac{\partial c_0}{\partial \xi}\frac{\partial}{\partial \xi} - \alpha^2 t^2\right)U = \frac{\mu^{*'}(c_0)}{\mu^*(c_0)}\alpha^2 t^2 C, \tag{4.44}$$

$$\left(\frac{\partial}{\partial t} + \frac{1}{t}\right)C = -\frac{F'(c_0)}{tF''(c_0)}U, \tag{4.45}$$

to be solved in $F'(1) < \xi < F'(0)$. Note that $c_0 = c_0(\xi)$ is independent of t for fixed ξ. Matching with the regions $\xi < 1/M$ and $\xi > M$, where any disturbance is neutrally stable, leads us to conclude that C and U are constant at $\xi = 1/M$ and $\xi = M$. We therefore need only consider interior maxima to determine whether the disturbance may grow unboundedly. For large αt we have, at least away from possible boundary layers

near $\xi = F'(1)$ and $\xi = F'(0)$, that

$$U = -\frac{\mu^{*'}(c_0)}{\mu^*(c_0)}C,$$

and so

$$\frac{\partial C}{\partial t} = \frac{1}{t}\left(\frac{\mu^{*'}(c_0)F'(c_0)}{\mu^*(c_0)F''(c_0)} - 1\right)C.$$

We solve to find that

$$C = C_0(\xi)t^{\sigma(\xi)},$$

where the algebraic growth rate is given by

$$\sigma(\xi) = \frac{\mu^{*'}(c_0(\xi))F'(c_0(\xi))}{\mu^*(c_0(\xi))F''(c_0(\xi))} - 1. \tag{4.46}$$

The disturbance will be stable if

$$\frac{\mathrm{d}}{\mathrm{d}c}\log\mu^*(c) \geq \frac{\mathrm{d}}{\mathrm{d}c}\log F'(c) \tag{4.47}$$

for all values of c, and unstable otherwise.

If we make the naïve assumption that the oil and solvent are always separate so that

$$F(c) = \frac{Mc}{1+(M-1)c} \quad \text{and} \quad \mu^*(c) = \frac{1}{1+(M-1)c},$$

the stability criterion (4.47) is always satisfied and from (4.46) we see that, for large αt, disturbances decay like $t^{-1/2}$. However, we have already seen in section 3.3.1 that the naïve assumption is not appropriate and fails to accurately predict the evolution of the fingering region. If instead we use the corrected expressions (4.22) and (4.25), then we find that

$$\sigma(\xi) = \frac{1}{2}\frac{M - M_e^2}{(M_e-1)(M_e+(M-M_e)c_0(\xi))}.$$

Since $M - M_e^2 > 0$ we see that the disturbance will grow algebraically for all α, with the growth rate largest for small values of the base-state concentration. This suggests that the largest growth rate of disturbances will be near the tips of the leading fingers. It is also possible to investigate the stability of the Todd & Longstaff model using (4.34) and (4.35) for the fractional flow function and harmonic average of viscosity respectively, and we have found that, for $\omega = 2/3$, disturbances are unstable for all values of c.

The mechanism of the instability is the same as that of viscous fingering, although it occurs at a larger length-scale and the rate of growth is controlled by the local gradient of the averaged viscosity. There are, however, the following two new mechanisms that

promote stability:

1. The spreading of the base-state average concentration, over the same time scale as the growth of fingers, reduces the local gradient of the averaged viscosity so that exponential growth of disturbances is no longer possible and only algebraic growth is observed.

2. The rate of increase in the fraction of the flow comprised of solvent decreases as the amount of solvent is increased, i.e. F is a concave, monotonic increasing function of c. Where there is a small, local increase in the concentration, this disturbance travels slower than the base-state, and where there is a small, local decrease in the concentration this disturbance travels faster than the base-state. The net effect is to promote the decay of such disturbances, entirely independently of the wavenumber of the disturbance.

As stated earlier, the concept of stability, or otherwise, is important in determining whether an averaged model is self-consistent. If we have averaged over a particular length scale then we should not see instabilities leading to ill-posedness arising at a length scale smaller than that over which we averaged. Our stability analysis of the generalised Koval model suggests that all wavelength disturbances, even arbitrarily small ones, will be unstable, but the growth-rate is bounded for all wavelengths, and so small-wavelength disturbances are not selected in preference of larger-wavelength disturbances. In addition we predict that, for all wavelength disturbances, growth is only algebraic, not exponential. Although small disturbances may grow in the generalised Koval model, the linearised problem is well-posed.

4.5 Conclusions

We have presented a systematic derivation of a generalised version of the Koval model, that allows for simulation in geometries other than a linear flood. The model also allows one to model flow past macroscopic heterogeneities in the porous medium, but does not take into account interaction between viscous fingering and heterogeneity at the same length scale as which the fingering occurs. The most important aspect of our model is in the discovery that it is the harmonic average of the viscosity across the fingers that is the appropriate effective macroscopic viscosity.

The harmonic average of the viscosity across many fingers can be determined by returning to our numerical simulations in the linear flood geometry. In principle it is not possible to determine the harmonic average of the viscosity without a fuller understanding of the tip problem encountered in Chapter 3; however we have been able to make a

practical suggestion for the harmonic average of the viscosity by taking averages of our numerical simulations. We have suggested an extremely simple form for the harmonic average of the viscosity by investigating the concentration-weighted average of the viscosity $\tilde{\mu}$ encountered in the tip problem in section 3.5, and our model appears to give excellent agreement with numerical simulations. We have only had to use a single parameter, the effective concentration suggested by Koval, to fit $F(\bar{c})$ and $\mu^*(\bar{c})$ to averages of our numerical simulations.

We have also shown that the generalised Koval model may be expressed in the terminology of 'relative permeabilities', frequently employed in studies of immiscible displacements. Writing the model in this form gives us new insight into the advantages of miscible displacement over immiscible displacement. We have seen that viscous fingering has a potentially benevolent effect, increasing the mixing of solvent and oil and, since the viscosity of a mixture of solvent and oil is very much less than that of oil alone, helping to transport oil through the reservoir. We have also been able to compare our model with that of Todd & Longstaff, one of the most widely-used models in industry, and seen that, although the basic form of the Todd & Longstaff model is sound, the ad hoc assumptions of the model are not justified. The generalised Koval model that we have presented, requires only a minor adaptation of the Todd & Longstaff model, but is better equipped to predict both the spreading of the solvent, and the correct pressure drop throughout the porous medium.

Finally, we have investigated the stability of solutions to our generalised Koval model. Although the spreading of the concentration does help to stabilise disturbances, we still find that our model permits the growth of disturbances of arbitrarily large wavenumber. Interestingly the naïve Koval model, in which one assumes that the oil and solvent are always separate is always stable. Although an instability is present it should be noted that the growth rate is algebraic and the growth rate is constant for large wavenumbers, so the linearised problem is well-posed and there is no preference for small-wavelength disturbances.

Chapter 5

Gravitational effects

Up to this point we have only considered the importance of viscosity differences in the formation of fingering instabilities during miscible displacements in porous media. In many applications there is a significant density difference between the injected solvent and the oil. When a more dense fluid lies above a less dense fluid, an instability may develop, leading to gravity-driven fingering or 'density fingering'.

One of the first treatments of both viscous fingering and density fingering in porous media is due to Hill [25]. Hill was concerned with the 'sweetening on' and 'sweetening off' processes which occur during the refining of sugar. Distilled water is used to wash out a sugar solution from a vertical column of porous media. This process is referred to as 'sweetening off'. The sugar solution is both more dense and more viscous than the distilled water used to displace it. The 'sweetening on' process involves the reintroduction of the sugar solution to replace the distilled water. Hill discovered that it was possible for instabilities to develop on a planar interface leading to fingering patterns. He realised that gravitational effects could stabilise flows that would otherwise be unstable due to viscous effects and that the reverse is also true , i.e. an interface that when stationary is unstable due to density differences may be stable when the viscosities are different and the interface is moving. We shall review the stability analysis of this problem in detail in the first section of this chapter.

In the oil recovery industry, gravitational effects are also important. The solvent injected in miscible flows is usually less dense than the oil recovered, and so the solvent tends to move upwards through the reservoir. This effect tends to reduce the amount of oil that can be recovered. One of the difficulties of modelling the effects of gravity in these miscible displacements is that the fluid is usually injected from a vertical well and so the applied pressure gradient acts in a horizontal direction. When we include gravity, we can no longer consider a one-dimensional problem and any fingering behaviour that forms will be immediately multidirectional.

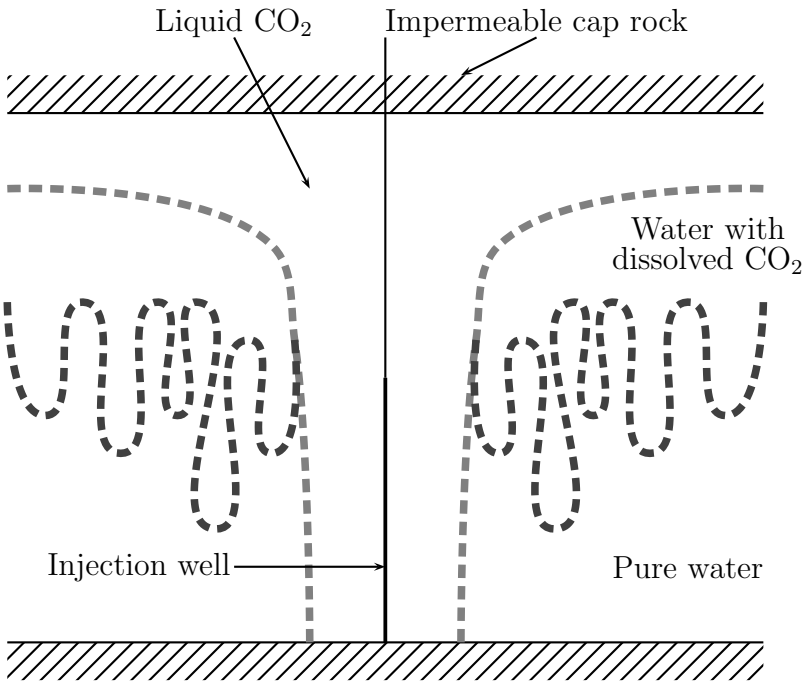

Figure 5.1: Gravity fingering in carbon sequestration. Liquid CO_2 is injected at the bottom of the oil reservoir. As the CO_2 is lighter than the surrounding water it rises until it becomes trapped beneath an impermeable cap rock. The carbon dioxide begins to dissolve into the surrounding water producing a dense mixture of water with dissolved CO_2. Gravity fingering then occurs between the dense, CO_2-rich water and the pure water lying beneath.

Another application of interest to the oil industry in which gravity-driven fingering is important involves the sequestration of carbon dioxide in aquifers. Carbon dioxide from industrial processes is injected into aquifers in an attempt to reduce the amount of carbon dioxide released into the atmosphere. It is thought that reducing carbon dioxide emissions could help to prevent global warming. The long term viability of carbon dioxide sequestration in aquifers may depend on the rate at which the carbon dioxide introduced into the aquifer dissolves into the water. As carbon dioxide is dissolved into water the density of the water increases. If water containing a large concentration of dissolved carbon dioxide is resting above water with a lower concentration of dissolved carbon dioxide then we may expect gravity fingering to develop. The dissolved carbon dioxide also reduces the viscosity of the fluid and this may increase the rate of growth of these fingers. In carbon sequestration the growth of these fingers is favourable, as their formation tends to increase the total amount of carbon dioxide that dissolves into the water in the aquifer.

We begin this chapter by reviewing the classical results of Hill [25] and Saffman and Taylor [49] for the stability of a planar interface between two fluids, of different viscosities and densities, moving through a porous medium. When the two fluids are miscible it is easy to extend the Peaceman model of Chapter 2 to account for the effect of gravity, with the density depending on the amount of solvent present. We show that, when gravitational effects are considered, there are some subtle differences between the stability

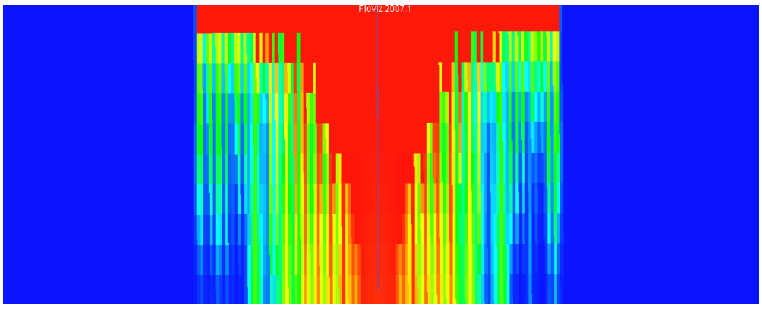

Figure 5.2: Numerical simulation of the carbon sequestration problem described in Figure 5.1. The colour represents the density of any water present, with red representing the highest density where the water is saturated with carbon dioxide and blue representing the lowest density where there is no carbon dioxide present. Image courtesy of Walter Sifuentes (Imperial College/Schlumberger), simulation uses ECLIPSE software.

properties of a miscible displacement and the corresponding Muskat problem. The systematic derivation of the Koval model in Chapter 3 can be extended to develop a novel model for the growth of fingers due to both density differences and viscosity differences. Our Koval-like model once again assumes that the fingers are unidirectional, representing only vertical flows, such as those encountered in the sugar refining problem of Hill, and the carbon sequestration problem. When the flow is not essentially one-dimensional, we may generalise the work of Chapter 4 to develop a model which allows us to average over multidirectional fingers engendered by both viscosity and density differences between the solvent and the oil.

5.1 The Muskat model

We first consider a moving boundary problem where a fluid with viscosity μ_1 and density ρ_1 displaces a fluid with viscosity μ_2 and density ρ_2. The two fluids are treated as immiscible at the macroscopic scale. Each fluid is incompressible, with velocity $\mathbf{u}_i$, where

$$\nabla \cdot \mathbf{u}_i = 0, \tag{5.1}$$

and satisfies Darcy's law,

$$\mathbf{u}_i = -\frac{k}{\mu_i}\nabla\left(p_i + \rho_i g z\right), \quad \text{for} \quad i = 1, 2. \tag{5.2}$$

At the interface between the two fluids we satisfy the dynamic boundary condition,

$$p_1 = p_2,$$

and the kinematic boundary condition

$$\mathbf{u}_1 \cdot \mathbf{n} = \mathbf{u}_2 \cdot \mathbf{n} = v_n,$$

where v_n is the normal velocity of the free surface. A planar solution exists, depicted in

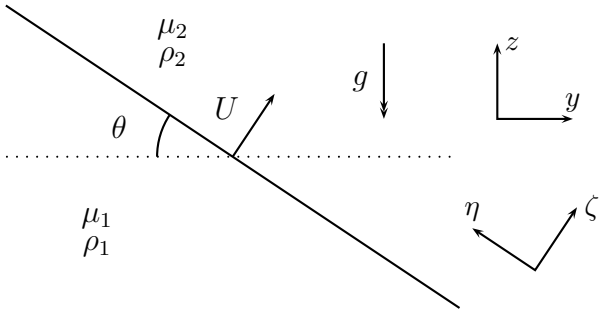

Figure 5.3: Solvent displacing oil in a porous medium in the presence of gravity.

Figure 5.3, in which the angle between the interface and the horizontal plane is θ and the interface moves with a normal velocity U. Introducing coordinates

$$\begin{aligned} \zeta &= y\sin\theta + z\cos\theta - Ut, \\ \eta &= -y\cos\theta + z\sin\theta, \end{aligned}$$

ensures that the interface is given by $\zeta = 0$. The velocity is U in the ζ-direction and is $-\frac{k}{\mu_i}\rho_i g\sin\theta$ in the η-direction. The pressure is given by

$$p_i = -\left(U\frac{\mu_i}{k} + \rho_i g\cos\theta\right)\zeta.$$

We now seek a solution where the interface is given by

$$\zeta = \epsilon L\Re\left(\exp(\sigma t + \mathrm{i}\alpha y)\right),$$

where $\epsilon \ll 1$ and L represents a typical length scale for the problem. We seek p_i of the form

$$p_i = -\left(U\frac{\mu_i}{k} + \rho_i g\cos\theta\right)\zeta + \epsilon\tilde{p}_i(\zeta)\Re\left(\exp(\sigma t + \mathrm{i}\alpha y)\right).$$

In each fluid, after linearising for small ϵ, $\tilde{p}_i$ satisfies

$$\frac{\partial^2\tilde{p}_i}{\partial\zeta^2} - \alpha^2\tilde{p}_i = 0,$$

and so the disturbance to pressure is given by

$$\begin{aligned} \tilde{p}_1 &= P_1 \mathrm{e}^{|\alpha|\zeta} \quad \text{for} \quad \zeta < 0, \\ \tilde{p}_2 &= P_2 \mathrm{e}^{-|\alpha|\zeta} \quad \text{for} \quad \zeta > 0, \end{aligned}$$

where we have ensured that the disturbance decays as $|\zeta| \to \infty$. The dynamic boundary condition yields

$$L\left(-U\frac{\mu_1}{k} - \rho_1 g\cos\theta\right) + P_1 = L\left(-U\frac{\mu_2}{k} - \rho_2 g\cos\theta\right) + P_2,$$

and the kinematic boundary condition gives

$$-\frac{k}{\mu_1}\,|\alpha|\,P_1 = \frac{k}{\mu_2}\,|\alpha|\,P_2 = \sigma L.$$

We find the dispersion relation

$$\sigma = \frac{|\alpha|}{\mu_1+\mu_2}\left(U(\mu_2-\mu_1) + gk(\rho_2-\rho_1)\cos\theta\right). \tag{5.3}$$

Note that when a lighter, less viscous fluid is displacing a heavier, more viscous fluid from below (i.e. $\cos\theta > 0$) the interface is always unstable. When the lighter, less viscous fluid is injected from above (i.e. $\cos\theta < 0$) the interface will be stable provided the velocity does not exceed the critical velocity

$$U_c = gk\,|\cos\theta|\,\frac{\rho_2-\rho_1}{\mu_2-\mu_1}.$$

If a heavier, more viscous fluid is displacing a lighter, less viscous fluid from above, it is even possible for there to exist a stable interface provided the interface is moving *faster* than the critical velocity. The two instabilities compete, with the viscous instability dominating at higher velocities and the gravity driven instability dominating at lower velocities.

The dispersion relation has the same linear dependence on the wavenumber as the Muskat problem without gravity and therefore, as in section 1.3.2, we find that the linear problem is therefore ill-posed whenever $\sigma > 0$. When $\sigma > 0$ we expect that a regularisation mechanism is required to ensure that the full problem is well-posed. In the case of miscible displacements, we expect diffusion to provide this regularisation mechanism.

5.2 The Peaceman model

The Peaceman model of Chapter 2 can be easily adapted to take account of gravitational effects. The only significant difficulty arises from the consideration of conservation of mass. In general there may be a change in volume associated with mixing; however, this change in volume is typically small and so we may apply the standard Boussinesq approximation (see e.g. [36]). Since the change in volume associated with mixing is small, conservation of mass is equivalent to conservation of volume. Density variations are only of importance in the momentum equation, and are neglected in the equation for conservation of mass. The model becomes

$$\nabla \cdot \mathbf{u} = 0, \tag{5.4}$$

$$\mathbf{u} = -\frac{k}{\mu(c)} \left(\nabla p^* - \rho(c)\mathbf{g} \right), \tag{5.5}$$

$$\phi \frac{\partial c}{\partial t} + \nabla \cdot (\mathbf{u}c) = \nabla \cdot (\mathbf{D}^* \nabla c), \tag{5.6}$$

where $\rho(c)$ is the density of the mixture, and is a function of the fraction of solvent present, and $\mathbf{D}^*$ is the diffusion tensor. A further consequence of the small volume-change on mixing is that the density must depend linearly on the concentration of solvent in the mixture (recall that the concentration of solvent is equal to the volume fraction of solvent), so that

$$\rho(c) = \rho_s c + \rho_o (1 - c). \tag{5.7}$$

We continue to use the empirical quarter-power mixing rule for $\mu(c)$,

$$\mu(c) = \left(\frac{c}{\mu_s^{1/4}} + \frac{1-c}{\mu_o^{1/4}} \right)^{-4}, \tag{5.8}$$

suggested by Koval [33], and commonly used in oil refinery calculations.

When we take $\mathbf{D}^*$ to be zero and consider an initial condition for which the solvent and oil are entirely separate, we can recover the moving boundary problem of section 5.1, as we shall now demonstrate. The equation for the advection of concentration, (5.6) becomes

$$\phi \frac{\partial c}{\partial t} + \mathbf{u} \cdot \nabla c = 0, \tag{5.9}$$

and so, with an initial condition where c takes only the values 0 and 1, c will only ever take the values 0 and 1. Away from any discontinuities in c it is clear that we must solve

(5.1) and (5.2). The pressure must satisfy

$$\nabla \cdot \left(\frac{k}{\mu(c)} \left(\nabla p^* - \rho(c)\mathbf{g} \right) \right) = 0.$$

Now suppose that c is discontinuous across a curve Γ. Physical conservation demands we require that

1. p^* is continuous across Γ,
2. $\dfrac{k}{\mu(c)} \left(\nabla p^* - \rho(c)\mathbf{g} \right) \cdot \mathbf{n}$ is continuous across Γ,

where $\mathbf{n}$ is the normal to the curve Γ. Since $\mathbf{u} \cdot \mathbf{n}$ is then continuous across Γ, we see from (5.9) that

$$\mathbf{u}_s \cdot \mathbf{n} = \mathbf{u}_o \cdot \mathbf{n} = v_n,$$

where $\mathbf{u}_s$ is the velocity in the solvent, $\mathbf{u}_o$ is the velocity in the oil and v_n is the normal velocity of the curve Γ.

We now nondimensionalise the Peaceman model. We write $\mathbf{g} = -g\mathbf{e}_3$, where $\mathbf{e}_3$ is the unit vector in the vertical direction. We introduce a reference value, D, for diffusion and define $\mathbf{D} = \mathbf{D}^*/D$. We set

$$p^* = \frac{U\mu_0 L p}{k} - \rho_0 g z,$$

and nondimensionalise $\mathbf{u}$ with U, $\mathbf{x}$ with L and t with $\phi L/U$, where U and L are, respectively, typical velocity and length scales. Applying (5.7) and (5.8) we obtain the nondimensional equations

$$\nabla \cdot \mathbf{u} = 0, \tag{5.10}$$

$$\mathbf{u} = -\frac{1}{\mu(c)} \left(\nabla p - \Lambda c\, \mathbf{e}_3 \right), \tag{5.11}$$

$$\frac{\partial c}{\partial t} + \nabla \cdot (\mathbf{u}c) = \frac{1}{\mathrm{Pe}} \nabla \cdot (\mathbf{D} \nabla c), \tag{5.12}$$

where

$$\mu(c) = \left(M^{1/4} c + 1 - c \right)^{-4} \tag{5.13}$$

and we have introduced the following non-dimensional parameters:

$$M = \frac{\mu_o}{\mu_s}, \quad \Lambda = \frac{k(\rho_o - \rho_s)g}{U\mu_o}, \quad \mathrm{Pe} = \frac{UL}{D}. \tag{5.14}$$

We expect the Péclet number to be large, just as we have already found in applications where gravitational effects are not important. As noted in a paper by Zimmerman and Homsy [64], for large Péclet number, all averaged quantities of the problem appear to

be entirely independent of any anisotropy or physically reasonable velocity-dependence of the diffusion tensor. We therefore believe that it is reasonable to model the diffusion as constant and isotropic provided $\mathrm{Pe} \gg 1$. Henceforth we shall assume that the diffusion is constant and isotropic so that (5.12) becomes

$$\frac{\partial c}{\partial t} + \nabla \cdot (\mathbf{u}c) = \frac{1}{\mathrm{Pe}} \nabla^2 c. \tag{5.15}$$

We have seen that, in the singular limit of $\mathrm{Pe} = \infty$, we recover the Muskat problem with a free surface separating a region containing only solvent from a region containing only oil. We therefore expect that this model will lead to the growth of long thin fingers when Pe is large. As for the case where gravity is not present, this will lead to difficulty in obtaining accurate numerical solutions of the model. For the moving boundary problem, the stability of a horizontal interface is given by (5.3) with $\theta = 0$. In non-dimensional form this gives a growth rate,

$$\sigma = \frac{M - 1 + \Lambda M}{M + 1} \left| \alpha \right|, \tag{5.16}$$

for disturbances of wavenumber α. The interface will be stable whenever

$$\Lambda \leq \frac{1}{M} - 1, \tag{5.17}$$

and unstable otherwise.

It has been suggested in [36] that there are some subtleties to the stability analysis when the Péclet number is large but not infinite. Hence we shall now look at the stability of a horizontal interface for the Peaceman model.

5.2.1 Stability analysis

Our stability analysis uses the techniques used in [24]. We seek a one-dimensional solution for our base state and so take the vertical velocity, $w = 1$ and the horizontal velocity, $v = 0$. For there to exist a well-defined global growth rate for the problem we require that our base-state is time-independent. There are no non-trivial solutions of (5.15) which are time-independent; however, provided we take an initial condition, $c = c_0(z)$, which is smooth, and provided $\mathrm{Pe} \gg 1$, our solution will take the form

$$c \sim c_0(\zeta) + \frac{1}{\mathrm{Pe}} c_1(\zeta, t) + \ldots, \tag{5.18}$$

where $\zeta = z - t$. This solution is valid provided $t \ll \mathrm{Pe}$. The base-state pressure must satisfy

$$-\mu(c_0) = \frac{\partial p}{\partial z} - \Lambda c_0,$$

and

$$\frac{\partial p}{\partial y} = 0.$$

The pressure is therefore given by

$$p \sim p_0(\zeta) = \int^{\zeta} -\mu(c_0) + \Lambda c_0 \,\mathrm{d}\zeta. \tag{5.19}$$

The equations, (5.18) and (5.19) define our base state. We seek a perturbed solution with the ansatz,

$$c \sim c_0(\zeta) + \epsilon \Re\left(C(\zeta)\mathrm{e}^{\mathrm{i}\alpha y + \sigma t}\right) + O\left(\epsilon^2, \frac{1}{\mathrm{Pe}}\right),$$

$$p \sim p_0(\zeta) + \epsilon \Re\left(P(\zeta)\mathrm{e}^{\mathrm{i}\alpha y + \sigma t}\right) + O\left(\epsilon^2, \frac{1}{\mathrm{Pe}}\right),$$

where $\frac{1}{\mathrm{Pe}} \ll \epsilon \ll 1$, and α is real and, without loss of generality, positive. On substituting this ansatz into (5.10), (5.11), (5.15) we recover from the $O(\epsilon)$ terms,

$$\frac{\mathrm{d}}{\mathrm{d}\zeta}\left(\frac{1}{\mu(c_0)}\frac{\mathrm{d}\mu}{\mathrm{d}c}(c_0)C + \frac{1}{\mu(c_0)}\frac{\mathrm{d}P}{\mathrm{d}\zeta} - \frac{\Lambda}{\mu(c_0)}C\right) - \frac{\alpha^2}{\mu(c_0)}P = 0, \tag{5.20}$$

$$\sigma C - \frac{1}{\mu(c_0)}\frac{\mathrm{d}\mu}{\mathrm{d}c}(c_0)\frac{\mathrm{d}c_0}{\mathrm{d}\zeta}C - \frac{1}{\mu(c_0)}\frac{\mathrm{d}c_0}{\mathrm{d}\zeta}\frac{\mathrm{d}P}{\mathrm{d}\zeta} + \frac{\Lambda}{\mu(c_0)}\frac{\mathrm{d}c_0}{\mathrm{d}\zeta}C = 0. \tag{5.21}$$

We can eliminate C to obtain the equation

$$\frac{\mathrm{d}}{\mathrm{d}\zeta}\left(\frac{\sigma\frac{\mathrm{d}P}{\mathrm{d}\zeta}}{\sigma\mu(c_0) - \frac{\mathrm{d}\mu}{\mathrm{d}c}(c_0)\frac{\mathrm{d}c_0}{\mathrm{d}\zeta} + \Lambda\frac{\mathrm{d}c_0}{\mathrm{d}\zeta}}\right) = \frac{\alpha^2}{\mu(c_0)}P. \tag{5.22}$$

Following Hickernell & Yortsos [24] we introduce a stream function defined by

$$\frac{\mathrm{d}\psi}{\mathrm{d}\zeta} = \frac{P}{\mu(c_0)}.$$

After integrating (5.22) we obtain

$$\frac{\mathrm{d}}{\mathrm{d}\zeta}\left(\mu_0\frac{\mathrm{d}\psi}{\mathrm{d}\zeta}\right) = \alpha^2\left(\mu_0 - \frac{1}{\sigma}\frac{\mathrm{d}\mu_0}{\mathrm{d}\zeta} + \frac{\Lambda}{\sigma}\frac{\mathrm{d}c_0}{\mathrm{d}\zeta}\right)\psi,$$

where $\mu_0(\zeta) = \mu(c_0(\zeta))$. Since $\mu_0 > 0$ we may simplify the problem further by introducing

a new variable, Z such that $\mathrm{d}Z = \mathrm{d}\zeta/\mu_0$, obtaining

$$\frac{\mathrm{d}^2\psi}{\mathrm{d}Z^2} = \alpha^2\left(\mu_0^2 - \frac{1}{\sigma}\frac{\mathrm{d}\mu_0}{\mathrm{d}Z} + \frac{\Lambda}{\sigma}\frac{\mathrm{d}c_0}{\mathrm{d}Z}\right)\psi. \tag{5.23}$$

We also need the disturbance to decay as $\zeta \to \pm\infty$ and so require that ψ tends to zero as $Z \to \pm\infty$.

The problem is now in the same form as (2.60), i.e. we can write

$$\frac{\mathrm{d}^2\psi}{\mathrm{d}Z^2} = \alpha^2 Q(Z)\psi,$$

where

$$Q(Z) = \mu_0(Z)^2 - \frac{1}{\sigma}\left(\frac{\mathrm{d}\mu_0}{\mathrm{d}Z} - \Lambda\frac{\mathrm{d}c_0}{\mathrm{d}Z}\right),$$

and we can therefore carry over many of the results of section 2.2.4. Firstly we require that, for some Z, the coefficient of ψ on the right-hand side of (5.23) must be negative and so for some Z

$$\sigma < \frac{1}{\mu_0^2}\frac{\mathrm{d}\mu_0}{\mathrm{d}Z} - \frac{\Lambda}{\mu_0^2}\frac{\mathrm{d}c_0}{\mathrm{d}Z},$$

or equivalently, for some ζ,

$$\sigma < V(\zeta) = \frac{1}{\mu_0}\frac{\mathrm{d}\mu_0}{\mathrm{d}\zeta} - \frac{\Lambda}{\mu_0}\frac{\mathrm{d}c_0}{\mathrm{d}\zeta}.$$

The growth rate is therefore bounded by

$$\sigma < \sigma_m = \sup_{\zeta} V(\zeta), \tag{5.24}$$

and so as in section 2.2.4, we see that the growth rate is bounded for large-wavenumber disturbances. This is in contrast to the stability analysis of the moving boundary problem in section 5.1.

For small-wavenumber disturbances, where $\alpha \ll 1$, we can follow the analysis of section 2.2.4.1 to find that

$$\psi \sim \psi_0 + \alpha\psi_1 + \dots\,, \qquad \sigma \sim \sigma_1\alpha + \dots\,,$$

with ψ_1 solving

$$\sigma_1\frac{\mathrm{d}^2\psi_1}{\mathrm{d}Z^2} = -\frac{\mathrm{d}\mu_0}{\mathrm{d}Z} + \Lambda\frac{\mathrm{d}c_0}{\mathrm{d}Z},$$

so that

$$\sigma_1\frac{\mathrm{d}\psi_1}{\mathrm{d}Z} = -\mu_0 + \Lambda c_0 + \text{constant}.$$

If as $Z \to \pm\infty$ we have that $c \to c_\pm$ and $\mu \to \mu_\pm$, then σ is given by

$$\sigma_1 = \frac{\mu_+ - \mu_- - \Lambda(c_+ - c_-)}{\mu_+ + \mu_-},$$

and so if we consider solvent displacing oil (i.e. $c_+ = 0$, $c_- = 1$, $\mu_+ = 1$ and $\mu_- = 1/M$) then we find that the growth rate for small wavenumbers is given by

$$\sigma = \frac{M - 1 + \Lambda M}{M + 1}\alpha. \tag{5.25}$$

This is the same dispersion relation as for the moving boundary problem as given by (5.16).

For large-wavenumber disturbances we can directly apply the analysis of section 2.2.4.2. The only possible complication is that since

$$\mu_0 - \Lambda c_0,$$

will not in general be a monotonic function of Z, it is possible for

$$Q_m(Z) = \mu_0^2 - \frac{1}{\sigma_m}\left(\frac{\mathrm{d}\mu_0}{\mathrm{d}Z} - \Lambda\frac{\mathrm{d}c_0}{\mathrm{d}Z}\right),$$

to be equal to zero for more than one value of Z. While we can consider this case, it is pathological, and we shall therefore assume that the concentration profile is such that this situation does not occur. We then have, by construction, that $Q_m(Z) \geq 0$ with equality only when $Z = Z_m$. With this assumption we then find that the maximum growth rate is given by

$$\sigma \sim \sigma_m - \frac{\sigma_m^2}{\alpha}\left(\frac{\mathrm{d}^2 Q_m}{\mathrm{d}Z^2}(Z_m)\right)^{1/2}\left(\frac{\mathrm{d}\mu_0}{\mathrm{d}Z}(Z_m) - \Lambda\frac{\mathrm{d}c_0}{\mathrm{d}Z}(Z_m)\right). \tag{5.26}$$

For large wavenumbers the growth rate of disturbances is almost constant. Hence, although for small wavenumber disturbances the growth rate is identical to that of the moving boundary analysis, it is very different for large wavenumbers. The most important consequence of the boundedness of the growth rate is that the linearised problem is well-posed. In particular the stability criterion that we obtained from the moving boundary analysis (5.17) does not, in general, hold for large wavenumber disturbances. This effect has already been noted in the paper of Manickam & Homsy [36]. A large-wavenumber instability may exist whenever

$$\frac{\mathrm{d}\mu_0}{\mathrm{d}Z} - \Lambda\frac{\mathrm{d}c_0}{\mathrm{d}Z} > 0,$$

for any Z. With $\mathrm{d}c_0/\mathrm{d}Z < 0$ the condition for large wavenumber instabilities to form is

that the inequality

$$\Lambda > \frac{\mathrm{d}\mu}{\mathrm{d}c}, \tag{5.27}$$

should hold for some value of c.

5.2.1.1 Transverse diffusion

Just as in section 2.2.4.3 we find that it is impossible to include the effect of transverse diffusion without losing the existence of a global growth rate. However, it is possible to see the effect of transverse diffusion if we neglect the terms involving longitudinal diffusion in (5.15), yielding

$$\frac{\partial c}{\partial t} + \nabla \cdot (\mathbf{u}c) = \frac{1}{\mathrm{Pe}} \frac{\partial^2 c}{\partial y^2}.$$

We can use the same base state as before, (5.20) still holds and (5.21) becomes

$$\sigma C - \frac{1}{\mu(c_0)} \frac{\mathrm{d}\mu}{\mathrm{d}c}(c_0) \frac{\mathrm{d}c_0}{\mathrm{d}\zeta} C - \frac{1}{\mu(c_0)} \frac{\mathrm{d}c_0}{\mathrm{d}\zeta} \frac{\mathrm{d}P}{\mathrm{d}\zeta} + \frac{\Lambda}{\mu(c_0)} \frac{\mathrm{d}c_0}{\mathrm{d}\zeta} C = -\frac{\alpha^2}{\mathrm{Pe}} C.$$

We observe that if we write

$$\tilde{\sigma} = \sigma + \frac{\alpha^2}{\mathrm{Pe}},$$

we recover the equations (5.20),(5.21) with σ replaced by $\tilde{\sigma}$. We conclude that for $\alpha \ll 1$

$$\sigma \sim \tilde{\sigma} \sim \frac{M - 1 + M\Lambda}{M + 1} \alpha + O(\alpha^2),$$

and for $\alpha \gg 1$

$$\sigma \sim \tilde{\sigma} - \frac{\alpha^2}{\mathrm{Pe}} \sim -\frac{\alpha^2}{\mathrm{Pe}} + \sigma_m - \frac{\sigma_m^2}{\alpha} \left(\frac{\mathrm{d}^2 Q_m}{\mathrm{d}Z^2}(Z_m) \right)^{1/2} \left(\frac{\mathrm{d}\mu_0}{\mathrm{d}Z}(Z_m) - \Lambda \frac{\mathrm{d}c_0}{\mathrm{d}Z}(Z_m) \right),$$

where σ_m is as defined in (5.24). With $\mathrm{Pe} \gg 1$ the cutoff wavenumber, beyond which all disturbances are stable, is $O(\mathrm{Pe}^{1/2})$ and the least-stable wavenumber is $O(\mathrm{Pe}^{1/3})$.

5.2.1.2 Summary of stability results

The stability of a disturbance in a miscible displacement in which both viscosity and density differences are important is quite complicated. An example of a dispersion relation is shown in Figure 5.4. The behaviour for small-wavenumber disturbances is the same as for the moving boundary model, and stability depends on a competition between the viscous fingering and density fingering instabilities. For large Λ which might correspond to small velocities, the density difference is of primary importance, while for small Λ, perhaps corresponding to large velocities, the viscosity difference is more important. The

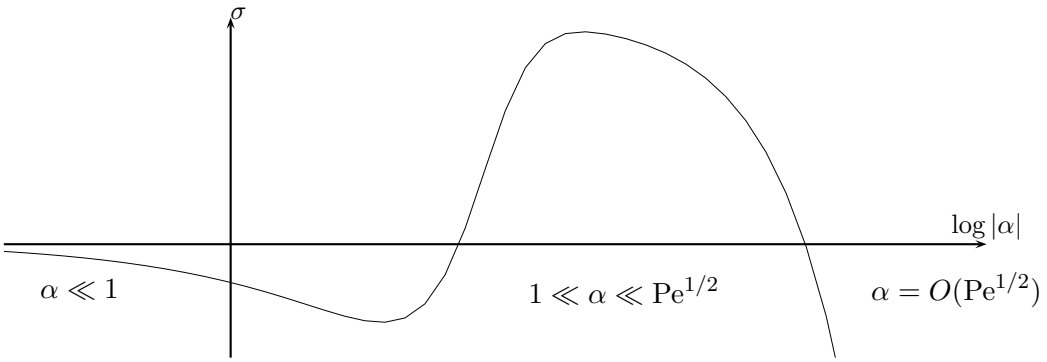

Figure 5.4: Dispersion relation for an interface which is stable for small wavenumber disturbances, but unstable for moderately large wavenumber disturbances, e.g. $\Lambda = -1$ and $M = 10$.

dispersion relation is given by

$$\sigma = \frac{M - 1 + \Lambda M}{M + 1} |\alpha| ,$$

and so stability is guaranteed whenever

$$\Lambda \leq \frac{1}{M} - 1.$$

For reasonably large-wavenumber disturbances ($1 \ll \alpha \ll \mathrm{Pe}^{1/2}$), the growth rate is almost constant, and depends on the maximum value of the density and viscosity gradients. The growth rate is given by

$$\sigma = \sigma_m = \sup_{\zeta} \frac{1}{\mu_0} \frac{\mathrm{d}\mu_0}{\mathrm{d}\zeta} - \frac{\Lambda}{\mu_0} \frac{\mathrm{d}c_0}{\mathrm{d}\zeta}.$$

Stability is guaranteed, provided

$$\Lambda \leq \frac{\mathrm{d}\mu}{\mathrm{d}c}, \tag{5.28}$$

for all values of c. When $M > 1$ the viscosity-concentration relationship is such that for sufficiently small values of c we have

$$\frac{\mathrm{d}\mu}{\mathrm{d}c} < \frac{1}{M} - 1,$$

and so stability of the moving boundary problem is a necessary, but not sufficient, condition for stability of the full, miscible problem. For very large-wavenumber disturbances ($\alpha = O(\mathrm{Pe}^{1/2})$), transverse diffusion ensures stability.

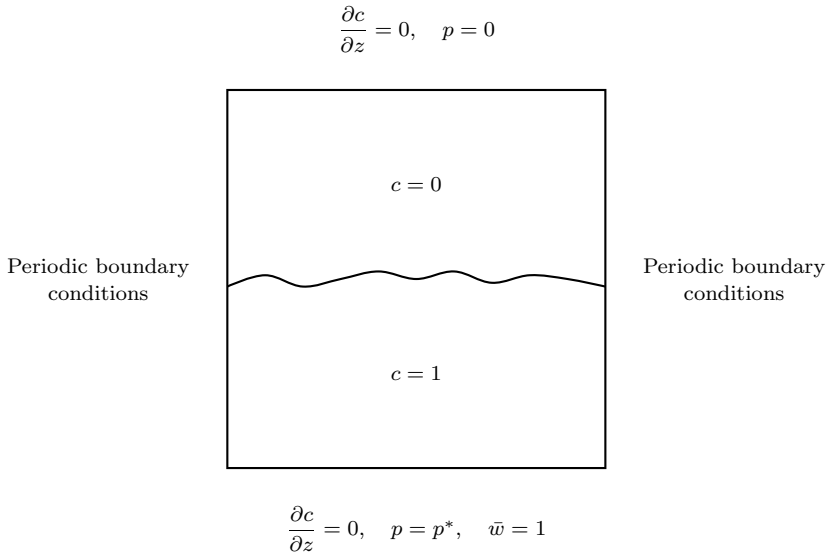

Figure 5.5: Schematic of the computational domain.

5.2.2 Numerical simulation

We now look at some numerical simulations of the Peaceman model, (5.10),(5.11),(5.15). We work in a coordinate system moving with the injection velocity. A schematic of the computational domain is depicted in Figure 5.5. Details of the numerical scheme used may be found in appendix A.

In Figure 5.6 we see a fingering instability develop although the stability analysis of section 5.1 leads us to believe that the displacement should be neutrally stable. As we have seen in section 5.2.1 the correct condition for stability in this problem is given by

$$\Lambda \leq \frac{\mathrm{d}\mu}{\mathrm{d}c},$$

for all c, rather than

$$\Lambda \leq \frac{1}{M} - 1.$$

Differentiating (5.13) we find that $-0.9 > \mathrm{d}\mu/\mathrm{d}c$ for all $c < 0.362$, and so we expect the one-dimensional solution to the Peaceman model to be unstable.

Figure 5.7 shows a simulation in which both a gravitational and a viscous instability is present. We note that there is a region of solvent and a region of oil separated by a mixing zone in which fingering takes place. The fingers are long and thin pointing in the direction of the mean flow and so this motivates the following attempt to use the same techniques as in Chapter 3 to develop a model for the average concentration.

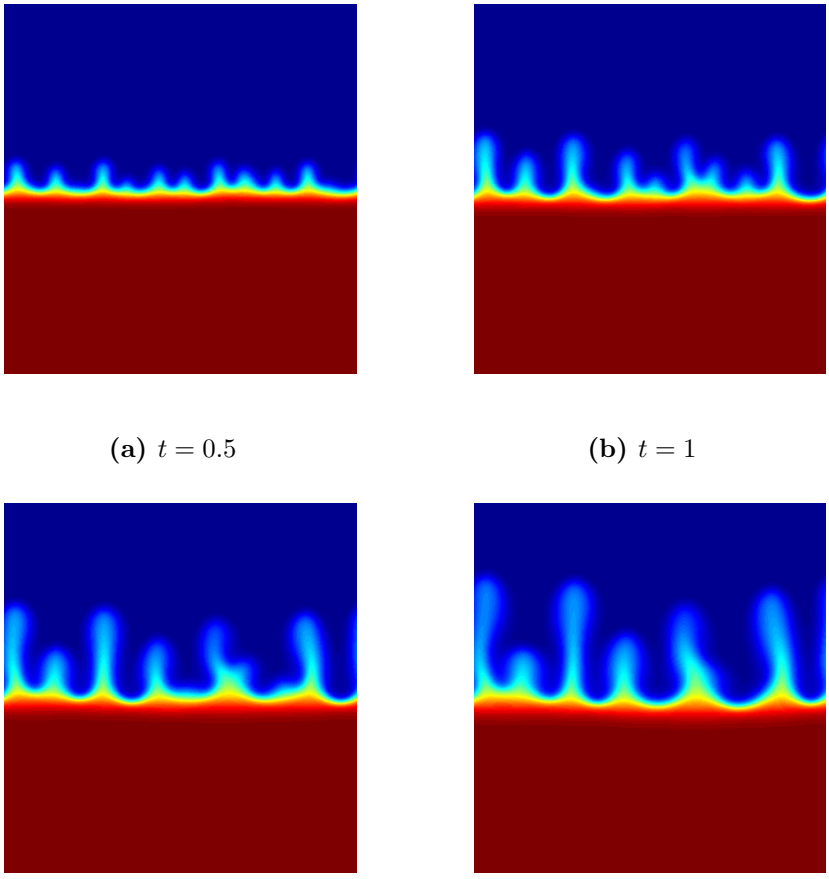

(a) $t = 0.5$ **(b)** $t = 1$

(c) $t = 1.5$ **(d)** $t = 2$

Figure 5.6: Numerical simulation of equations (5.10), (5.11), (5.15) where viscous fingering is being damped by gravitational effects. Here $M = 10$, $\Lambda = -0.9$ and $\mathrm{Pe} = 2000$, with red representing the less viscous, denser fluid ($c = 1$) and blue representing the more viscous, lighter fluid ($c = 0$).

5.3 The unidirectional finger model

We now extend the model that we developed in Chapter 3 to account for unidirectional fingering when the effects of both gravity and viscosity differences are important.

We assume that the prescribed flow is vertical so that any fingers formed point in the direction of the z-axis. As with our previous derivation of the Koval model, we assume that the fingers have a large aspect ratio. Our stability analysis has suggested that the existence of long thin fingers is a consequence of the large Péclet number for our problem. We need to determine the relevant relationship between the aspect ratio of the fingers and the Péclet number.

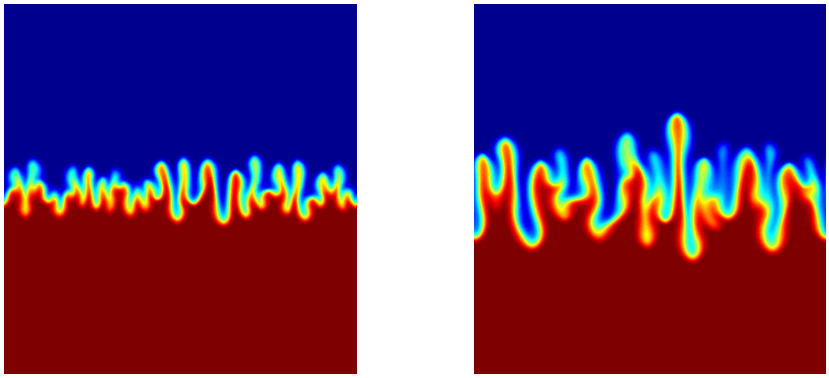

(a) $t = 0.2$ **(b)** $t = 0.4$

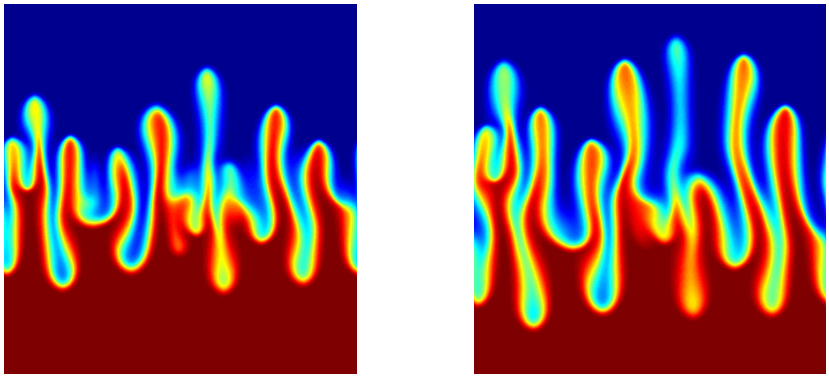

(c) $t = 0.6$ **(d)** $t = 0.8$

Figure 5.7: Numerical simulation of equations (5.10), (5.11), (5.15) where viscous fingering is enhanced by gravitational effects. Here $M = 3$, $\Lambda = 0.5$ and $\mathrm{Pe} = 2000$, with red representing the less viscous, lighter fluid ($c = 1$) and blue representing the more viscous, denser fluid ($c = 0$).

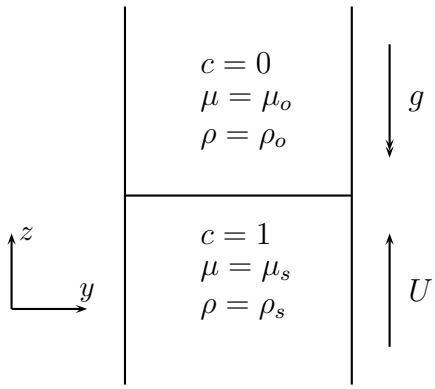

Figure 5.8: Geometry of unidirectional problem

5.3.1 Scaling of diffusion

The fingers are long and thin, and so we rescale the distance across the fingers,

$$y = \epsilon Y,$$

where $\epsilon \ll 1$. The continuity equation, (5.10), becomes

$$\frac{1}{\epsilon}\frac{\partial v}{\partial Y} + \frac{\partial w}{\partial z} = 0.$$

To achieve a sensible balance we require that the transverse velocity is small and scales as

$$v = \epsilon V.$$

The equation for conservation of solvent is now

$$\frac{\partial c}{\partial t} + \frac{\partial}{\partial Y}(Vc) + \frac{\partial}{\partial z}(wc) = \frac{1}{\epsilon^2 \mathrm{Pe}}\frac{\partial^2 c}{\partial Y^2} + \frac{1}{\mathrm{Pe}}\frac{\partial^2 c}{\partial z^2}, \tag{5.29}$$

where we recall that $\epsilon \ll 1$ and $\mathrm{Pe} \gg 1$. The second term on the right-hand side of (5.29), representing longitudinal diffusion, will always be small with this scaling. If $\epsilon^2\mathrm{Pe} \ll 1$ then we cannot achieve a sensible balance in (5.29) and we find that c is independent of Y. We may achieve a sensible balance if $\epsilon^2\mathrm{Pe} \gg 1$; however, diffusion does not then play a rôle in the microscopic problem and so we expect fingering instabilities to develop in this microscopic problem. If we take $\epsilon^2\mathrm{Pe} = O(1)$ then the $O(1)$ diffusion at the microscopic scale may prevent fingering instabilities while still leading to a solution dependent on Y. We therefore rescale the Péclet number,

$$\mathrm{Pe} = \frac{\mathrm{Pe}^*}{\epsilon^2},$$

where $\mathrm{Pe}^* = O(1)$.

5.3.2 Homogenisation of unidirectional fingers

With the aforementioned scaling of the Péclet number the pressure and concentration must satisfy

$$\nabla \cdot \left(\frac{1}{\mu(c)} (\nabla p - \Lambda c\, \mathbf{e}_3) \right) = 0, \tag{5.30}$$

and

$$\frac{\partial c}{\partial t} - \nabla \cdot \left(\frac{c}{\mu(c)} (\nabla p - \Lambda c\, \mathbf{e}_3) \right) = \frac{\epsilon^2}{\mathrm{Pe}^*} \nabla^2 c. \tag{5.31}$$

As with our previous derivation of the Koval model, we assume that the fingers are long, thin and unidirectional pointing in the direction of the z-axis, so that the concentration of solvent has the multiple-scales asymptotic expansion

$$c \sim c_0(y, Y, z, t) + \epsilon c_1(y, Y, z, t) + \dots\,, \quad \text{where} \quad Y = \frac{y}{\epsilon}. \tag{5.32}$$

We also seek a multiple-scales solution for the pressure of the form

$$p \sim p_0(y, Y, z, t) + \epsilon p_1(y, Y, z, t) + \epsilon^2 p_2(y, Y, z, t) + \dots ,$$

and we shall treat the variables y, Y as independent. To leading order in (5.30), we find that

$$\frac{\partial}{\partial Y}\left(\frac{1}{\mu(c_0)}\frac{\partial p_0}{\partial Y}\right) = 0,$$

and so as in (3.7) we find that p_0 is independent of Y, provided a well-defined local average of $\mu(c_0)$ can be found. Such a well-defined local average of $\mu(c_0)$ is, as usual, assured if for instance c is periodic or defined by a stationary and ergodic random variable. At next order in (5.30)

$$\frac{\partial}{\partial Y}\left(\frac{1}{\mu(c_0)}\frac{\partial p_1}{\partial Y}\right) + \frac{\partial}{\partial Y}\left(\frac{1}{\mu(c_0)}\frac{\partial p_0}{\partial y}\right) = 0$$

which implies that

$$\frac{\partial p_1}{\partial Y} = -\frac{\partial p_0}{\partial y} + \mu(c_0)b(y, z, t), \tag{5.33}$$

and so

$$p_1 = -Y\frac{\partial p_0}{\partial y}(y, z, t) + b(y, z, t)\int_0^Y \mu(c_0(y, Y, z, t))\,\mathrm{d}Y + \hat{p}_1(y, z, t).$$

As in (3.9), we find that

$$b(y, z, t) = \frac{1}{\bar{\mu}}\frac{\partial p_0}{\partial y}(y, z, t),$$

where $\bar{\mu}$ is the average of $\mu(c_0)$ across the fingers, defined as in section 3.2. Finally the order one terms of (5.30) yield

$$\frac{\partial}{\partial Y}\left(\frac{1}{\mu(c_0)}\frac{\partial p_2}{\partial Y} + \frac{1}{\mu(c_0)}\frac{\partial p_1}{\partial y} - c_1\frac{\mu'(c_0)}{\mu(c_0)^2}\left(\frac{\partial p_0}{\partial y} + \frac{\partial p_1}{\partial Y}\right)\right) + \frac{\partial}{\partial y}\left(\frac{1}{\mu(c_0)}\frac{\partial p_1}{\partial Y}\right) + \frac{\partial}{\partial y}\left(\frac{1}{\mu(c_0)}\frac{\partial p_0}{\partial y}\right) + \frac{\partial}{\partial z}\left(\frac{1}{\mu(c_0)}\frac{\partial p_0}{\partial z}\right) - \Lambda\frac{\partial}{\partial z}\left(\frac{c_0}{\mu(c_0)}\right) = 0.$$

Analogously to our derivation of (3.11), we find that in order to ensure that p_2 does not grow like Y^2 for large Y we require

$$\frac{\partial}{\partial y}\left(\frac{1}{\bar{\mu}}\frac{\partial p_0}{\partial y}\right) + \frac{\partial}{\partial z}\left(\frac{1}{\mu^*}\frac{\partial p_0}{\partial z}\right) - \Lambda\frac{\partial}{\partial z}\left(\overline{\left(\frac{c_0}{\mu(c_0)}\right)}\right) = 0, \tag{5.34}$$

where μ^* is the harmonic average of $\mu(c_0)$, defined in (3.10). To make analytical progress we now seek an essentially one-dimensional solution with $c = c(Y, z, t)$ and $p_0 = p_0(z, t)$. We see that

$$\frac{\partial p_0}{\partial z} = \Lambda\mu^*\overline{\left(\frac{c_0}{\mu(c_0)}\right)} + \gamma\mu^*, \tag{5.35}$$

where γ is constant. The leading-order equation for conservation of mass is

$$\frac{\partial v_1}{\partial Y} + \frac{\partial w_0}{\partial z} = 0, \tag{5.36}$$

and by integrating with respect to Y and using the boundary conditions $w_0 = 1$ as $z \to \pm\infty$ we conclude that $\bar{w}_0 = 1$. From Darcy's law and (5.35), the vertical velocity is given by

$$w_0 = -\frac{1}{\mu(c_0)}\left(\Lambda\mu^*\overline{\left(\frac{c_0}{\mu(c_0)}\right)} + \gamma\mu^* - \Lambda c_0\right), \tag{5.37}$$

and so, to ensure that $\bar{w}_0 = 1$, we require that $\gamma = -1$. The leading-order velocity transverse to the direction of flow can then be determined from (5.36). Finally, the conservation of solvent equation (5.31) becomes

$$\frac{\partial c_0}{\partial t} + \frac{\partial}{\partial Y}(v_1 c_0) + \frac{\partial}{\partial z}\left(-\frac{c_0}{\mu(c_0)}\left(\Lambda\mu^*\overline{\left(\frac{c_0}{\mu(c_0)}\right)} - \mu^* - \Lambda c_0\right)\right) = \frac{1}{\mathrm{Pe}^*}\frac{\partial^2 c_0}{\partial Y^2}. \tag{5.38}$$

As in section 3.3 we may integrate this equation with respect to Y to find that for some arbitrary function $e(y, z, t)$,

$$\begin{aligned}\frac{1}{\mathrm{Pe}^*}\frac{\partial c_0}{\partial Y} - v_1 c_0 &= \int_0^Y \frac{\partial c_0}{\partial t} + \frac{\partial}{\partial z}\left(-\frac{c_0}{\mu(c_0)}\left(\Lambda\mu^*\overline{\left(\frac{c_0}{\mu(c_0)}\right)} - \mu^* - \Lambda c_0\right)\right)\mathrm{d}Y' + e(y,z,t)\\ &\sim \left(\frac{\partial \bar{c}_0}{\partial t} + \frac{\partial}{\partial z}\left(\mu^*\overline{\left(\frac{c_0}{\mu(c_0)}\right)} + \Lambda\left(\overline{\left(\frac{c_0^2}{\mu(c_0)}\right)} - \mu^*\overline{\left(\frac{c_0}{\mu(c_0)}\right)}^2\right)\right)\right)Y,\end{aligned}$$

for large Y. To ensure that the left-hand side of the above equation does not grow unboundedly as $Y \to \infty$ we therefore require that

$$\frac{\partial \bar{c}}{\partial t} + \frac{\partial}{\partial z}\left(\mu^*\overline{\left(\frac{c}{\mu(c)}\right)} + \Lambda\left(\overline{\left(\frac{c^2}{\mu(c)}\right)} - \mu^*\overline{\left(\frac{c}{\mu(c)}\right)}^2\right)\right) = 0, \tag{5.39}$$

where we have now suppressed the 0 subscripts. This is our fundamental model for the evolution of the averaged concentration; however, it is not yet closed. The averaged functions of c are not known as functions of $\bar{c}$.

5.3.3 Closure of the problem

We now make the naïve assumption, encountered in section 3.3, that c only ever takes the values 0 and 1. In Chapter 3 and in section 5.3.1, we have suggested that this assumption is not likely to be correct as we are left with a microscale problem that is susceptible to

further fingering instabilities. It is nevertheless instructive to consider this possibility and, for the Koval model in section 3.3.1, it proved possible to combine this approach with some empirical results to develop a model that agrees with experimental data. When we assume that c may only take the values 0 and 1 we find that

$$\mu^* = \frac{1}{M\overline{c} + 1 - \overline{c}}, \quad \overline{\left(\frac{c}{\mu}\right)} = \overline{\left(\frac{c^2}{\mu}\right)} = M\overline{c}.$$

From (5.39) we obtain

$$\frac{\partial \overline{c}}{\partial t} + \frac{\partial}{\partial z}\left(M\frac{\overline{c} + \Lambda(\overline{c} - \overline{c}^2)}{M\overline{c} + 1 - \overline{c}}\right) = 0. \tag{5.40}$$

Note that, when $\Lambda = 0$, we recover the naïve version of the Koval model (3.18) and when $M = 1$ we recover the model mentioned in a paper by Menon and Otto [39].

For convenience, we write (5.40) in the form

$$\frac{\partial \bar{c}}{\partial t} + \frac{\partial}{\partial z}\left(F(\bar{c})\right) = 0,$$

where

$$F(\bar{c}) = \frac{M\bar{c}(1 + \Lambda(1 - \bar{c}))}{M\bar{c} + 1 - \bar{c}}.$$

An elementary application of the method of characteristics gives us the implicit solution

$$\bar{c} = \bar{c}_0(z - F'(\bar{c})t),$$

where $\bar{c} = \bar{c}_0(z)$ is our initial condition when $t = 0$. To determine whether we get shock or rarefaction wave solutions, we need to determine the sign of $F''(\bar{c})$. For this problem

$$F'(\bar{c}) = \frac{M(1 - \Lambda((M-1)\bar{c}^2 + 2\bar{c} - 1))}{(M\bar{c} + 1 - \bar{c})^2},$$
$$F''(\bar{c}) = \frac{2M(1 - M(1 + \Lambda))}{(M\bar{c} + 1 - \bar{c})^3}.$$

The sign of $F''(\bar{c})$ is independent of $\bar{c}$ and so we get a rarefaction wave solution whenever

$$\Lambda > \frac{1}{M} - 1; \tag{5.41}$$

otherwise there will be a shock solution. Note that the condition for obtaining a rarefaction wave solution, (5.41), is the same as the condition for the interface to be unstable in the moving-boundary model, (5.17).

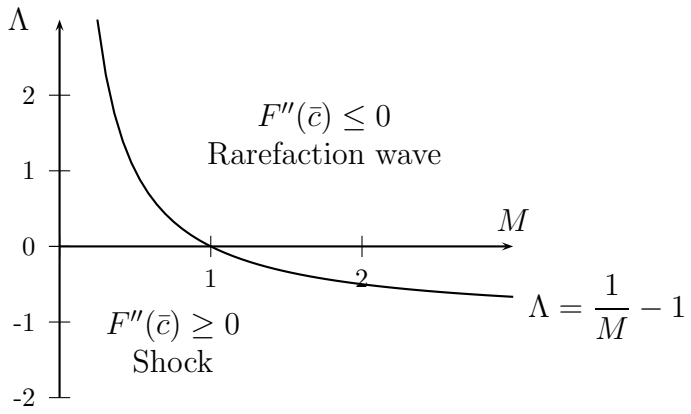

Figure 5.9: Condition for existence of rarefaction wave solutions

If we take as our initial condition

$$\begin{aligned} \bar{c}_0 &= 1 \quad \text{for} \quad z < 0, \\ \bar{c}_0 &= 0 \quad \text{for} \quad z > 0, \end{aligned} \tag{5.42}$$

then when (5.41) holds, the solution is

$$\begin{aligned} &\bar{c} = 1 \quad \text{for} \quad \frac{z}{t} = \zeta \leq \frac{1}{M} - \Lambda, \\ &\bar{c} = 0 \quad \text{for} \quad \zeta \geq M(1+\Lambda), \\ &\bar{c} = \frac{\sqrt{M\frac{M-1+M\Lambda}{(M-1)\zeta+M\Lambda}} - 1}{(M-1)} \\ &\text{for} \quad \frac{1}{M} - \Lambda \leq \zeta \leq M(1+\Lambda). \end{aligned} \tag{5.43}$$

If instead

$$\Lambda < \frac{1}{M} - 1$$

a shock solution will occur. If the shock is at $z = z_s(t)$ then the shock speed is given by

$$\frac{\mathrm{d}z_s}{\mathrm{d}t} = \frac{[F(\bar{c})]^+_-}{[\bar{c}]^+_-} = 1.$$

The interface moves as a travelling wave with the same speed as the injected fluid. The criterion for the formation of shocks is the same as the criterion for stability of the moving boundary problem (5.17), instead of the stability criterion of the full Peaceman model (5.28).

5.3.3.1 Introduction of effective parameters

By comparing (5.43) with experimental data and numerical simulations, we have found that our naïve model fails to accurately predict the speed at which the mean concentration spreads out. This comes as no surprise, since we have encountered this failure of the naïve Koval model in Chapter 3, and a similar observation has been made in [39] for the problem of fingering driven solely by gravitational effects. It can be seen from our numerical simulations (Figure 5.7) that there is significant mixing between the oil and solvent at the microscopic scale, even at large values of the Péclet number. We therefore believe that it is the use of the naïve approximation that is responsible for our model's failure to capture the correct growth rate for the mixing zone. Nevertheless, as discussed in Chapter 3, for the Koval model it has proved possible to adapt the parameter M to produce an effective model which agrees with empirical data. If such an approach is to be applicable here then we must use the effective value of M used in the Koval model as otherwise our model would not agree with the Koval model when $\Lambda = 0$. The effective mobility ratio suggested by Koval [33] that we have already encountered in Chapter 3 is

$$M_e = (0.78 + 0.22M^{1/4})^4.$$

We also aim to determine an effective parameter Λ_e to replace Λ. When the viscosity is constant, and only gravitational effects need to be considered, we may use the results of experiments of Wooding [61] in addition to our numerical simulations. When the viscosity is constant in (5.39) we can write $z = t + \Lambda\tilde{z}$, to obtain the equation

$$\frac{\partial \bar{c}}{\partial t} + \frac{\partial}{\partial \tilde{z}}\left(\overline{c^2} - \bar{c}^2\right) = 0,$$

and so the dependence of the averaged concentration on Λ is equivalent to a linear rescaling in z. The effective parameter Λ_e must therefore depend linearly on Λ. When $M = 1$ and Λ is replaced with Λ_e in (5.43) we find

$$\bar{c} = \frac{1}{2}\left(1 - \frac{z/t - 1}{\Lambda_e}\right), \quad \text{for} \quad 1 - \Lambda_e < \frac{z}{t} < 1 + \Lambda_e, \tag{5.44}$$

with $\bar{c} = 1$ for $z/t < 1 - \Lambda_e$ and $\bar{c} = 0$ for $z/t > 1 + \Lambda_e$. Wooding [61] reported that his experiments gave a growth rate for the mixing zone of approximately 0.446Λ, in our nondimensional coordinates. If our effective model is to agree with Wooding's result we must therefore take

$$\Lambda_e = 0.223\Lambda. \tag{5.45}$$

Note the appearance of the constant 0.223 in the above expression; this value is close

to the value of c_e reported by Koval. This result is not a coincidence as we now show. When the mobility ratio is close to 1, (5.40) becomes

$$\frac{\partial \bar{c}}{\partial t} + \Lambda \frac{\partial}{\partial \xi}\left(\overline{c^2} - \bar{c}^2\right) = 0,$$

where $\xi = x - t$ and $\Lambda = M - 1$. This equation is identical to (5.39) for fingering driven solely by density differences. We also note that when M is close to 1, Koval's effective mobility ratio (3.22) is

$$M_e = 1 + \Lambda c_e,$$

and so the rate of growth of the mixing zone will be equal to $2\Lambda c_e$. We therefore expect to find $c_e = \Lambda_e/\Lambda$, which is indeed the case. There are therefore two entirely independent pieces of experimental evidence that the value of c_e chosen by Koval is correct, namely

- Koval [33] fitting data, from Blackwell's experiments [6] of viscous fingering in miscible displacement in a porous medium, to the Koval model and finding that $c_e = 0.22$.
- Wooding [61] measuring the growth of the mixing zone of density-driven fingering in miscible displacement in a Hele-Shaw cell, and finding that $\Lambda_e = 0.223\Lambda$.

That two entirely independent pieces of evidence should be in such close agreement with each other, and with our numerical simulations, suggests that we should have a high degree of confidence in the estimation of the parameter c_e.

It is not possible to determine the shape of the averaged concentration profile from Wooding's experiments and so we also compare our model with our numerical simulations. In Figure 5.11, our numerical simulations show that, in the mixing zone, the transversely-averaged concentration profile is approximately a straight line, agreeing with (5.44). At larger times, diffusion and coalescence of fingers have acted to reduce the aspect ratio of the fingers, which perhaps explains the slight deviation from the straight line at later times. There is also good agreement with the value of the growth rate of the mixing zone reported in Wooding's experiments. Using least-squares to fit (5.44) to our numerical simulations we obtain values for Λ_e/Λ in the range of 0.215-0.227.

Our effective model for when $c = c(Y, z, t)$ is

$$\frac{\partial \bar{c}}{\partial t} + \frac{\partial}{\partial z}\left(M_e \frac{\bar{c} + \Lambda_e(\bar{c} - \bar{c}^2)}{M_e \bar{c} + 1 - \bar{c}}\right) = 0, \tag{5.46}$$

where

$$M_e = (0.78 + 0.22M^{1/4})^4, \quad \Lambda_e = 0.223\Lambda.$$

We now check that our model agrees with numerical simulations. Figure 5.12 shows

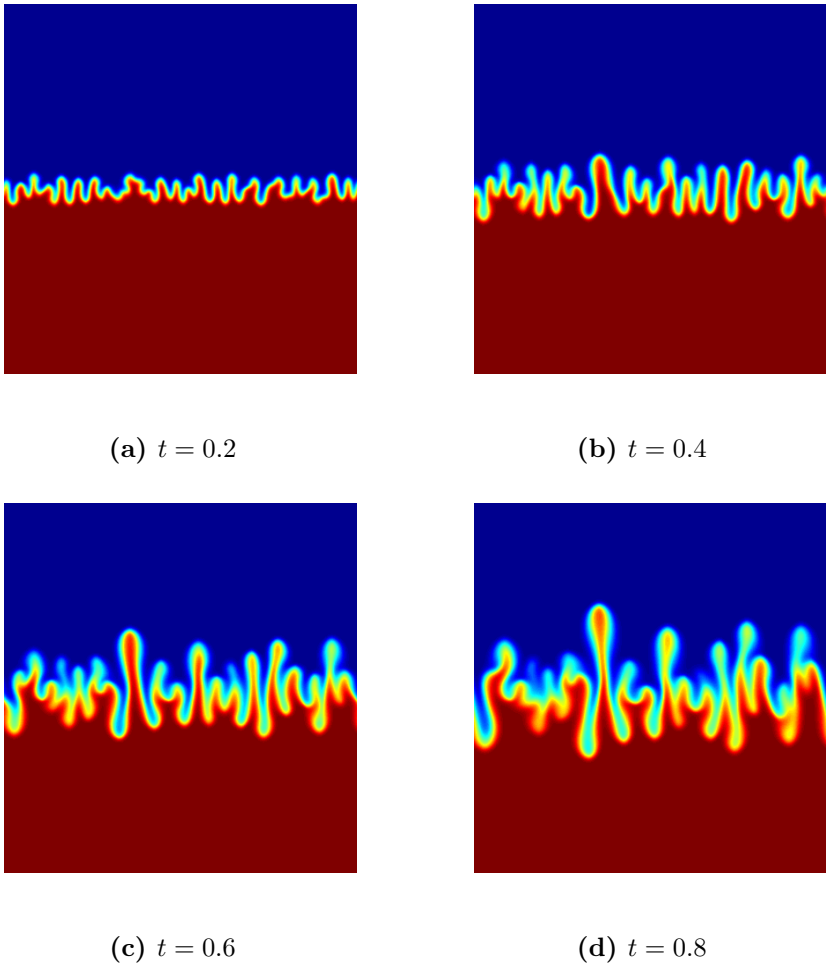

(a) $t = 0.2$ **(b)** $t = 0.4$

(c) $t = 0.6$ **(d)** $t = 0.8$

Figure 5.10: Numerical simulations of equations (5.10), (5.11), (5.15) for gravity-driven fingering. Red represents the lighter fluid ($c = 1$) and blue represents the heavier fluid ($c = 0$). We have taken $\mathrm{Pe} = 2000$ for these simulations.

the transverse average of a two-dimensional simulation along with the theoretical solution of (5.46). We see a close agreement between the numerical simulation and the theoretical solution. When gravitational effects are competing with viscous effects our model is not in such close agreement with the numerical simulations. The effective model (5.46), produces shock solutions, and hence a stable displacement, whenever

$$\Lambda_e < \frac{1}{M_e} - 1.$$

This criterion is not equivalent to the correct stability criterion, (5.27). Further work is needed to accurately close the model, and to ensure that a rarefaction solution exists whenever the displacement is unstable. Perhaps treating the unstable concentrations that appear in our linear stability analysis separately from the stable concentrations could improve the model.

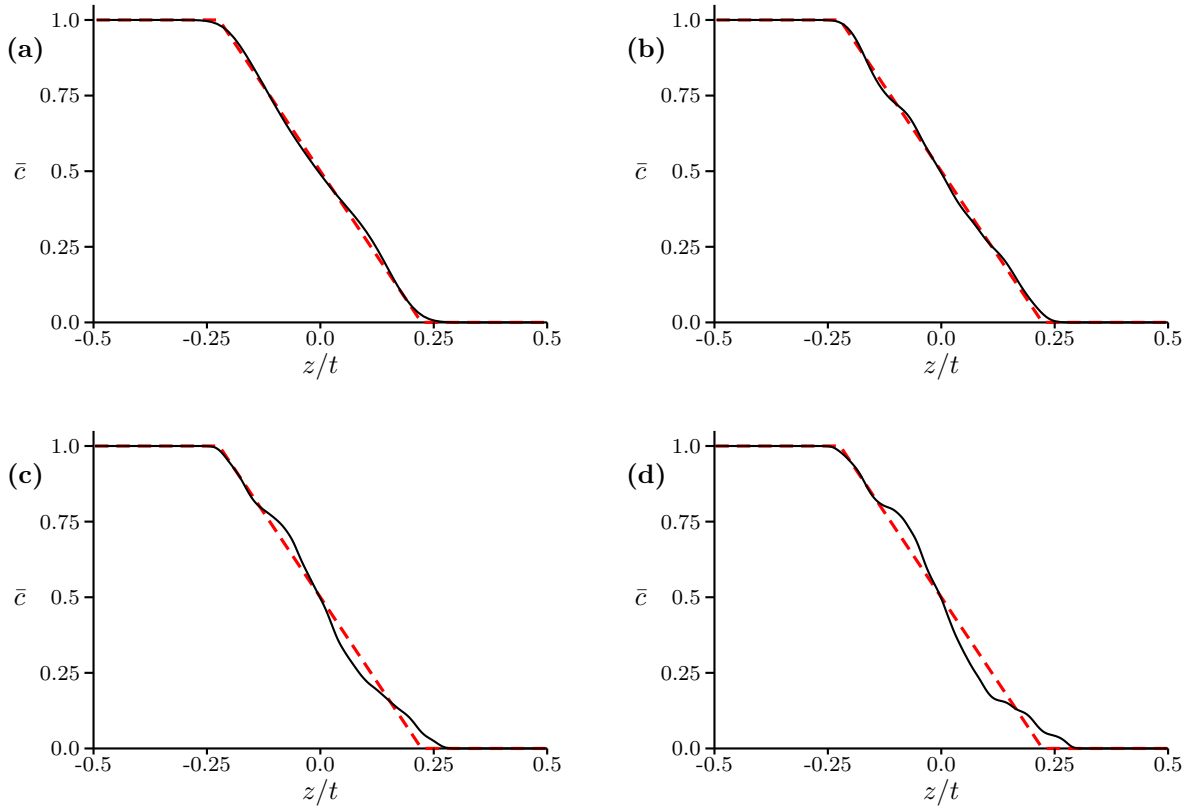

Figure 5.11: The transversely-averaged concentration profiles of the simulation shown in Figure 5.10. The black, unbroken line represents the average of the two-dimensional numerical simulations and the dashed, red line shows the theoretical solution of the averaged concentration as given by (5.44) with $\Lambda_e = 0.223\Lambda$.

All of the work in this section assumes that the fingers are unidirectional, pointing in the vertical direction. This assumption is appropriate when considering the Hill problem [25], in which the flow is confined in a vertical column, or the carbon sequestration problem in which, at least in the region of interest, there is no significant mean flow. In most oil recovery applications the oil is injected horizontally and so any fingers that form will not be unidirectional. In the next section we work towards developing the multidirectional model of Chapter 4 for such applications.

5.4 Oblique viscous/gravity fingering

We would like to extend the work to situations in which the applied flow is not in the vertical direction. While the small disturbances to the interface in section 5.1 grow perpendicular to the interface, it is not clear in which direction nonlinear fingers will grow. In the absence of further evidence about the direction of growth of the fingers, we shall assume that the fingers grow parallel to the direction of mean flow, the same assump-

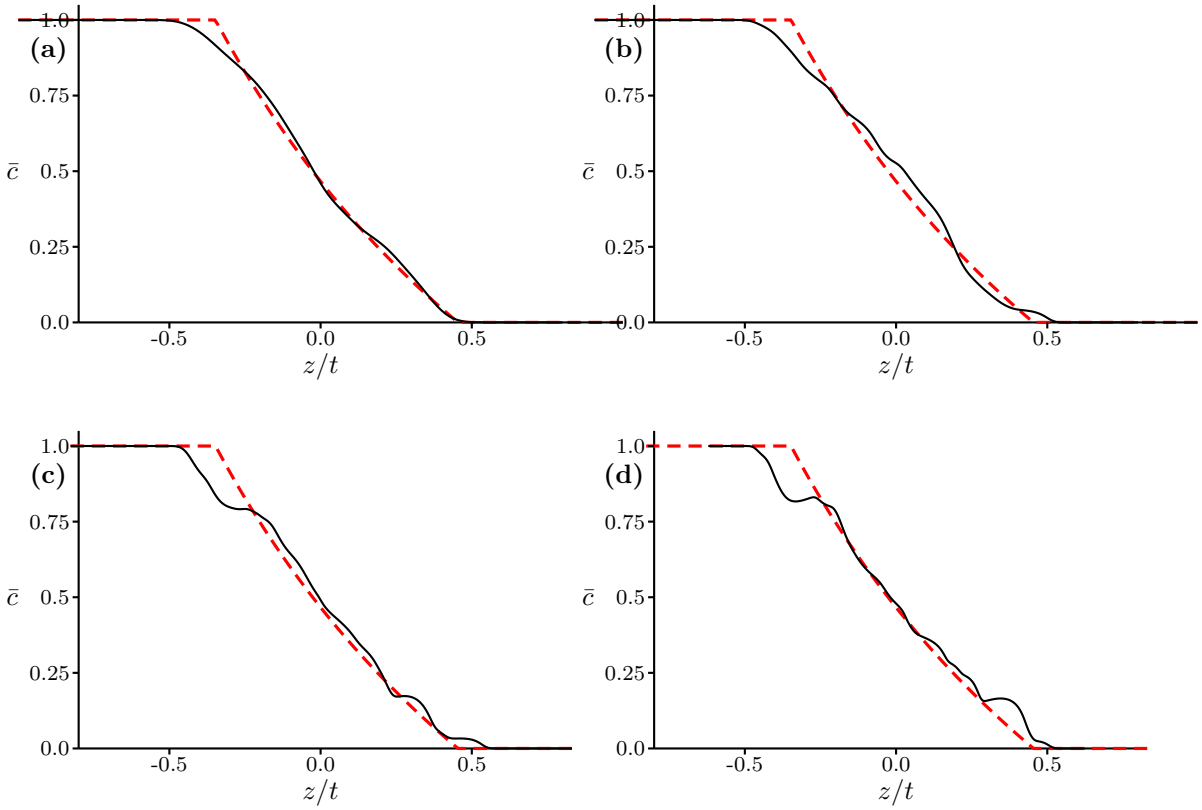

Figure 5.12: The transversely-averaged concentration profiles of the numerical simulations shown in Figure 5.7. The black unbroken line represent the average of the two-dimensional numerical simulation and the dashed, red line shows the theoretical solution of the averaged concentration as given by (5.46).

tion that we successfully applied in Chapter 4. We shall comment on the validity of this assumption at the end of the section. We must still solve equations (5.4)-(5.6),

$$\mathbf{u} = -\frac{1}{\mu(c)}\left(\nabla p - \Lambda c\,\mathbf{e}_3\right), \tag{5.47}$$

$$\nabla \cdot \mathbf{u} = 0, \tag{5.48}$$

$$\frac{\partial c}{\partial t} + \nabla \cdot (\mathbf{u}c) = \frac{\epsilon^2}{\mathrm{Pe}^*}\nabla^2 c. \tag{5.49}$$

As in Chapter 4 we assume that the fingers point in the direction of ∇r, where $r = r(y, z)$, and we also introduce $s = s(y, z)$ as a second coordinate, chosen to ensure that (r, s) is an orthogonal coordinate system (i.e. ∇r is perpendicular to ∇s). Our postulated existence of long thin fingers leads us to suggest the following form for the concentration,

$$c \sim c_0(r, s, S, t) + \epsilon c_1(r, s, S, t) + \dots\,, \quad \text{where} \quad S = \frac{s}{\epsilon} \quad \text{and} \quad \epsilon \ll 1.$$

We therefore take the following asymptotic expansion for the pressure,

$$p \sim p_0(r,s,S,t) + \epsilon p_1(r,s,S,t) + \epsilon^2 p_2(r,s,S,t) + \dots \ .$$

By analogy with section 4.1 we find that in (r,s) coordinates the pressure satisfies

$$\nabla \cdot \left(\begin{pmatrix} \frac{1}{\mu^*} & 0 \\ 0 & \frac{1}{\bar{\mu}} \end{pmatrix} \nabla p_0 - \Lambda \begin{pmatrix} \overline{\left(\frac{c_0}{\mu(c_0)}\right)} \frac{\partial r}{\partial z} \\ \frac{\bar{c}}{\bar{\mu}} \frac{\partial s}{\partial z} \end{pmatrix} \right) = 0, \tag{5.50}$$

with the leading order pressure indpendent of S, i.e. $p_0 = p_0(r,s,t)$. To transform to Cartesian coordinates we use the tensor transformation rule:

$$A^i{}_j(\mathbf{x}) = \frac{\partial x^i}{\partial \xi^l} \frac{\partial \xi^m}{\partial x^j} \tilde{A}^l{}_m(\boldsymbol{\xi}) \ , \tag{5.51}$$

where

$$\tilde{A}^l{}_m(\boldsymbol{\xi}) = \begin{pmatrix} \frac{1}{\mu^*} & 0 \\ 0 & \frac{1}{\bar{\mu}} \end{pmatrix},$$

so that

$$\begin{aligned} A^1{}_1 &= y_r r_y \tilde{A}^1{}_1 + y_s s_y \tilde{A}^2{}_2, \\ A^1{}_2 = A^2{}_1 &= y_r r_z \tilde{A}^1{}_1 + y_s s_y \tilde{A}^2{}_2, \\ A^1{}_1 &= z_r r_z \tilde{A}^1{}_1 + z_s s_z \tilde{A}^2{}_2. \end{aligned}$$

The partial derivatives are related by

$$\begin{pmatrix} y_r & z_r \\ y_s & z_s \end{pmatrix} = \frac{1}{r_y s_z - r_z s_y} \begin{pmatrix} s_z & -s_y \\ -r_z & r_y \end{pmatrix}, \tag{5.52}$$

and also, since (r,s) are orthogonal coordinates, by

$$r_y s_y + r_z s_z = 0.$$

We find that

$$\begin{aligned} A^1{}_1 &= \frac{1}{r_y^2 + r_z^2} \left(\frac{r_y^2}{\mu^*} + \frac{r_z^2}{\bar{\mu}} \right), \\ A^1{}_2 = A^2{}_1 &= \frac{r_y r_z}{r_y^2 + r_z^2} \left(\frac{1}{\mu^*} - \frac{1}{\bar{\mu}} \right), \\ A^2{}_2 &= \frac{1}{r_y^2 + r_z^2} \left(\frac{r_y^2}{\bar{\mu}} + \frac{r_z^2}{\mu^*} \right). \end{aligned}$$

Similarly

$$b^i(\mathbf{x}) = \frac{\partial x^i}{\partial \xi^l}\tilde{b}^l(\boldsymbol{\xi}), \tag{5.53}$$

where

$$\tilde{b}^l(\boldsymbol{\xi}) = \begin{pmatrix} \overline{\left(\frac{c_0}{\mu(c_0)}\right)}\frac{\partial r}{\partial z} \\ \frac{\bar{c}_0}{\bar{\mu}}\frac{\partial s}{\partial z} \end{pmatrix},$$

and so

$$\begin{aligned} b^1 &= \frac{r_y r_z}{r_y^2 + r_z^2}\left(\overline{\left(\frac{c_0}{\mu(c_0)}\right)} - \frac{\bar{c}_0}{\bar{\mu}}\right), \\ b^2 &= \frac{1}{r_y^2 + r_z^2}\left(r_y^2\frac{\bar{c}_0}{\bar{\mu}} + r_z^2\overline{\left(\frac{c_0}{\mu(c_0)}\right)}\right). \end{aligned}$$

In Cartesian coordinates equation (5.50) can be expressed as

$$\frac{\partial \bar{v}_0}{\partial y} + \frac{\partial \bar{w}_0}{\partial z} = 0, \tag{5.54}$$

where the mean Cartesian velocities, $\bar{v}$ and $\bar{w}$, are given by:

$$\begin{aligned} \bar{v} = -\frac{1}{r_y^2 + r_z^2}\Bigg(\left(\frac{r_y^2}{\mu^*} + \frac{r_z^2}{\bar{\mu}}\right)\frac{\partial p_0}{\partial y} &+ r_y r_z\left(\frac{1}{\mu^*} - \frac{1}{\bar{\mu}}\right)\frac{\partial p_0}{\partial z} \\ &- \Lambda r_y r_z\left(\overline{\left(\frac{c_0}{\mu(c_0)}\right)} - \frac{\bar{c}_0}{\bar{\mu}}\right)\Bigg), \end{aligned} \tag{5.55}$$

$$\begin{aligned} \bar{w} = -\frac{1}{r_y^2 + r_z^2}\Bigg(r_y r_z\left(\frac{1}{\mu^*} - \frac{1}{\bar{\mu}}\right)\frac{\partial p_0}{\partial y} &+ \left(\frac{r_y^2}{\bar{\mu}} + \frac{r_z^2}{\mu^*}\right)\frac{\partial p_0}{\partial z} \\ &- \Lambda\left(r_y^2\frac{\bar{c}_0}{\bar{\mu}} + \overline{\left(\frac{c_0}{\mu(c_0)}\right)}r_z^2\right)\Bigg). \end{aligned} \tag{5.56}$$

Recall that we are assuming that the fingers immediately align themselves to point in the direction of the mean flow of fluid. This assumption yields the requirement that ∇r is parallel to $\overline{\mathbf{u}}$, or

$$\lambda(y,z) = \frac{r_z}{r_y} = \frac{\bar{w}_0}{\bar{v}_0}. \tag{5.57}$$

Using (5.55) and (5.56) we find that λ satisfies

$$p_{0y}\lambda^3 - (p_{0z} - \Lambda\bar{c}_0)\lambda^2 + p_{0y}\lambda - (p_{0z} - \Lambda\bar{c}_0) = 0, \tag{5.58}$$

which has the solutions

$$\lambda = \pm \mathrm{i}, \quad \lambda = \frac{p_{0z} - \Lambda \bar{c}_0}{p_{0y}}.$$

The physically relevant solution is

$$\lambda(y,z) = \frac{r_z}{r_y} = \frac{p_{0z} - \Lambda \bar{c}_0}{p_{0y}}. \tag{5.59}$$

We find that the mean velocities are given by

$$\bar{v}_0 = -\frac{\Pi}{\mu^*} p_{0y}, \qquad \bar{w}_0 = -\frac{\Pi}{\mu^*}(p_{0z} - \Lambda \bar{c}), \tag{5.60}$$

where

$$\Pi = \frac{p_{0y}^2 + (p_{0z} - \Lambda \bar{c}_0)(p_{0z} - \Lambda F)}{p_{0y}^2 + (p_{0z} - \Lambda \bar{c}_0)^2},$$

and F is the usual fractional flow function defined by

$$F = \mu^* \overline{\left(\frac{c_0}{\mu(c_0)} \right)}.$$

To find the pressure field we must then solve

$$\nabla \cdot \bar{\mathbf{u}}_0 = 0,$$

using (5.60).

We now must return to the equation for the transport of solvent,

$$\frac{\partial c}{\partial t} - \nabla \cdot \left(\frac{c}{\mu} \left(\nabla p - \Lambda c \mathbf{e}_3 \right) \right) = \frac{\epsilon^2}{\mathrm{Pe}^*} \nabla^2 c.$$

In (r,s) coordinates this becomes

$$\begin{aligned} \frac{\partial c_0}{\partial t} &- \frac{1}{\sqrt{g}} \frac{\partial}{\partial r} \left(\frac{c_0 \sqrt{g}}{\mu(c_0)} \left(g^{11} \frac{\partial p_0}{\partial r} - \Lambda c_0 \frac{\partial r}{\partial z} \right) \right) \\ &- \frac{1}{\sqrt{g}} \frac{\partial}{\partial s} \left(\frac{c_0 \sqrt{g}}{\mu(c_0)} \left(g^{22} \left(\frac{\partial p_0}{\partial s} + \frac{\partial p_1}{\partial S} \right) - \Lambda c_0 \frac{\partial s}{\partial z} \right) \right) \\ &- \frac{1}{\epsilon \sqrt{g}} \frac{\partial}{\partial S} \left(\frac{c_0 \sqrt{g}}{\mu(c_0)} \left(g^{22} \left(\frac{\partial p_0}{\partial s} + \frac{\partial p_1}{\partial S} + \epsilon \frac{\partial p_1}{\partial s} + \epsilon \frac{\partial p_2}{\partial S} \right) - \Lambda c_0 \frac{\partial s}{\partial z} \right) \right) \\ &= \frac{1}{\mathrm{Pe}^* \sqrt{g}} \frac{\partial}{\partial S} \left(\sqrt{g} g^{22} \frac{\partial c_0}{\partial S} \right) + O(\epsilon). \end{aligned} \tag{5.61}$$

As with (3.23) and (4.21), this equation is not simple to solve and requires us to think about local 2-D problems. We can however make some progress if we integrate over the

small scale variable, S, and use empirical closure conditions. Integrating over S gives

$$\frac{\partial \overline{c}}{\partial t} - \frac{1}{\sqrt{g}}\frac{\partial}{\partial r}\left(\sqrt{g}\overline{\left(\frac{c}{\mu}\right)}g^{11}\frac{\partial p}{\partial r} - \sqrt{g}\Lambda\overline{\left(\frac{c^2}{\mu}\right)}\frac{\partial r}{\partial z}\right) - \frac{1}{\sqrt{g}}\frac{\partial}{\partial s}\left(\sqrt{g}\left(\frac{\overline{c}}{\overline{\mu}}g^{22}\frac{\partial p}{\partial s} - \Lambda\frac{\overline{c}^2}{\overline{\mu}}\frac{\partial s}{\partial z}\right)\right) = 0, \tag{5.62}$$

or

$$\frac{\partial \overline{c}}{\partial t} - \nabla\cdot\left(\begin{pmatrix}\overline{\left(\frac{c}{\mu}\right)} & 0\\ 0 & \frac{\overline{c}}{\overline{\mu}}\end{pmatrix}\nabla p - \Lambda\begin{pmatrix}\overline{\left(\frac{c^2}{\mu}\right)}\frac{\partial r}{\partial z}\\ \frac{\overline{c}^2}{\overline{\mu}}\frac{\partial s}{\partial z}\end{pmatrix}\right) = 0, \tag{5.63}$$

where we have now suppressed the 0 subscripts from the leading order terms. We may rewrite this in Cartesian coordinates, eventually finding that the mean concentration satisfies

$$\frac{\partial \overline{c}}{\partial t} + \nabla\cdot\left(F\tilde{\Pi}\bar{\mathbf{u}}\right) = 0, \tag{5.64}$$

where

$$\tilde{\Pi} = \frac{p_y^2 + (p_z - \Lambda\overline{c})(p_z - \Lambda G)}{p_y^2 + (p_z - \Lambda\overline{c})(p_z - \Lambda F)},$$

and

$$G = \overline{\left(\frac{c^2}{\mu}\right)}\Big/\overline{\left(\frac{c}{\mu}\right)}.$$

In summary we must solve

$$\nabla\cdot\bar{\mathbf{u}} = 0, \tag{5.65}$$

$$\bar{\mathbf{u}} = -\frac{\Pi}{\mu^*}\begin{pmatrix}p_y\\ p_z - \Lambda\overline{c}\end{pmatrix}, \tag{5.66}$$

$$\frac{\partial \overline{c}}{\partial t} + \nabla\cdot\left(F\tilde{\Pi}\bar{\mathbf{u}}\right) = 0. \tag{5.67}$$

If we make the naïve assumption that c only takes the values 0 and 1 then we find that

$$\mu^* = \frac{1}{M\overline{c} + 1 - \overline{c}}, \qquad F = \frac{M\overline{c}}{M\overline{c} + 1 - \overline{c}}, \qquad G = 1.$$

5.4.1 Ellipticity of pressure problem

Our model shows that the leading order pressure satisfies

$$\nabla\cdot\left(\frac{\Pi(\nabla p, \bar{c})}{\mu^*(\bar{c})}\begin{pmatrix}p_y\\ p_z - \Lambda\bar{c}\end{pmatrix}\right) = 0. \tag{5.68}$$

The dependence of Π on ∇p leads us to question whether this is an elliptic problem for p. Expanding (5.68) gives

$$\begin{aligned}\left(1-\frac{\Lambda(F-\overline{c})(p_z-\Lambda\overline{c})}{p_y^2+(p_z-\Lambda\overline{c})^2}+\frac{2\Lambda(F-\overline{c})(p_z-\Lambda\overline{c})p_y^2}{(p_y^2+(p_z-\Lambda\overline{c})^2)^2}\right)p_{yy} &+\\ \left(-\frac{\Lambda(F-\overline{c})p_y}{p_y^2+(p_z-\Lambda\overline{c})^2}+\frac{4\Lambda(F-\overline{c})p_y(p_z-\Lambda\overline{c})^2}{(p_y^2+(p_z-\Lambda\overline{c})^2)^2}\right)p_{yz} &+\\ \left(1-\frac{2\Lambda(F-\overline{c})(p_z-\Lambda\overline{c})}{p_y^2+(p_z-\Lambda\overline{c})^2}+\frac{2\Lambda(F-\overline{c})(p_z-\Lambda\overline{c})^3}{(p_y^2+(p_z-\Lambda\overline{c})^2)^2}\right)p_{zz} &+ \tilde{g}(\nabla p,\nabla\overline{c},\overline{c})=0.\end{aligned}$$

We define

$$\beta=\Lambda(\overline{c}-F),$$

$$p_y=P\cos\theta,\quad p_z-\Lambda\overline{c}=P\sin\theta,$$

where

$$P=\sqrt{p_y^2+(p_z-\Lambda\overline{c})^2}.$$

Our equation, (5.68) now simplifies to

$$\begin{aligned}\left(P+\beta\sin\theta-2\beta\sin\theta\cos^2\theta\right)p_{yy} &+\\ \beta\left(\cos\theta-4\cos\theta\sin^2\theta\right)p_{yz} &+\\ \left(P+2\beta\sin\theta-2\beta\sin^3\theta\right)p_{zz} &+ g(\nabla p,\nabla\overline{c},\overline{c})=0.\end{aligned}$$

The discriminant is

$$-4P^2-4P\beta\sin\theta+\beta^2(1-\sin^2\theta), \tag{5.69}$$

and hence, for $\beta>0$, the problem is:

elliptic for $P>\frac{1}{2}\beta(1-\sin\theta)$;

parabolic for $P=\frac{1}{2}\beta(1-\sin\theta)$;

hyperbolic for $P<\frac{1}{2}\beta(1-\sin\theta)$.

The model that we have developed does not seem to be physically appropriate when the pressure gradient is small, so that the equation can change type. We infer that the assumption that the fingers follow the direction of the mean flow is only likely to be valid when viscosity differences are the primary mechanism for finger formation.

When density differences are the primary mechanism for finger formation we might instead choose the direction of fingering so that $r=z$. However, it does not seem clear that transport perpendicular to the direction of fingering is possible, without destroying the

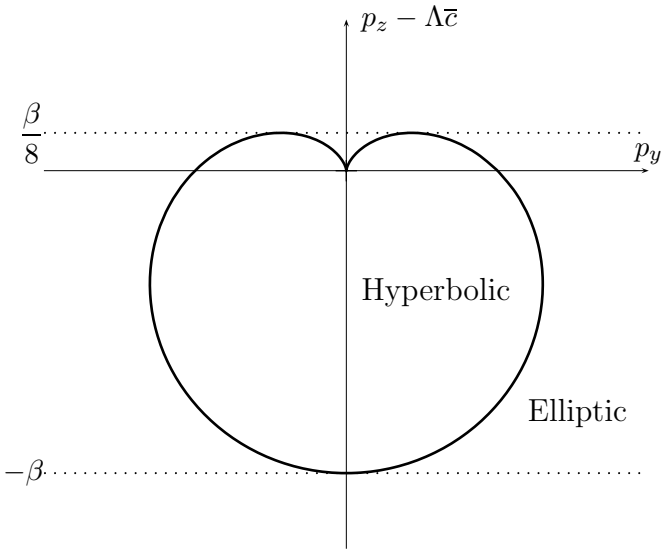

Figure 5.13: Region of ellipticity.

fingering pattern. We suspect that often neither of these assumptions for the direction of fingering is valid, and perhaps even the assumption that there is a simple fingering pattern with a clear directionality is suspect. For oblique viscous/gravity fingering with important interaction between the viscous fingering instability and the density fingering instability, more direct numerical simulations of the full problem are required before any reasonable conjectures are made.

5.5 Conclusions

In this chapter we have considered displacements where there are both density and viscosity differences between the two fluids. We have seen that the stability of the interface between two immiscible fluids of differing densities and viscosities can be quite complicated. There is a competition between the density-difference driven instability and the viscosity-difference driven instability. When a heavier, more viscous fluid displaces a lighter, less viscous fluid from above, the density-driven instability can be overcome, provided that the interface moves sufficiently fast. Similarly a viscous fingering instability can be stabilised provided the lighter fluid lies above the heavier fluid and the interface moves sufficiently slow.

In miscible displacements, this result is altered surprisingly. As one might expect from our stability analysis of Chapter 2, we find that the growth-rate is bounded and sufficiently large wavenumber disturbances are always stable. However, it is also possible for the displacement of a heavier, more viscous fluid by a lighter, less viscous fluid from above to be unstable, even when our moving boundary analysis suggests that it should be

stable. The instability is largely a consequence of the nonlinear viscosity-concentration relationship, resulting in a large viscosity gradient for small concentrations of the less viscous fluid.

We have applied the methodology of Chapter 3 to develop a model for the evolution of the averaged concentration of solvent, as solvent is injected to displace oil from a vertical column. As with Chapter 3 we ultimately have to rely on some experimental evidence to close our model. Our model can predict the influence of viscosity differences in vertical, gravity-driven fingering.

We have also attempted to extend the generalised Koval model, developed in Chapter 4, to include gravitational effects. The essential difficulty that we have encountered is that it is not now clear in which direction the fingers should point. In our model we have first assumed that fingering instabilities grow in the direction of the mean flow; however, we then obtained an unphysical equation for the pressure when the pressure gradient is small. The assumption that fingering instabilities grow in the direction of the mean flow is only likely to be reasonable when gravity-driven fingering is of secondary importance to the viscous fingering instability. Away from this limit, and when the mean flow is not entirely vertical, it is not clear that a fingering pattern will persist, and perhaps direct numerical simulation is preferable.

Chapter 6

Conclusions

We now briefly summarise the important results of this thesis, making clear how our results can be applied in practical situations. We also list some unanswered questions and possibilities for further work that have arisen from this investigation.

6.1 Summary of results

The principal goal of this thesis has been to systematically derive an effective model for the industrial process of a miscible displacement of oil by a solvent. In Chapter 2 we have derived the Peaceman model from first principles, with molecular diffusion acting at the pore scale to produce a homogeneous mixture of oil and solvent. We have therefore, throughout, treated the Peaceman model as the fundamental model for miscible displacements. We have shown how the rapid variations in the velocity lead to an enhanced dispersion effect at the macroscopic scale, but that the flow is nevertheless convection-dominated at the macroscopic scale, i.e. Pe, the Péclet number, is large. We have shown that instabilities may grow, in the form of fingers, although the growth of these fingers is inhibited when compared to the growth of fingers in the immiscible Muskat problem. This is the result of the following two mechanisms:

- longitudinal diffusion, which acts to reduce the viscosity gradient leading to a bounded growth rate for large wavenumber disturbances;
- and transverse diffusion, which acts to cause large wavenumber disturbances to decay.

The combination of these two stabilising mechanisms leads to the selection of a particular length scale for the width of the fingering instabilities, and we have shown that this width is of $O(\mathrm{Pe}^{-1/2})$. We have also shown that, with some care, it is possible to numerically

simulate the fine details of miscible displacements through porous media; however, the detailed simulation is numerically costly, and so an averaged model needs to be constructed. The numerical simulations suggested that a "mixing zone" or "mushy region" exists in which fingering occurs and there is some diffusion of the solvent into the oil. Our numerical simulations also suggested that the growth of this mushy region was predictable, and did not depend on the fine details of the fingering, suggesting that an averaged model is possible.

In Chapter 3 we modelled the fingering behaviour, under the important assumption that the fingers had a large aspect ratio. By assuming that the mean flow is one-dimensional we were able to explicitly solve for the velocity in terms of the concentration field. This led to a homogenised model (3.23) for the growth of thin fingers in which the pressure variation across each finger was negligible. When we made the naïve assumption that the oil and solvent did not mix at all we found, on averaging our homogenised model across the fingers, that the rate of growth of fingers was dramatically different to the true rate of growth of fingers, as predicted by the numerical simulation of the Peaceman model. Our numerical simulations supported Koval's supposition [33] that, when calculating the fractional flow function, it was possible to model the mixing of solvent and oil by replacing the solvent by a fictitious mixture of oil and solvent that is treated as immiscible with the oil. However, although effective in practice, Koval's model has still not been justified, and so we proceeded to study the growth of thin fingers in more detail.

We found that our homogenised model for large-aspect-ratio fingers predicted the formation of shocks aligned perpendicular to the direction of flow. We identified these shocks with the roots and tips of the finger, and showed that the large-aspect-ratio assumption breaks down close to the shocks. We could analyse our homogenised model away from shocks, but, to obtain the correct shock conditions, we needed to match with the solution to a local tip-scale problem. Previous works have attempted to bound the growth of fingers by considering shocks that are regularised by small longitudinal diffusion, analogous to the viscous shock solutions of Burgers' equation. However, we have shown that this is not appropriate here since the assumption of large-aspect-ratio fingers breaks down at a length scale that is still so long that longitudinal diffusion remains negligible.

We therefore introduced a fully two-dimensional flow problem (3.40)-(3.41). To make further progress we limited attention to the leading finger-tips, for which we have concluded that the only possible family of solutions are the famous Saffman-Taylor fingers, with no mixing between the solvent and oil in the tip-region scaling, although of course mixing will occur at a still smaller length scale. Almost all the mixing between solvent and oil must take place in the "mushy region" where the large aspect-ratio fingers are found. We have also concluded that it is realistic to model the leading finger-tips as being

periodic in the direction perpendicular to that of the flow, although further interior finger-tips will also exist. On the basis of our numerical simulations of the Peaceman model, we have suggested that a shape selection mechanism that results from this tip analysis may exist, and explain the observed rate of growth of the mixing zone. Some preliminary ideas concerning the mechanism of periodic finger-tip formation were also presented.

In Chapter 4 we have applied the ideas of Chapter 3 to problems in which the mean flow is not one-dimensional, but there are still many thin fingers present. This allows us to relax the requirements that the permeability is homogeneous and isotropic at the macroscopic scale, although at the finger length scale homogeneity is still required. We assumed that the direction of the mean flow did not change rapidly so that the direction of fingering followed that of the mean flow. Our resultant model (4.19)-(4.20) was a two-dimensional generalisation of the Koval model in which, crucially, we had to determine μ^*, the harmonic average of the viscosity, in addition to the usual fractional flow function that has to be determined for the original Koval model (3.21). By analysing our numerical simulations we were able to suggest a sensible expression for μ^* as a function of the transversely averaged concentration, without introducing any new fitting-parameters beyond that of the effective concentration introduced in the original Koval model.

We have compared our generalised Koval model with the standard model for immiscible flow through porous media, and have shown that we can reformulate the generalised Koval model in the terminology of "relative permeabilities". These relative permeabilities that may be identified with the generalised Koval model are simple quadratic functions of the averaged concentration of solvent. This reformulation provides extra intuitive understanding of the advantage of using miscible displacements over immiscible displacements, namely that the injection of solvent in the porous medium may actually promote the flow of oil, whereas the injection of a fluid immiscible with the oil hinders the flow of oil.

We have also compared our generalised Koval model with the widely-used Todd & Longstaff model, and noted that while the basic structure of the Todd & Longstaff model is sound, certain effective parameters have been introduced in an ad hoc way. The generalised Koval model is structurally identical to the Todd & Longstaff model, but is algebraically simpler and is more effective at predicting both the growth of the mixing zone and the pressure drop across the mixing zone for a wide range of different mobility ratios.

In Chapter 5 we have extended our analysis to consider miscible displacements in which the density difference between the two fluids is important in addition to the viscosity difference. We have discussed the stability of miscible displacements in which both the density difference and viscosity difference is important and shown the possibility of instability in the miscible problem even though the corresponding immiscible problem

is stable! We also produced a model (5.46), analogous to the Koval model, for vertical miscible displacements between two fluids of differing densities and viscosities, although the model disagreed with numerical simulations of the Peaceman model when the viscous instability and gravity-driven instability were competing. We have also attempted to derive a model for fingering when the mean flow is not vertical, and considered whether or not the fingering structure remains, and, if it does, how to determine in which direction the fingers grow. We have been able to produce a model when viscous fingering is the dominant process, with the fingers aligned with the mean direction of flow as in Chapter 4.

6.2 Future work

Throughout this thesis we have stumbled upon many interesting questions which we have either been unable to answer or which have been outside our central theme. We therefore conclude with some areas for potential future work.

- In section 2.1 we derived the Peaceman model, and in particular investigated diffusion through porous media. The resulting cell problem (2.21) is not easy to solve, and so it is not easy to determine how the magnitude of the effective diffusion coefficients depend on the flow of fluid through the porous medium. We found in section 2.1.2.4 that, when the pore-scale Péclet number is large, the assumption of periodicity of the medium may lead to unrealistic behaviour. In modelling diffusion through porous media there remains a wide gulf between the predictions for periodic media [7, 47] and the predictions for random media [50, 32]. We believe that further study of flow through periodic media in which the flow is not aligned with the periodic medium may help to bridge this divide.

- In section 2.1.4 we derived the Muskat problem as the limit of the Peaceman model with negligible diffusion and an interface that was slightly diffuse. A potential regularisation of the Muskat problem might be obtained by determining the next order correction to the kinematic condition.

- In Chapter 3 we encountered the most compelling problem of the thesis, namely the explanation of the growth rate of the mixing zone, as predicted by numerical simulations of the Peaceman model. It seems that it is the growth of the tips and roots that control the growth of the mixing zone, and so we think that these regions are worthy of further study. The appearance of the Saffman-Taylor finger family of solutions in the finger-tip regions suggests that these solutions may lead to a shape

selection mechanism, analogous to the shape selection obtained with the surface tension regularisation of the Muskat problem. The "fading" mechanism observed in [64], may also be important in explaining the growth rate of finger-tips and further work is needed in studying the interaction between finger-tips and the main body of other fingers.

- One problem of great practical importance that remained unanswered in Chapter 4 is how to model the interaction between fingering and heterogeneities with a characteristic length scale of the same size as the width of the fingers. However, at present this problem appears to be too difficult for a systematic mathematical treatment, allowing only bounds on the rate of growth.

- In section 5.3 we extended the Koval model to consider vertical miscible displacements in which both the density differences and the viscosity differences between the solvent and oil were important. When there was a competition between gravity and viscous fingering, the validity of our model (5.46) is not clear since the existence of a mixing zone did not correspond exactly with the disturbance being unstable. Perhaps considering the concentrations for which the problem is linearly stable separately from the concentrations for which the problem is linearly unstable would correct the model.

- Finally, more work is needed on the interaction between viscous fingering and density fingering when the miscible displacement is not vertical. The crucial question that needs to be answered is whether a fingering structure remains, and, if so, what is its direction. Further numerical simulations may be useful in answering this question.

Appendix A

Numerical algorithms

To produce a numerical solution of the Peaceman model (2.32)-(2.33) we have followed the same basic approach as Peaceman [46] or Farmer [17]. At each time-step the problem is split into three parts:

1. First we solve for the pressure field using the viscosity obtained from the previous time-step (or the initial condition for the first time-step);

2. Next we calculate the velocity of the fluid, using the pressure field calculated in the previous time-step, and apply a finite-volume method to advect the concentration of solvent;

3. Finally we introduce the physical diffusion via a simple explicit method.

All our numerical simulations take place in a rectangular domain, split up into rectangular cells of width h_x and height h_y. Each cell is indexed (i, j) with i running from 1 to $N_x = L_x/h_x$, where L_x is the width of the domain and j running from 1 to $N_y = L_y/h_y$, where L_y is the height of the domain.

A.1 Elliptic problem for the pressure field

Darcy's law and incompressibility of the fluid leads us to solve

$$\nabla \cdot \left(\frac{\mathbf{K}}{\mu(c)} \nabla p \right) = 0.$$

All of the numerical simulations that are presented in this thesis have assumed that the permeability is isotropic and homogeneous, however our numerical method is equally valid for heterogeneous media, and only needs a slight adaptation to allow for anisotropic media. For an isotropic medium with permeability k, we work in terms of the mobility

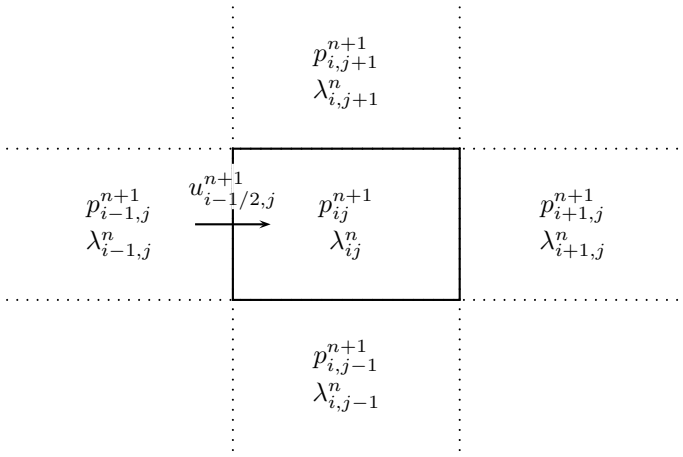

Figure A.1: Definition of pressure and flux in numerical scheme.

$\lambda = k/\mu(c)$. In each cell (i, j) we know the mobility calculated from the concentration profile at the previous time-step, denoted by λ^n_{ij}, and we need to find the pressure at this time step, i.e. p^{n+1}_{ij}. We introduce the flux per unit area of fluid between cell $(i-1, j)$ and (i, j), at the current time-step, as $u^{n+1}_{i-1/2,j}$, and the flux per unit area of fluid between cell $(i, j-1)$ and (i, j) as $v^{n+1}_{i,j-1/2}$. Our numerical approximations of these fluxes are

$$u^{n+1}_{i-1/2,j} = \frac{2}{h_x} \frac{p^{n+1}_{ij} - p^{n+1}_{i-1,j}}{1/\lambda^n_{ij} + 1/\lambda^n_{i-1,j}}, \tag{A.1}$$

and

$$v^{n+1}_{i,j-1/2} = \frac{2}{h_y} \frac{p^{n+1}_{ij} - p^{n+1}_{i,j-1}}{1/\lambda^n_{ij} + 1/\lambda^n_{i,j-1}}, \tag{A.2}$$

these being the analytical solutions for the fluxes in one-dimensional problems with a discontinuous mobility. In each cell we must conserve mass and so we require that the total flux of fluid entering the cell is equal to the total flux of fluid leaving the cell or

$$h_y \left(u^{n+1}_{i-1/2,j} - u^{n+1}_{i+1/2,j} \right) + h_x \left(v^{n+1}_{i,j-1/2} - v^{n+1}_{i,j+1/2} \right) = 0. \tag{A.3}$$

We apply periodic boundary conditions in the y direction, and set $p = 1$ at the inlet boundary and $p = 0$ at the outlet. This gives us a system of equations for p^n_{ij} that can be solved for this time step. We have set $p = 1$ at the inlet boundary, however in practice we wish to ensure that the total flux is constant, rather than apply a constant pressure. By conservation of mass

$$\overline{u} = \int_0^{L_y} u \, \mathrm{d}y$$

will be equal to the total flux of fluid, and since the problem has a linear dependence on the value of p at the inlet, we can obtain the correct pressure field and fluxes simply by

scaling the pressure and fluxes with $U/\overline{u}$, where U is the flux of fluid introduced at the inlet. After scaling we obtain the pressure throughout the medium, as well as the fluxes of fluid throughout the medium. We now need to update the concentration profile, as the solvent is transported through the medium by convection and diffusion.

A.2 Advection of solvent

After solving the elliptic problem we know the concentration profile at the previous time step and the flux of fluid at the current time-step. We now need to solve the equation

$$\frac{\partial c}{\partial t} + \nabla \cdot (\mathbf{u}c) = \frac{1}{\mathrm{Pe}} \nabla \cdot (\mathbf{D}\nabla c)\,,$$

for the transport of the solvent. Since the Péclet number is large, there are two distinct timescales for the problem. We therefore think that it is sensible to split the problem for the advection of the solvent from the problem for the diffusion the solvent. Our scheme is of the form

$$\tilde{c}^{n+1} = c^n + \tau \mathcal{F}(c^n, u^{n+1}, v^{n+1}, \tau), \qquad c^{n+1} = \tilde{c}^{n+1} + \tau \mathcal{G}(\tilde{c}^{n+1}),$$

where τ is the size of the time step, $\tilde{c}$ is our intermediate variable, and $\mathcal{F}$ and $\mathcal{G}$, represent our schemes for solving the advection and diffusion processes respectively. It may appear that these two processes are equivalent to a time step of 2τ, however, since we have only approximated some of the terms from the equation in each part, it can be seen to be equivalent to only a time step of τ. This scheme has the advantage of allowing us to carefully control the amount of numerical diffusion that we introduce into the problem.

The chief difficulty that we have encountered in simulating viscous fingering in miscible flow is the appearance of numerical diffusion. Simulating hyperbolic problems inevitably leads to numerical errors, which have the effect of introducing an artificial diffusion into the problem. Since our problem is extremely sensitive to the magnitude of diffusion, and the magnitude of the actual physical diffusion is small, numerical diffusion can affect our simulations. To obtain an accurate numerical simulation we must ensure that the magnitude of our actual physical diffusion is much larger than the magnitude of the numerical diffusion. We have applied the following strategies to reduce the magnitude of numerical diffusion:

- We have used an explicit scheme and have chosen the largest possible time-step permissible without violating the Courant stability condition.
- We have solved the problem in a moving reference frame, to reduce the maximum

value of the velocity and also to allow us to use a smaller domain.

- We have used the corner-transport upwind method with flux-limiters.

Our scheme is of the form

$$\begin{aligned} \tilde{c}_{ij}^{n+1} = c_{i,j} &- \frac{\tau}{h_x}\left((u_{i-1/2,j}-U)^+(c_{i,j}-c_{i-1,j}) + (u_{i+1/2,j}-U)^-(c_{i+1,j}-c_{i,j})\right) \\ &- \frac{\tau}{h_y}\left(v^+_{i,j-1/2}(c_{i,j}-c_{i,j-1}) + v^-_{i,j+1/2}(c_{i,j+1}-c_{i,j})\right) \\ &- \frac{\tau}{h_x}\left(\tilde{F}_{i+1/2,j}-\tilde{F}_{i-1/2,j}\right) - \frac{\tau}{h_y}\left(\tilde{G}_{i,j+1/2}-\tilde{G}_{i,j-1/2}\right), \end{aligned} \tag{A.4}$$

where we have suppressed the appearance of n from c_{ij} and $n+1$ from $u_{i-1/2,j}, v_{i,j-1/2}$. The expression $(u_{i-1/2,j}-U)^+$ is equal to the maximum of $(u_{i-1/2,j}-U)$ and 0, and $(u_{i-1/2,j}-U)^-$ is equal to the minimum of $(u_{i-1/2,j}-U)$ and 0, and similarly for $v^+_{i,j-1/2}$ and $v^-_{i,j-1/2}$. The expressions $\tilde{F}$ and $\tilde{G}$ are the corrective fluxes, which would be equal to zero if we applied a donor-cell upwind method without flux limiters [35]. The donor-cell upwind method has a five-point stencil, and does not consider the flux from diagonally adjacent cells. For solving the simplest two-dimensional advection equation,

$$\frac{\partial c}{\partial t} + u\frac{\partial c}{\partial x} + v\frac{\partial c}{\partial y} = 0, \tag{A.5}$$

with u and v constant, the Courant condition for stability of the donor-cell method is

$$\left|\frac{u\tau}{h_x}\right| + \left|\frac{v\tau}{h_y}\right| \leq 1, \tag{A.6}$$

and so, for a given speed, the largest possible time step has a strong dependence on the orientation of the grid to the flow. The donor-cell upwind method does not have the best possible stability properties [35]. For these reasons we use the corner-transport upwind method, which uses a nine-point stencil and does model the flux from diagonally adjacent cells, to model the advection of the solvent.

The corrective fluxes $\tilde{F}$ and $\tilde{G}$ for the corner-transport upwind method are algebraically complicated since one has to consider many different cases for different signs of u and v. Full details of the corrective fluxes can be found in [35], but as an example we give the correction fluxes for when $u-U$ and v are everywhere positive:

$$\begin{aligned} \tilde{F}_{i-1/2,j} &= -\frac{1}{2}\frac{\tau}{h_y}(u_{i-1/2,j}-U)v_{i-1,j-1/2}(c_{i-1,j}-c_{i-1,j-1}), \\ \tilde{G}_{i,j-1/2} &= -\frac{1}{2}\frac{\tau}{h_x}v_{i,j-1/2}(u_{i-1/2,j-1}-U)(c_{i,j-1}-c_{i-1,j-1}). \end{aligned}$$

The Courant condition for the corner-transport upwind method when solving (A.5)

$$\max\left(\left|\frac{u\tau}{h_x}\right|,\left|\frac{v\tau}{h_y}\right|\right)\leq 1, \tag{A.7}$$

which is an improvement over (A.6). To reduce the magnitude of numerical diffusion throughout our domain we have taken the largest possible time-step τ, while satisfying the Courant condition throughout the domain. Since the maximum component of the velocity throughout the domain will change over time we must use a time-step that changes with time. At the start of the advection simulation at each time step we choose the size of our time step to be

$$\tau=\tau^{n+1}=\left(\max_{i,j}\max\left(\left|\frac{u^{n+1}_{i-1/2,j}}{h_x}\right|,\left|\frac{v^{n+1}_{i,j-1/2}}{h_y}\right|\right)\right)^{-1}. \tag{A.8}$$

This choice of the time step minimises numerical diffusion throughout the domain and especially in the tip regions, where the velocities are largest, and accurate numerical simulation is particularly important.

In addition to using the corner-transport upwind method, we have also included flux-limiters to reduce the magnitude of numerical diffusion still further. Flux limiters have the effect of allowing us to use a higher order scheme, thus reducing numerical diffusion and improving accuracy, wherever the application of such a scheme does not lead to spurious oscillations (i.e. flux-limited schemes are total-variation diminishing). Flux limiters may be included by the following modification of the corrective fluxes:

$$\begin{aligned}\tilde{F}_{i-1/2,j} &= \hat{\tilde{F}}_{i-1/2,j}+\frac{1}{2}\left|u_{i-1/2,j}-U\right|\left(1-\frac{\tau}{h_x}\left|u_{i-1/2,j}-U\right|\right)\tilde{\mathcal{W}}_{i-1/2,j},\\ \tilde{G}_{i,j-1/2} &= \hat{\tilde{F}}_{i,j-1/2}+\frac{1}{2}\left|v_{i,j-1/2}\right|\left(1-\frac{\tau}{h_y}\left|v_{i,j-1/2}\right|\right)\tilde{\mathcal{W}}_{i,j-1/2},\end{aligned}$$

where $\hat{\tilde{F}}$ and $\hat{\tilde{G}}$ are the corrective fluxes obtained from the corner-transport upwind method and $\tilde{\mathcal{W}}_{i-1/2,j}$ is a "limited wave", obtained by comparing $c_{i,j}-c_{i-1,j}$ with either $c_{i-1,j}-c_{i-2,j}$ or $c_{i+1,j}-c_{i,j}$ depending on the sign of $u_{i-1/2,j}-U$. More precisely, we have

$$\tilde{\mathcal{W}}_{i-1/2,j}=\phi(\theta_{i-1/2,j})(c_{i,j}-c_{i-1,j}), \tag{A.9}$$

where

$$\theta_{i-1/2,j}=\frac{c_{i-1,j}-c_{i-2,j}}{c_{i,j}-c_{i-1,j}}\quad\text{if}\quad u_{i-1/2,j}-U>0,$$

and

$$\theta_{i-1/2,j} = \frac{c_{i+1,j} - c_{i,j}}{c_{i,j} - c_{i-1,j}} \quad \text{if} \quad u_{i-1/2,j} - U < 0,$$

and $\phi(\theta)$ is a flux-limiter function, for which we have chosen the minmod function:

$$\phi(\theta) = \min(1, |\theta|),$$

although various other functions can be used instead [35, 54]. The "limited wave" in the $y-$direction, $\tilde{\mathcal{W}}_{i,j-1/2}$ is defined in an identical fashion.

With both the corner-transport and flux-limited corrections added to (A.4) we are able to find the updated, advected concentration field $\tilde{c}_{ij}^{n+1}$. We now complete the final stage of each time-step: the simulation of diffusion.

A.3 Diffusion of solvent

In our numerical simulations we assume that the diffusion tensor is constant and diagonal in our coordinate system. We must therefore solve

$$\frac{\partial c}{\partial t} + \nabla \cdot (\mathbf{u}c) = \frac{1}{\mathrm{Pe}_x}\frac{\partial^2 c}{\partial x^2} + \frac{1}{\mathrm{Pe}_y}\frac{\partial^2 c}{\partial y^2}. \tag{A.10}$$

To simulate diffusion we use a simple explicit finite difference scheme:

$$c_{i,j}^{n+1} = \tilde{c}_{i,j}^{n+1} + \tau\left(\frac{\tilde{c}_{i+1,j}^{n+1} - 2\tilde{c}_{i,j}^{n+1} + \tilde{c}_{i-1,j}^{n+1}}{\mathrm{Pe}_x h_x^2} + \frac{\tilde{c}_{i,j+1}^{n+1} - 2\tilde{c}_{i,j}^{n+1} + \tilde{c}_{i,j-1}^{n+1}}{\mathrm{Pe}_y h_y^2}\right). \tag{A.11}$$

In general if we use the time-step given by (A.8) in (A.11) then we find that the scheme is unstable, since the criterion for stability of (A.11) (see e.g. [40]) is

$$\tau \leq \frac{1}{2}\left(\frac{1}{\mathrm{Pe}_x h_x^2} + \frac{1}{\mathrm{Pe}_y h_y^2}\right)^{-1}.$$

We therefore have to split up each advective time-step further to simulate diffusion using (A.11) while ensuring stability. It is possible to instead use an alternating-direction-implicit method (ADI) (see e.g. [40]) to simulate diffusion; however, for most of our simulations this did not appear to be as time-efficient, since the effect of diffusion over each advective time-step was small. An ADI method is more time-efficient when Pe_x and Pe_y are not large, however this case was not of primary interest.

At the end of simulating diffusion we have finished one (advective) time-step, and can return to the start, simulating the new pressure-field.

Appendix B

Brinkman porous media

Although Darcy's law is by far the most widely-used model for single-phase flow through porous media, there are other models which aim to capture additional physics. We include here a discussion of one such model, the Brinkman model, and consider the stability of a free surface in this model. For the application to miscible oil recovery, Darcy's law is quite sufficient, and our motivation for studying Brinkman's model is to present a novel result which adds a new possible physical mechanism for regularisation of the Muskat problem.

Brinkman's model applies to very porous media, where the porosity is very close to 1, i.e. almost all of space is pore-space. The simplest derivation of Brinkman's model considers Stokes flow past a fixed 3-dimensional array of spheres, with radius a, and separation L. We assume that both the size of the spheres and their separation are small compare to some macroscopic length-scale of interest, l, i.e. $a/l, L/l \ll 1$. We also assume that the spheres are well-separated so that $a/L \ll 1$, this ensures that the porosity is asymptotically equal to 1. With the spheres well-separated, the drag on each sphere is simply given by the formula for the Stokes drag i.e. $6\pi\mu a\mathbf{u}$, where $\mathbf{u}$ is the velocity of the fluid away from each sphere. The number of spheres per unit volume is equal to $(l/L)^3$. The spheres therefore exert a force on the fluid per unit volume of

$$\frac{6\pi\mu a}{L^3}\mathbf{u},$$

which may be treated as a body-force on the fluid. The flow of the fluid is therefore governed by

$$\nabla p = \mu\nabla^2\mathbf{u} - \frac{6\pi\mu a}{L^3}\mathbf{u},$$

which after nondimensionalising $\mathbf{x}$ with l; $\mathbf{u}$ with U, a typical velocity; and p with $\mu U/l$, becomes

$$\nabla p = \nabla^2\mathbf{u} - \frac{6\pi a_\delta}{\delta^3}\mathbf{u}, \tag{B.1}$$

where $a_\delta = a/l$ and $\delta = l/L$. There are now three possible cases:

1. $\delta^3 \ll a_\delta$. We rescale the pressure $p = a_\delta P/\delta^3$ to recover Darcy's law with the permeability $k = 1/6\pi$.
$$\mathbf{u} = -k\nabla P. \tag{B.2}$$

2. $\delta^3 \gg a_\delta$. The effect of the drag due to the spheres is negligible. We recover Stokes flow
$$\nabla p = \nabla^2 \mathbf{u}. \tag{B.3}$$

3. $\delta^3 = \mathcal{O}(a_\delta)$, $\quad a_\delta/\delta^3 = \beta = \mathcal{O}(1)$ say. We obtain the Brinkman model for flow through very porous media with (a nondimensional) permeability $k = 1/6\pi\beta$,
$$\nabla p = \nabla^2 \mathbf{u} - \frac{1}{k}\mathbf{u}. \tag{B.4}$$

The result can be generalised to a random array of non-spherical particles with qualitatively similar results, [27].

We now suppose that a free surface is present in a Brinkman medium. In the fluid region the flow is described by

$$\nabla \cdot \mathbf{u} = 0, \qquad \nabla p = \nabla^2 \mathbf{u} - \frac{1}{k}\mathbf{u},$$

and at the free surface the fluid should satisfy the kinematic boundary condition,

$$\mathbf{u} \cdot \mathbf{n} = v_n,$$

where $\mathbf{n}$ is the normal to the surface and v_n is the normal velocity of the surface. The fluid should also satisfy the dynamic boundary condition that the normal and tangential stresses at the interface are zero (neglecting surface tension), and so we require that

$$\boldsymbol{\sigma}\mathbf{n} = 0,$$

where

$$\boldsymbol{\sigma} = \begin{pmatrix} -p + 2\frac{\partial u}{\partial x} & \left(\frac{\partial u}{\partial y} + \frac{\partial v}{\partial x}\right) \\ \left(\frac{\partial u}{\partial y} + \frac{\partial v}{\partial x}\right) & -p + 2\frac{\partial v}{\partial y} \end{pmatrix}.$$

We have a one-dimensional base-state solution in which $u = 1$, $v = 0$ in $\xi = x - t \leq 0$, and the pressure is given by $p = -\xi/k$. We now seek a slightly perturbed solution in

which the location of the free surface is given by

$$\xi = \epsilon \mathrm{e}^{\mathrm{i}\alpha y + \sigma t},$$

where $\epsilon \ll 1$, and we (implicitly) take real parts throughout. The linearised problem gives

$$\begin{aligned} p &\sim -\frac{1}{k}\xi + \epsilon P \mathrm{e}^{|\alpha|\xi + \mathrm{i}\alpha y + \sigma t}, \\ u &\sim 1 + \epsilon\left(-|\alpha| kP \mathrm{e}^{|\alpha|\xi} + U \mathrm{e}^{\sqrt{\alpha^2+\frac{1}{k}}\xi}\right)\mathrm{e}^{\mathrm{i}\alpha y + \sigma t}, \\ v &\sim \epsilon\left(-\mathrm{i}\alpha k P \mathrm{e}^{|\alpha|\xi} + V \mathrm{e}^{\sqrt{\alpha^2+\frac{1}{k}}\xi}\right)\mathrm{e}^{\mathrm{i}\alpha y + \sigma t}. \end{aligned}$$

We must also ensure that $\nabla \cdot \mathbf{u} = 0$, and so we find that

$$V = \frac{U\mathrm{i}}{\alpha}\sqrt{\alpha^2 + \frac{1}{k}}.$$

The kinematic boundary condition yields,

$$-|\alpha| kP + U = \sigma.$$

Zero normal stress at the free surface gives

$$\frac{1}{k} - P + 2\left(U\sqrt{\alpha^2 + \frac{1}{k}} - \alpha^2 kP\right) = 0,$$

and zero tangential stress at the free surface gives

$$-2|\alpha| kP + \left(2 + \frac{1}{\alpha^2 k}\right)U = 0.$$

Combining these conditions we find that

$$\frac{1}{\sigma} = 4\alpha^2 k^2\left(\sqrt{\alpha^2 + \frac{1}{k}} - |\alpha| - \frac{1}{|\alpha| k}\right) - \frac{1}{|\alpha|}. \tag{B.5}$$

Note that in the limits of large and small k we find that

$$\begin{aligned} \sigma &\to 0 \quad \text{as} \quad k \to \infty, \\ \sigma &\to -|\alpha| \quad \text{as} \quad k \to 0. \end{aligned}$$

These are the appropriate dispersion relations for the stability of a free surface in Stokes

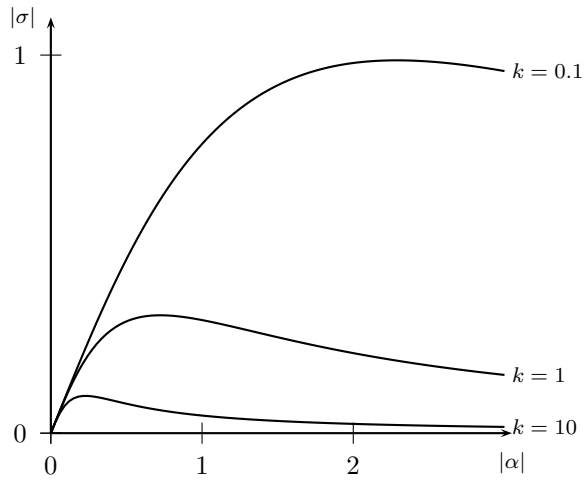

Figure B.1: Dispersion relation of disturbances to a free surface moving through a Brinkman porous medium.

flow and a Hele-Shaw cell respectively.[1]

A receding free surface in a Brinkman porous medium is unstable to all wavelength disturbances but, in contrast to a receding free surface in a porous medium modelled by Darcy's law, the growth rate of the disturbance is bounded, and large wavenumber disturbances are, asymptotically, neutrally stable. The linearised problem is therefore not ill-posed: we do not get blow-up of the solution in finite time. Modelling flow through porous media by Brinkman's model leads to a regularisation of the ill-posed Hele-Shaw problem, but for oil recovery applications it is an inappropriate regularisation since the porosity of oil-bearing rocks is emphatically not close to 1, more typically in the range 0.05-0.4, [2].

[1]Note that we have predicted a stable interface for the Hele-Shaw cell since we have an advancing front. The time-reversed problem in which a receding front is present is correspondingly unstable.

Bibliography

[1] R. Aris. On the dispersion of a solute in a fluid flowing through a tube. Proceedings of the Royal Society A, **235**:67–78, 1956.

[2] J. Bear. Dynamics of Fluids in Porous Media. Elsevier, 1972.

[3] A. Yu. Beliaev and S. M. Kozlov. Darcy equation for random porous media. Communications on Pure and Applied Mathematics, **XLIX**:1–34, 1996.

[4] R. B. Bird, W. E. Stewart, and E. N. Lightfoot. Transport Phenomena. New York: Wiley, 1960.

[5] R. J. Blackwell. Laboratory studies of microscopic dispersion phenomena. Society of Petroleum Engineers Journal, **2**:1–8, 1962.

[6] R. J. Blackwell, J. R. Rayne, and W. M. Terry. Factors influencing the efficiency of miscible displacement. Trans. AIME, **216**:1–8, 1959.

[7] H. Brenner. A general theory of Taylor dispersion phenomena. Physico-Chemical Hydrodynamics, **1**:91–123, 1980.

[8] R. Burridge and J. B. Keller. Poroelasticity equations derived from microstructure. The Journal of the Acoustical Society of America, **70**:1140–1146, 1981.

[9] S. J. Chapman. On the rôle of Stokes lines in the selection of Saffman-Taylor fingers with small surface tension. European Journal of Applied Mathematics, **10**:513–534, 1999.

[10] S. J. Chapman and J. R. King. The selection of Saffman-Taylor fingers by kinetic undercooling. J. Eng. Math., **46**:1–32, 2003.

[11] R. E. Collins. Flow of Fluids Through Porous Materials. Reinhold, 1961.

[12] R. Combescot, V. Hakim, T. Dombre, Y. Pomeau, and A. Pumir. Shape selection of saffman-taylor fingers. Physics Review Letters, **56**:2036–2039, 1986.

[13] H. Darcy. Les fontaines publiques de la ville de Dijon. Victor Dalmont, 1856.

[14] P. Daripa and G. Paşa. New bounds for stabilizing Hele-Shaw flows. Applied Mathematics Letters, **18**:1293–1303, 2005.

[15] P. Daripa and G. Paşa. On the growth rate for three-layer Hele-Shaw flows: Variable and constant viscosity cases. International Journal of Engineering Science, **43**:877–884, 2005.

[16] J. D. Evans and J. R. King. Asymptotic results for the Stefan problem with kinetic undercooling. Quarterly Journal of Mechanics and Applied Mathematics, **53**:449–473, 2000.

[17] C. L. Farmer. The numerical calculation of unstable miscible displacement. Technical report, Oil Recovery Projects Division, AEE Winfrith, June 1983.

[18] F. J. Fayers. An approximate model with physically interpretable parameters for representing viscous fingering. SPE Reservoir Engineering, **285**:551–558, 1988.

[19] W. E. Forsythe. Smithsonian Physical Tables (9th Revised Edition). Knovel, 1954;2003.

[20] A. C. Fowler. Mathematical Models in the Applied Sciences. CUP, 1997.

[21] J. J. Fried and M. A. Combarnous. Dispersion in porous media. Advances in Hydroscience, **7**:169–282, 1971.

[22] L. W. Gelhar, C. Welty, and K. R. Rehfeldt. A critical review of data on field-scale dispersion in aquifers. Water Resources Research, **28**:1955–1974, 1992.

[23] Sheldon B. Gorell and G. M. Homsy. A theory of the optimal policy of oil recovery by secondary displacement processes. SIAM Journal on Applied Mathematics, **43**:79–98, 1983.

[24] F. J. Hickernell and Y. C. Yortsos. Linear stability of miscible displacement processes in porous media in the absence of dispersion. Studies in Applied Mathematics, **74**:93–115, 1986.

[25] S. Hill. Channelling in packed columns. Chemical Engineering Science, **6**:247–253, 1952.

[26] G. M. Homsy. Viscous fingering in porous media. Annual Review of Fluid Mechanics, **19**:271–311, 1987.

[27] U. Hornung. Homogenization and Porous Media. Springer, 1997.

[28] S. D. Howison. Fingering in Hele-Shaw cells. Journal of Fluid Mechanics, **167**:439–453, 1986.

[29] S. D. Howison, J. R. Ockendon, and A. A. Lacey. Singularity developments in moving-boundary problems. Quarterly Journal of Mechanics and Applied Mathematics, **38**:343–354, 1985.

[30] G. P. Ivantsov. The temperature field around a spherical, cylindrical, or point crystal growing in a cooling solution. Doklady Akademii Nauk SSSR, **58**:567–569, 1947.

[31] P. Jacquard and P. Séguier. Mouvement de deux fluides en contact dans un milieu poreux. Journal de Mécanique, **1**:367–394, 1962.

[32] D. L. Koch and J. F. Brady. Dispersion in fixed beds. J. Fluid Mech., **154**:399–427, 1985.

[33] E.J. Koval. A method for predicting the performance of unstable miscible displacement in heterogenous media. Society of Petroleum Engineers Journal, **450**:145–154, 1963.

[34] A. A. Lacey, S. D. Howison, J. R Ockendon, and P. Wilmott. Irregular morphologies in unstable Hele-Shaw free-boundary problems. Quarterly Journal of Mechanics and Applied Mathematics, **43**:387–405, 1990.

[35] Randall J. LeVeque. Finite Volume Methods for Hyperbolic Problems. CUP, 2002.

[36] O. Manickam and G.M. Homsy. Fingering instabilities in vertical miscible displacement flows in porous media. Journal of Fluid Mechanics, **288**:75–102, 1995.

[37] A.J. McConnell. Applications of Tensor Analysis. Dover, 1957.

[38] J. W. McLean and P. G. Saffman. The effect of surface tension on the shape of fingers in a hele-shaw cell. J. Fluid Mech., **102**:455–469, 1981.

[39] G. Menon and F. Otto. Dynamic scaling in miscible viscous fingering. Commun. Math. Phys., **257**:303–317, 2005.

[40] K. W. Morton and D. F. Mayers. Numerical Solution of Partial Differential Equations. CUP, second edition, 2005.

[41] H. Ockendon and J.R. Ockendon. Viscous Flow. CUP, 1995.

[42] J. R. Ockendon, S. D. Howison, A. A. Lacey, and A. B. Movchan. Applied Partial Differential Equations. OUP, 1999.

[43] G. C. Papanicolaou and S. R. S. Varadhan. Boundary value problems with rapidly oscillating random coefficients. Seria Colloquia Mathematica Societatis János Bolyai, **27**:835–873, 1981.

[44] C.-W Park, S. Gorell, and G. M. Homsy. Two-phase displacement in Hele-Shaw cells: experiments on viscously driven instabilities. Journal of Fluid Mechanics, **141**:257–287, 1984.

[45] C.-W. Park and G. M. Homsy. Two-phase displacement in Hele-Shaw cells: theory. Journal of Fluid Mechanics, **139**:291–308, 1984.

[46] D.W. Peaceman and H.H. Rachford Jr. Numerical calculation of multidimensional miscible displacement. Society of Petroleum Engineers Journal, **2**:327–339, 1962.

[47] J. Rubinstein and R. Mauri. Dispersion and convection in periodic porous media. SIAM Journal on Applied Mathematics, **46**:1018–1023, 1986.

[48] P. G. Saffman. Exact solutions for the growth of fingers from a flat interface between two fluids in a porous medium or Hele-Shaw cell. Quarterly Journal of Mechanics and Applied Mathematics, **12**:146–150, 1959.

[49] P. G. Saffman and G. I. Taylor. The penetration of a fluid into a porous medium or Hele-Shaw cell containing a more viscous fluid. Proceedings of the Royal Society A, **245**:312–329, 1958.

[50] P.G. Saffman. A theory of dispersion in a porous medium. Journal of Fluid Mechanics, **6**:321–349, 1959.

[51] Muhammad Sahimi. Flow and Transport in Porous Media and Fractured Rock. VCH, 1995.

[52] Michael Siegel, Russel E. Caflisch, and Sam Howison. Global existence, singular solutions, and ill-posedness for the Muskat problem. Communications on Pure and Applied Mathematics, **LVII**:1374–1411, 2004.

[53] Lisa Stewart, editor. Oilfield Review, chapter Highlighting Heavy Oil, pages 34–53. Schlumberger, Summer 2006.

[54] P.K. Sweby. High resolution schemes using flux limiters for hyperbolic conservation laws. SIAM Journal on Numerical Analysis, **21,5**:995–1011, 1984.

[55] C.T. Tan and G.M. Homsy. Stability of miscible displacements in porous media - rectilinear flow. Physics of Fluids, **29**:3549–3556, 1986.

[56] C.T. Tan and G.M. Homsy. Simulation of nonlinear viscous fingering in miscible displacement. Physics of Fluids, **31**:1330–1338, 1988.

[57] G.I. Taylor. Dispersion of soluble matter in solvent flowing slowly through a tube. Proceedings of the Royal Society A, **219**:186–203, 1953.

[58] M.R. Todd and W.J. Longstaff. The development, testing and application of a numerical simulator for predicting miscible flood performance. Journal of Petroleum Technology, **253**:874–882, 1972.

[59] I. White, P. M. Colombera, and J. R. Philip. Experimental study of wetting front instability induced by gradual change of pressure gradient and by heterogeneous porous media. Soil Science Society of America Journal, **41**:483–489, 1976.

[60] R.A. Wooding. The stability of an interface between miscible fluids in a porous medium. Zeitschrift für Angewandte Mathematik und Physik, **13**:255–265, 1962.

[61] R.A. Wooding. Growth of fingers at an unstable diffusing interface in a porous medium or Hele-Shaw cell. Journal of Fluid Mechanics, **39**:477–495, 1969.

[62] Z.M. Yang, Y.C. Yortsos, and D. Salin. Asymptotic regimes in unstable miscible displacements in random porous media. Advances in Water Resources, **25**:885–898, 2002.

[63] Y.C. Yortsos and D. Salin. On the selection principle for viscous fingering in porous media. Journal of Fluid Mechanics, **557**:225–236, 2006.

[64] W.B. Zimmerman and G.M. Homsy. Nonlinear viscous fingering in miscible displacement with anisotropic dispersion. Physics of Fluids A, **3**:1859–1872, 1991.

[65] W.B. Zimmerman and G.M. Homsy. Viscous fingering in miscible displacements: Unification of effects of viscosity contrast, anisotropic dispersion, and velocity dependence of dispersion on nonlinear finger propagation. Physics of Fluids A, **4**:2348–2359, 1992.